ABDALHAMEED, MANAHIL MIRGHANI ALI, Ph.D. Design, Synthesis, and Structure-Activity Relationships of GPR35 Agonists and Antagonists and Design, Synthesis, and Anti-microbial Evaluation of Pyrazole Derivatives. (2015)
Directed by Dr. Mitchell Croatt. 163 pp.

GPR35, a G protein-coupled receptor (GPCR), was discovered and specified as an orphan receptor in 1998. GPR35 has been described as a prospective therapeutic target as a result of its association with many diseases including type-2 diabetes, nociceptive pain, inflammation, mild mental retardation syndrome, metabolic disorders, and gastric cancer. A GPR35 antagonist benzothiazole was identified via high-throughput screening of approximately 300,000 compounds. Based on the docking of the benzothiazole into a homology model of GPR35, analogs were designed, synthesized, and evaluated as antagonists at GPR35. The study examines various regions of the GPR35 binding site for the benzothiazole ligand. The results provided information that was used as a guide to design and synthesized potent GPR35 ligands.

A heterocyclic ring, pyrazole, has gained special consideration as a result of its significant biological properties including anti-cancer, anti-microbial, anti-bacterial, anti-fungal, and anti-inflammatory. Structurally novel pyrazole derivatives were designed, synthesized and evaluated for antagonist activity at the GPR35 receptor. Due to the scarcity in the anti-microbial drugs and limited scaffold with potentially unique mode of action and different resistance mechanism, these pyrazoles were also evaluated for their anti-microbial activity. SAR study on the pyrazole core presented potential antimicrobial agents that will serve as basis for designing and developing novel antimicrobial drugs.

DESIGN, SYNTHESIS, AND STRUCTURE-ACTIVITY RELATIONSHIPS OF GPR35 AGONISTS AND ANTAGONISTS AND DESIGN, SYNTHESIS, AND ANTI-MICROBIAL EVALUATION OF PYRAZOLE DERIVATIVES

by

Manahil Mirghani Ali Abdalhameed

A Dissertation Submitted to
the Faculty of the Graduate School at
The University of North Carolina at Greensboro
in Partial Fulfillment
of the Requirements for the Degree
Doctor of Philosophy

Greensboro
2015

Approved by

_____
Committee Chair

For my daughters, Dan and Ayan

APPROVAL PAGE

This dissertation, written by Manahil Mirghani Ali Abdalhameed, has been approved by the following committee of the Faculty of The Graduate School at The University of North Carolina at Greensboro.

Committee Chair Mitchell Croatt

Committee Members Patricia Reggio

Jerry Walsh

Gregory Raner

_____

Date of Acceptance by Committee

_____

Date of Final Oral Examination

ACKNOWLEDGMENTS

First of all, I want to thank God for the blessings of health, wellness and success in completing this work. Second, I offer my sincerest gratitude to my supervisor, Dr. Mitchell Croatt, who has supported me throughout my research with his knowledge, experience and understanding whilst allowing me the room to work in my own way. I would also like to thank Dr. Patricia Reggio, Dr. Gregory Raner and Dr. Jerry Walsh for serving as my dissertation committee members and providing their invaluable time, guidance and suggestions. I would like to thank our collaborator Dr. Mary Abood and also Dr. Nadja Cech for offering the antimicrobial evaluation for the pyrazole derivatives.

I would like to thanks the Department of chemistry and biochemistry for providing the support and equipment I needed to produce and complete my dissertation and offering to me a friendly and cheerful group of fellow students and post doctors. Further, I would like to acknowledge the National Science Foundation (CHE-1351883) and the NIH (R21NS077347 and R01DA023204) for funding my studies.

I would like to thank my mom and dad for always loving me, believing in me, and praying for me. My special thanks go to my best friend, my husband Mohamed, for offering me unconditional love, understanding, and outstanding support throughout my PhD program. He taught me the meaning of loyalty and the true meaning of success. I would like to give my full thanks to my daughters Dan and Ayan for sacrificing their first years of their childhood as a gift for me to complete this works, and also my two sisters for giving me motivation.

TABLE OF CONTENTS

Page

LIST OF TABLES

Page

LIST OF FIGURES

Page

CHAPTER I

DESIGN, SYNTHESIS, AND EVALUATION OF GPR35 AGONISTS

Introduction

G protein-coupled receptors (GPCRs) represent the largest family of proteins in the mammalian genome.[1] There are two major characteristics associated with GPCRs. First, all the receptors interact with G-protein. Second, all the receptors consists of seven α-helices imbedded in the cell membrane. The endogenous ligands for GPCRs are considerably diverse, including proteins, lipids, peptides, amines, nucleotides, and hormones.[1] These ligands bind to the GPCRs and trigger a series of reactions with multiple alternative signaling pathways to ultimately deliver the messages and generate the appropriate physiological responses. More than half of today's drugs are targeted at GPCRs which reflect the physiological and pharmacological importance of these receptors.[2]

Cloning and sequencing of the human genome led to the discovery of new GPCRs, however, many of the GPCRs are still orphan receptors. By definition, an orphan receptor is a receptor that lacks the identification of endogenous ligands.[3] GPR35 was discovered and specified as an orphan receptor in 1998 using molecular cloning techniques.[3] The study described and assigned the signal of GPR35 to chromosome 2, region q37.3. Initially, GPR35 was discovered as an open reading frame encoding a protein of 309 amino acids. The sequence of these amino acids showed the identity of

GPR35. GPR35 sequenced amino acids resembled amino acid sequences of many receptors including nicotinic acid receptor HM74, nucleotide receptors P2Ys, GPR27, and GPR55.[1, 3]

First detection of GPR35 was in the rat intestine.[3] High levels of GPR35 were detected in gastrointestinal tissue and immune cells.[4] Significant expression of human GPR35 were reported in small intestine, colon, spleen and immune cells; with lower levels of GPR35 reported in heart, pancreas, kidney, liver, and adipose tissues.

Although limited information on GPR35 has appeared and some certainty might change when the crystal structure of GPR35 is determined, the discovery of a GPR35 endogenous ligand has been confirmed. A metabolite of amino acid L-tryptophan, kynurenic acid, was reported as the first endogenous ligand for the GPR35 receptor with a moderate to low potency agonist activity.[4] The moderate potency of kynurenic acid makes deorphanization of the GPR35 still under debate. 2-Acyl lysophosphatidic acid (LPA) was also described as another endogenous ligand for the GPR35 receptor.[5] Zaprinast, a well characterized cyclic guanosine monophosphate-specific phosphodiesterase inhibitor, was described as a first-rate GPR35 exogenous ligand that moderately activates human GPR35[6] (Table 1).

Since GPR35's discovery, it has attracted a lot of attention in the area of drug design and development. In 2000, GPR35 has been suggested to have significant role in type-2 diabetes.[7] Genome-wide screening of type-2 diabetes genes reported linkage between the disease and GPR35. Association of GPR35 with type-2 diabetes was

dependent on the finding of 19 polymorphisms in GPR35 region and 4 in the intergenic region of GPR35.

Table 1

GPR35 Endogenous and Exogenous Agonists

Agonist	Structure	EC_{50}
LPA	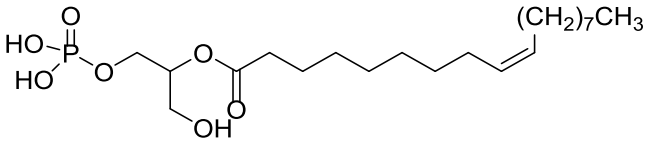	–
Kynurenic acid	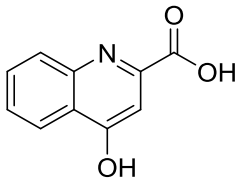	217 µM
cGMP	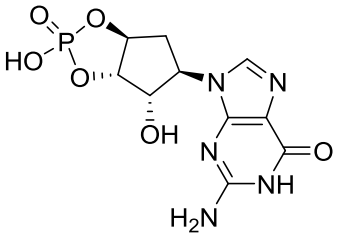	131 µM
Reverse T3	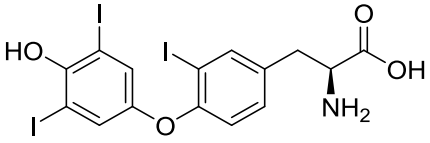	100 µM
DHICA	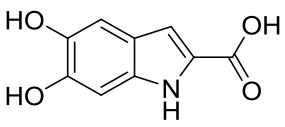	22 µM

Table 1

(Cont.)

Agonist	Structure	EC_{50}
Furosemide	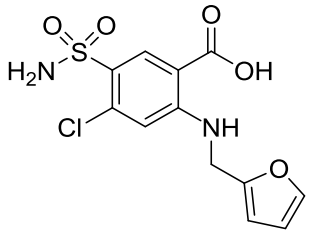	8.3 µM
Tyrphostin-51	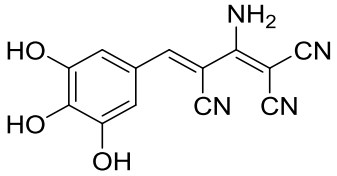	8 µM
Zaprinast	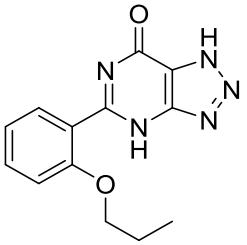	8 µM
Cromolyn	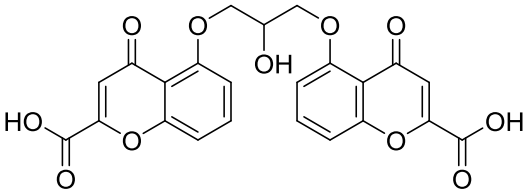	7 µM
Amlexanox	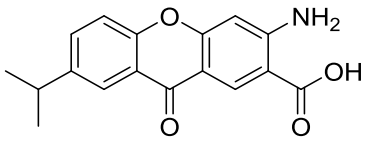	4 µM

Table 1

(Cont.)

Agonist	Structure	EC_{50}
Pamoic acid	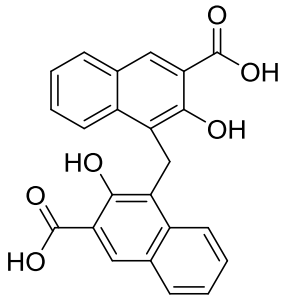	50 nM
Compound 1	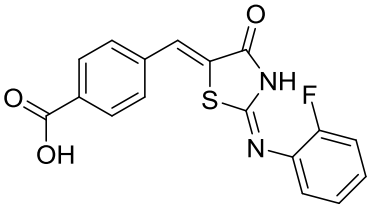	26 nM
Bufrolin	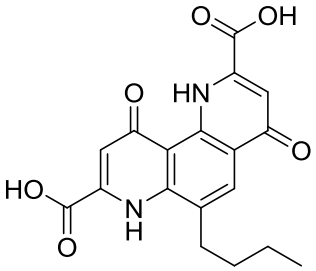	13 nM
PSB-13253	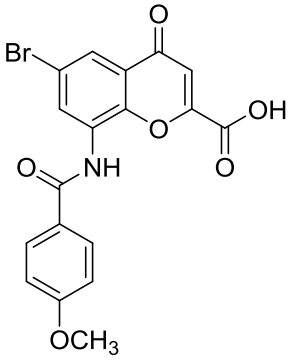	12 nM

Table 1

(Cont.)

Agonist	Structure	EC_{50}
Lodoxamide	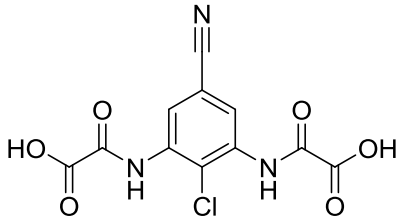	4 nM

GPR35 is proposed to be strongly involved in pain signaling.[8] Based on the expression of GPR35 in the rat nociceptive neurons and the involvement of GPR35 in antinociceptive mechanism, the study demonstrated that GPR35 might be a novel therapeutic target for nociceptive pain.

High expression of GPR35 in immune cells hints at linkage between GPR35 and immune response. Although the potential role of GPR35 in immunomodulation remains unexplored, involvement of this receptor in inflammation response has been confirmed.[4] The study connected an elevated level of kynurenic acid during inflammation and involvement of GPR35 in inflammation. A number of subsequent studies linked GPR35 with inflammatory regulation,[9] inflammatory macrophage,[10] and inflammatory bowel disease.[11]

GPR35 has been suggested as a prospective therapeutic target in the treatment of cardiovascular diseases. Linkage between the GPR35 and heart failure was determined via screening study of 12 genes in rat cardiomyocytes.[12] Another screening study using single nucleotide polymorphisms strongly linked GPR35 with coronary artery disease.[13]

GPR35 has been suggested to have a significant role in Albright hereditary osteodystrophy and mild mental retardation syndrome associated with the deletion on chromosome 2q37.3.[14] GPR35 has also been suggested to be involved in metabolic disorders,[15] asthma,[16] and gastric cancer.[17]

Association of GPR35 with that number of diseases urges the need to characterize the GPR35 receptor, to define the chemistry and biochemistry of this receptor, to regulate this receptor, and to ultimately provide compounds that utilize this information for potential therapeutic advantages. As a consequence, many studies focus on the synthesis of new compounds with agonist activity on GPR35 to reach this goal.[18, 19, 20, 21] Table 1 showed numbers of endogenous and exogenous ligands act as moderate to potent agonists at GPR35.[21] For instance, similar to zaprinast, furosemide, tyrphostin-51, cromolyn, and amlexanox showed moderate agonist activity at GPR35. Until recently, pamoic acid was significantly more potent than the endogenous and synthetic GPR35 agonists with an EC_{50} of 50 nM (Table 1). However, thus far, these endogenous and synthetic ligands have proved ineffectual in characterizing GPR35 receptor due to moderate potency or poor selectivity. For these reasons, pamoic acid was selected as a lead to develop more potent and selective agonists of human GPR35 receptor. The proposed hypothesis is constructed to attain extremely potent and selective GPR35 agonist for therapeutic targets and radio labeling purposes which will facilitate the characterization of the GPR35 receptor.

Modeling of GPR35 Active State

Although the crystal structure of GPR35 is not available, the Reggio group was able to build a homology model of GPR35 based on known crystal structure of other

related GPCRs. This homology model can be used to spot the ligand binding site for GPR35 and identify the amino acid interactions when the ligands bind to the receptor as well as supporting the therapeutic potential for GPR35. Construction of the GPR35 homology model is discussed in detail in Chapter II. However, the focus of this chapter is the modeling of the active state of the GPR35.

The GPR35 active state was built based on a sequence comparison with the β_2-adrenergic receptor.[23] In the GPR35 active form intracellular and extracellular loops were modified to mimic the class A conserved disulfide bridge. The activated state model was generated to maintain the hydrogen bonds, loops and termini. Also the helicity was kept using the harmonic constraint on the backbone. Finally, the loops were energy minimized using the conformational memories technique.

Design of GPR35 Agonists

There have been a considerable number of studies focusing on the screening of chemical libraries in an attempt to identify potential GPR35 ligands.[19, 22] The chemical library of Prestwick has been broadly targeted for the aim of identifying potential GPR35 ligands. From the screening of 1120 small molecules in the Prestwick chemical library, Dr. Mary Abood and coworkers discovered new and potent GPR35 ligands.[22] Pamoic acid, a well-known and presumably inactive drug ingredient, was revealed to have GPR35 agonist activity. The study disclosed that pamoic acid effectively recruits β-arrestin2 to GPR35 and activates ERK1/2. The study also demonstrated that pamoic acid is more potent than any other known ligands, endogenous or exogenous, for GPR35 with an EC_{50} of 50 nM.

Despite the fact that pamoic acid was reported as the most potent GPR35 exogenous ligand, it is still not ideal as a radioligand due to non-selectivity and moderate potency. For these reasons the collaboration between our departments' labs and Dr. Mary Abood selected pamoic acid for initial compound development in order to achieve a more potent and selective GPR35 agonist and ultimately provide means to characterize GPR35.

As pamoic acid deprotonated readily in physiological pH (pk_{a1} = 2.51, pk_{a2} = 3.1), the lowest energy conformation was calculated for the dianionic form of pamoic acid.[23] Interaction of the binding site of activated form of GPR35 with the pamoic acid was examined based on the deprotonated pamoic acid. Pamoic acid binding pocket is located mainly in TMH3, 4, 5, and 6 region of the GPR35 activated form. Pamoic acid provides a handful of favorable interaction with the residue of the binding site. Due to the deprotonation of pamoic acid, the arginine residue was considered the main contributing residue. The residues R4.60(151), R3.36, R(164), and R(167) provide a salt bridge with the carboxylic acid moieties of pamoic acid. Residues R(164), Q3.29 and S5.39 provide hydrogen bonding also with carboxylic acid moieties. The residues T166, L6.55, and L3.33 provide van der Waals interactions with the pamoic acid. Finally R4.60 form cation-π interactions with the fused ring of pamoic acid (Figure 1). These interactions of pamoic acid with the GPR35 binding site supported our selection of pamoic acid as a lead for this study.

About eight analogs of pamoic acid were subjected to computational analysis in the Reggio lab to predict the interaction, or the lack of interaction, at the binding site of the GPR35 model activated form (R*). Three compounds show proper fitting into the

binding pocket of GPR35 model (R*). Figure 2 shows pamoic acid and the three selected analogs **1.1**, **1.2**, and **1.3**. Analog **1.1** lacks the hydroxyl groups on the naphthalene rings while analog **2** has additional methoxy groups at position 7 of each naphthalene ring. Analog **1.3** has two methyl groups at the methylene position of the pamoic acid.

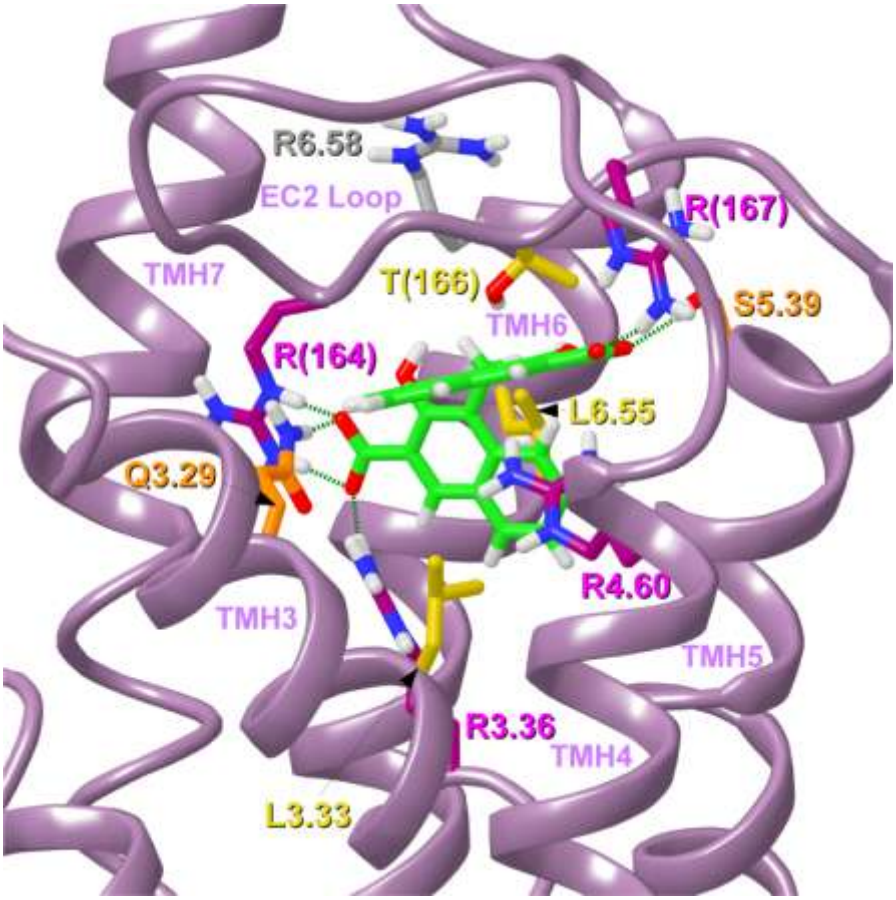

Figure 1. Docking of Pamoic Acid in the GPR35 Homology Model Active State.

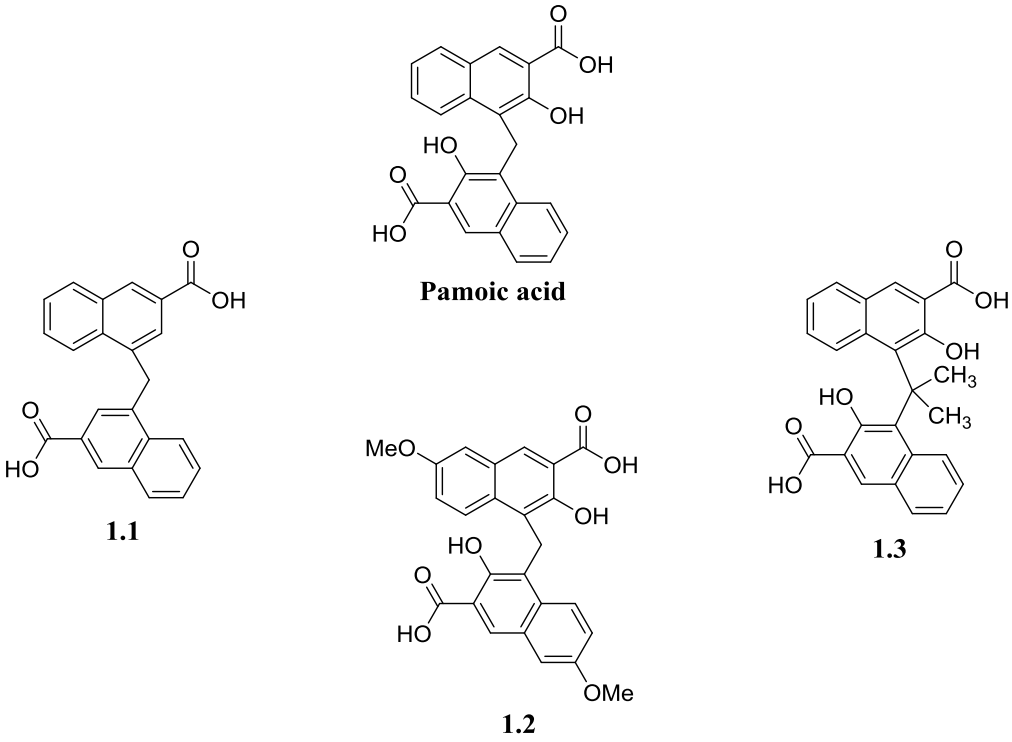

Figure 2. Pamoic Acid and Analogs **1.1**, **1.2** and **1.3**.

Synthesis of Pamoic Acid Analogs

The proposed synthesis of analog **1.1** is shown in the retrosynthesis scheme (Figure 3). The synthetic route includes replacement of the hydroxyl groups of pamoic acid with triflate groups using triflic anhydride and then reduction using palladium and a reducing agent.

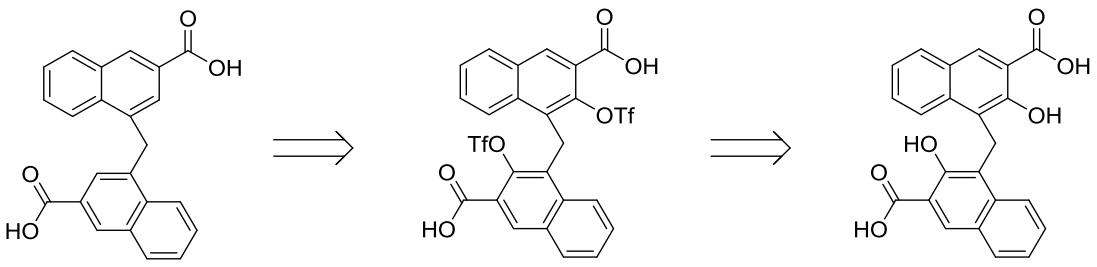

Figure 3. Retrosynthesis Analysis of Analog **1.1**.

The synthesis of analog **1.1** initiated with treating commercially available pamoic acid with triflic anhydride and pyridine to produce compound **1.4** (Figure 4). However, the intended product was not observed which is assumed to be due to the presence of carboxylic acid groups. Esterification of the carboxylic acid groups of pamoic acid to obtain ester **1.5** was then suggested as a solution. Because pamoic acid possesses multiple OH functionalities, esterifiction of pamoic acid proved to be ineffectual (Figure 4). As a result, another synthetic pathway was pursued.

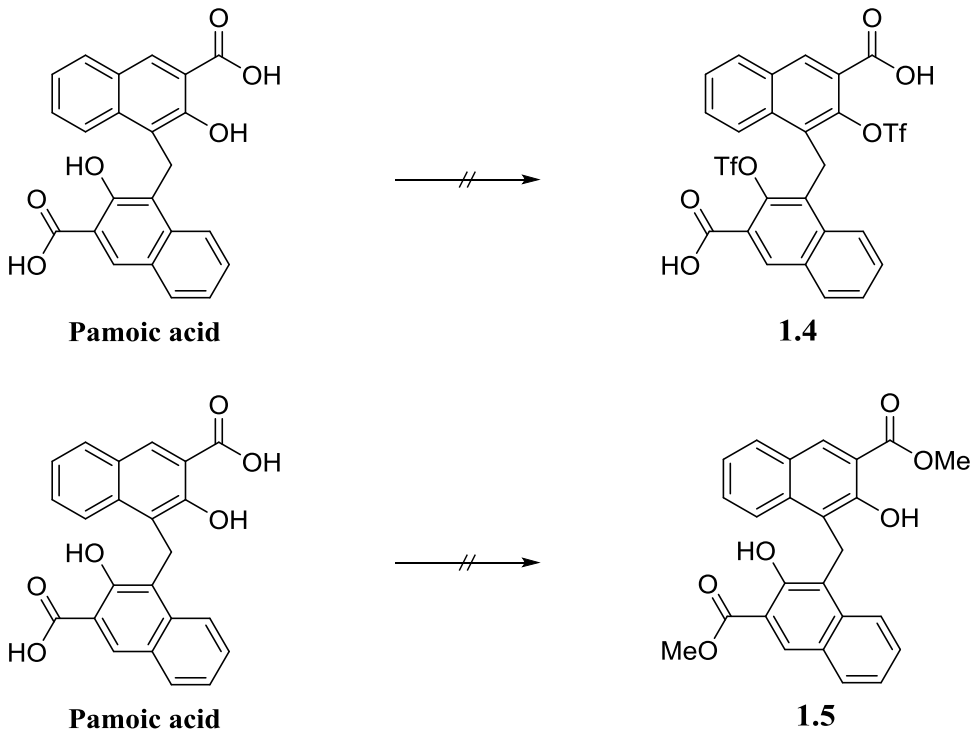

Figure 4. Unsuccessful Attempts to Synthesize Analog **1.1** Using Pamoic Acid.

The synthesis (Figure 5) began with esterification of the commercially available 3-hydroxy-2-naphthoic acid to form methyl 3-hydroxy-2-naphthoate **1.6** in high yield. The resulting methyl 3-hydroxy-2-naphthoate undergoes a condensation reaction with

formaldehyde to result in the formation of methyl pamoate **1.7**.[24] Methyl pamoate was then treated with triflic anhydride and pyridine to yield the ditriflate **1.8** in high yield.[25] The resulting product was then subjected to palladium-catalyzed reduction using formic acid as a reducing agent,[26] thus effectively removing the hydroxyl groups in the original compound. Subsequent column chromatographic purification confirms the successful substitution of the triflates with hydrogens to form intermediate **1.9** in good yield (Figure 5).

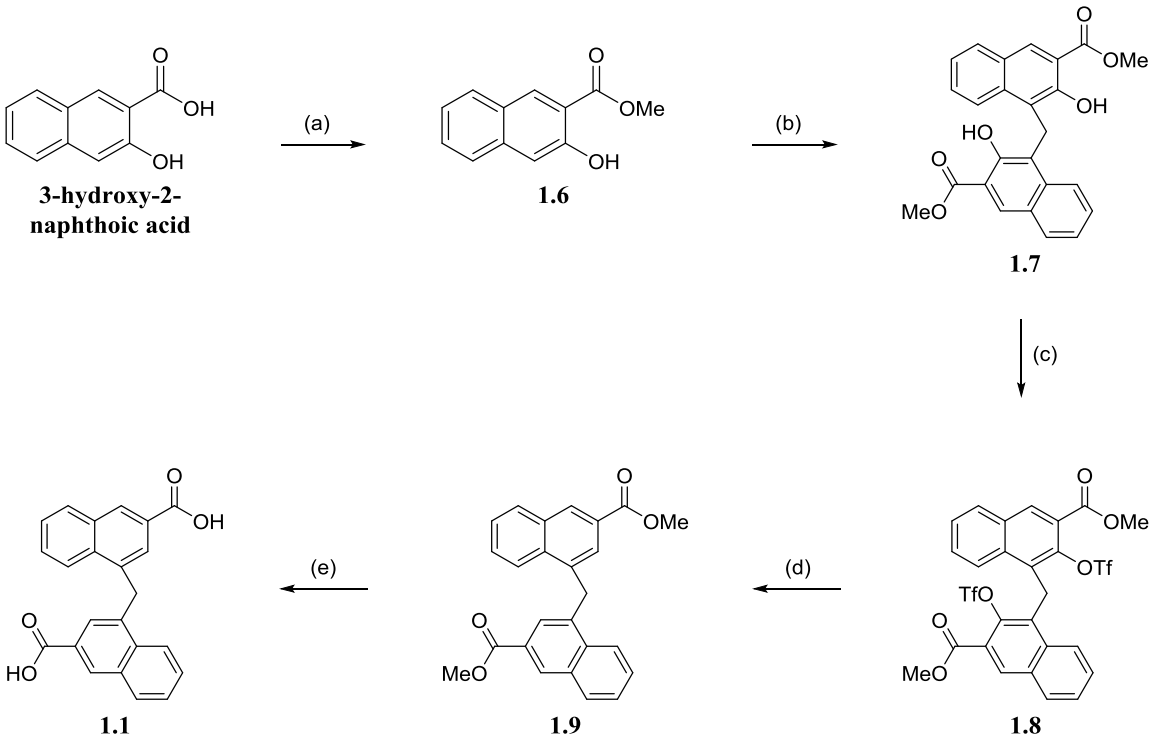

Figure 5. Synthesis of Analog **1.1**. (a) MeOH, H_2SO_4, 93% (b) HCOH, CH_3CO_2H, 85% (c) Tf_2O, pyridine, CH_2Cl_2, 94% (d) $Pd(OAc)_2$, PPh_3, DMF, TEA, HCO_2H, 69% (e) $(CH_3)_4NOH$, CH_2Cl_2, 92%.

Although the last step in the synthesis seems to be simple deprotection of carboxylic acid to produce final analog **1.1**, numerous attempted experiments resulted in

decomposition or recovery of the starting material (Table 2). As solubility was likely the cause of failure, tetramethylammonium hydroxide was attempted so that a nonpolar solvent could be used (Figure 5).

The second analog (**1.2**) contains two methoxy groups at position 7 of each naphthalene ring. Analog **1.2** was synthesized using commercially available 3-hydroxy-7-methoxy-2-naphthoate sodium salt (Figure 6). Because the 3-hydroxy-7-methoxy-2-naphthoate ring comprises multiple activated positions including positions 4, 6, and 8 (see the numbering system), the condensation reaction of 7-methyl-3-hydroxy-2-naphthoate sodium salt with formaldehyde could produce a mixture of products.[24] However, position 4, which is activated by a hydroxyl group, is more active than position 6 and 8 which are activated by methoxy groups. As a result, close monitoring of the reaction was required to successfully produce the desired product in 64% yield (Figure 6).

Table 2

Experimental Condition for Deesterificaton Reaction

Entry	Reagent	Result
1	EtOH, CH_2Cl_2, NaOH, H_2O	starting material
2	NaOH, MeOH	starting material
3	NaOH, H_2O	starting material
4	LiOH, H_2O	starting material
5	H_2SO_4, H_2O	starting material
6	$(Et)_3BnNBr$, CH_2Cl_2, NaOH	decomposition
7	$(CH_3)_4NOH$, CH_2Cl_2	desired product

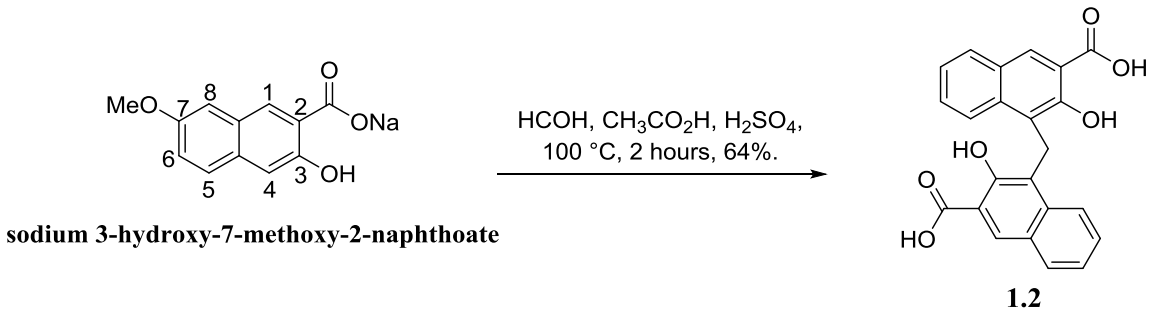

sodium 3-hydroxy-7-methoxy-2-naphthoate

1.2

Figure 6. Synthesis of Analog **1.2**.

Pamoic acid analog **1.3** required installation of two methyl groups at methylene position of pamoic acid. Numerous experiments were conducted including different routes. Specifically, a route incorporating condensation of acetone or acetone surrogates using 3-hydroxy-2-naphthoic acid or methyl-3-hydroxy-2-naphthoate turned out undesired products or the starting materials. Oxidation of the methylene position of pamoic acid followed by nucleophilic addition of the methyl groups was suggested as alternative route. However, the intended product was not synthesized (Table 3). The steric hindrance effect and the geometry of the product were expected to be the reasons for unsuccessful reactions.

Results and Discussion

The measurement of the agonist activity of the synthesized analogs was carried out using β-arrestin assay. The bioassay results showed that analog **1.2** was slightly less potent than the pamoic acid. Whereas, removing the hydroxyl groups from position 3 in analog **1.1** diminished the activity of pamoic acid (Table 4).

Table 3

Unsuccessful Trails to Synthesize Analog **1.3**

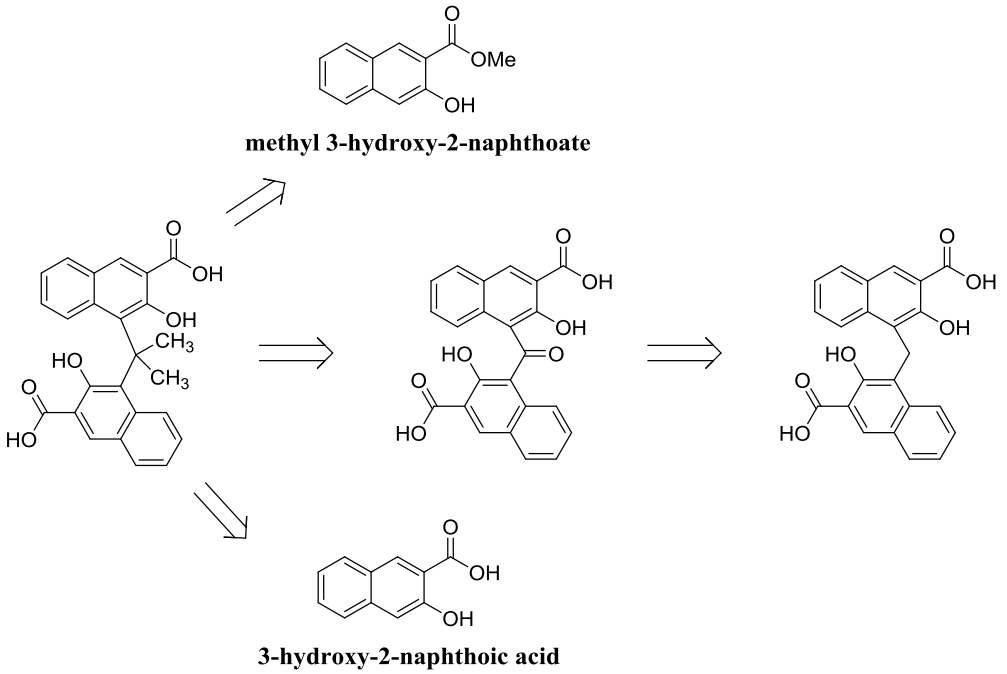

Starting material	Reagents	Results
3-hydroxy-2-naphthoic acid	$(CH_3)_2CO$, CH_3COOH	Undesired product
3-hydroxy-2-naphthoic acid	$(CH_3)_2CO$	Starting material
3-hydroxy-2-naphthoic acid	$(CH_3)_2C(OCH_3)_2$, CH_3COOH	Undesired product
3-hydroxy-2-naphthoic acid	$(CH_3)_2C(OCH_3)_2$, CH_3COOH, H_2SO_4	Undesired product
Methyl-3-hydroxy-2-naphthoate	$(CH_3)_2CO$, CH_3COOH	Starting material
Methyl-3-hydroxy-2-naphthoate	$(CH_3)_2C(OCH_3)_2$, CH_3COOH	Undesired product
Methyl-3-hydroxy-2-naphthoate	$(CH_3)_2C(OCH_3)_2$, CH_3COOH, H_2SO_4	Undesired product
Pamoic acid	$(Et)_3BnNBr$, $KMnO_4$, DCM	Decomposition

Table 3

(Cont.)

Starting material	Reagents	Results
Pamoic acid	Acetic anhydride, CrO_3	Starting material
Pamoic acid	$(Bu)_4NHSO_4$, $KMnO_4$, DCM	Starting material

Table 4

Biological Results of Pamoic Acid Analogs

	EC_{50} (nM)
Pamoic acid	50
Analog **1.1**	604
Analog **1.2**	61

Analysis of these results provides information on pamoic acid as an agonist ligand for GPR35. The result implies the significance of hydroxyl groups on position 3 of each naphthalene ring of pamoic acid. This probably indicates a type of interaction between the hydroxyl groups and the residue at the binding site of GPR35 or interaction of this hydroxyl groups with carboxylic acid functional groups. The slight decreasing of the potency of pamoic acid upon modifying position 7 suggests that this modification has low influence on the agonist activity. However, the binding site at this region of the receptor could prefer positively charged surfaces. As a result, a likewise response will emerge if the modification was performed at position 6 or 8.

The analysis of the bioassay indicates that the possibility of improving the potency or selectivity of pamoic acid is most likely limited. Additionally, numerous research groups are focusing on the identification and creation of novel and potent GPR35 agonists (Table 1). Milligan Group reached their goal with a novel and potent GPR35 agonist (EC_{50} = 26 nM).[27] Whereas the Muller Group was able to synthesize a novel radio-labeled GPR.335 agonist with high potency (EC_{50} = 5.5 nM)[28] (Figure 1.4). This approach is the basis to pursue a different but related unsolved dilemma.

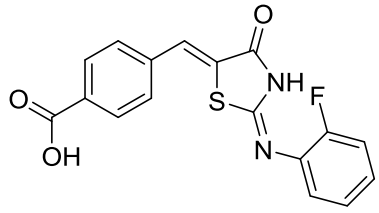

4-((*Z*)-((*E*)-2-((2-fluorophenyl)imino)
-4-oxothiazolidin-5-ylidene)methyl)
benzoic acid
EC_{50} = 26 nM

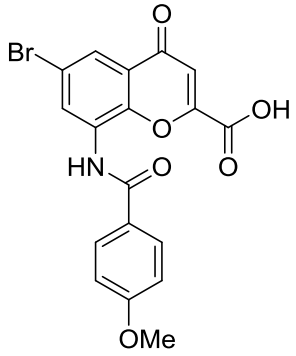

6-bromo-8-(4-methoxybenzamido)
-4-oxo-4H-chromene-2-carboxylic acid
EC_{50} = 5.54 nM

Figure 7. Potent GPR35 Agonists.

Experimental Procedures and Characterization

All anhydrous reactions were performed in oven dried glassware under a nitrogen atmosphere. All commercial reagents and solvents were used without further purification. Chromatographic purification was performed using silica gel (60 Å, 32-63μm). Analytical thin-layer chromatography (TLC) was performed on SiO_2 plates and visualizing by UV irradiation at 254 nm. NMR spectra were recorded in $CDCl_3$, DMSO-

d_6, methanol-d_4, or acetone-d_6 using JEOL ECA spectrometer (500 MHz for ^{1}H, 125 MHz for ^{13}C). All ^{1}H NMR experiments are reported in δ units, parts per million (ppm) downfield of TMS, and were measured relative to the signals for chloroform (7.26 ppm), DMSO (2.50 ppm), methanol (3.31 ppm), or acetone (2.05 ppm). All ^{13}C NMR spectra were reported in ppm relative to the signals for chloroform (77 ppm), DMSO (39.5 ppm), methanol (49 ppm), acetone (29.8 ppm) and. Coupling constants, *J*, are reported in hertz (Hz) and multiplicities are listed as singlet (s), doublet (d), triplet (t), doublet of doublets (dd), triplet of doublets (td), quintet (quint), multiplet (m), etc. High resolution mass spectra were acquired on a Thermo Fisher Scientific LTQ Orbitrap XL MS system using electrospray ionization (ESI).

To a solution of 3-hydroxy naphthalene-2-carboxylic acid (3.60 g, 19.1 mmol) in dry methanol (20 mL) was added concentrated sulfuric acid (0.22 mL) and the mixture was refluxed for 17 hours (Figure 8). The excess methanol was evaporated off under reduced pressure. The residue was then dissolved in ethyl acetate (50 mL), washed several times with 5% aqueous K_2CO_3 and brine, and then dried using Na_2SO_4. The product was crystallized as yellow crystal during solvent evaporation under reduced pressure (3.6 g, 93% yield). The product matched spectral data from reference 29.[29]

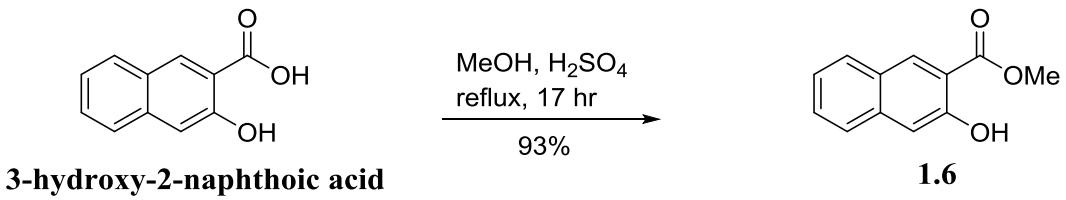

3-hydroxy-2-naphthoic acid **1.6**

Figure 8. Synthesis of Methyl 3-hydroxyl-2-Naphthoate.

Following a reported procedure,[24] methyl 3-hydroxy-2-naphthoate (0.49 g, 2.47 mmol) was dissolved in 37% aqueous formaldehyde (0.58 mL, 7.42 mmol) and glacial acetic acid (0.58 mL) and the mixture was refluxed at 110 °C for 17 hours (Figure 9). The product was cooled in an ice bath, filtered under vacuum, washed with cold water (125 mL) and then with ethyl alcohol to produce the desired product (0.88 g, 85% yield).

^{1}H NMR (500 MHz, $CDCl_3$) δ 11.26 (s, 2H), 8.40 (s, 2H), 8.23 (d, *J* = 8.59 Hz, 2H), 7.69 (d, *J* = 8.02 Hz, 2H), 7.33 - 7.38 (m, 2H), 7.19 (t, *J* = 7.16 Hz, 2H), 4.95 (s, 2H), 4.05 (s, 6H).

^{13}C NMR (126 MHz, $CDCl_3$) δ 171.1(2C), 153.4 (2C), 137.3 (2C), 131.6 (2C), 130.0 (2C), 129.0 (2C), 127.2 (2C), 124.3 (2C), 123.5 (2C), 121.9 (2C), 113.5 (2C), 52.8 (2C), 20.6.

HRMS (ESI): $C_{25}H_{21}O_6$ $[M+H]^+$, Calculated: 417.13381**,** Found:417.1327.

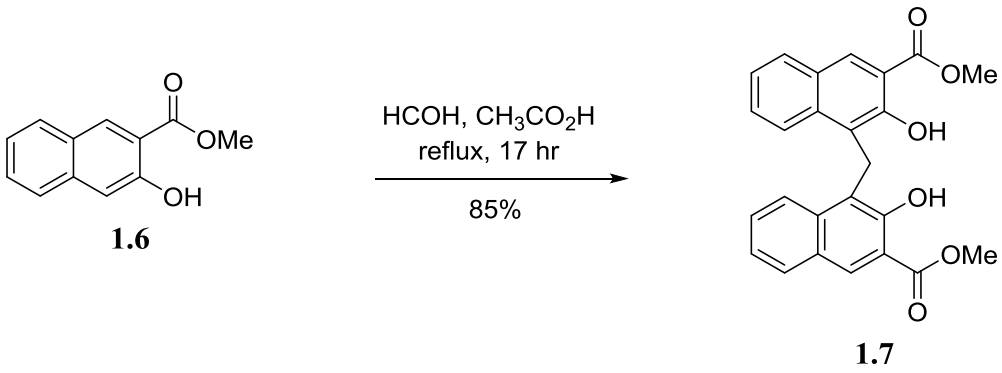

1.6 **1.7**

Figure 9. Synthesis of Methyl Pamoate.

Following a reported procedure,[25] to a solution of methyl pamoate (0.10 g, 0.24 mmol) in dry dichloromethane (3 mL) under N_2 atmosphere was added dry pyridine (0.10 mL, 1.20 mmol) followed by triflic anhydride (0.12 mL, 0.72 mmol) and the mixture was

stirred at room temperature for 17 hours (Figure 10). Saturated solution of $NaHCO_3$ (10 mL) was added to the reaction mixture and the product was extracted with ethyl acetate, dried over Na_2SO_4, and evaporated off under reduced pressure to obtain 0.15 g of paige solid (94% yield).

^{1}H NMR (500 MHz, $CDCl_3$) δ 8.49 (s, 2H), 7.86 (dd, *J* = 3.44, 6.30 Hz, 2H), 7.82 (dd, *J* = 3.44, 6.30 Hz, 2H), 7.45 - 7.49 (m, 4H), 5.10 (s, 2H), 4.06 (s, 6H).

^{13}C NMR (126 MHz, $CDCl_3$) δ 165.2 (2C), 142.1 (2C), 134.2 (2C), 133.9 (2C), 131.5 (2C), 130.1 (2C), 129.9 (2C), 129.4 (2C), 127.8 (2C), 124.3 (2C), 122.8 (2C), 53.0 (2C), 24.8.

HRMS (ESI): $C_{27}H_{19}F_6O_{10}S_2$ $[M+H]^+$, Calculated: 681.03238**,** Found:681.0311.

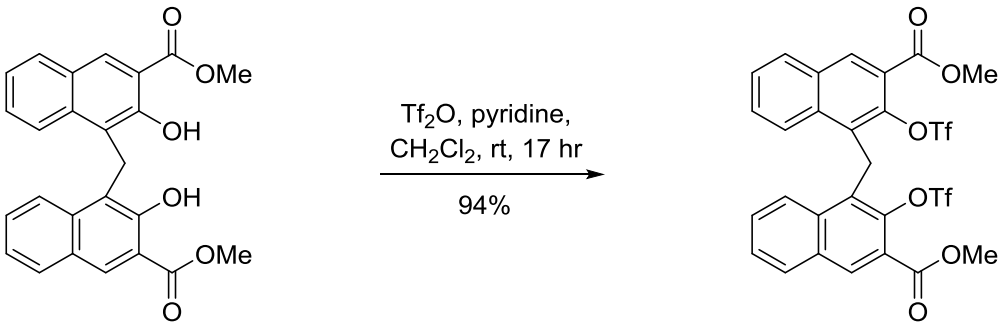

1.7 **1.8**

Figure 10. Synthesis of Ditriflate **1.8**.

Following a reported procedure,[26] an oven dry round bottom flask was equipped with starting material (0.10 g, 0.15 mmol), palladium acetate (0.003 g, 0.015 mmol), and triphenyl phosphine (0.01 g, 0.03 mmol). Dry DMF (1 mL) and TEA (0.10 mL, 0.74 mmol) were added at room temperature under N_2 followed by formic acid (0.02 mL, 0.59 mmol) and then the mixture was stirred at 100 °C for 17 hours (Figure 11). The mixture

was cooled to room temperature, brine (10 mL) was added and the product was extracted with ether, washed with brine, and dried over Na_2SO_4. The crude mixture was then evaporated and purified by column chromatography using solvent system of hexane and ethyl acetate (15/ 85) to obtain 0.039 g of white solid (69% yield).

^{1}H NMR (500 MHz, $CDCl_3$) δ 8.53 (s, 2H), 7.99 - 8.05 (m, 4H), 7.68 (d, *J* = 1.72 Hz, 2H), 7.55 - 7.59 (m, 4H), 4.90 (s, 2H), 3.87 (s, 6H).

^{13}C NMR (126 MHz, $CDCl_3$) δ 167.3 (2C), 136.3 (2C), 134.3 (2C), 133.1 (2C), 130.6 (2C), 130.5 (2C), 128.7 (2C), 127.2 (2C), 126.6 (2C), 126.3 (2C), 123.9 (2C), 52.3 (2C), 35.8.

HRMS (ESI): $C_{25}H_{21}O_4$ $[M+H]^+$, Calculated: 385.14398**,** Found:385.1068.

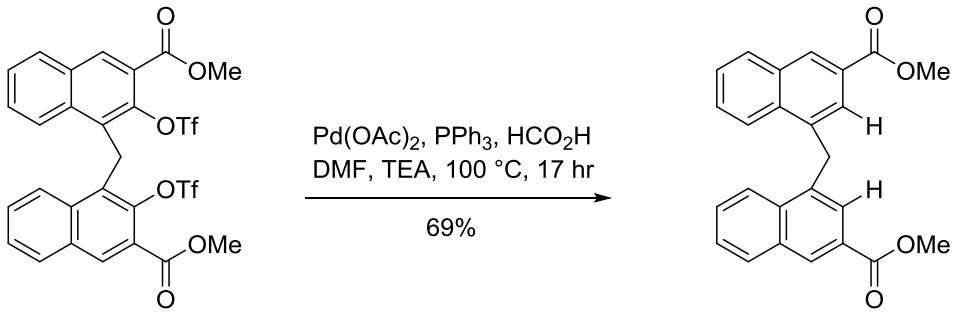

1.8 **1.9**

Figure 11. Synthesis of Methyl Ester **1.9**.

To a stirred solution of the methyl ester (0.21 g, 0.055 mmol) in DCM (2 mL), was added 25% solution of $(CH_3)_4NOH$ (0.4 mL, 1.09 mmol) in methanol and the mixture was refluxed at 45 °C for overnight (Figure 12). The mixture was acidified to pH~2 using HCl (1M), extracted with DCM and washed with water many times. The

product was precipitated out of the DCM layer, collected by filtration and dried on high vacuum to yield 0.02 g (92% yield) of a white solid.

^{1}H NMR (500 MHz, Acetone-d_6) δ 8.61 (s, 2H), 8.22 (d, *J* = 8.02 Hz, 2H), 8.17 (d, *J* = 9.17 Hz, 2H), 7.75 (s, 2H), 7.62 - 7.71 (m, 4H), 5.07 (s, 2H).

^{13}C NMR (126 MHz, Acetone-d_6) δ 166.2 (2C), 136.4 (2C), 133.8 (2C), 132.7 (2C), 129.8 (2C), 129.7 (2C), 128.1 (2C), 127.0 (2C), 126.2 (2C), 125.6 (2C), 123.6 (2C), 34.5.

HRMS (ESI): $C_{23}H_{17}O_4$ $[M+H]^+$, Calculated: 357.11268**,** Found:357.1119.

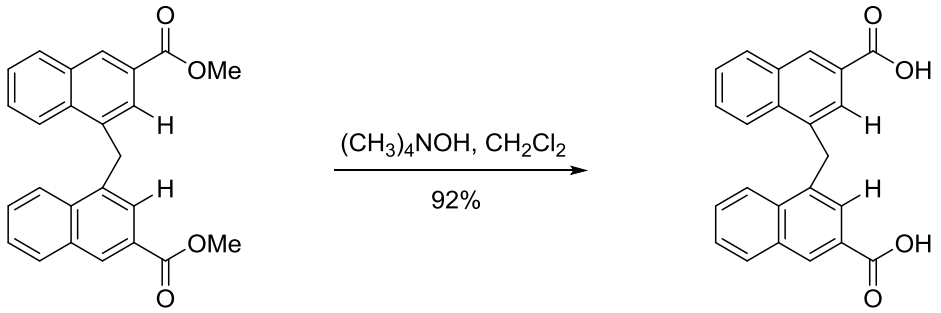

1.9 **1.1**

Figure 12. Synthesis of Analog **1.1**.

Sodium 7-methoxy-3-hyroxy-2-naphthoate (0.50 g, 2.08 mmol) was dissolved in 37% aqueous formaldehyde (0.51 mL, 6.24 mmol) and glacial acetic acid (0.51 mL) and the mixture was refluxed at 100 °C for 2 hours (Figure 13). The product was cooled in an ice bath and then filtered under vacuum, washed with cold water (125 mL) and then with cold ethyl alcohol. Product was purified by silica gel column chromatography using a solvent system of ethyl acetate and methanol (90/10) to yield 0.60 g of the desired product (64% yield) as yellow solid.

^{1}H NMR (500 MHz, DMSO-d_6) δ 11.80 (br. s, 2H), 8.34 (s, 2H), 8.00 (d, *J* = 9.16 Hz, 2H), 7.28 (s, 2H), 7.03 (dd, *J* = 2.29, 9.16 Hz, 2H), 4.70 (s, 2H), 3.71 (s, 6H).

^{13}C NMR (126 MHz, DMSO-d_6) δ 173.1 (2C), 155.7 (2C), 152.4 (2C), 132.2 (2C), 130.4 (2C), 128.3 (2C), 125.4 (2C), 122.0 (2C), 121.5 (2C), 114.8 (2C), 108.5 (2C), 55.6 (2C), 20.5.

HRMS (ESI): $C_{25}H_{21}O_8$ $[M+H]^+$, Calculated: 449.12364**,** Found:449.1179.

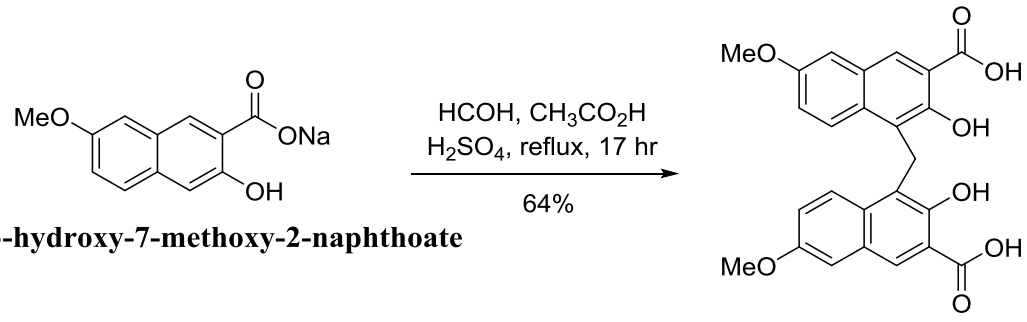

sodium 3-hydroxy-7-methoxy-2-naphthoate

1.2

Figure 13. Synthesis of Analog **2.2**.

NMR Spectra of Compounds

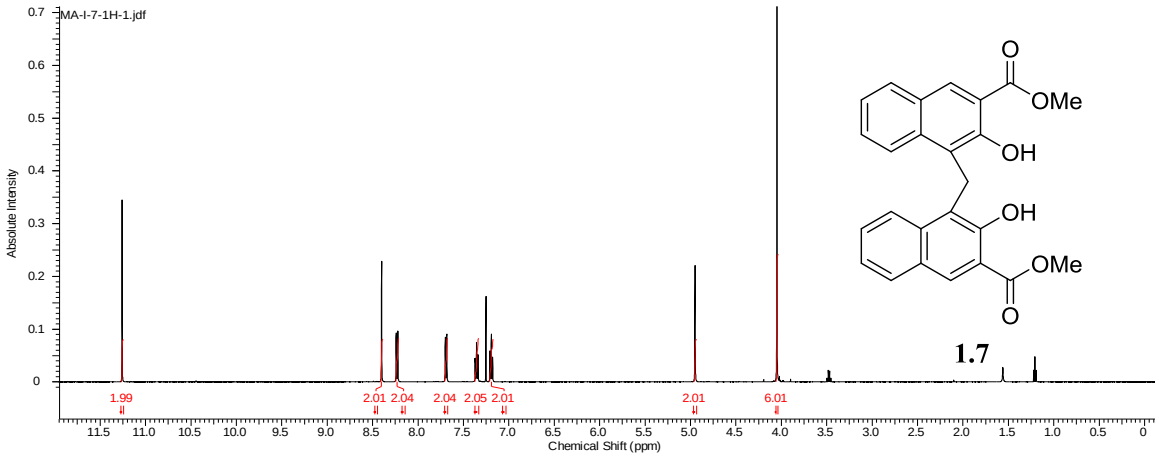

Figure 14. ^{1}H NMR Spectra of Compound **1.7**.

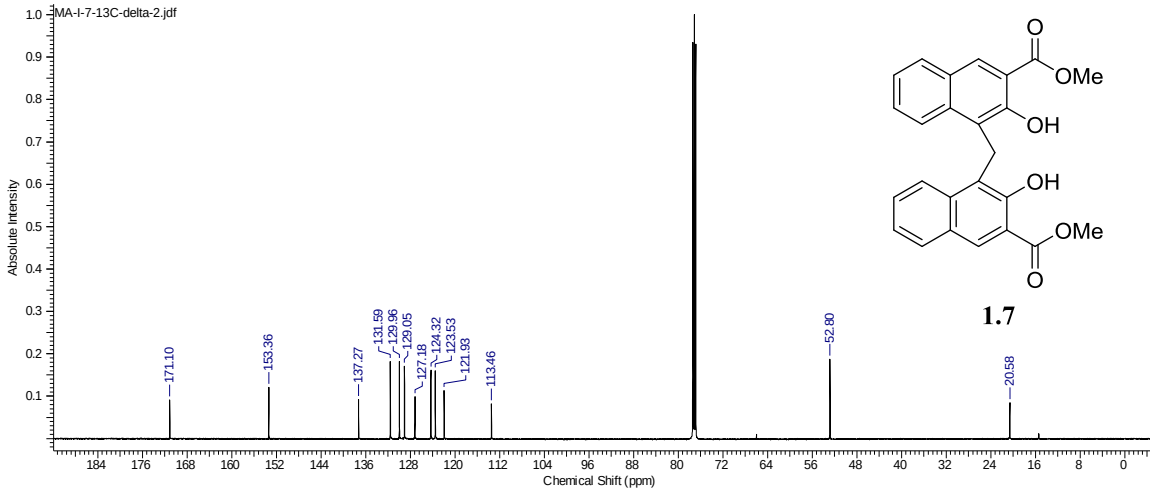

Figure 15. ^{13}C NMR Spectra of Compound **1.7**.

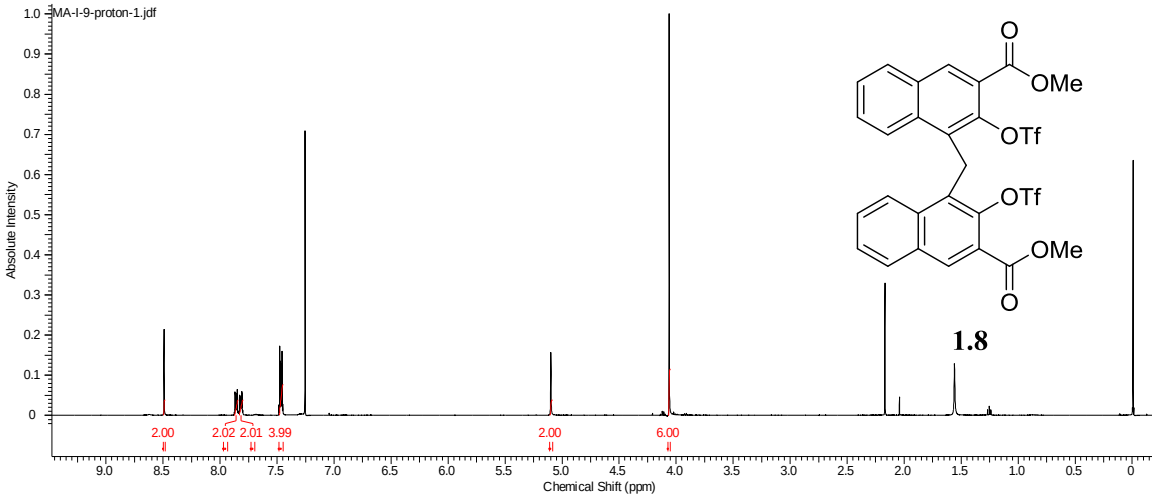

Figure 16. ^{1}H NMR Spectra of Compound **1.8**.

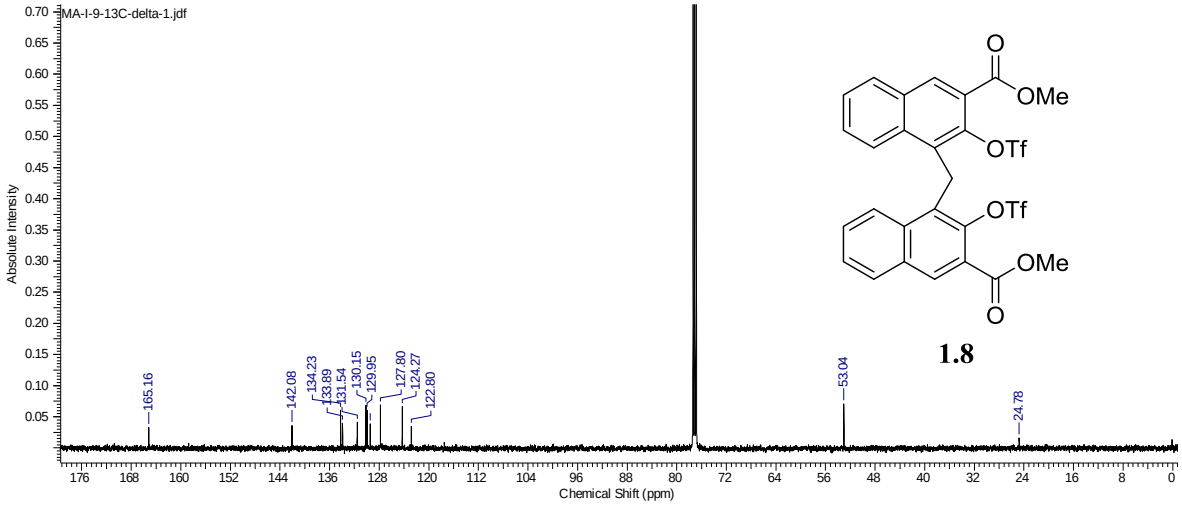

Figure 17. ^{13}C NMR Spectra of Compound **1.8**.

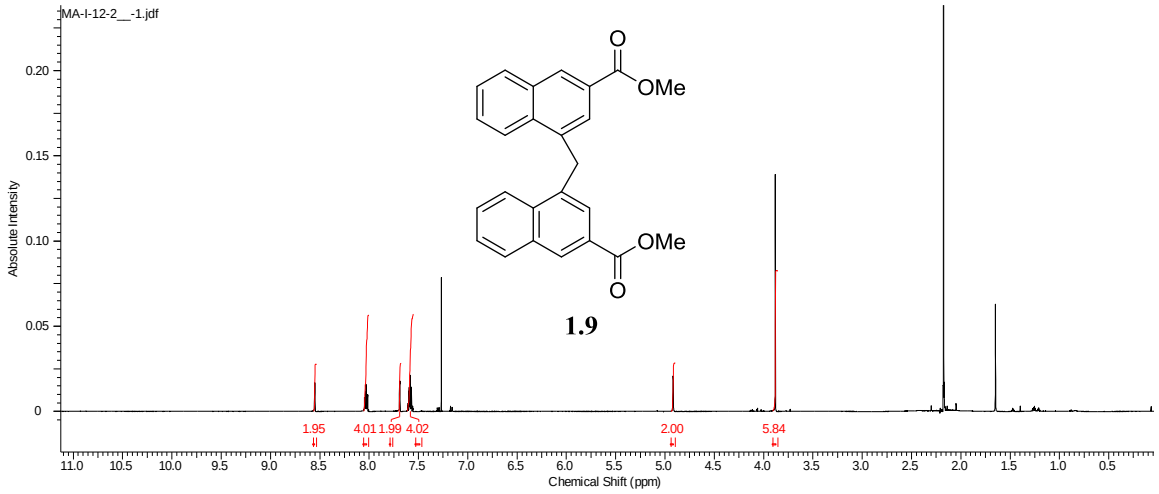

Figure 18. ^{1}H NMR Spectra of Compound **1.9**.

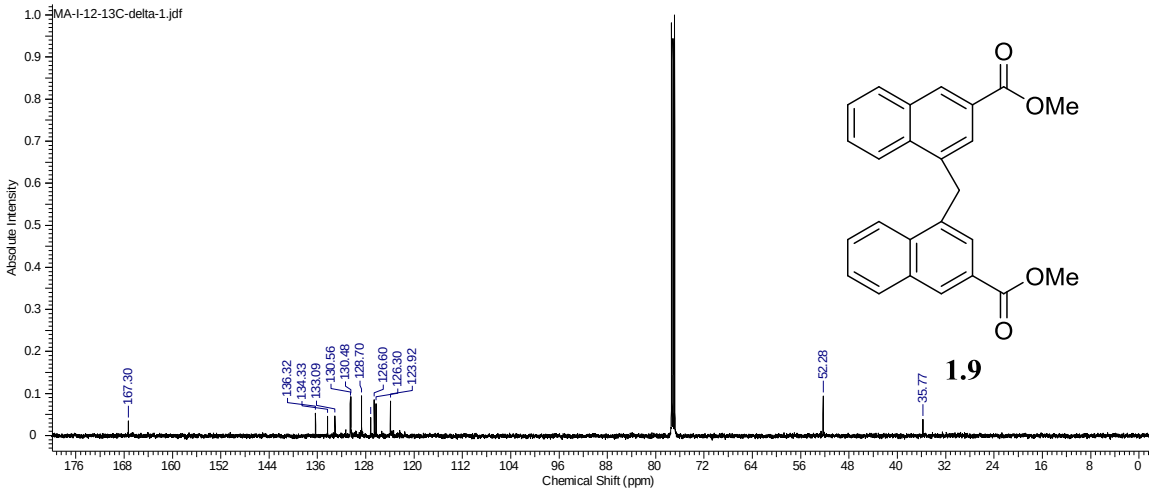

Figure 19. ^{13}C NMR Spectra of Compound **1.9**.

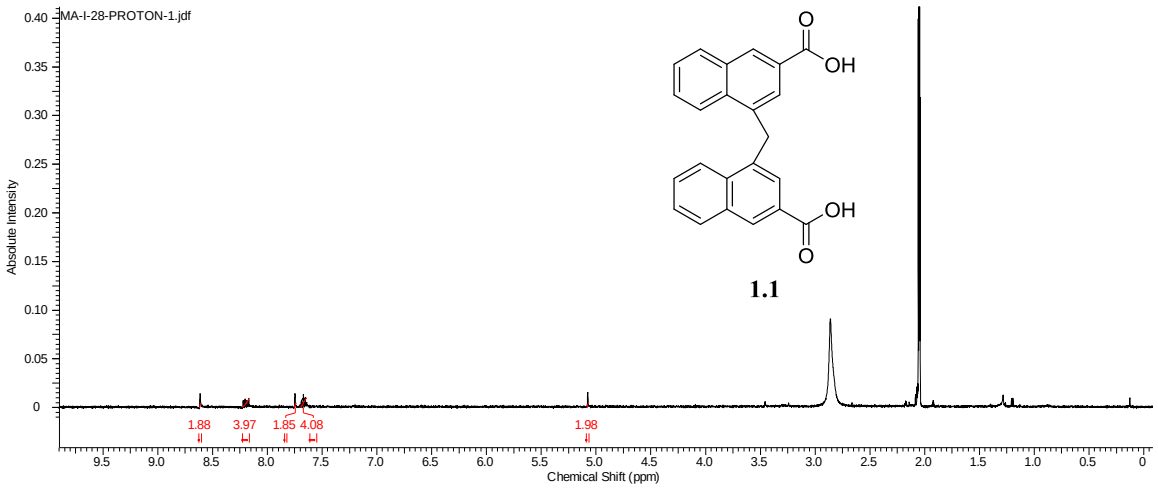

Figure 20. ^{1}H NMR Spectra of Compound **1.1**.

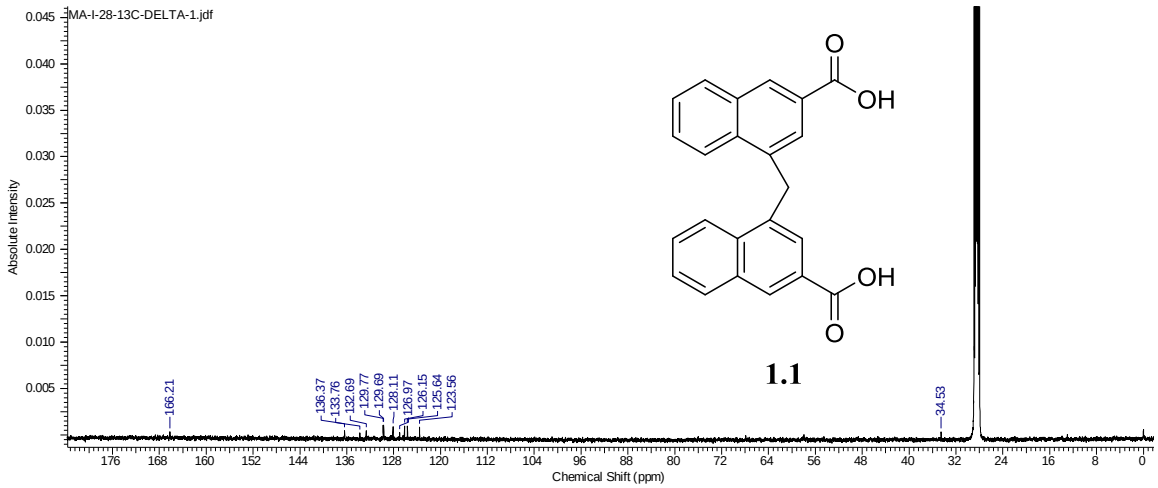

Figure 21. ^{13}C NMR Spectra of Compound **1.1**.

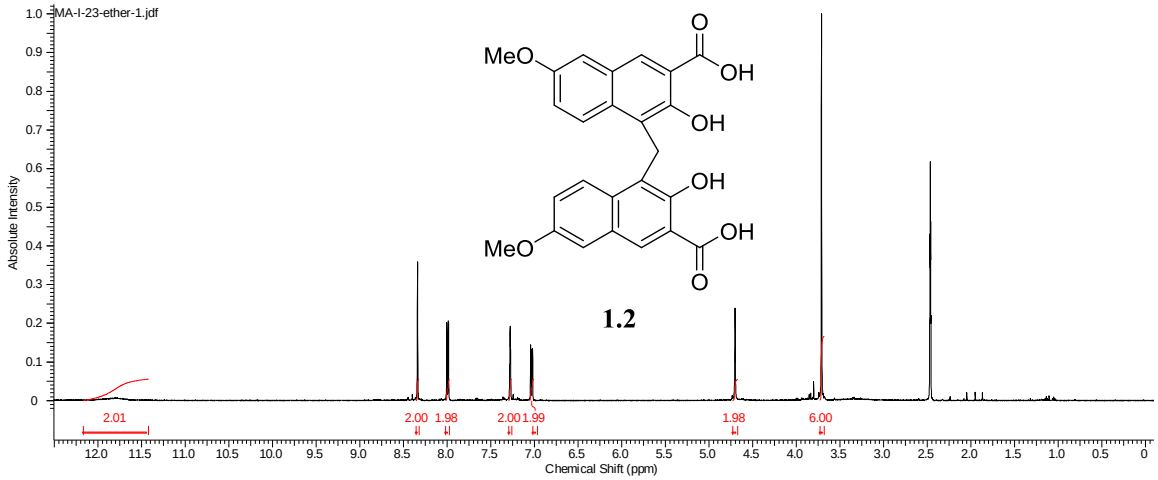

Figure 22. ^{1}H NMR Spectra of Compound **1.2**.

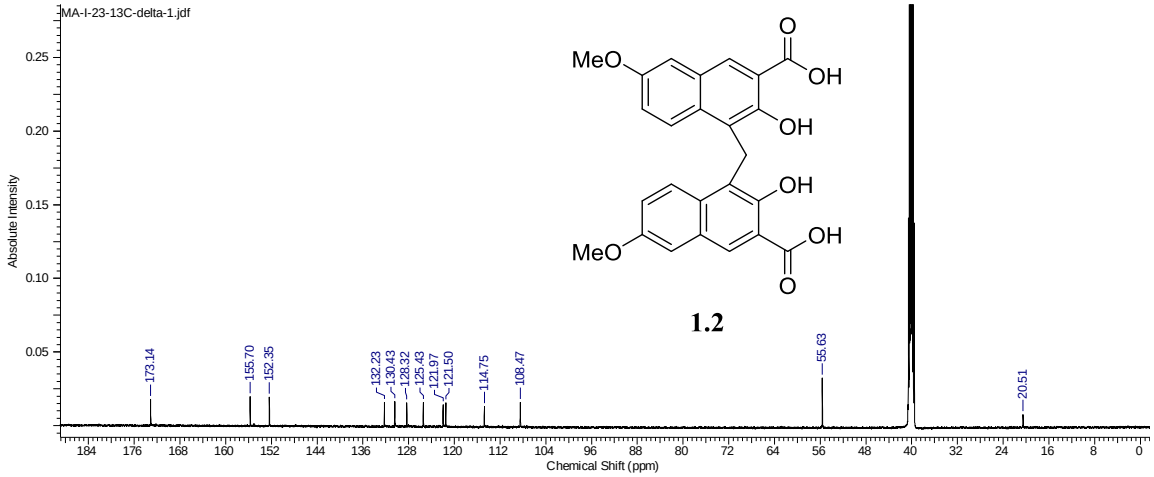

Figure 23. ^{13}C NMR Spectra of Compound **1.2**.

References

[1] Fredriksson, R.; Lagerstrom M. C.; Lundin, L. G.,; Schioth, H. B. The G-protein-coupled receptors in the human genome form five main families. Phylogenetic analysis, paralogon groups, and fingerprints. *Mol. Pharmacol*. **2003**, *63*, 1256-1272.

[2] Flower, D. R. Modelling G-protein-coupled receptors for drug design. *Biochimica et Biophysica Acta* **1999**, *1422*, 207-234.

[3] O'Dowd, B. F.; Nguyen, T.; Marchese, A.; Cheng, R.; Lynch, K. R.; Heng, H. H.; Kolakowski, L. F. Jr.; George, S. R. Discovery of three novel G-protein-coupled receptor genes. *Genomics* **1998**, *47*, 310-313.

[4] Wang, J.; Simonavicius, N.; Wu, X.; Swaminath, G., Reagan, J.; Tian, H.; Ling, L. Kynurenic Acid as a Ligand for Orphan G Protein-coupled Receptor GPR35. *J. Biol. Chem.* **2006**, *281*, 22021-22028.

[5] Oka, S.; Ota, R.; Shima, M.; Yamashita, A.; Sugiura, T. GPR35 is a novel lysophosphatidic acid receptor. *Biochem. Biophys. Res. Commun*. **2010**, *395*, 232-237.

[6] Taniguchi, Y.; Tonai-Kachi, H.; Shinjo, K. Zaprinast, a well-known cyclic guanosine monophosphate-specific phosphodiesterase inhibitor, is an agonist for GPR35. *FEBS Letters* **2006**, *580*, 5003–5008.

[7] Horikawa, Y.; Oda, N.; Cox, N. J.; Li, X.; Orho-Melander, M.; Hara, M.; Hinokio, Y.; Lindner, T. H.; Mashima, H.; Schwarz, P. E. H.; Bosque-Plata, L. D.; Horikawa, Y.; Oda, Y.; Yoshiuchi, I.; Colilla, S.; Polonsky, K. S.; Wei, S.; Concannon, P.; Iwasaki, N.; Schulze, J.; Baier, L. J.; Bogardus, C.; Groop, L.; Boerwinkle, E.; Hanis, C. L.; Bell, G. Genetic variation in the gene encoding calpain-10 is associated with type 2 diabetes mellitus, *Nat. Genet.* **2000**, *26*, 163-175.

[8] Ohshiro, H.; Tonai-Kachi, H.; Ichikawa, K. GPR35 is a functional receptor in rat dorsal root ganglion neurons, *Biochem. Biophys. Res. Commun*. **2008**, *365*, 344-348.

[9] Sparfel, L.; Pinel-Marie, M. L.; Boize, M.; Koscielny, S.; Desmots, S.; Pery, A.; Fardel, O. Transcriptional signature of human macrophages exposed to the environmental contaminant benzo(a)pyrene. *Toxicol. Sci*. **2010**, *114*, 247- 259.

[10] Lattin, J. E.; Schroder, K.; Su, A. I.; Walker, J. R.; Zhang, J.; Wiltshire, T.; Saijo, K.; Glass, C. K.; Hume, D. A., Kellie, S.; Sweet, M. J. Expression analysis of G Protein-Coupled Receptors in mouse macrophages. *Immunome Res.* **2008**, *4*, 5.

[11] Imielinski, M.; Baldassano, R. N.; Griffiths, A.; Russell, R. K.; Annese, V.; Dubinsky, M.; Kugathasan, S.; Bradfield, J. P.; Walters, T. D.; Sleiman, P.; Kim, C. E.; Muise, A.; Wang, K.; Glessner, J. T.; Saeed, S.; Zhang, H.; Frackelton, E. C.; Hou, C.; Flory, J. H.; Otieno, G.; Chiavacci, R. M.; Grundmeier, R.; Castro, M.; Latiano, A.; Dallapiccola, B.; Stempak, J.; Abrams, D. J.; Taylor, K.; McGovern, D.; Heyman, M. B.; Ferry, G. D.; Kirschner, B.; Lee, J.; Essers, J.; Grand, R.; Stephens, M.; Levine, A.; Piccoli, D.; Limbergen, J. V.; Cucchiara, S.; Monos, D. S.; Guthery, S. L.; Denson, L.; Wilson, D. C.; Grant, S. F. A.; Daly, M.; Silverberg, M. S.; Satsangi, J.; Hakonarson, H. Common variants at five new loci associated with early-onset inflammatory bowel disease. *Nat. Genet.* **2009**, *41*, 1335-1340.

[12] Min, K. D.; Asakura, M.; Liao, Y.; Nakamaru, K.; Okazaki, H.; Takahashi, T.; Fujimoto, K.; Ito, S.; Takahashi, A.; Asanuma, H.; Yamazaki, S.; Minamino, T.; Sanada, S.; Seguchi, O.; Nakano, A.; Ando, Y.; Otsuka, T.; Furukawa, H.; Isomura, T.; Takashima, S.; Mochizuki, N.; Kitakaze, M. Identification of genes related to heart failure using global gene expression profiling of human failing myocardium, *Biochem. Biophys. Res. Commun*. **2010**, *393*, 55-60.

[13] Sun, Y. V.; Bielak, L. F.; Peyser, P. A.; Turner, S. T.; Sheedy, P. F.; Boerwinkle, E.; Kardia, S. L. Application of machine learning algorithms to predict coronary artery calcification with a sibship-based design. *Genet Epidemiol*. **2008**, *32*, 350-360.

[14] Shrimpton, A. E.; Braddock, B. R.; Thomson, L. L.; Stein, C. K. Hoo, J. J. Molecular delineation of deletions on 2q37.3 in three cases with an Albright hereditary osteodystrophy-like phenotype. *Clin. Genet.* **2004**, *66*, 537-544.

[15] Leonard, J. N.; Chu, Z. L.; Unett, D. J.; Gatlin, J. E.; Gaidarov, I.; Qui, J.; Skinner, P. J.; Boatman, P.D. GPR35 and modulators thereof for the treatment of metabolic-related disorders, US 20070077602 A1.

[16] Yang, Y.; Lu, J. Y.; Wu, X.; Summer, S.; Whoriskey, J.; Saris, C.; Reagan, J. D. G-protein-coupled receptor 35 is a target of the asthma drugs cromolyn disodium and nedocromil sodium. *Pharmacology* **2010**, *86*, 1-5.

[17] Okumura, S.; Baba, H.; Kumada, T.; Nanmoku, K.; Nakajima, H.; Nakane, Y.; Hioki, K.; Ikenaka, K. Cloning of a G-protein-coupled receptor that shows an activity to transform NIH3T3 cells and is expressed in gastric cancer cells. *Cancer Sci*. **2004**, *95*, 131-135.

[18] Taniguchi, Y.; Tonai-Kachi, H.; Shinjo, K. 5-Nitro-2-(3-phenylpropylamino) benzoic acid is a GPR35 agonist. *Pharmacology*, **2008**, *82*, 245-249.

[19] Jenkins, L.; Brea, J.; Smith, N. J.; Hudson, B. D.; Reilly, G.; Bryant, N. J.; Castro, M.; Loza, M. I.; Milligan, G. Identification of novel species-selective agonists of the G-protein-coupled receptor GPR35 that promote recruitment of β-arrestin-2 and activate Gα13. *Biochem J.*, **2010**, *432*, 451-459.

[20] Deng, H.; Hu, H.; Fang, Y. Tyrphostin analogs are GPR35 agonists. *FEBS Lett*. **2011**, *585*, 1957-1962.

[21] Divorty, N.; Mackenzie, A. E.; Nicklin, S. A.; Milligan, G. Protein-coupled receptor 35: an emerging target in inflammatory and cardiovascular disease. *Front. Pharmacol.* 6:41. Doi:10.3389/fphar.**2015**.00041].

[22] Zhao, P.; Sharir, H.; Kapur, A.; Cowan, A.; Geller, E. B.; Adler,M. W.; Seltzman, H. H.; Reggio, P. H.; Heynen-Genel, S.; Sauer, M.; Chung,T. D.Y.; Bai, Y.; Chen, W.; Caron, M. G.; Barak, L. S.; Abood, M. E. Targeting of the Orphan Receptor GPR35 by Pamoic Acid: A Potent Activator of Extracellular Signal-Regulated Kinase and β-Arrestin2 with Antinociceptive Activity, *Mol. Pharmacol*. **2010**, *78*, 560-568.

[23] Zhao, P.; Lane, T. R.; Gao, H. G.; Hurst, D. P.; Kotsikorou, E.; Le, L.; Brailoiu, E.; Reggio, P. H.; Abood, M. E.; Crucial positively charged residues for ligand activation of the GPR35 receptor, *J Bio. Chem*., **2014**, *6*, 3625-3638.

[24] Kondekar, N.; Potnis, S. P. Condensation of 3-Hydroxy-2-naphthoic Acid with Formaldehyde. *Ind. Eng. Chem. Prod. Res. Develop*., **1973**, *12*, 135-137.

[25] Cai, D.; Payack, J. F.; Bender, D. R.; Hughes, D. L.; Verhoeven, T. R.; Reider, P. J. *Org. Synth. Coll. Vol*., **1999**, 76, 6.

[26] Wang, G.; He, Y.; Sun, J.; Das, D.; Hu, M., Huang, J.; Ruhrmund, D.; Hooi, L.; Misialek, S.; Ravi Rajagopalan, P. T.; Stoycheva, A.; Buckman, B. O.; Kossen, K.; Seiwert, S. D.; Beigelman, L. HCV NS5B polymerase inhibitors 1: Synthesis and in vitro activity of 2-(1,1-dioxo-2H-[1,2,4]benzothiadiazin-3-yl)-1-hydroxynaphthalene derivatives. *Bioorg. Med. Chem. Lett*. **2009**, *19*, 4476-4479.

[27] Neetoo-Isseljee, Z.; Mackenzie, A. E.; Southern, C.; Jerman, J.; McIver, E. G.; Harries, N.; Taylor, D. L.; Milligan, G., High-Throughput Identification and Characterization of Novel, Species-selective GPR35 Agonists. *J. Pharmacol. Exp. Ther.* **2013**, *344*, 568-578

[28] Funke, M.; Thimm, D.; Schiedel, A. C.; Muller, C. E. 8-Benzamidochromen-4-one-2-carboxylic Acids: Potent and Selective Agonists for the Orphan G Protein-Coupled Receptor GPR35. *J. Med. Chem*. **2013**, *56*, 5182-5197.

[29] Burmaoglu, S.; Altundas, R.; Secen, H. A short and efficient synthesis of cytotoxic 3-isopropylnaphthalene-1,2-dione *via* 3-hydroxy-2-naphthoic acid. ARKIVOC **2008**, 269-273.

CHAPTER II

STRUCTURE-ACTIVITY RELATIONSHIPS OF GPR35 ANTAGONISTS

Manahil M. Abdalhameed, Dow P. Hurst, Pingwei Zhao, Mary E. Abood*, Patricia H. Reggio*, and Mitchell P. Croatt*, 2015, *in press…*

Introduction

GPR35, a G protein-coupled receptor (GPCR), was discovered and classified as an orphan GPCR in 1998[1] and deorphanized in 2006 by the discovery of kynurenic acid as the endogenous agonist.[2] Since the discovery of GPR35, limited references on the GPR35 receptor have appeared and there is a scarcity of ligands, endogenous or exogenous, that regulate GPR35. The deorphanization of GPR35 receptor has even been debated due to the poor potency of kynurenic acid (EC_{50} of 39 μM). Recently, GPR35 has gained special consideration as a result of its association with many diseases including type-2 diabetes,[3] nociceptive pain,[4] inflammation,[1] mild mental retardation syndrome,[5] metabolic disorders,[6] and gastric cancer.[7] Based on the association of GPR35 with these major diseases and disorders, there is a current and urgent need for compounds to regulate the GPR35 receptor and to serve as research tools in molecular characterization of GPR35 receptor. In this chapter, we report an initial structure-activity relationship (SAR) study of GPR35 that was enabled by an inactivate state homology model. This research will assist in the design of potent and selective ligands that act as antagonists at GPR35.

Homology Model

Only small numbers of GPCRs have been crystallized including, rhodopsin (Rho), meta-rhodopsin, β_2-adrenergic receptor (β_2-AR), β_1-adrenergic receptor (β_1-AR), adenosine (A2A) receptor, $CXCR_4$, dopamine D3 receptor, and the Histamine H receptor.[8] These crystal structures share fundamental topologies specifically; the seven transmembrane alpha helices (TMHs) arrange to form a closed bundle and connected with loops that extended intracellular and extracellular membrane surface with C-terminus and N-terminus respectively. Finally, with exception of some crystal structures when ligand binding occurs within extracellular loops, ligand binding takes place in the TMH bundle. Sharing these topologies makes it possible to use a template crystal structure of crystallized receptors to build a homology model of un-crystallized receptor. Thus, it is possible to build a homology model of GPR35 based on available crystal structure. This homology model can then be used to explore the GPR35 ligand binding pocket and key amino acid interactions for GPR35 ligands and will serve as a research tool or basis for designing and developing novel drugs.

The construction of GPR35 homology model was done based upon sequence-dictated differences with the template of β_2-adrenergic receptor (Figure 24).[9] These differences included TMH2, TMH4, TMH5, and TMH7. TMH2 has proline shift from P2.59 in β_2-AR to P2.58 in GPR35 receptor. In GPR35 receptor TMH4 losses proline P4.60 and TMH5 has an additional proline P5.43. TMH7 has DAICY in GPR35 instead of NPXXY in β_2-AR. Conformational memories were used to explore conformational differences in these helices dictated by sequence variations. The GPR35 inactive state

binding site is shaped for a long horizontal ligand with one end near TMH5 and the other reaching past TMH2 and TMH7. The pocket near TMH3, 4, 5 and 6 is larger than the pocket near TMH2 and TMH7. The narrow channel connecting the two pockets is bracketed by R6.58 above and Y3.32 below.

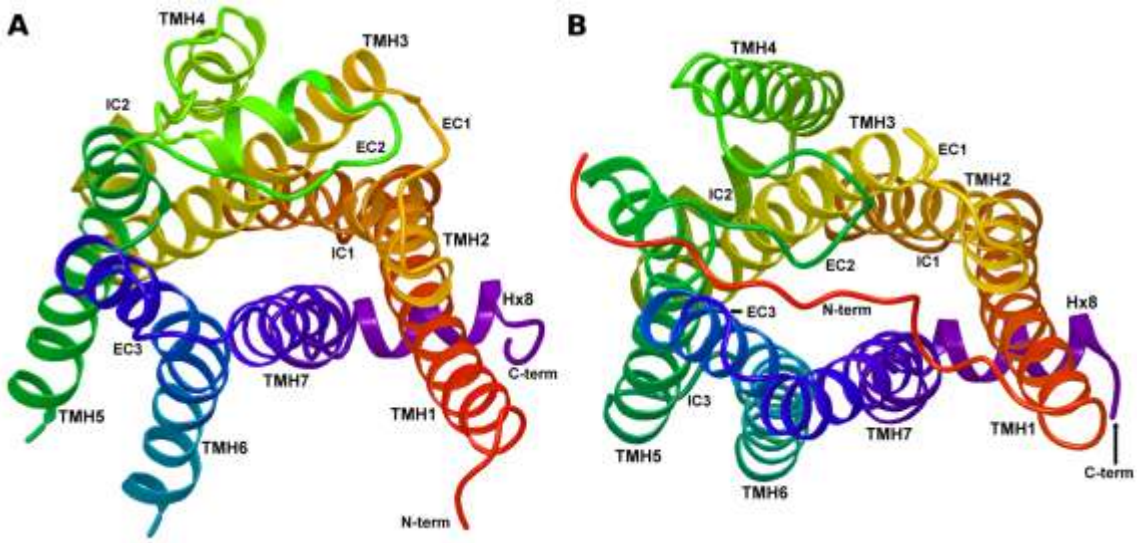

Figure 24. Comparison between β_2-AR Crystal Structure (A) and GPR35 Homology Model (B).

Chemical Library Screening

To date, there is no potent and selective GPR35 antagonist. The reported GPR35 antagonist either nonpotent or nonselective. Table 5 shows the only reported antagonists. A screen performed with the Molecular Libraries Probe Production Initiative evaluated ~300,000 compounds in an image-based high-throughput, high-content primary screen.[10] This screen identified a few relatively potent and selective GPR35 antagonists, rhodanine **2.28** (CID2286812), pyrrazole **2.29** (CID2745684), benzothiazole **2.1** (CID1231538), and pyrimidine **2.30** (CID1542103) (Table 5). Compound **2.28** displayed

high antagonism activity on GPR35 (IC_{50}/EC_{50} = 20.1 nM), however this compound has a rhodanine ring. Compounds with a rhodanine ring have been recommended to be excluded from libraries screening results due to the misleading potential through various chemical effects, as described as Pan Assay Interference Compounds (PAINS).[11] The misleading potential resulted from structure reactivity, chelation probability, and aggregation. Compound **2.29** is also a potent GPR35 antagonist (IC_{50}/EC_{50} = 160 nM), but we were concerned that the thiourea hydrazone functionality could react in a nonselective manner, similar to the rhodanine ring.[11] In addition to these concerns, the GPR35 inactive state (R) model has a binding site that appears to be more suitable for elongated ligands. For these reasons, benzothiazole **2.1** was selected for this ligand-based homology model optimization. Although compound **2.1** has a moderate antagonism activity at GPR35 (IC_{50}/EC_{50} = 0.55 μM), its structural features and conformation could be modified to improve on its activity.

Table 5

GPR35 Antagonists

Antagonist	Structure	IC50/EC50
2.28 (CID2286812)	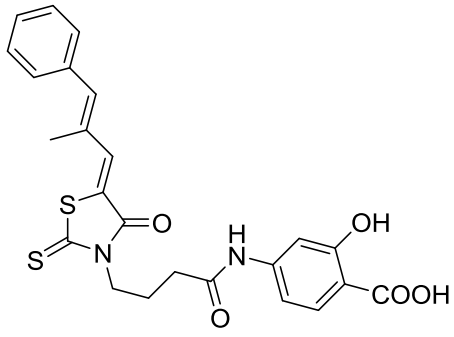	20.1 nM

Table 5

(Cont.)

Antagonist	Structure	IC50/EC50
2.29 (CID2745684)	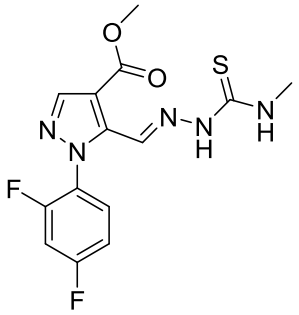	160 nM
2.1 (CID1231538)	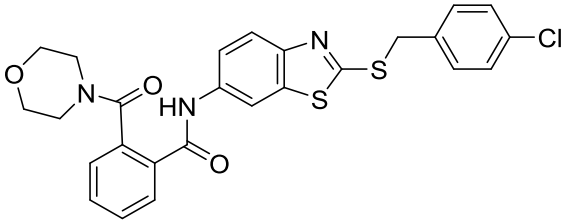	0.55 µM
2.30 (CID1542103)	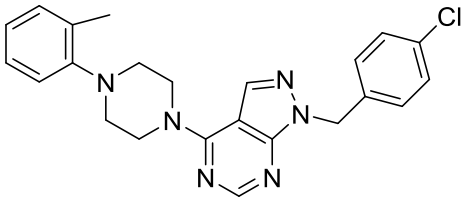	2.2 µM

Docking Study

Docking of benzothiazole **2.1** into this homology model of GPR35 (Figure 25) indicated that benzothiazole **2.1** possessed a handful of favorable interaction with the binding site. Specifically, residues R4.60(151)[12] and R6.58(240) provide hydrogen bonding with the morpholine amide oxygen and the heterobicyclic nitrogen, respectively. Residue S7.39(262) provided weak hydrogen bonding with the exocyclic sulfur. Also residue Y3.37(101) and Y7.36(259) provide aromatic stacking interactions with the

phthalamide and the aryl connected to the thiol, respectively. In spite of the fact that benzothiazole **2.1** has moderate potency, these favorite interactions, together with the scarcity of GPR35 antagonists, enforced our decision to choose benzothiazole **2.1** as a probe for this ligand-based structure-activity relationships study.

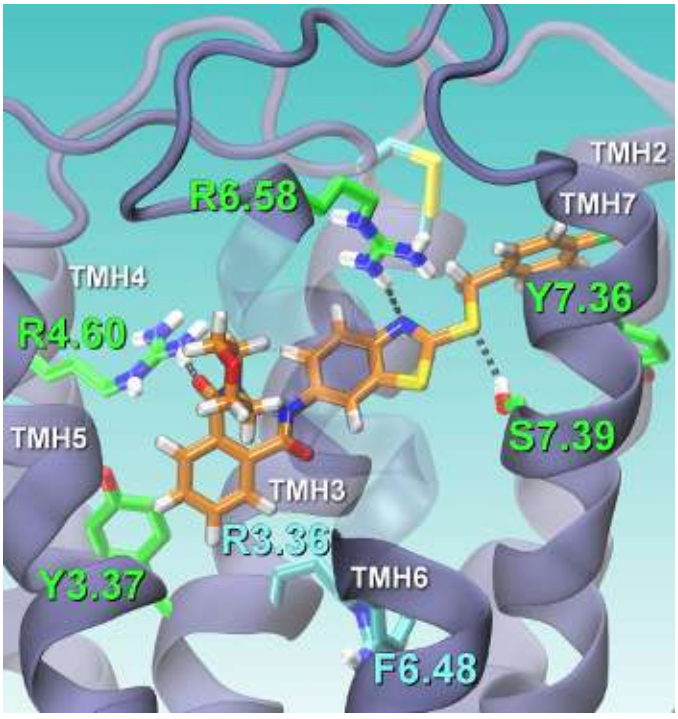

Figure 25. Docking of Benzothiazole **2.1** in the GPR35 Homology Model.

Further scrutiny of the dock of benzthiazole into the homology model of GPR35 identified additional information. It was hypothesized that the position of the morpholine is important because it blocks the F6.48(230) $\chi 1$ g+ $\rightarrow$ trans rotation. Since the rotation of F6.48 is hypothesized to be important for activation of many GPCRs,[13] the position of the morpholine ring could be crucial for this ligand to act as an antagonist. Based on the model, there were no residues in that area of the binding pocket available for hydrogen

bonding so the influence on the toggle switch seems to be solely steric in nature. Thus, piperidine **2.2** and pyrrolidine **2.3** were prepared to examine this supposition. The GPR35 R model suggests that the exocyclic sulfur in benzothiazole **2.1** is only weakly hydrogen bonding to S7.39 (262) (S-O distance = 3.4 Å). Oxidation of the sulfur would shorten the distance (O-O distance = 2.6 Å) and provided stronger hydrogen bonding. Therefore, sulfoxide **2.4** and sulfone **2.5** were synthesized to improve this interaction (Scheme 2.6). Due to the chiral nature of the sulfoxide, enantiomers **2.6** and **2.7** were individually synthesized (Scheme 2.7). The GPR35 R model implied that the terminal aryl group adjacent to the thiol has no influence in the binding pocket other than the aromatic stacking interactions. To test that assumption, benzene **2.8** and pyridine **2.9** were synthesized (Scheme 2.6). The GPR35 R model suggests that in the heterocyclic core of benzothiazole **2.1** the nitrogen can be hydrogen bonded with R6.58(240) but the sulfur does not have any discernible interactions. To exploit this, the benzimidazole **2.10** was made (Scheme 2.6). Benzimidazole **2.10** may provide a positive potential surface instead of negative potential surface of the sulfur near the electron rich region of S7.39 (262). The benzylic methylene of benzothiazole **2.1** provided beneficial van der Waals interactions. Based on the current model, the S-enantiomer of a benzylic methyl group (compound **2.11**) will fit nicely into the binding pocket and enhance the predicted van der Waals interactions with R6.58(240), whereas the R-enantiomer will have detrimental steric clashes (Scheme 2.10).

Compounds **2.2-2.11** were docked individually into the GPR35 homology model inactive state to perceive the binding site interactions. The residues R4.60 and R6.58

provide hydrogen bonding interaction for compound **2.1**-**2.11**. The residue S7.39 provide hydrogen bonds to the thio ether group in compound **2.1**-**2.3**, **2.8**-**2.11**, and to the oxygen in **2.1**-**2.7** (Table 6). In contrast between GPR35 and other related GPCRs, in GPR35 R model the residue R3.36 blocks the movement of F6.48 and H6.52 stacks with F6.48 from above. Thus, it is possible that the toggle switch for GPR35 is more complex than other related GPCRs with three residue required to move to reach the active state. All these compounds were synthesized and biologically evaluated.

Synthesis of GPR35 Antagonists

The synthesis of this family of compounds was designed so that many diverse analogs could be rapidly accessed (Figure 26). The proposed synthetic route involves the opening of phthalic anhydride with commercially available cyclic amines to produce an amide and carboxylic acid. The acid will be coupled to the heterobicyclic aryl amine and then the thiol will be alkylated with commercially available aryl groups.

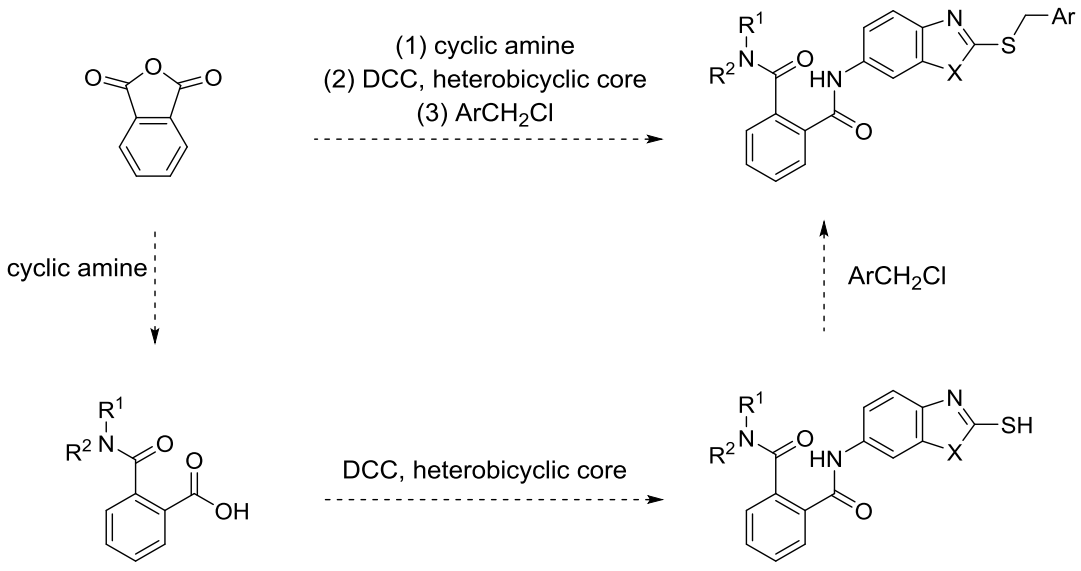

Figure 26. Proposed Synthetic Route for GPR35 Antagonists.

The first step in the synthesis was the opening of the phthalic anhydride using the amine functionality of morpholine to successfully produce the amide and carboxylic acid. The reaction took 4 hours under refluxed temperature to produce the intermediate **2.31** in good yield (Figure 27).

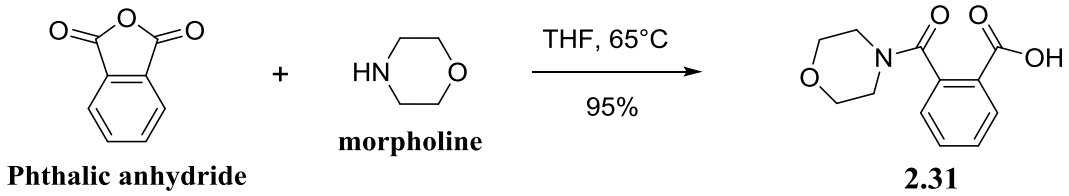

Figure 27. Synthesis of Compound **2.31**.

The following step is the coupling of intermediate **2.31** with 5-amino-2-mercaptobenzothiazole using *N,N'*-dicyclohexylcarbodiimide (DCC) to form compound **2.32**. One equivalent of DCC was added to a solution of starting material, *N*-hydroxysuccinimide (HOSu), triethylamine (TEA) and 5-amino-2-mercaptobenzothiazole in dimethylformamide (DMF). The DCC coupling reaction produced mixture of products that did not include the intended product (Figure 28). An alternative procedure was suggested which include formation of acyl chloride followed by nucleophilic addition elimination reaction (Figure 28). The acyl chloride was prepared using thionyl chloride followed by the addition of the 5-amino-2-mercaptobenzothiazole, however, the anticipated product was not formed. It was observed that the coupling reaction of 5-amino-2-mercaptobenzothiazole incorporated some difficulties. As a result another synthetic route was proposed.

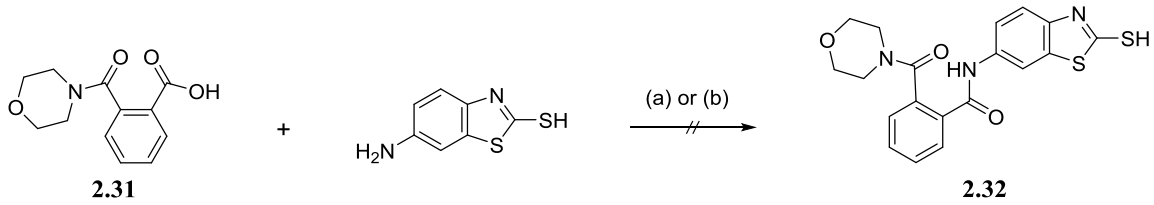

Figure 28. Unsuccessful Trails to Synthesize Compound **2.32**. Reagents and conditions: (a) 5-amino-2-mercaptobenzothiazole, DMF, HOSu, TEA, DCC, rt., 17 hr; (b) 1) $SOCl_2$, DCM 2) 5-amino-2-mercaptobenzothiazole, TEA, DCM, THF.

This route relied on the formation of phthalisoimide ring as substantial intermediate that will be reopened with the amine function of the cyclic amines (Figure 29). The synthetic route to synthesis compound **2.1** was exemplified in Figure 28. The synthetic route began with ring-opening of the commercially available phthalic anhydride with the amine functionality of 5-amino-2-mercaptobenzothiazole to form benzoate **2.33**. The resulting product was a good candidate for phthalisoimide ring formation (Figure 30). This was achieved through treatment of the resulting product with acetic anhydride and triethylamine to produce phthalisoimide **2.34**.[14] Although the phthalisoimide ring seems to be unstable, the product of this reaction was precipitated out of cold water with a yield of 90%. Following the same protocol, the phthalisoimide ring was opened by the amine function of morpholine to generate **2.35**. The reaction was straightforward; however, formation of the morpholinium salt decreases the yield and required special treatment. The resulting products were purified by recrystalization in 46% yield. The last step is a typical S_N2 reaction of the thiol moiety and 4-chloro benzyl chloride, however the benzothiazole **2.1** was isolated in low yield (Scheme 2.3).

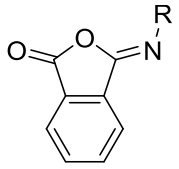

Phthalisoimide

Figure 29. Phthalisoimide Ring.

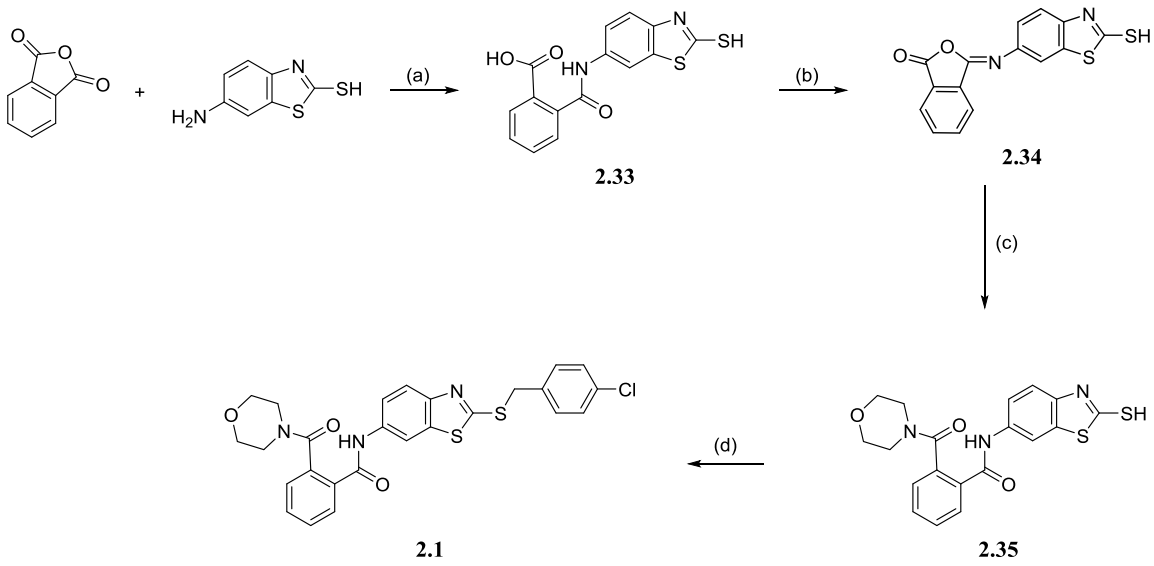

Figure 30. Synthesis of Benzothiazole **2.1**. Reagents and conditions: (a) THF, 30 °C, 17 hr, 89%; (b) $(CH_3CO)_2O$, TEA, 1,4 Dioxane, rt, 17 hr, 90%; (c) morpholine, THF, reflux, 2 hr, HCl, 46%; (d) *p*-ClBzCl, DMF, NaH, 4 hr, 32%.

The preceding synthetic route was followed to synthesize analog **2.2** and **2.3**. As previously mentioned, analogs **2.2** and **2.3** have piperidine or pyrrolidine as replacement of morpholine, respectively. Opening the phthalisoimide ring with piperidine or pyrrolidine produced intermediates **2.36** and **2.37** in 24% and 31% respectively (Figure 31).

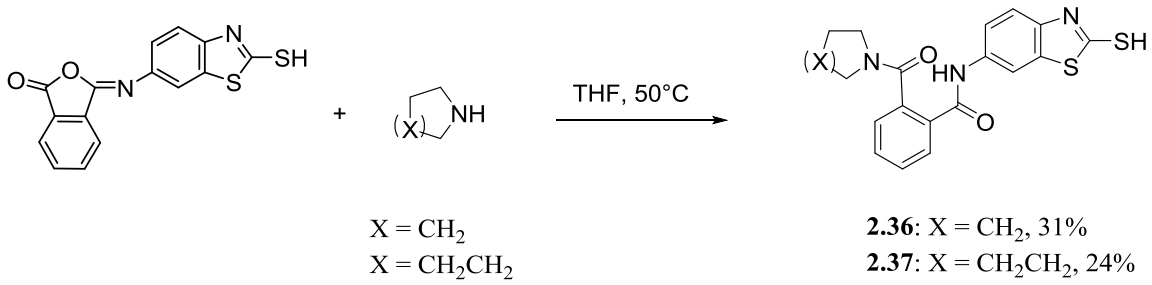

Figure 31. Synthesis of Intermediate **2.36** and **2.37**.

In spite of the lower yields, formation of iminium salts, and the demand for satisfactory yield to access analogs **2.4**, **2.5**, **2.6**, and **2.7**, following the same synthetic route to synthesize analog **2.9** encountered with some difficulties. Analog **2.9** has a pyridine as a replacement of aryl group on the lead compound. Following the established synthetic route proved to be unsuccessful due to the presence of the weakly basic nitrogen. After various experimental conditions had been attempted, another pathway was devised. This modified route enabled us to access many different structures with good to satisfactory yields.

The synthetic route to synthesize compounds **2.1**-**2.3**, and **2.8**-**2.10** initiated with ring-opening of phthalic anhydride with the amine functionality of 6-amino-2-mercaptobenzothiazole to form acid **2.12** in 96% yield or with 5-amino-2-mercaptobenzoimidazole to form compound **2.19**, also in good yield (95%) (Figure 32). Addition of thiol **2.12** and 4-chlorobenzyl chloride, benzyl chloride, or 4-(chloromethyl) pyridine hydrochloride to a solution of sodium hydroxide in ethanol successfully produced thioethers **2.13**, **2.15**, and **2.17** respectively.[15] The subsequent step is the formation of the phthalisoimide ring using acetic anhydride and triethylamine.[14]

Phthalisoimide intermediates **2.14**, **2.16**, and **2.18** were produced in 91%, 96%, and 87% yields respectively. The phthalisoimide rings were opened using morpholine, piperidine, or pyrolidine to produce final analogs **2.1**, **2.2**, **2.3**, **2.8**, and **2.9**. Analog **2.10** was synthesized following the same protocol using 5-amino-2-mercaptobenzoimidazole as starting substrate through intermediates **2.19**, **2.20**, and **2.21**.

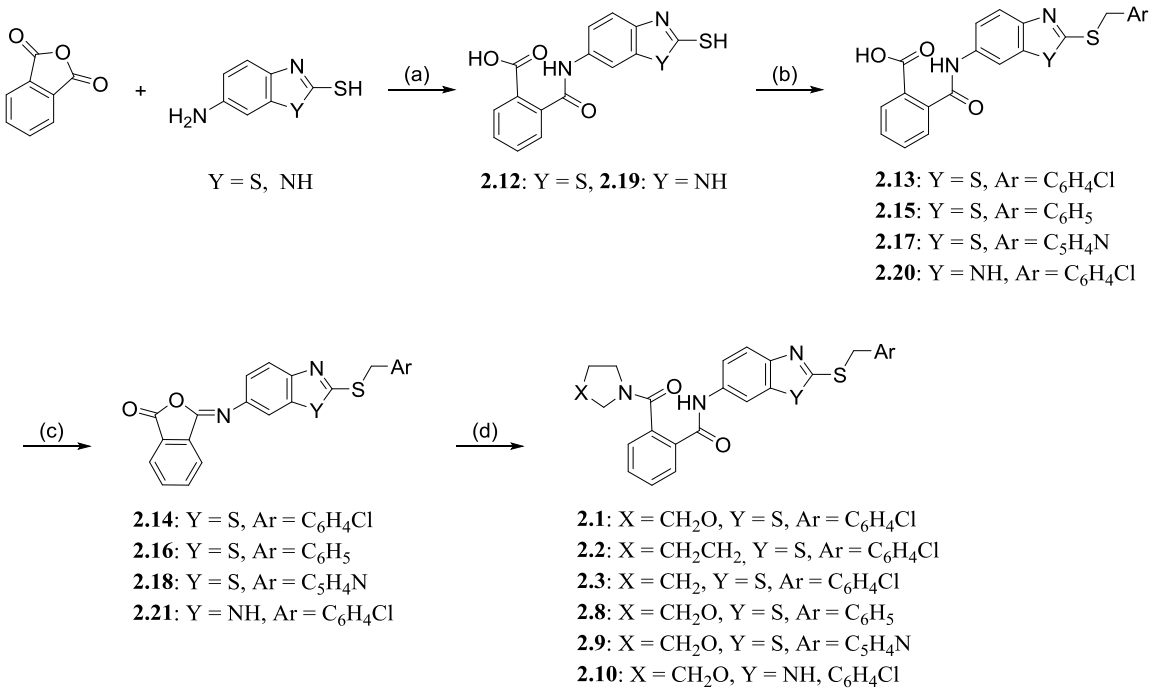

Figure 32. General Synthetic Route. Reagents and conditions: (a) THF, 30 °C, 17 hr; (b) NaOH, EtOH, 0 °C to rt, $ArCH_2Cl$, 17 hr; (c) $(CH_3CO)_2O$, TEA, 1,4 dioxane, rt, 17 hr; (d) R_2NH, THF, 50-35°C, 15 hr.

Oxidation of the exocyclic sulfur of the benzothiazole **2.1** was accomplished to generate racemic sulfoxide **2.4**, sulfone **2.5**, and the individual enantiomers of sulfoxide **2.4** (Figure 33). Racemic sulfoxide **2.4** was synthesized in 82% yield using an equimolar amount of substrate and oxidizing agent *meta*-chloroperoxybenzoic acid (*m*CPBA). The

same approach was employed to synthesize sulfone **2.5** using excess of *m*CPBA. The individual sulfoxide enantiomers (**2.6** and **2.7**) were synthesized using cumene hydroperoxide, titanium tetraisopropoxide and the respective enantiomer of diethyl tartrate.[16]

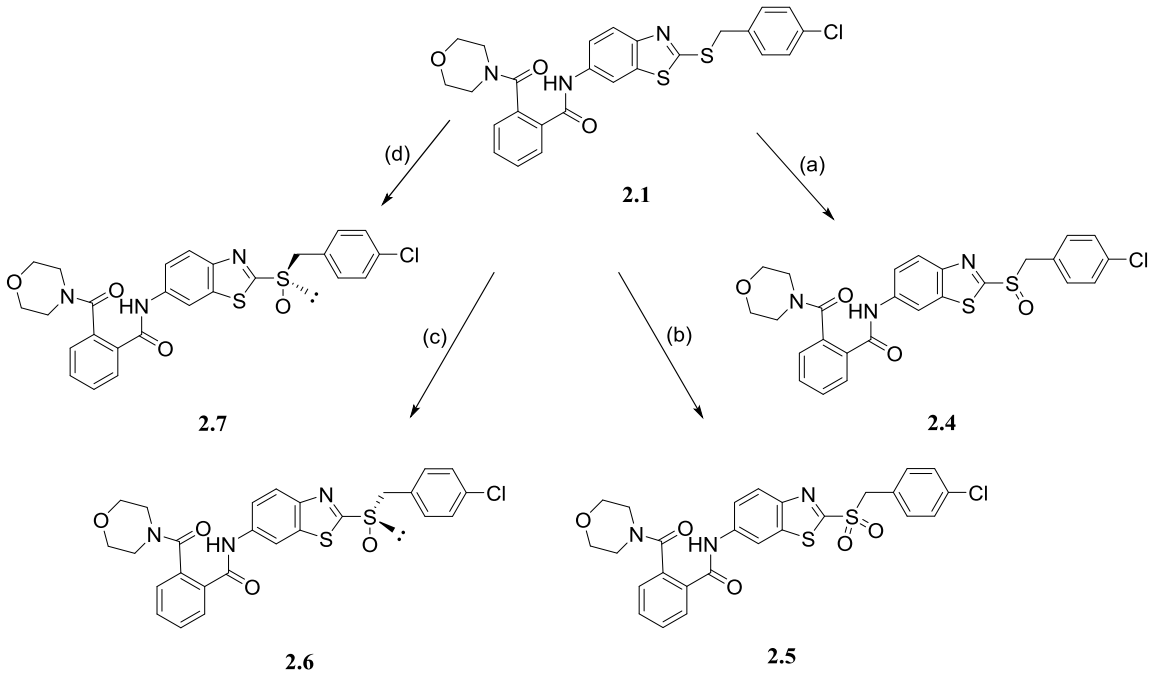

Figure 33. Oxidation of the Exocyclic Sulfur. Reagents and conditions: (a) *m*CPBA, CH_2Cl_2, 0 °C to rt., 3 hr, 82%; (b) *m*CPBA, CH_2Cl_2, 0 °C to rt., 5 hr, 83%; (c) (+) DET, Ti(Oi-Pr)$_4$, $C_6H_5C(CH_3)_2OOH$, DIPEA, toluene, 2 h, 59%; (d) (-) DET, Ti(Oi-Pr)$_4$, $C_6H_5C(CH_3)_2OOH$, DIPEA, toluene, 2 h, 53%.

The retrosynthesis analysis to synthesize the *S*-enantiomer of compound **2.11** is demonstrated in Figure 34. The synthesis proposed to use nucleophilic substitution (S_N2) to set the stereo center using commercially available (*S*)-4-chloro-α-methyl-benzyl alcohol and thiol **2.35** (Figure 30). Formation of a good leaving group is a requisite for successful S_N2 reaction.

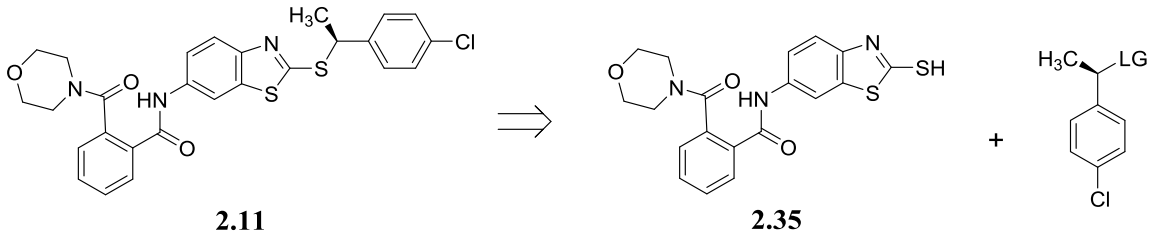

Figure 34. Retrosynthesis Analysis of Compound **2.11**.

Conversion of the hydroxyl group to triflate group was done using triflic anhydride and pyridine (Figure 35). Replacement of hydroxyl group by triflate group was completely achieved as indicated by the NMR, nevertheless the substitution of triflate leaving group by nucleophilic sulfur was unsuccessful. (*S*)-4-chloro-α-methyl-benzyl alcohol was then reacted with mesityl chloride to form mesityl leaving group. The reaction was done at -20 ºC and completed in one hour at the same temperature. Replacement of OH with OMs was achieved also as indicated by the NMR; however the S_N2 reaction was ineffective (Figure 35).

Various experiments were attempted including *in situ* replacement of OH with Cl using (*S*)-4-chloro-α-methyl-benzyl alcohol (Figure 35). (*S*)-4-chloro-α-methyl-benzyl alcohol reacted with oxalyl chloride at 0 °C followed by addition of compound **2.35**. However the intended product was not observed. Also (*R*)-4-chloro-α-methyl-benzyl alcohol was subjected to Mitsunobu reaction condition, triphenylphosphine (PPh_3) and diethyl azodicarboxylate (DEAD); likewise the desired product was not achieved (Figure 36).

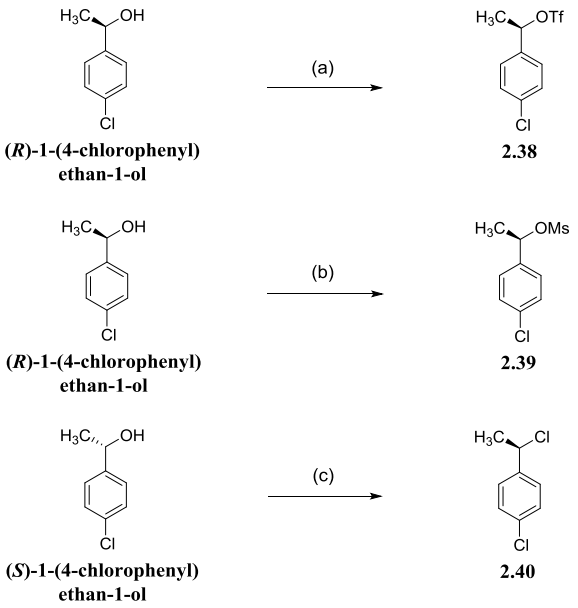

Figure 35. Conversion of OH to a Good Leaving Group. Reagents and conditions: (a) Tf_2O, pyridine, DCM, rt, 76%; (b) MsCl, TEA, DCM, -20 °C; (c) $(COCl)_2$, TEA, DMF, DCM, 0 °C.

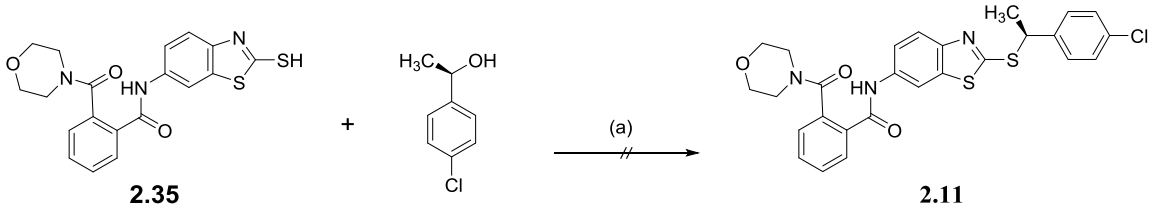

Figure 36. Mitsunobu Condition to Synthesize Compound **2.11**. Reagents and conditions: (a) PPh_3, DIAD, THF, 0°C to rt.

Due to the ineffectuality of the S_N2 reaction on the secondary position, synthesis of compound **2.11** followed a slightly different synthetic route (Figure 37). Compound **2.11** was synthesized in a racemic fashion with this study and plans for an enantioselective synthesis could be developed based on the activity of racemic **2.11**. The synthesis began with nucleophilic addition of the commercially available 1-phenylethyl mercaptan to 2-chloro-6-nitrobenzothiazole to form nitrobenzothiazole **2.22** in 80% yield.

The nitro group was then reduced to amine **2.23** through catalytic hydrogenation. The resulting primary amine was used to open phthalic anhydride to produce the intended product **2.24** in high yield (98%). The following step is the formation of the phthalisoimide ring **2.25** in 70% yield which was reopened by morpholine to successfully produce analog **2.11** in 76% yield (Figure 37).

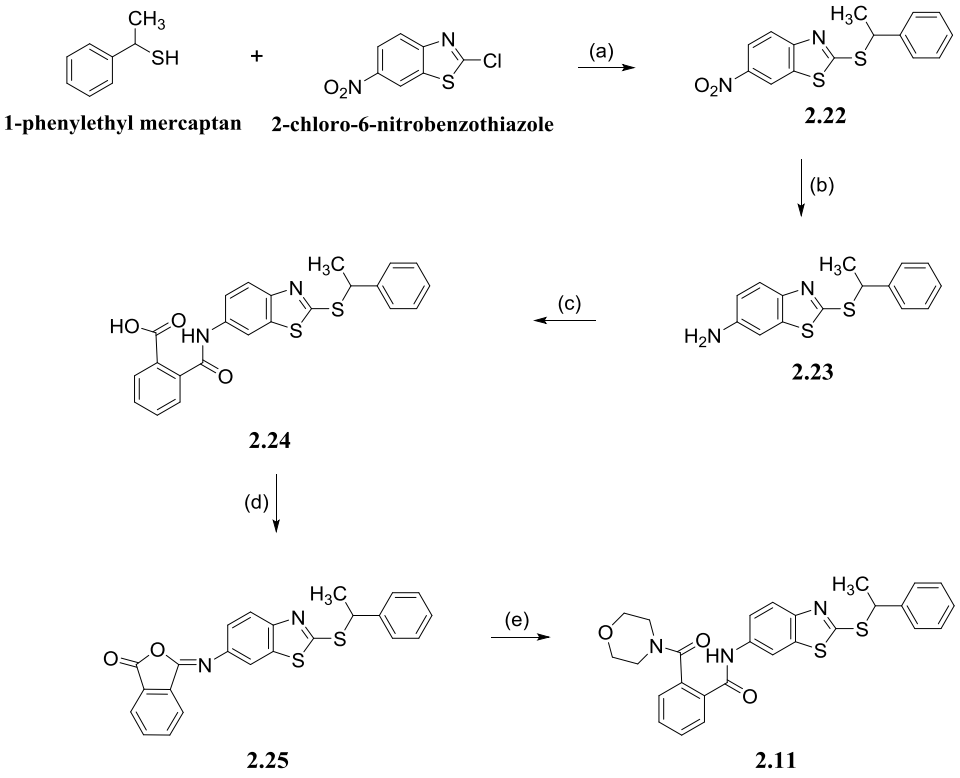

Figure 37. Reagents and Conditions. (a) NaH, DMF, 5 hr, 80%; (b) H_2, Pd/C, EtOH, 17 hr, 89%; (c) phthalic anhydride, THF, 30 °C, 17 hr, 98%; (d) $(CH_3CO)_2O$, TEA,1,4 dioxane, rt, 17 hr, 70%; (e) morpholine, THF, 35 °C, 15 hr, 76%.

β-Arrestin Assay

The activities of the synthesized analogs as antagonists at GPR35 was examined using β-arrestin-2-recruitment assay. U2OS cells permanently expressing HA-GPR35a

and βarr2-GFP (UGPR35β) were utilized for most experiments. Cells were plated onto coverslips that were placed in 24 well plates. Cells were maintained at 37 °C in 5% CO_2 until ready for experiments (80-85% confluent). Cells were washed once with Hank's buffered salt solution (HBSS) before drug application and experiments were performed in HBSS. Cells were incubated with drug for 40 minutes at room temperature then fixed with 4% paraformaldehyde for 20 minutes. Glass coverslips were mounted on slides and were imaged on a (Nikon E800) fluorescence microscope using a 40 X oil objective and 488 nm excitation for GFP.

Data Analysis of β-Arrestin Assay

βarr2-GFP aggregates were quantified by using the ImageJ software (http://rsbweb.nih.gov/ij/). Concentration-effect curves for agonist-mediated receptor activation were analyzed by nonlinear regression techniques using GraphPad Prism 5.0 software (GraphPad) and data were fitted to sigmoidal dose-response curves to obtain IC_{50} (Figure 38).

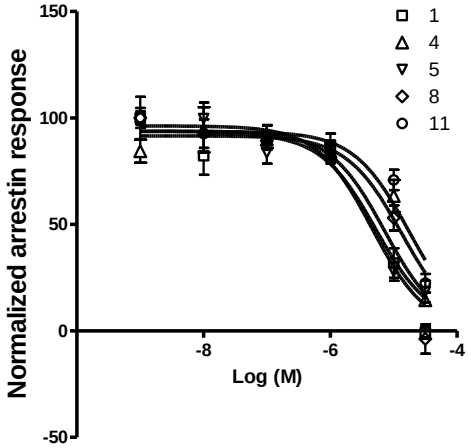

Figure 38. Concentration-effect Curves for GPR35 Antagonists.

Results and Discussion

The evaluations of the analogs comprise considerable information (Table 6). The fact that piperidine **2.2** and pyrolidine **2.3** are devoid of activity as GPR35 antagonists indicate that there is likely to be a strong interaction between the oxygen of the morpholine ring and a residue in the binding site in this region. We assumed that the morpholine ring affected the toggle switch, but without any hydrogen bonding to lock the ring in place.

Table 6

Biological Results

Antagonist	Structure	IC_{50}(CI range)
2.1	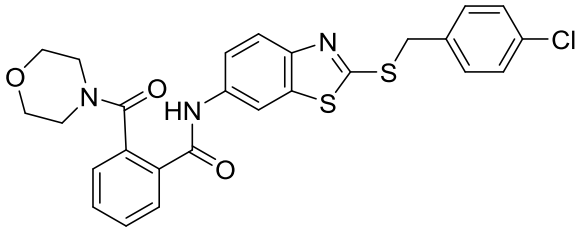	4.6 (1.8-12)
2.2	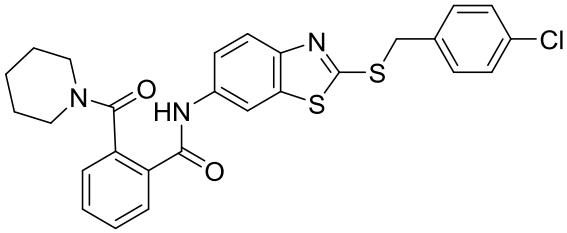	>30
2.3	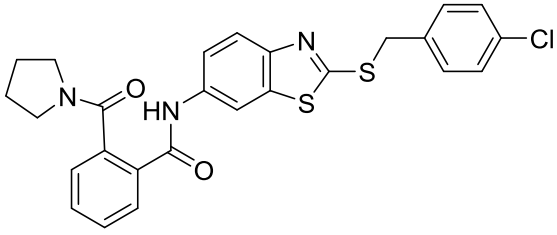	>30

Table 6

(Cont.)

Antagonist	Structure	IC_{50}(CI range)
2.4	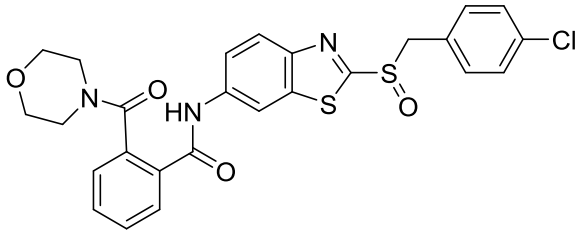	13 (4.0-45)
2.5	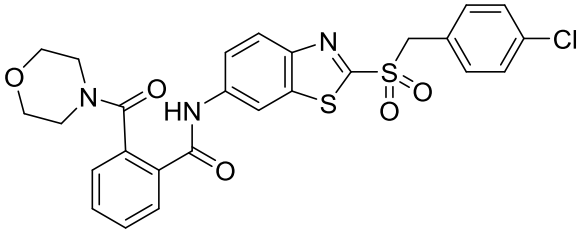	5.2 (2.2-13)
2.6	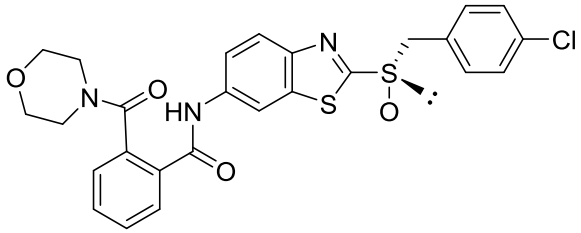	>30
2.7	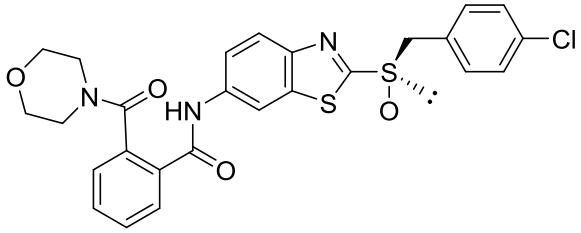	>30
2.8	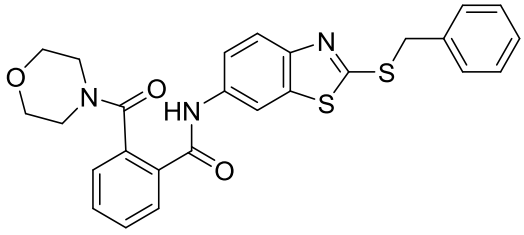	7.2 (2.3-23)
2.9	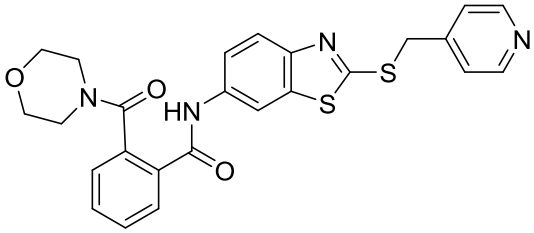	>30

Table 6

(Cont.)

Antagonist	Structure	IC_{50}(CI range)
2.10	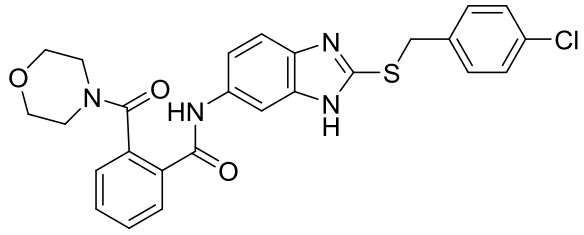	>30
2.11	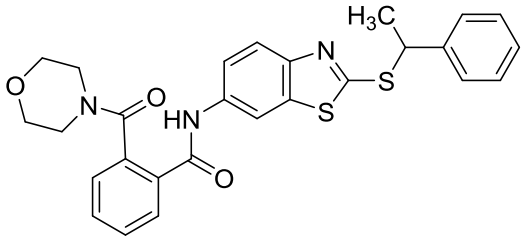	17 (5.6-54)

Oxidation of the exocyclic sulfur to sulfoxide **2.4** and sulfone **2.5** decreased the activity as an antagonist; we assumed that this small detrimental activity was perhaps due to electronic effect rather than unfavorable binding site interaction. The sulfoxide enantiomers **2.6** and **2.7** are inactive and this is probably due to a combination of steric and electronic effects. Replacement of the aryl group connected to sulfur with pyridine in compound **2.9** was done to examine the influence of the aryl group on the binding pocket. Compound **2.9** was found to be inactive GPR35 antagonist which is an indication that the basicity of the nitrogen of the pyridine ring produced unfavorable negative potential surface. The same scenario exists when the cyclic sulfur is replaced with nitrogen in benzimidazole **2.10.** These results provided us with key binding pocket interactions which will be utilized in the further development of the model of GPR35 and also will be used as guidance for designing novel antagonists for GPR35.

The paramount aim of this work is to gain a precise understanding of the function and pharmacology of GPR35 receptor by means of pharmacological tools. These tools include mainly accessing a potent and selective GPR35 ligand and building a computational modeling of the GPR35 receptor. Although the outcomes of this study lack a potent compound with antagonist activity at GPR35 receptor, the study provides a delicate understanding on the binding pocket of the GPR35 inactive state. The toggle switch occurrence required strong hydrogen-bonding with the residue to lock the antagonist in place. This piece of information assists in developing and refining the homology model of the GPR35 receptor. Likewise, the homology model refining includes the residue at the binding site of terminal aryl group connected to the thiol. This area was found to be, depending on the results, preferred a positively potential surface. The refinement also included the region of S7.39 (262) in view of the fact that the positively charged surface was found to be unfavored. The initial structure-activity relationships study is used to further refine a homology model of GPR35 receptor. The SAR provides us with precise key binding pocket interactions which are used as a foundation in the refinement process of the GPR35 homology model. This model will serve as a research tools or basis for designing and developing novel drugs.

Experimental Procedures

All anhydrous reactions were performed in oven dried glassware under a nitrogen atmosphere. All commercial reagents and solvents were used without further purification. Chromatographic purification was performed using silica gel (60 Å, 32-63μm). Analytical thin-layer chromatography (TLC) was performed on SiO_2 plates and

visualizing by UV irradiation at 254 nm. NMR spectra were recorded in $CDCl_3$, DMSO-d_6, methanol-d_4, or acetone-d_6 using JEOL ECA spectrometer (500 MHz for ^1H, 125 MHz for ^{13}C). All ^1H NMR experiments are reported in δ units, parts per million (ppm) downfield of TMS, and were measured relative to the signals for chloroform (7.26 ppm), DMSO (2.50 ppm), methanol (3.31 ppm), or acetone (2.05 ppm). All ^{13}C NMR spectra were reported in ppm relative to the signals for chloroform (77 ppm), DMSO (39.5 ppm), methanol (49 ppm), acetone (29.8 ppm) and. Coupling constants, *J*, are reported in hertz (Hz) and multiplicities are listed as singlet (s), doublet (d), triplet (t), doublet of doublets (dd), triplet of doublets (td), quintet (quint), multiplet (m), etc. High resolution mass spectra were acquired on a Thermo Fisher Scientific LTQ Orbitrap XL MS system using electrospray ionization (ESI).

Phthalic anhydride (1.00 g, 6.75 mmol) was added to a solution of mercaptobenzothiazole (1.23 g, 6.75 mmol) in THF (50 mL) and the mixture was stirred at 30 °C for 17 hours (Figure 39). THF was then evaporated under reduced pressure and the product was purified by recrystallization out of ethanol/ water mixture to yield yellow crystal (2.13 g, 96%).

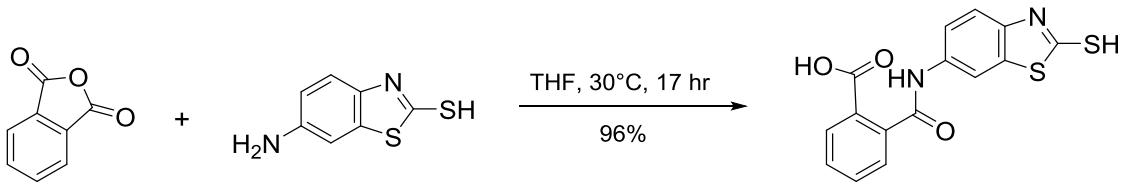

2.12

Figure 39. Synthesis of Compound **2.12**.

^{1}H NMR (500 MHz, DMSO-d_6) δ 13.05 (br. s, 1H), 10.52 (s, 1H), 8.13 (d, J = 1.7 Hz, 1H), 7.89 (dd, J = 1.1, 7.4 Hz, 1H), 7.66 (td, J_d = 1.4, J_t = 7.7 Hz, 1H), 7.56 - 7.61 (m, 2H), 7.54 (d, J = 8.0 Hz, 1H), 7.27 (d, J = 9.2 Hz, 1H).

^{13}C NMR (126 MHz, DMSO-d_6) δ 189.5, 168.0, 167.9, 139.2, 137.7, 136.9, 132.3, 130.42, 130.37, 130.1, 130.0, 128.3, 119.7, 113.0, 112.6.

HRMS (ESI): $C_{15}H_{11}N_2O_3S_2$ $[M+H]^+$, Calculated: 331.02111, Found: 331.01990.

To a solution of NaOH (0.23 g, 5.68 mmol) in ethanol (40 mL) under 0 °C was added compound **2.12** (1.25 g, 3.78 mmol) and 4-chlorobenzyl chloride (0.61 g, 3.78 mmol). The mixture was stirred at 0 °C for 30 minutes and then at room temperature for 17 hours (Figure 40). The ethanol was removed under reduced pressure and water (20 mL) was added to the residue. The aqueous layer was washed with dichloromethane (3 X 20 mL) and then acidified to pH~2 using hydrochloric acid (1 M). The aqueous layer was then placed on an ice bath and the resultant precipitate was collected by vacuum filtration, washed with water, and dried on vacuum to yield the desired product as pale yellow powder (1.63 g, 95%).

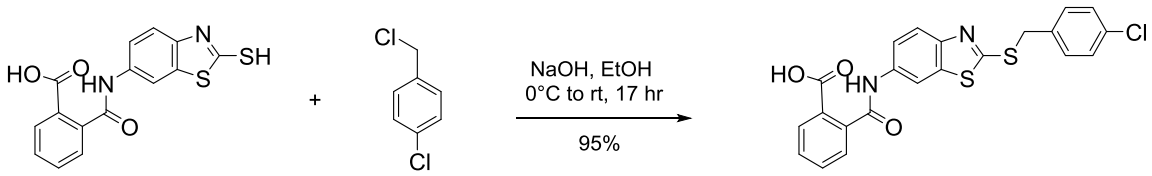

2.12 **2.13**

Figure 40. Synthesis of Compound **2.13**.

^{1}H NMR (500 MHz, DMSO-d_6) δ 10.62 (s, 1H), 8.48 (d, *J* = 2.3 Hz, 1H), 7.90 (dd, *J* = 1.1, 7.4 Hz, 1H), 7.84 (d, *J* = 8.6 Hz, 1H), 7.67 (td, J_d = 1.1, J_t = 7.4 Hz, 1H), 7.55 - 7.62 (m, 3H), 7.52 (d, *J* = 8.6 Hz, 2H), 7.40 (d, *J* = 8.6 Hz, 2H), 4.63 (s, 2H).

^{13}C NMR (126 MHz, DMSO-d_6) δ 168.1, 167.9, 164.5, 149.2, 139.2, 137.1, 136.5, 135.9, 132.7, 132.4, 131.5 (2C), 130.4, 130.1, 130.1, 129.1 (2C), 128.4, 121.7, 119.5, 112.1, 36.4.

HRMS (ESI): $C_{22}H_{16}ClN_2O_3S_2$ $[M+H]^+$, Calculated: 455.02909, Found: 455.02704.

Following a reported procedure,[14] a mixture of acetic anhydride (0.70 mL, 0.75 g, 7.39 mmol) and triethylamine (2.06 mL, 1.49 g, 14.77 mmol) was added dropwise to a suspension of compound **2.13** (1.12 g, 2.46 mmol) in dry 1,4 dioxane (20 mL). The suspension turned to clear yellowish solution upon completion of the addition. The reaction mixture was allowed to stir at room temperature for 17 hours (Figure 41). The mixture was poured into ice and product was precipitated instantly. The product was collected by filtration, washed with water, sodium bicarbonate, water, and dried on vacuum to yield the desired product as a yellow powder (0.98 g, 91%).

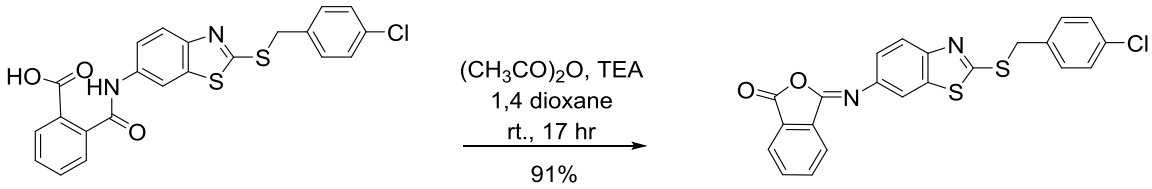

2.13 **2.14**

Figure 41. Synthesis of Compound **2.14**.

^{1}H NMR (500 MHz, $CDCl_3$) δ 7.96 - 8.00 (m, 3H), 7.84 (d, *J* = 1.7 Hz, 1H), 7.81 (dd, *J* = 2.9, 5.2 Hz, 2H), 7.51 (dd, *J* = 2.3, 8.6 Hz, 1H), 7.40 (d, *J* = 8.6 Hz, 2H), 7.29 (d, *J* = 8.6 Hz, 2H), 4.58 (s, 2H).

^{13}C NMR (126 MHz, $CDCl_3$) δ 167.5, 167.4 (2C), 152.5, 135.9, 134.9, 134.7 (2C), 133.8, 131.7, 130.6 (2C), 129.0 (2C), 128.0, 124.9, 124.0 (2C), 121.9, 119.5 (2C), 37.0.

HRMS (ESI): $C_{22}H_{14}ClN_2O_2S_2$ $[M+H]^+$,Calculated: 437.01852, Found: 437.01680.

Morpholine (1.19 mL, 1.17 g, 13.48 mmol) was added to a solution of compound **2.14** (0.98 g, 2.25 mmol) in THF (30 mL) and the mixture was stirred at 50 °C for 2 hours then at 35 °C for 15 hours (Figure 42). THF was removed under reduced pressure and water (20 mL) was added to the resultant residue. The mixture was acidified to pH~2 using hydrochloric acid (1 M). The product was extracted with ethyl acetate (3 X 40 mL), washed with water (4 X 25 mL), and dried over sodium sulfate. The product was crystallized during solvent evaporation under reduced pressure to yield 1.19 g of pale yellow crystal (99%).

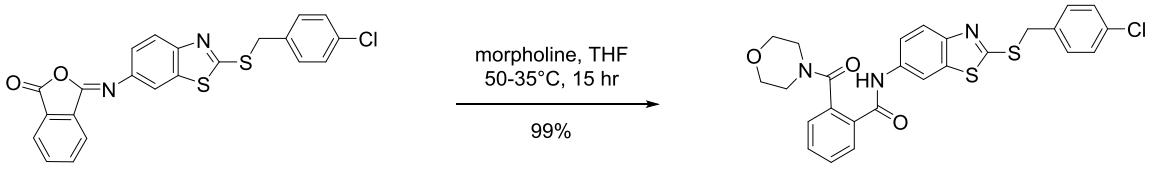

2.14 **2.1**

Figure 42. Synthesis of Analog **2.1**.

^{1}H NMR (500 MHz, $CDCl_3$) δ 9.52 (s, 1H), 8.31 (d, *J* = 1.7 Hz, 1H), 7.77 (dd, *J* = 1.4, 7.7 Hz, 1H), 7.70 (d, *J* = 9.2 Hz, 1H), 7.34 - 7.42 (m, 5H), 7.28 (d, *J* = 8.6 Hz, 2H), 7.14

(dd, *J* = 1.7, 6.9 Hz, 1H), 4.52 (s, 2H), 3.98 (br. s, 1H), 3.70 (br. s, 3H), 3.61 (br. s., 2H), 3.25 (t, *J* = 4.9 Hz, 2H).

^{13}C NMR (126 MHz, $CDCl_3$) δ 170.7, 165.7, 164.9, 149.7, 136.1, 135.2, 135.0, 134.5, 133.8, 133.7, 131.1, 130.6 (2C), 129.4, 129.3, 128.9 (2C), 126.1, 121.3, 118.9, 111.8, 66.7, 66.6, 48.0, 42.6, 37.1.

HRMS (ESI): $C_{26}H_{23}ClN_3O_3S_2$ $[M+H]^+$, Calculated: 524.08694, Found: 524.08498.

Piperidine (0.07 mL, 0.06 g, 0.69 mmol) was added to a solution of compound **2.14** (0.05 g, 0.11 mmol) in THF (10 mL) and the mixture was stirred at 50 °C for 2 hours then at 35 °C for 15 hours (Figure 43). THF was removed under reduced pressure and water (10 mL) was added to the resultant residue. The mixture was acidified to pH~2 using hydrochloric acid (1 M). The product was extracted with ethyl acetate (3 X 20 mL), washed with water (4 X 15 mL), and dried over sodium sulfate. The product was crystallized during solvent evaporation under reduced pressure to yield 0.06 g of yellow crystal (100%).

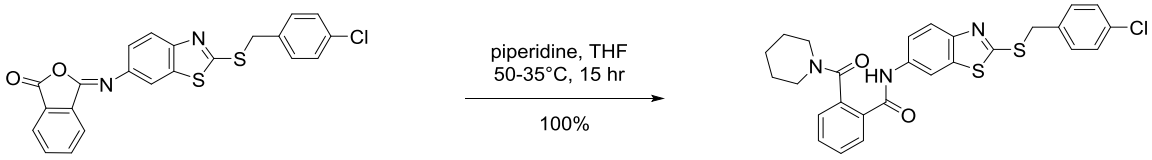

2.14 **2.2**

Figure 43. Synthesis of Analog **2.2**.

^{1}H NMR (500 MHz, $CDCl_3$) δ 9.59 (s, 1H), 8.40 (d, *J* = 1.7 Hz, 1H), 7.87 (dd, *J* = 1.7, 7.4 Hz, 1H), 7.75 (d, *J* = 9.2 Hz, 1H), 7.40 - 7.48 (m, 3H), 7.38 (d, *J* = 8.6 Hz, 2H), 7.28

(d, *J* = 8.6 Hz, 2H), 7.19 (dd, *J* = 1.7, 6.9 Hz, 1H), 4.53 (s, 2H), 3.88 (br. s, 1H), 3.61 (br. s, 1H), 3.16 (br. s, 2H), 1.59 (br. s., 3H), 1.44 (br. s., 3H).

^{13}C NMR (126 MHz, $CDCl_3$) δ 170.2, 165.6, 164.7, 149.6, 136.1, 135.2, 134.9, 134.8, 133.5, 133.1, 131.1, 130.5 (2C), 129.9, 129.1, 128.8 (2C), 125.8, 121.3, 118.8, 111.7, 48.7, 43.0, 37.0, 26.2, 25.6, 24.3.

HRMS (ESI): $C_{27}H_{25}ClN_3O_2S_2$ $[M+H]^+$, Calculated: 522.10767, Found: 522.10489.

Pyrrolidine (0.06 mL, 0.05 g, 0.69 mmol) was added to a solution of compound **2.14** (0.05 g, 0.11 mmol) in THF (10 mL) and the mixture was stirred at 50 °C for 2 hours then at 35 °C for 15 hours (Figure 44). THF was removed under reduced pressure and water (10 mL) was added to the resultant residue. The mixture was acidified to pH~2 using hydrochloric acid (1 M). The product was extracted with ethyl acetate (3 X 20 mL), washed with water (4 X 15 mL), and dried over sodium sulfate. The product was crystallized during solvent evaporation under reduced pressure to yield 0.06 g of yellow crystal (99%).

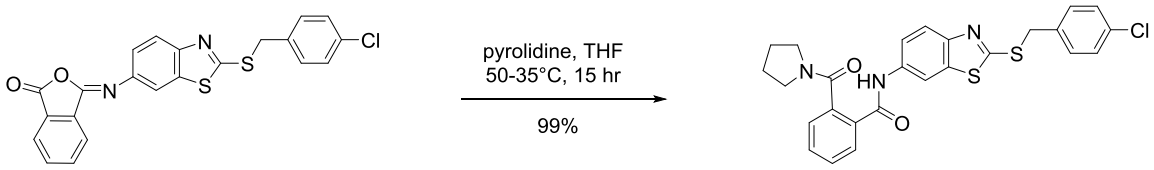

2.14 **2.3**

Figure 44. Synthesis of Analog **2.3**.

^{1}H NMR (500 MHz, $CDCl_3$) δ 9.81 (s, 1H), 8.44 (d, *J* = 1.7 Hz, 1H), 7.94 - 7.97 (m, 1H), 7.80 (d, *J* = 9.2 Hz, 1H), 7.50 - 7.53 (m, 2H), 7.48 (dd, *J* = 2.3, 8.6 Hz, 1H), 7.39 (d, *J* =

8.6 Hz, 2H), 7.31 (d, *J* = 3.4 Hz, 1H), 7.30 (d, *J* = 8.6 Hz, 2H), 4.55 (s, 2H), 3.65 (t, *J* = 6.9 Hz, 2H), 3.20 (t, *J* = 6.6 Hz, 2H), 1.94 (quin, *J* = 6.3 Hz, 2H), 1.87 (quin, *J* = 6.3 Hz, 2H).

^{13}C NMR (126 MHz, $CDCl_3$) δ 170.4, 166.0, 164.6, 149.6, 136.0, 135.8, 135.6, 135.0, 133.6, 133.3, 131.0, 130.7 (2C), 129.8, 129.2, 128.9 (2C), 126.3, 121.3, 119.2, 111.9, 49.4, 46.1, 37.1, 25.9, 24.6.

HRMS (ESI): $C_{26}H_{23}ClN_3O_2S_2$ [M+H], Calculated: 508.09202, Found: 508.08904.

To a solution of compound **2.1** (0.10 g, 0.19 mmol) in CH_2Cl_2 (12 mL) at 0 °C was added a solution of 70-75% *m*CPBA (0.033 g, 0.19 mmol) in CH_2Cl_2 (4 mL) drop wise (Figure 45). The ice bath was removed and reaction mixture was stirred at room temperature until the starting material was completely consumed in 3 hours (reaction was monitored by TLC). A saturated solution of sodium bicarbonate was added and the mixture was stirred for 10 minutes. The CH_2Cl_2 layer was separated and the aqueous layer was extracted with CH_2Cl_2 (2 X 20 mL). The organic layers were combined, washed with aqueous sodium bicarbonate, dried over sodium sulfate, and concentrated on vacuum. The product was purified by silica gel column chromatography using a solvent system of hexane, ethyl acetate and methanol (78/20/2) to obtain 0.08 g (yield 82%) of a white powder.

^{1}H NMR (500 MHz, $CDCl_3$) δ 9.81 (br. s, 1H), 8.47 (d, *J* = 2.3 Hz, 1H), 7.84 (d, *J* = 8.0 Hz, 1H), 7.77 (d, *J* = 6.9 Hz, 1H), 7.52 (d, *J* = 7.4 Hz, 1H), 7.34 - 7.42 (m, 2H), 7.25 - 7.30 (m, 1H), 7.23 (br. s., 1H), 7.05 - 7.18 (m, 3H), 4.47 (d, *J* = 13.2 Hz, 1H), 4.33 (br. s, 1H), 3.98 (br. s, 1H), 3.75 (br. s, 3H), 3.63 (br. s, 2H), 3.27 (t, *J* = 4.6 Hz, 2H).

^{13}C NMR (126 MHz, $CDCl_3$) δ 175.0, 170.8, 165.9, 150.1, 136.93, 136.89, 135.0, 134.5, 133.6, 131.9 (2C), 131.3, 129.4 (2C), 129.0 (2C), 127.1, 126.2, 123.7, 120.0, 112.3, 66.7, 66.6, 61.9, 48.1, 42.6.

HRMS (ESI): $C_{26}H_{23}ClN_3O_4S_2$ $[M+H]^+$, Calculated: 540.08185, Found: 540.07997.

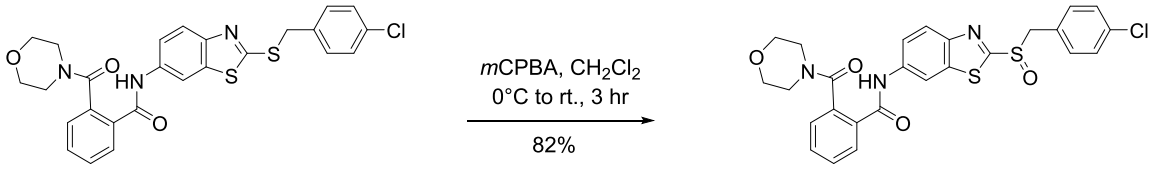

2.1 **2.4**

Figure 45. Synthesis of Analog **2.4**.

To a solution of compound **2.1** (0.1 g, 0.19 mmol) in CH_2Cl_2 (12 mL) at 0 °C was added a solution of 70-75 % *m*CPBA (0.12 g, 0.48 mmol) in CH_2Cl_2 (4 mL) drop wise (Figure 46). The ice bath was removed and reaction mixture was stirred at room temperature until the starting material was completely consumed in 5 hours (reaction was monitored by TLC). A saturated solution of sodium bicarbonate was added and the mixture was stirred for 10 minutes. The CH_2Cl_2 layer was separated and the aqueous layer was extracted with CH_2Cl_2 (2 X 20 mL). The organic layers were combined, washed with aqueous sodium bicarbonate, dried over sodium sulfate, and concentrated on vacuum. The product was purified by silica gel column chromatography using a solvent system of hexane, ethyl acetate and methanol (76/20/4) to obtain 0.088 g (yield 83%) of a whitish paige powder.

^{1}H NMR (500 MHz, $CDCl_3$) δ 9.76 (s, 1H), 8.58 (d, *J* = 1.7 Hz, 1H), 8.04 (d, *J* = 8.6 Hz, 1H), 7.83 (dd, *J* = 1.7, 7.4 Hz, 1H), 7.57 (dd, *J* = 2.0, 8.9 Hz, 1H), 7.41 - 7.49 (m, 2H),

7.26 - 7.31 (m, 4H), 7.20 (dd, *J* = 1.1, 7.4 Hz, 1H), 4.74 (s, 2H), 3.96 (br. s, 1H), 3.73 (br. s, 3H), 3.62 (t, *J* = 4.6 Hz, 2H), 3.27 (t, *J* = 5.2 Hz, 2H).

^{13}C NMR (126 MHz, $CDCl_3$) δ 170.7, 166.0, 163.7, 149.0, 138.4, 138.3, 135.7, 134.3, 133.4, 132.6 (2C), 131.5, 129.69, 129.67, 129.3 (2C), 126.3, 125.5, 124.9, 120.9, 111.9, 66.7 (2C), 60.3, 48.2, 42.6.

HRMS (ESI): $C_{26}H_{23}ClN_3O_5S_2$ $[M+H]^+$, Calculated: 556.07676, Found: 556.07480.

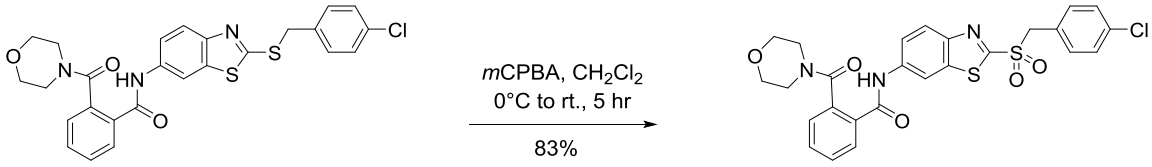

2.1 **2.5**

Figure 46. Synthesis of Analog **2.5**.

Following a reported procedure,[15] to a suspension of compound **2.1** (0.3 g, 0.57 mmol) in toluene (15 mL) at 50 °C were added (-) diethyl tartrate (0.01 mL, 0.01 g, 0.05 mmol) and triisopropoxide (0.006 mL, 0.006 g, 0.02 mmol) (Figure 47). After the mixture was stirred for 45 minutes at 50 °C, heat was removed and the mixture allowed to warm to room temperature. At this point, N-ethyldiisopropylamine (0.004 mL, 0.003 g, 0.02 mmol) and cumene hydroperoxide (0.09 mL, 0.09 g, 0.57 mmol) were added. The mixture was stirred until conversion of most of the starting material to product was observed by TLC (about an hour). A saturated solution of sodium bicarbonate (15 mL) was added and the product was extracted with ethyl acetate (3 X 30 mL). The organic layers were combined, washed with water (2 X 20 mL), dried with sodium sulfate, and concentrated on vacuum. The product was purified by column chromatography using a

solvent system of hexane, ethyl acetate and methanol (78/20/2) to obtain 0.18g (yield 59%) of a white powder.

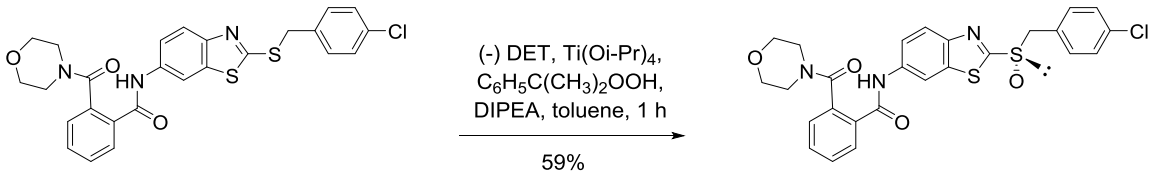

2.1 **2.6**

Figure 47. Synthesis of Analog **2.6**.

^{1}H NMR (500 MHz, $CDCl_3$) δ 9.81 (br. s, 1H), 8.47 (s, 1H), 7.84 (d, *J* = 8.0 Hz, 1H), 7.77 (d, *J* = 6.9 Hz, 1H), 7.52 (d, *J* = 7.4 Hz, 1H), 7.34 - 7.43 (m, 2H), 7.26 - 7.31 (m, 1H), 7.24 (br. s., 1H), 7.07 - 7.18 (m, 3H), 4.48 (dd, *J* = 4.0, 13.2 Hz, 1H), 4.33 (br. s, 1H), 3.98 (br. s, 1H), 3.76 (br. s, 3H), 3.64 (br. s, 2H), 3.27 (t, *J* = 4.6 Hz, 2H).

^{13}C NMR (126 MHz, $CDCl_3$) δ 175.0, 170.8, 165.9, 150.1, 136.93, 136.89, 135.0, 134.5, 133.6, 131.9 (2C), 131.3, 129.4 (2C), 129.0 (2C), 127.1, 126.2, 123.7, 120.0, 112.3, 66.7, 66.6, 61.9, 48.1, 42.6.

HRMS (ESI): $C_{26}H_{23}ClN_3O_4S_2$ $[M+H]^+$, Calculated: 540.08185, Found: 540.07994.

Following a reported procedure,[15] to a suspension of compound **2.1** (0.30 g, 0.57 mmol) in toluene (15 mL) at 50 °C were added (+) diethyl tartrate (0.01 mL, 0.01 g, 0.05 mmol) and triisopropoxide (0.006 mL, 0.006 g, 0.02 mmol) (Figure 48). After the mixture was stirred for 45 minutes at 50 °C, heat was removed and the mixture allowed to warm to room temperature. At this point, N-ethyldiisopropylamine (0.004 mL, 0.003 g, 0.02 mmol) and cumene hydroperoxide (0.09 mL, 0.09 g, 0.57 mmol) were added. The mixture was stirred until conversion of most of the starting material to product was

observed by TLC (about an hour). A saturated solution of sodium bicarbonate (15 mL) was added and the product was extracted with ethyl acetate (3 X 30 mL). The organic layers were combined, washed with water (2 X 20 mL), dried with sodium sulfate, and concentrated on vacuum. The product was purified by column chromatography using a solvent system of hexane, ethyl acetate and methanol (78/20/2) to obtain 0.16 g (yield 53%) of a white powder.

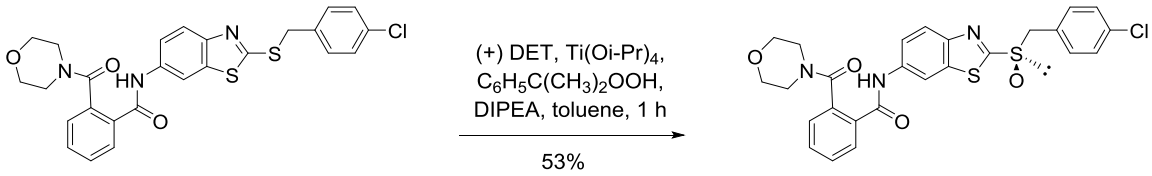

2.1 **2.7**

Figure 48. Synthesis of Analog **2.7**.

^{1}H NMR (500 MHz, $CDCl_3$) δ 9.81 (br. s, 1H), 8.47 (s, 1H), 7.84 (d, *J* = 8.0 Hz, 1H), 7.77 (d, *J* = 6.9 Hz, 1H), 7.52 (d, *J* = 7.4 Hz, 1H), 7.34 - 7.44 (m, 2H), 7.26 - 7.31 (m, 1H), 7.24 (br. s., 1H), 7.05 - 7.17 (m, 3H), 4.48 (d, *J* = 13.2 Hz, 1H), 4.33 (br. s, 1H), 3.98 (br. s, 1H), 3.76 (br. s, 3H), 3.64 (br. s, 2H), 3.27 (d, *J* = 4.6 Hz, 2H).

^{13}C NMR (126 MHz, $CDCl_3$) δ 175.0, 170.8, 165.9, 150.1, 136.9, 136.9, 135.0, 134.5, 133.6 (2C), 131.9 (2C), 131.3, 129.4 (2C), 129.0, 127.1, 126.2, 123.7, 120.0, 112.3, 66.7, 66.6, 61.9, 48.1, 42.6.

HRMS (ESI): $C_{26}H_{23}ClN_3O_4S_2$ $[M+H]^+$, Calculated: 540.08185, Found: 540.07990.

To a solution of NaOH (0.02g, 0.45 mmol) in ethanol (5 mL) under 0 °C was added compound **2.12** (0.10 g, 0.30 mmol) and benzyl bromide (0.05 g, 0.30 mmol). The mixture was stirred at 0 °C for 30 minutes and then at room temperature for 17 hours

(Figure 49). The ethanol was removed under reduced pressure and water (15 mL) was added to the residue. The aqueous layer was washed with dichloromethane (3 X 15 mL) and then acidified to pH~2 using hydrochloric acid (1 M). The aqueous layer was then placed on an ice bath and the resultant precipitate was collected by vacuum filtration, washed with water, and dried on vacuum to yield the desired product as a pale yellow powder (0.10 g, 77%).

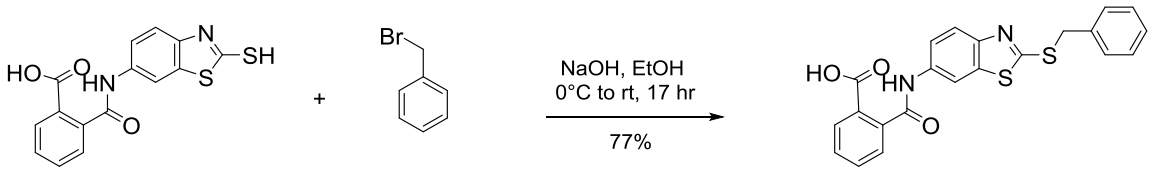

2.12 **2.15**

Figure 49. Synthesis of Compound **2.15**.

^{1}H NMR (500 MHz, DMSO-d_6) δ 13.07 (br. s, 1H), 10.56 (s, 1H), 8.45 (d, J = 1.7 Hz, 1H), 7.86 (dd, J = 1.1, 7.4 Hz, 1H), 7.81 (d, J = 8.6 Hz, 1H), 7.64 (td, J_d = 1.1, J_t = 7.4 Hz, 1H), 7.52 - 7.59 (m, 3H), 7.46 (d, J = 7.4 Hz, 2H), 7.32 (td, J_d = 1.7, J_t = 6.9 Hz, 2H), 7.23 - 7.27 (m, 1H), 4.60 (s, 2H).

^{13}C NMR (126 MHz, DMSO-d_6) δ 168.1, 167.9, 164.8, 149.3, 139.3, 137.1, 137.0, 135.8, 132.3, 130.4, 130.1, 130.0, 129.6 (2C), 129.1 (2C), 128.4, 128.2, 121.7, 119.5, 112.1, 37.3.

HRMS (ESI): $C_{22}H_{17}N_2O_3S_2$ $[M+H]^+$, Calculated: 421.06806, Found: 421.06649.

Following a reported procedure,[1] a mixture of acetic anhydride (0.02 mL, 0.02 g, 0.21 mmol) and triethylamine (0.06 mL, 0.04 g, 0.43 mmol) was added drop wise to a suspension of compound **2.15** (0.03 g, 0.07 mmol) in dry 1,4 dioxane (6 mL). The

suspension turned to clear solution upon completion of the addition. The reaction mixture was allowed to stir at room temperature for 17 hours (Figure 50). The mixture was poured into ice and the product was precipitated instantly. The product was collected by filtration, washed with water, sodium bicarbonate solution, water, and dried on vacuum to obtain the desired product as a pale yellow powder (0.027 g, yield 96%).

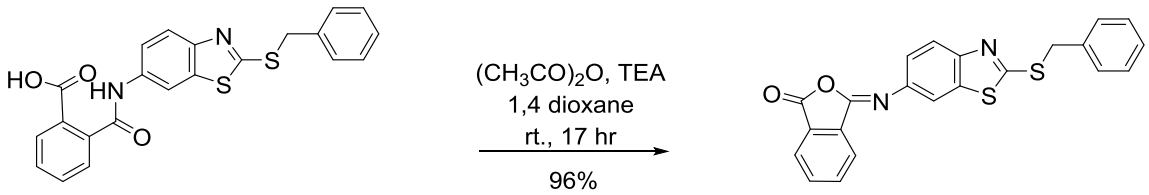

2.15 **2.16**

Figure 50. Synthesis of Compound **2.16**.

^{1}H NMR (500 MHz, $CDCl_3$) δ 7.93 - 8.02 (m, 3H), 7.78 - 7.86 (m, 3H), 7.49 (dd, *J* = 1.7, 8.6 Hz, 1H), 7.45 (d, *J* = 7.4 Hz, 2H), 7.33 (t, *J* = 7.4 Hz, 2H), 7.29 (d, *J* = 7.4 Hz, 1H), 4.62 (s, 2H).

^{13}C NMR (126 MHz, $CDCl_3$) δ 168.1, 167.4 (2C), 152.6, 136.1, 135.9, 134.7 (2C), 131.7, 129.2 (2C), 128.9 (2C), 127.89, 127.95, 124.9 (2C), 124.0 (2C), 121.8, 119.4, 37.8.

HRMS (ESI): $C_{22}H_{15}N_2O_2S_2$ $[M+H]^+$, Calculated: 403.05749, Found: 403.05574.

Morpholine (0.02 mL, 0.02 g, 0.22 mmol) was added to a solution of compound **2.16** (0.015 g, 0.037 mmol) in THF (6 mL) and the mixture was stirred at 50 °C for 2 hours then at 35 °C for 15 hours (Figure 51). THF was removed under reduced pressure and water (10 mL) was added to the resultant residue. The mixture was acidified to pH~2 using hydrochloric acid (1 M) and the product was extracted with ethyl acetate (3 X 15

mL). All organic layers were combined, washed with water (4 X 15 mL), dried over sodium sulfate, and concentrated under reduced pressure. The product was precipitated by addition of cold hexane to yield 0.018 g of white yellowish crystal (100%).

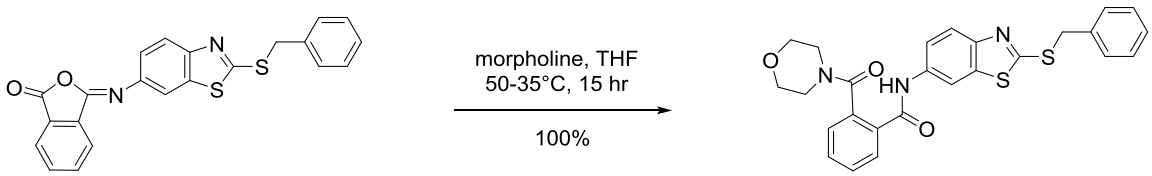

2.16 **2.8**

Figure 51. Synthesis of Analog **2.8**.

^{1}H NMR (500 MHz, $CDCl_3$) δ 9.22 (s, 1H), 8.38 (d, *J* = 1.7 Hz, 1H), 7.83 (dd, *J* = 1.7, 6.9 Hz, 1H), 7.77 (d, *J* = 9.2 Hz, 1H), 7.42 - 7.50 (m, 4H), 7.37 (dd, *J* = 2.3, 8.6 Hz, 1H), 7.27 - 7.35 (m, 3H), 7.22 (dd, *J* = 1.7, 7.4 Hz, 1H), 4.58 (s, 2H), 3.97 (br. s, 1H), 3.66 (br. s, 3H), 3.58 (t, *J* = 4.6 Hz, 2H), 3.24 (t, *J* = 4.6 Hz, 2H).

^{13}C NMR (126 MHz, $CDCl_3$) δ 170.5, 165.8, 165.6, 150.0, 136.3, 136.1, 134.9, 134.3, 133.7, 131.3, 129.6, 129.5, 129.3 (2C), 128.8 (2C), 127.9, 126.2, 121.5, 118.8, 111.9, 66.7 (2C), 48.0, 42.6, 37.9.

HRMS (ESI): $C_{26}H_{24}N_3O_3S_2$ $[M+H]^+$, Calculated: 490.12591, Found: 490.12318.

To a solution of NaOH (0.03g, 0.76 mmol) in ethanol (6 mL) under 0 °C was added compound **2.12** (0.13 g, 0.38 mmol) and 4-(chloromethyl)pyridine hydrochloride (0.06 g, 0.38 mmol). The mixture was stirred at 0 °C for 30 minutes and then at room temperature for 17 hours (Figure 52). The ethanol was removed under reduced pressure and water (20 mL) was added to the residue. The aqueous layer was washed with dichloromethane (3 x 20 mL) and then acidified to pH~2 using hydrochloric acid (1 M).

The aqueous layer was then placed on an ice bath and the resultant precipitate was collected by vacuum filtration, washed with water, and dried on vacuum to yield the desired product as a pale yellow powder (0.15 g, 94%).

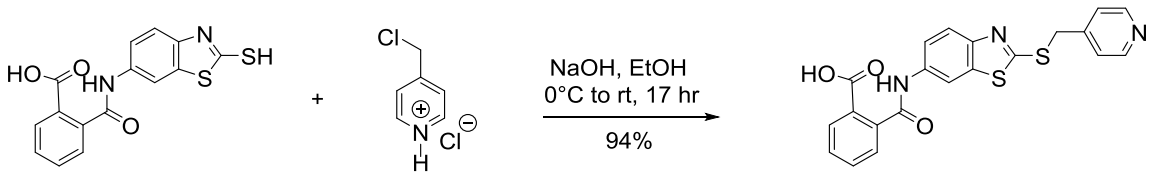

2.12 **2.17**

Figure 52. Synthesis of Compound **2.17**.

^{1}H NMR (500 MHz, DMSO-d_6) δ 12.99 (br.s, 1H), 10.63 (s, 1H), 8.73 (d, *J* = 6.3 Hz, 2H), 8.46 (d, *J* = 1.7 Hz, 1H), 7.94 (d, *J* = 6.3 Hz, 2H), 7.85 (dd, *J* = 1.1, 7.4 Hz, 1H), 7.78 (d, *J* = 8.6 Hz, 1H), 7.58 - 7.65 (m, 2H), 7.51 - 7.57 (m, 2H), 4.80 (s, 2H).

^{13}C NMR (126 MHz, DMSO-d_6) δ 168.1, 167.9, 163.4, 149.0, 144.0 (2C), 139.2, 137.3, 136.1, 132.4, 130.4, 130.15, 130.07, 128.3, 127.0 (3C), 121.8, 119.6, 112.2, 35.8.

HRMS (ESI): $C_{21}H_{16}N_3O_3S_2$ $[M+H]^+$, Calculated: 422.06331, Found: 422.06170.

A mixture of acetic anhydride (0.07 mL, 0.07 g, 0.71 mmol) and triethylamine (0.2 mL, 0.14 g, 1.42 mmol) was added drop wise to a suspension of compound **2.17** (0.10 g, 0.24 mmol) in dry 1,4 dioxane (6 mL). The suspension turned to clear pale yellowish solution upon completion of the addition. The reaction mixture was allowed to stir at room temp for 17 hours (Figure 53). The mixture was poured into ice and product was precipitated instantly. The product was collected by filtration, washed with water, sodium bicarbonate solution, water, and dried on vacuum to obtain the desired product as a yellow powder (0.08 g, yield 87%).

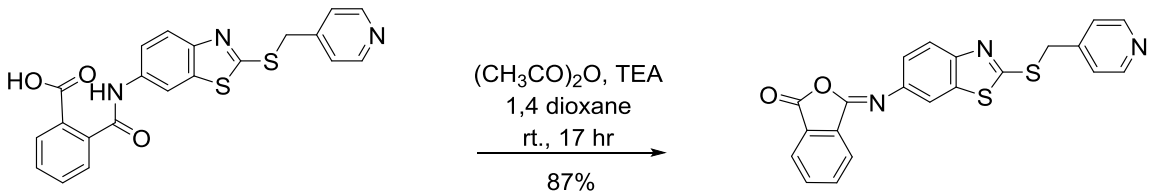

2.17 **2.18**

Figure 53. Synthesis of Compound **2.18**.

^{1}H NMR (500 MHz, $CDCl_3$) δ 8.57 (d, *J* = 6.3 Hz, 2H), 7.95 - 8.01 (m, 3H), 7.85 (d, *J* = 1.7 Hz, 1H), 7.82 (dd, *J* = 2.9, 5.2 Hz, 2H), 7.51 (dd, *J* = 2.3, 8.6 Hz, 1H), 7.39 (d, *J* = 5.2 Hz, 2H), 4.58 (s, 2H).

^{13}C NMR (126 MHz, $CDCl_3$) δ 167.4 (2C), 166.7, 152.4, 150.2 (3C), 145.8, 136.0, 134.7 (3C), 131.7, 128.2, 125.0, 124.04 (2C), 124.01, 122.0, 119.5, 36.1.

HRMS (ESI): $C_{21}H_{14}N_3O_3S_2$ $[M+H]^+$, Calculated: 404.05274, Found: 404.05149.

Morpholine (0.03 mL, 0.03 g, 0.30 mmol) was added to a solution of compound **2.18** (0.02 g, 0.05 mmol) in THF (6 mL) and the mixture was stirred at 50 °C for 2 hours then at 35 °C for 15 hours (Figure 54). THF was removed under reduced pressure and water (10 mL) was added to the resultant residue. The mixture was acidified to pH~2 using hydrochloric acid (1 M) and the product was extracted with ethyl acetate (3 X 15 mL). All organic layers were combined, washed with water (4 X 15 mL), dried over sodium sulfate, and concentrated under reduced pressure. The product was crystallized by addition of cold hexane to yield 0.024 g of pale yellowish crystal (99%).

^{1}H NMR (500 MHz, $CDCl_3$) δ 9.82 (s, 1H), 8.54 (d, *J* = 6.3 Hz, 2H), 8.23 (d, *J* = 2.3 Hz, 1H), 7.69 (d, *J* = 6.9 Hz, 1H), 7.63 (d, *J* = 8.6 Hz, 1H), 7.37 (d, *J* = 1.7 Hz, 2H), 7.35 (d,

J = 2.3 Hz, 1H), 7.26 - 7.33 (m, 2H), 7.07 (d, *J* = 6.9 Hz, 1H), 4.50 (s, 2H), 3.97 (br. s., 1H), 3.75 (br. s., 2H), 3.65 (br. s, 3H), 3.25 (t, *J* = 4.6 Hz, 2H).

^{13}C NMR (126 MHz, CHLOROFORM-d) δ 170.5, 165.6, 164.3, 150.2 (2C), 149.8, 145.9, 136.5, 135.1, 134.2, 133.6, 131.4, 129.7, 129.6, 126.3, 124.1 (2C), 121.7, 118.9, 111.9, 66.7 (2C), 48.1, 42.6, 36.2.

HRMS (ESI): $C_{25}H_{23}N_4O_3S_2$ $[M+H]^+$, Calculated: 491.12116, Found: 491.11949.

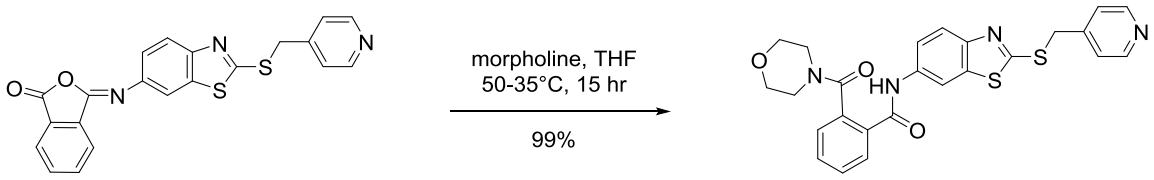

2.18 **2.9**

Figure 54. Synthesis of Analog **2.9**.

Phthalic anhydride (0.20 g, 1.35 mmol) was added to a solution of 5-amino-2-mercaptobenzoimidazole (0.22 g, 1.35 mmol) in THF (20 mL) and the mixture was stirred at room temperature for 17 hours (Figure 55). THF was then evaporated under reduced pressure and the product was precipitated out of ethanol/ water mixture (0.40 g, yield 95%).

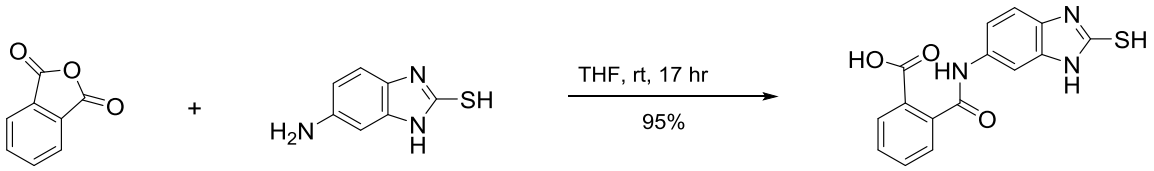

2.19

Figure 55. Synthesis of Compound **2.19**.

^{1}H NMR (500 MHz, DMSO-d_6) δ 12.96 (br. s, 1H), 12.42 (s, 2H), 10.34 (br. s., 1H), 7.82 - 7.85 (m, 1H), 7.79 (d, J = 1.7 Hz, 1H), 7.62 (dt, J_d = 1.1, J_t = 7.4 Hz, 1H), 7.49 - 7.56 (m, 2H), 7.23 (dd, J = 1.7, 8.6 Hz, 1H), 7.04 (d, J = 8.6 Hz, 1H).

^{13}C NMR (126 MHz, DMSO-d_6) δ 168.6, 168.0, 167.7, 139.4, 135.4, 132.8, 132.2, 130.6, 130.0, 129.9, 128.8, 128.3, 115.1, 109.8, 101.5.

HRMS (ESI): $C_{15}H_{12}ClN_3O_3S$ $[M+H]^+$, Calculated: 314.05994, Found: 314.05894.

To a solution of NaOH (0.02 g, 0.48 mmol) in ethanol (5 mL) at 0 °C was added compound **2.19** (0.10 g, 0.32 mmol) and 4-chlorobenzyl chloride (0.05 g, 0.32 mmol). The mixture was stirred at 0 °C for 30 minutes and then at room temperature for 17 hours (Figure 56). The ethanol was removed under reduced pressure and water (20 mL) was added to the residue. The aqueous layer was washed with dichloromethane (3 X 15 ml) and then acidified to pH~2 using hydrochloric acid (1 M). The aqueous layer was then placed on ice bath and the resultant precipitate was collected by vacuum filtration, washed with water, and dried on vacuum to yield the desired product as a yellowish white powder (0.09 g, 66%).

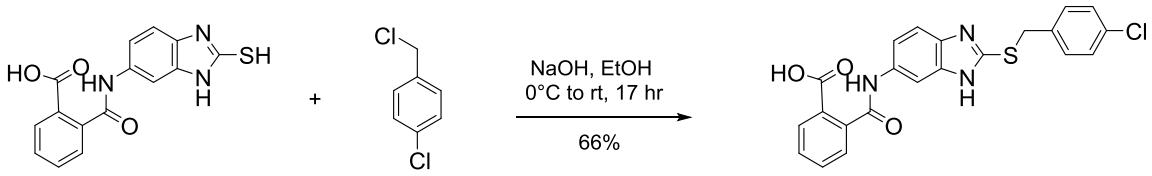

2.19 **2.20**

Figure 56. Synthesis of Compound **2.20**.

^{1}H NMR (500 MHz, DMSO-d_6) δ 12.98 (br. s, 1H), 12.51 (br. s, 1H), 10.29 (s, 1H), 8.02 (s, 1H), 7.87 (dd, *J* = 1.1, 7.4 Hz, 1H), 7.65 (td, J_d = 1.1, J_t = 7.4 Hz, 1H), 7.53 - 7.60 (m, 2H), 7.46 (d, *J* = 8.0 Hz, 2H), 7.37 (d, *J* = 8.6 Hz, 2H), 7.27 (br. s, 2H), 4.54 (s, 2H).

^{13}C NMR (126 MHz, DMSO-d_6) δ 168.1, 167.6, 139.6, 137.7, 132.4, 132.2 (2C), 131.2 (5C), 130.6, 130.0, 129.8, 129.0 (4C), 128.3 (2C), 35.0.

HRMS (ESI): $C_{22}H_{17}ClN_3O_3S$ $[M+H]^+$, Calculated: 438.06791, Found: 438.06628.

A mixture of acetic anhydride (0.02 mL, 0.02 g, 0.21 mmol) and triethylamine (0.06 mL, 0.04 g, 0.41 mmol) was added drop wise to a suspension of compound **2.20** (0.03 g, 0.07 mmol) in dry 1,4 dioxane (6 mL) (Figure 57). The suspension turned to clear yellowish solution upon completion of the addition. The reaction mixture was allowed to stir at room temp for 17 hours. The mixture was poured into ice and product was precipitated instantly. The product was collected by vacuum filtration, washed with water, sodium bicarbonate solution, water, and dried on vacuum to obtain the desired product as paige powder (0.028 g, yield 97%).

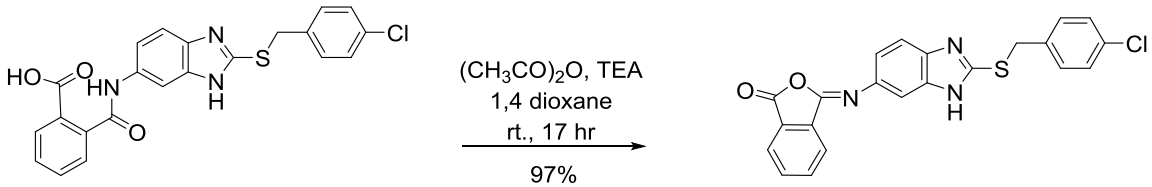

2.20 **2.21**

Figure 57. Synthesis of Compound **2.21**.

^{1}H NMR (500 MHz, $CDCl_3$) δ 7.97 (dd, *J* = 2.9, 5.2 Hz, 2H), 7.80 (dd, *J* = 3.1, 5.4 Hz, 2H), 7.49 - 7.62 (m, 2H), 7.33 (d, *J* = 8.6 Hz, 2H), 7.26 (d, *J* = 8.6 Hz, 2H), 7.21 (dd, *J* = 1.7, 8.6 Hz, 1H), 4.52 (s, 2H).

^{13}C NMR (126 MHz, $CDCl_3$) δ 167.9 (2C), 151.1, 135.5, 134.5 (4C), 133.7, 131.9 (2C), 130.4 (2C), 129.0 (2C), 126.1, 123.9 (3C), 121.5 (2C), 36.4.

HRMS (ESI): $C_{22}H_{15}ClN_3O_2S$ $[M+H]^+$, Calculated: 420.05735, Found: 420.05586.

Morpholine (0.02 mL, 0.02 g, 0.21 mmol) was added to a solution of compound **2.21** (0.02 g, 0.04 mmol) in THF (6 mL) and the mixture was stirred at 50 °C for 2 hours then at 35 °C for 15 hours (Figure 58). THF was removed under reduced pressure and water (15 mL) was added to the resultant residue. The mixture was acidified to pH~2 using hydrochloric acid (1 M). The product was extracted with ethyl acetate (3 X 20 mL), washed with water (4 X 15 mL), and dried over sodium sulfate. The product was crystallized from ethyl acetate/ hexane, filtered and dried under vacuum to obtain 0.017 g of a pale yellow product (93%).

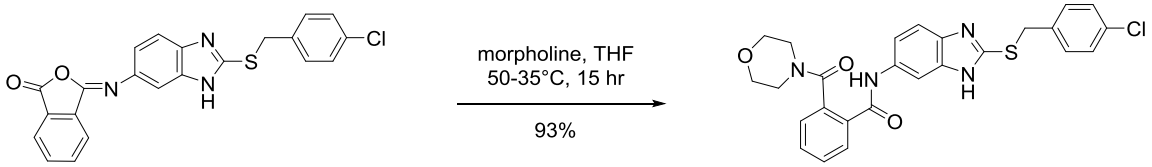

2.21 **2.10**

Figure 58. Synthesis of Compound **2.10**.

^{1}H NMR (500 MHz, $CDCl_3$) δ 10.13 (br. s, 1H), 8.90 (s, 1H), 8.05 (s, 1H), 7.88 (d, *J* = 6.9 Hz, 1H), 7.45 - 7.59 (m, 3H), 7.26 - 7.32 (m, 3H), 7.23 (d, *J* = 8.6 Hz, 2H), 7.04 (s, 1H), 4.45 (s, 2H), 3.94 (br. s, 1H), 3.63 (br. s, 3H), 3.50 (br. s, 2H), 3.21 (br. s., 2H).

^{13}C NMR (126 MHz, $CDCl_3$) δ170.6, 168.0, 165.8, 149.9, 135.6, 134.7, 134.6, 133.9, 133.5, 132.8, 131.8, 131.4, 130.4 (2C), 129.7, 129.2, 128.9, 128.9 (2C), 126.4, 123.9, 66.64, 66.61, 48.0, 42.5, 36.3.

HRMS (ESI): $C_{26}H_{24}ClN_4O_3S$ $[M+H]^+$, Calculated: 507.12576, Found: 507.12397.

To a solution of 1-phenylethyl mercaptan (0.06 g, 0.06 mL, 0.47 mmol) in DMF (3 mL) was added 60% NaH (0.02 g, 0.47 mmol) in mineral oil (Caution: 1-Phenylethyl mercaptan has an unpleasant odor[17]). The mixture stirred for 10 minutes before a solution of 2-chloro, 6-nitrobenzothiazole (0.1 g, 0.47 mmol) in DMF (1 mL) was added (Figure 59). After 4 hours the complete conversion of starting materials to product was observed by TLC (Ethyl acetate: hexane; 10:90%). Water (10 mL) was added to the reaction mixture followed by ethyl acetate (30 mL). The organic layer was separated and concentrated. Cold hexane was added to precipitate 0.12 g of the product in 80% yield.

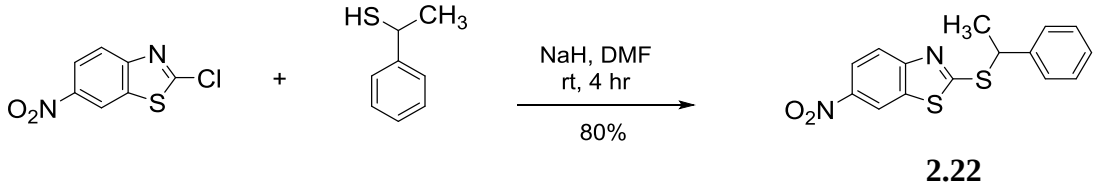

2.22

Figure 59. Synthesis of Compound **2.22**.

^{1}H NMR (500 MHz, $CDCl_3$) δ 8.64 (d, *J* = 2.3 Hz, 1H), 8.29 (dd, *J* = 2.3, 8.6 Hz, 1H), 7.92 (d, *J* = 9.2 Hz, 1H), 7.48 (d, *J* = 7.4 Hz, 2H), 7.36 (t, *J* = 7.4 Hz, 2H), 7.29 (t, *J* = 7.4 Hz, 1H), 5.23 (q, *J* = 7.1 Hz, 1H), 1.88 (d, *J* = 7.1 Hz, 3H).

^{13}C NMR (126 MHz, $CDCl_3$) δ 173.4, 157.0, 144.2, 141.3, 135.7, 128.9 (2C), 128.2, 127.5 (2C), 122.0, 121.5, 117.5, 47.9, 22.7.

To a solution of compound **2.22** (0.10 g, 0.32 mmol) in ethanol (10 mL) was added 20% Pd/C (0.02 g) and the system was pressurized with a balloon fill with H_2. The closed system was stirred at 50 °C for 4 hours (Figure 60). The mixture was filtered

through celite and washed with ethanol and chloroform. The solvent was evaporated under reduced pressure and the product (0.08 g) was carried on to the next step without further purification due to the unpleasant odor.

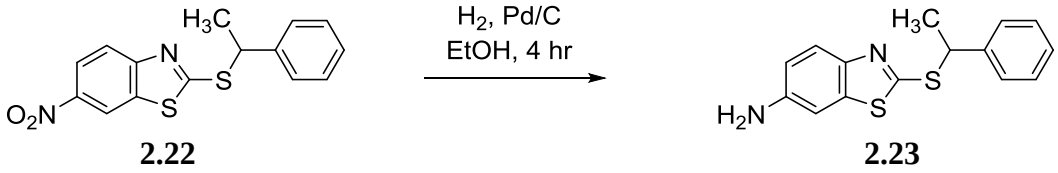

2.22 **2.23**

Figure 60. Synthesis of Compound **2.23**.

To a solution of compound **2.23** (0.06 g, 0.20 mmol) in THF (20 mL), was added phthalic anhydride (0.03 g, 0.20 mmol) and the mixture was stirred at room temperature for 17 hours (Figure 61). THF was then evaporated under reduced pressure and the product (0.083 g) was taken to the next step without further purification.

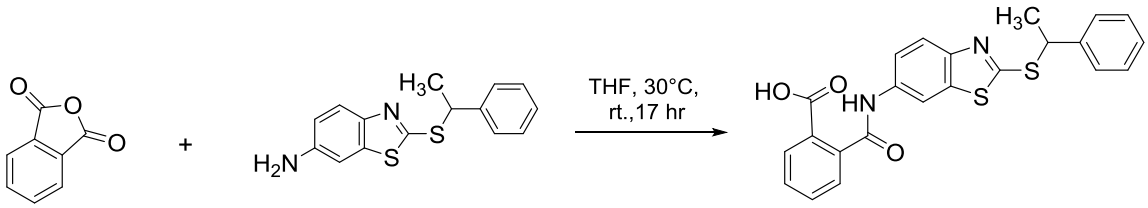

2.23 **2.24**

Figure 61. Synthesis of Compound **2.24**.

A mixture of acetic anhydride (0.05 mL, 0.05 g, 0.48 mmol) and triethyl amine (0.07 mL, 0.05 g, 0.48 mmol) was added drop wise to a suspension of compound **2.24** (0.073 g, 0.16 mmol) in dry 1,4 dioxane (12 mL). The reaction mixture was allowed to stir at room temp for 17 hours (Figure 62). Water (20 mL) was added to the reaction mixture and the product was extracted with ethyl acetate (3 X 20 mL). The organic layers

were combined and washed with sodium bicarbonate solution, water, dried over anhydrous Na_2SO_4, and evaporated to dryness. A yield of 0.045 g was obtained and was carried on to the next step without further purification.

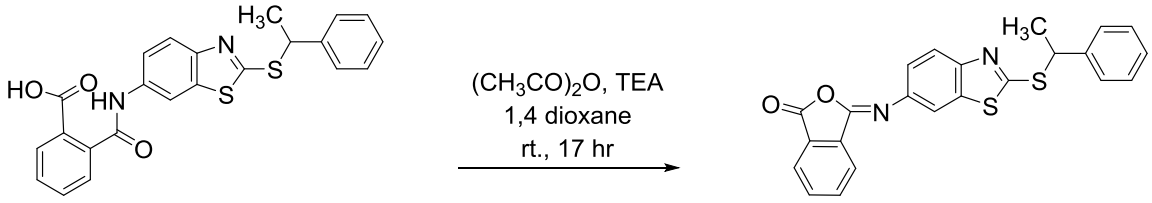

2.24 **2.25**

Figure 62. Synthesis of Compound **2.25**.

Morpholine (0.05 mL, 0.05 g, 0.58 mmol) was added to a solution of compound **2.25** (0.04 g, 0.1 mmol) in THF (10 mL) and the mixture was stirred at 50 °C for 3 hours then at 35 °C for 15 hours (Figure 63). THF was removed under reduced pressure and water (10 mL) was added to the resultant residue. The mixture was acidified to pH~2 using hydrochloric acid (1 M). The product was extracted with ethyl acetate (3 X 20 mL), washed with water (4 X 10 mL), and dried over sodium sulfate. The solvent was then evaporated and the crude mixture purified by column chromatography to obtain 0.036 g, yield 67%.

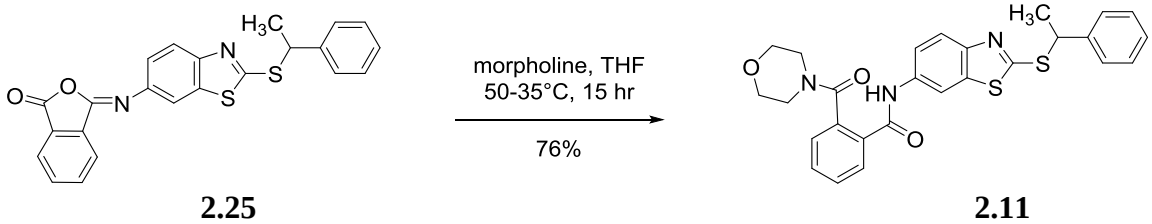

2.25 **2.11**

Figure 63. Synthesis of Analog **2.11**.

^{1}H NMR (500 MHz, $CDCl_3$) d 9.00 (s, 1H), 8.40 (d, *J* = 2.3 Hz, 1H), 7.88 (dd, *J* = 1.7, 6.9 Hz, 1H), 7.81 (d, *J* = 8.6 Hz, 1H), 7.49 - 7.56 (m, 2H), 7.47 (d, *J* = 8.0 Hz, 2H), 7.35 - 7.38 (m, 1H), 7.33 (d, *J* = 8.0 Hz, 2H), 7.26 - 7.29 (m, 2H), 5.11 (q, *J* = 6.9 Hz, 1H), 3.92 (br. s, 1H), 3.68 (br. s, 3H), 3.55 (br. s, 2H), 3.22 (t, *J* = 4.6 Hz, 2H), 1.84 (d, *J* = 6.9 Hz, 3H).

^{13}C NMR (126 MHz, $CDCl_3$) δ 170.4, 165.5, 165.3, 150.2, 141.9, 136.6, 134.8, 134.1, 133.6, 131.5, 129.8, 129.7, 128.8 (2C), 127.9, 127.5 (2C), 126.3, 121.8, 118.7, 111.9, 66.8 (2C), 48.0, 47.8, 42.5, 22.8.

HRMS (ESI): $C_{27}H_{26}N_3O_3S_2$ $[M+H]^+$, Calculated: 504.14156**,** Found: 504.13915.

NMR Spectra

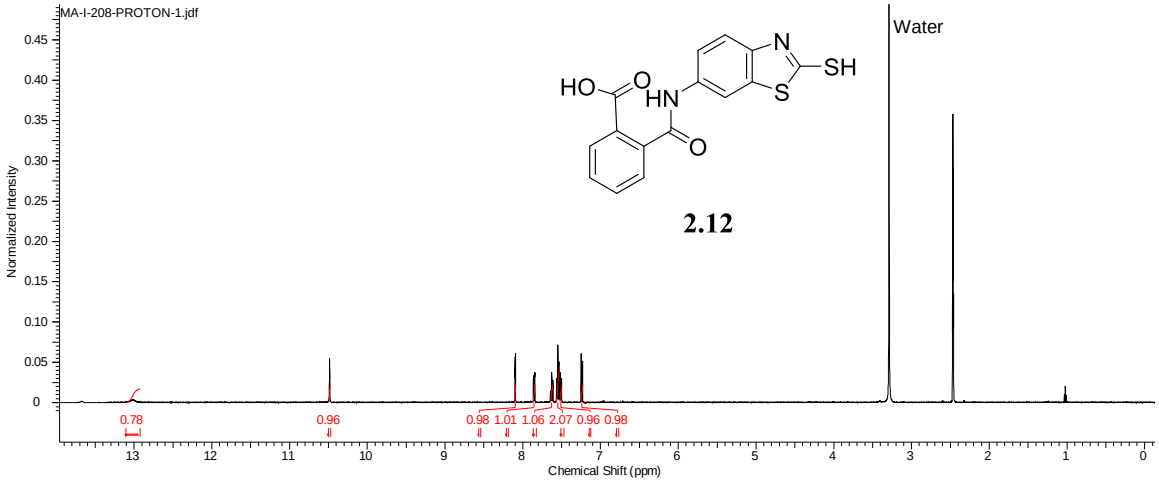

Figure 64. ^{1}H NMR Spectra of Compound **2.12**.

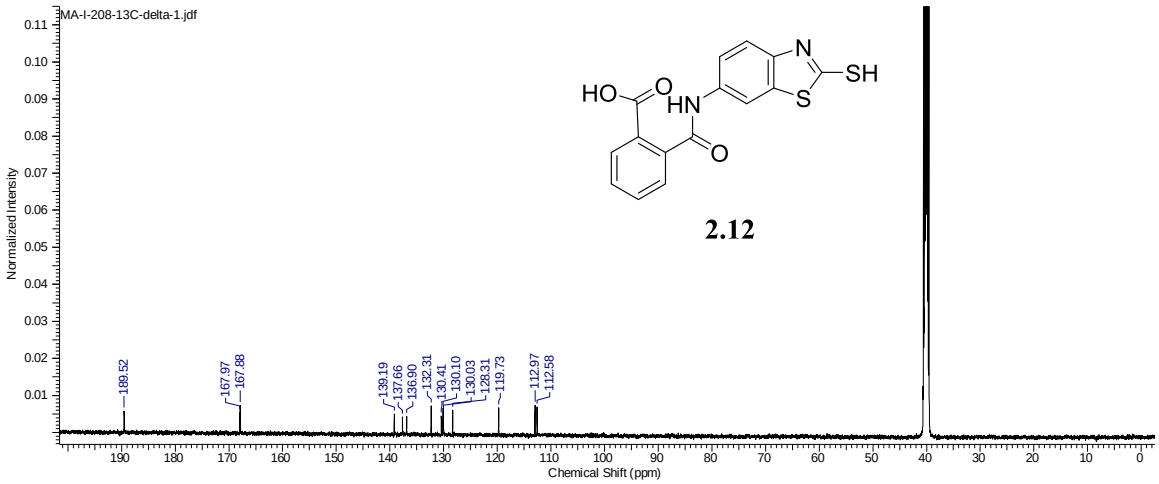

Figure 65. ^{13}C NMR Spectra of Compound **2.12**.

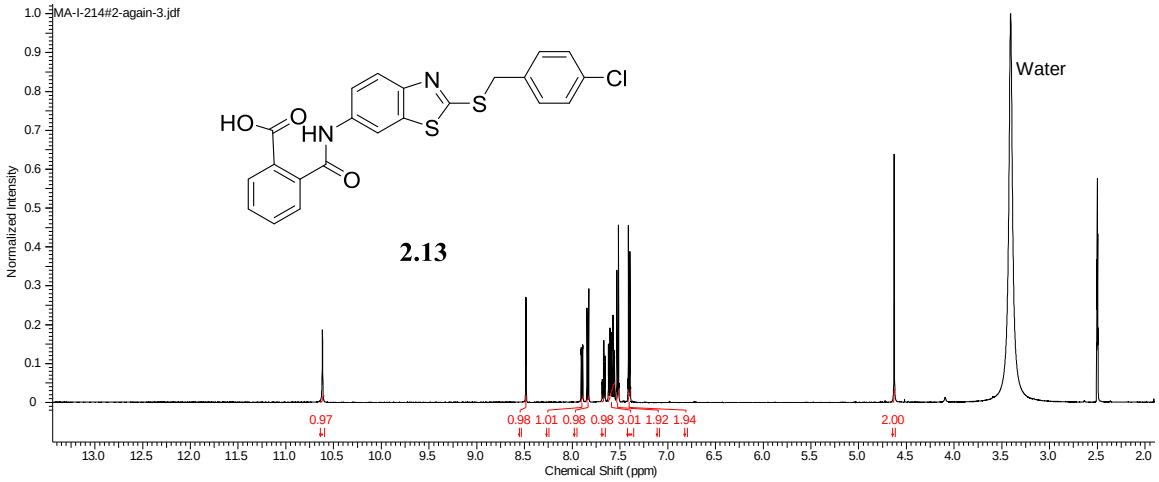

Figure 66. ^{1}H NMR Spectra of Compound **2.13**.

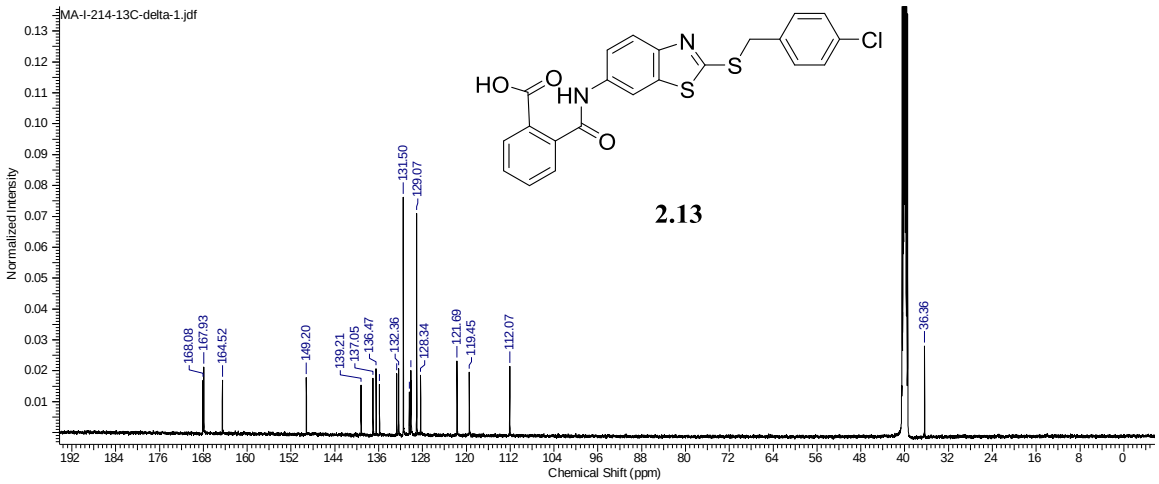

Figure 67. ^{13}C NMR Spectra of Compound **2.13**.

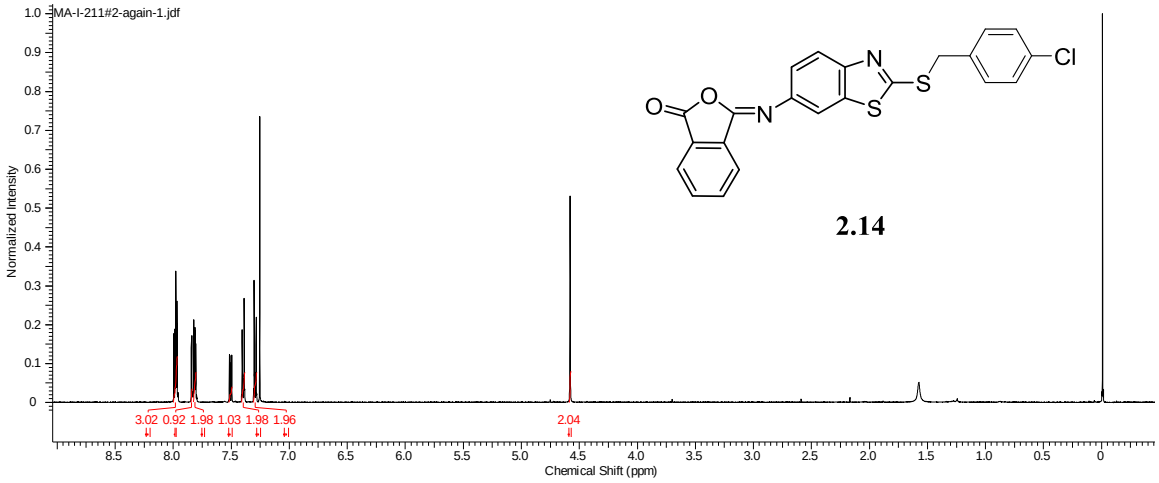

Figure 68. ^{1}H NMR Spectra of Compound **2.14**.

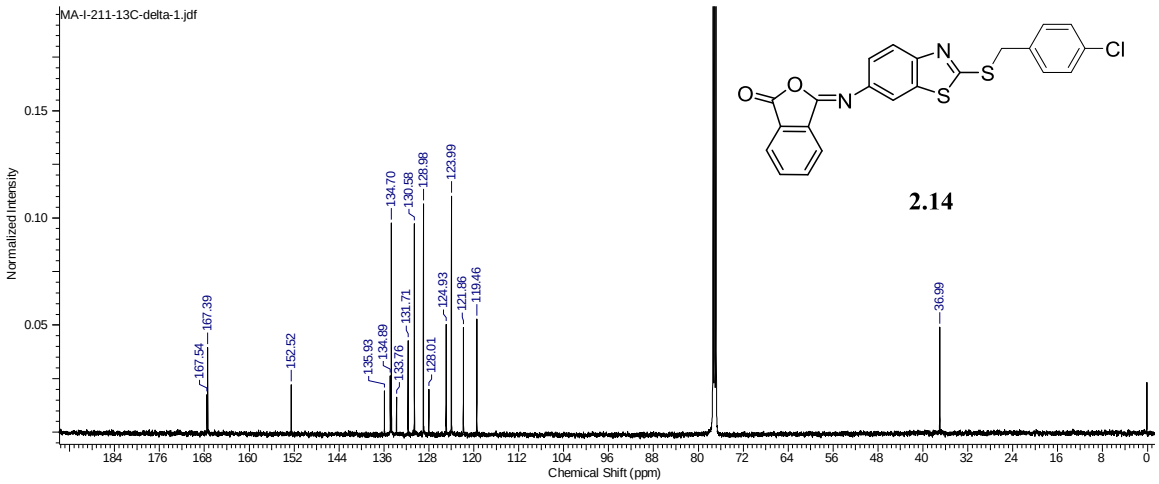

Figure 69. ^{13}C NMR Spectra of Compound **2.14**.

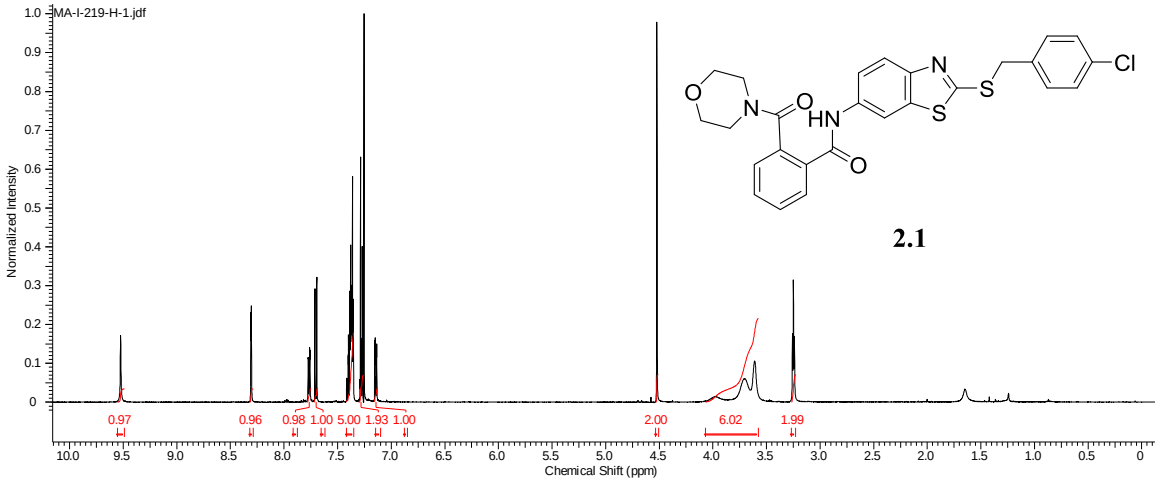

Figure 70. ^{1}H NMR Spectra of Compound **2.1**.

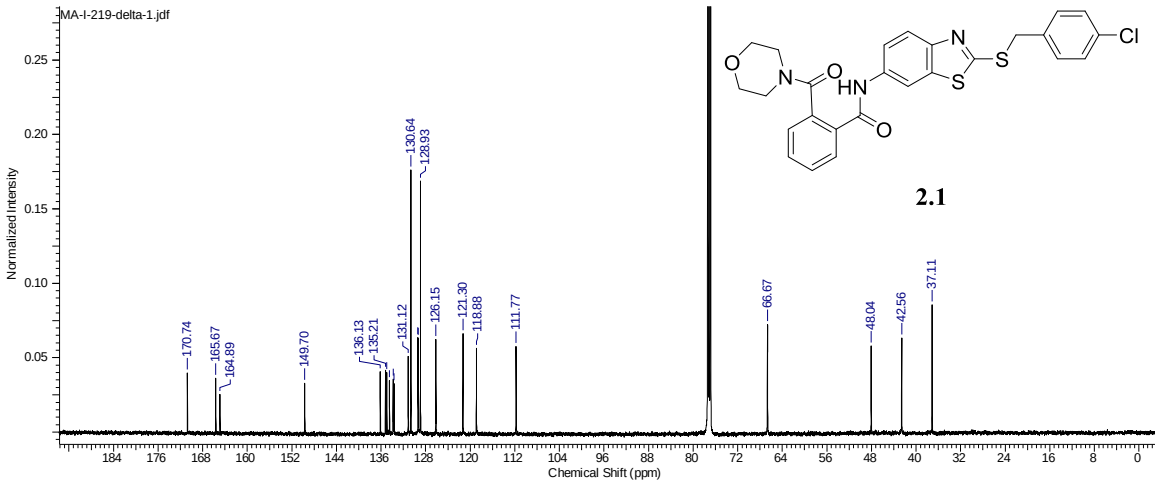

Figure 71. ^{13}C NMR Spectra of Compound **2.1**.

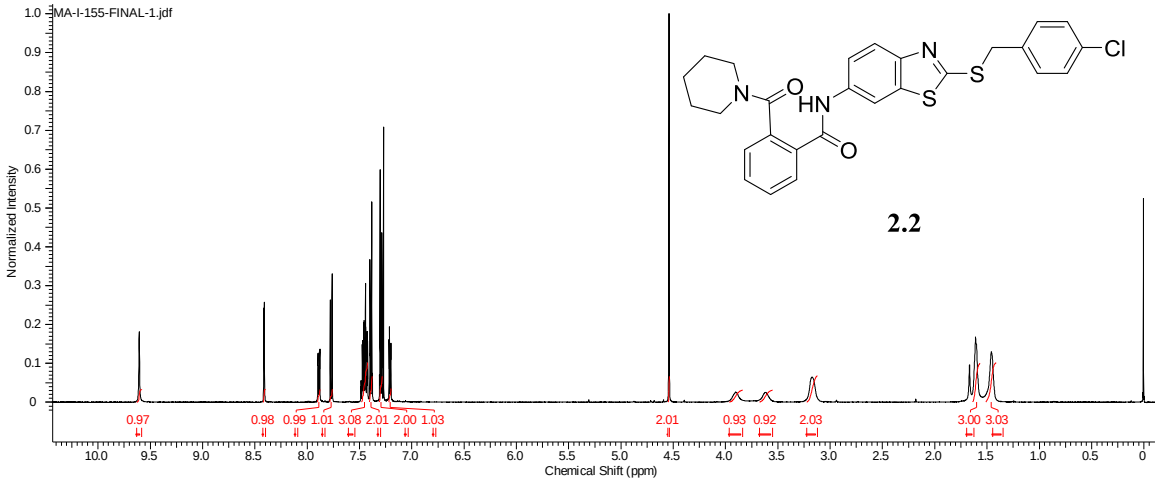

Figure 72. ^{1}H NMR Spectra of Compound **2.2**.

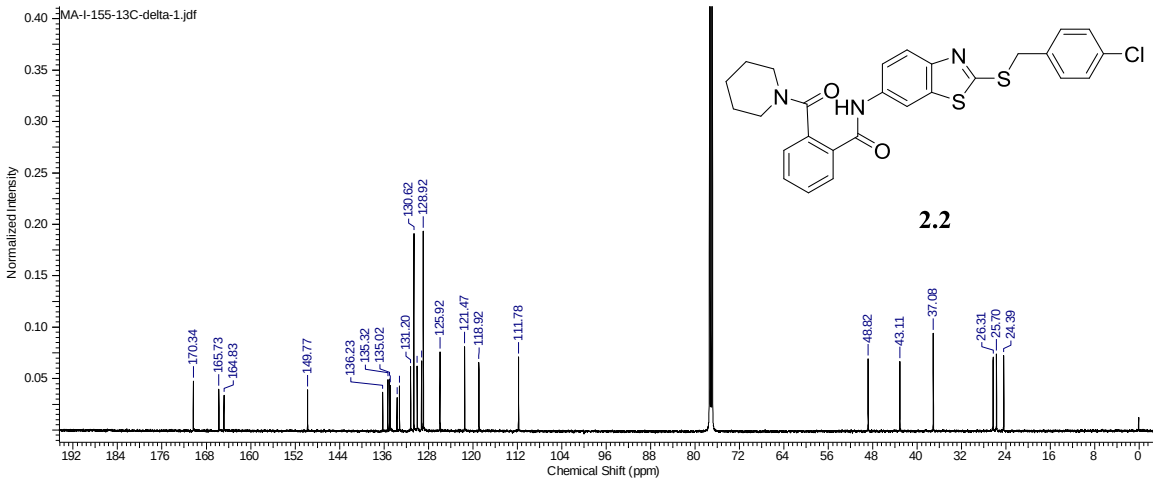

Figure 73. ^{13}C NMR Spectra of Compound **2.2**.

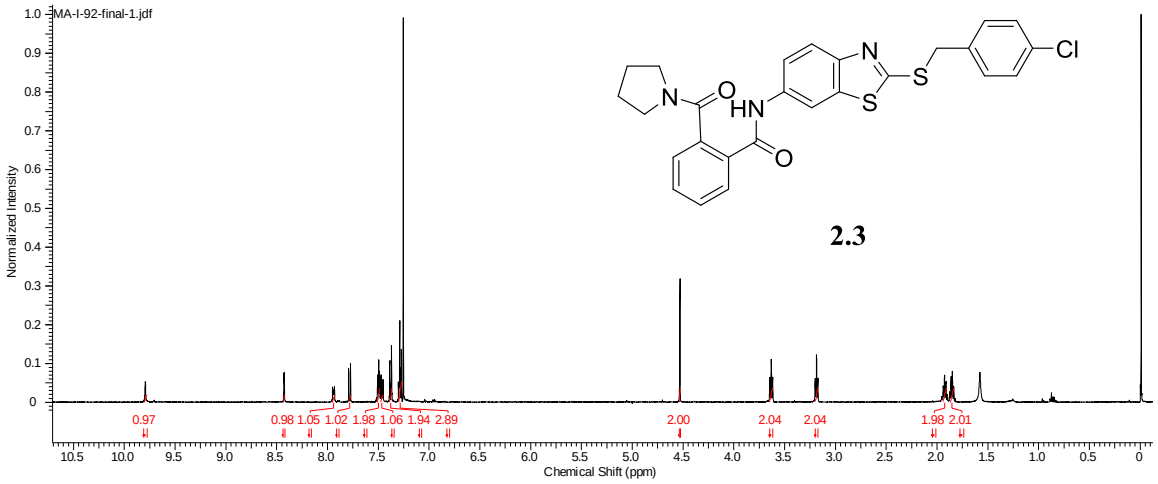

Figure 74. ^{1}H NMR Spectra of Compound **2.3**.

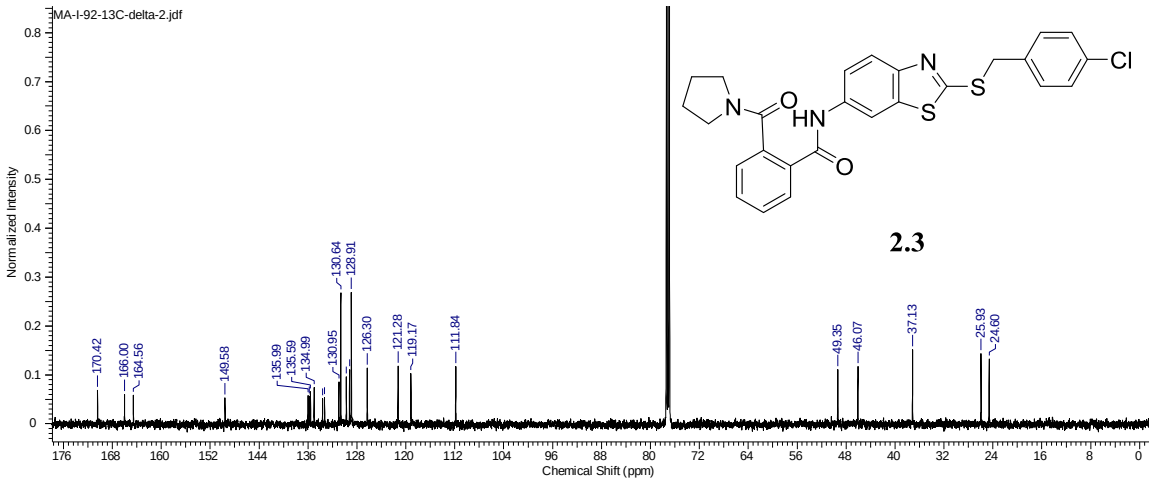

Figure 75. ^{13}C NMR Spectra of Compound **2.3**.

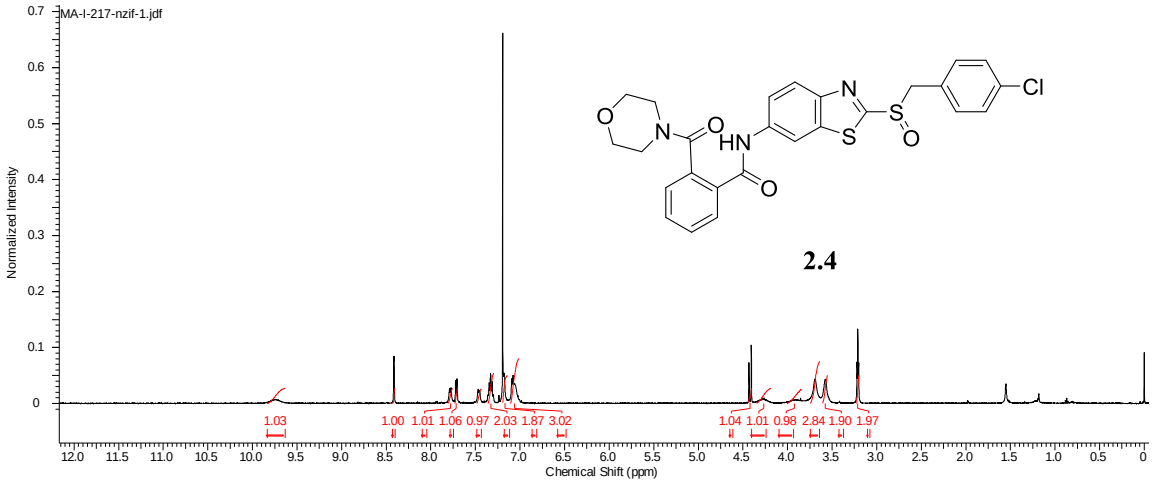

Figure 76. ^{1}H NMR Spectra of Compound **2.4**.

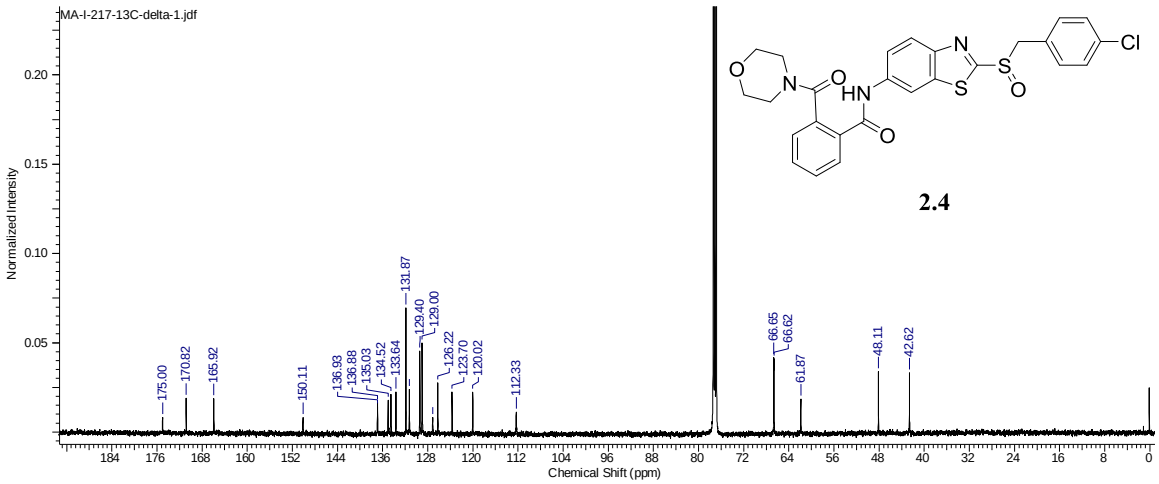

Figure 77. ^{13}C NMR Spectra of Compound **2.4**.

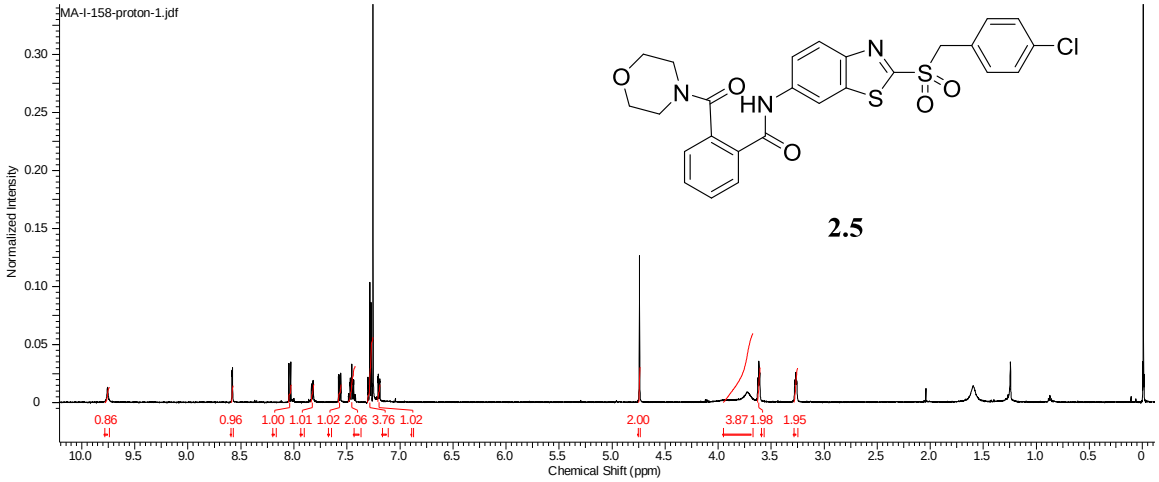

Figure 78. ^{1}H NMR Spectra of Compound **2.5**.

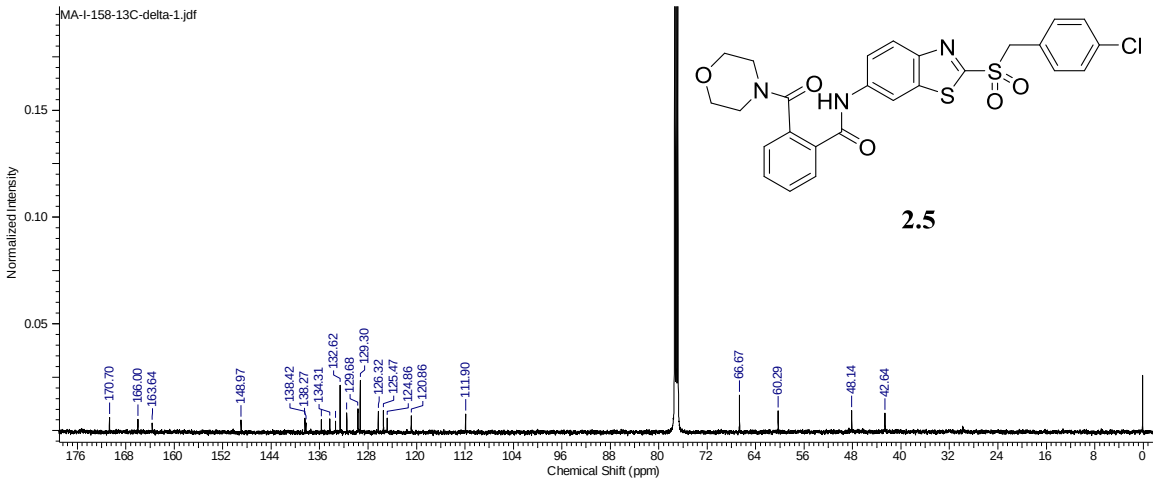

Figure 79. ^{13}C NMR Spectra of Compound **2.5**.

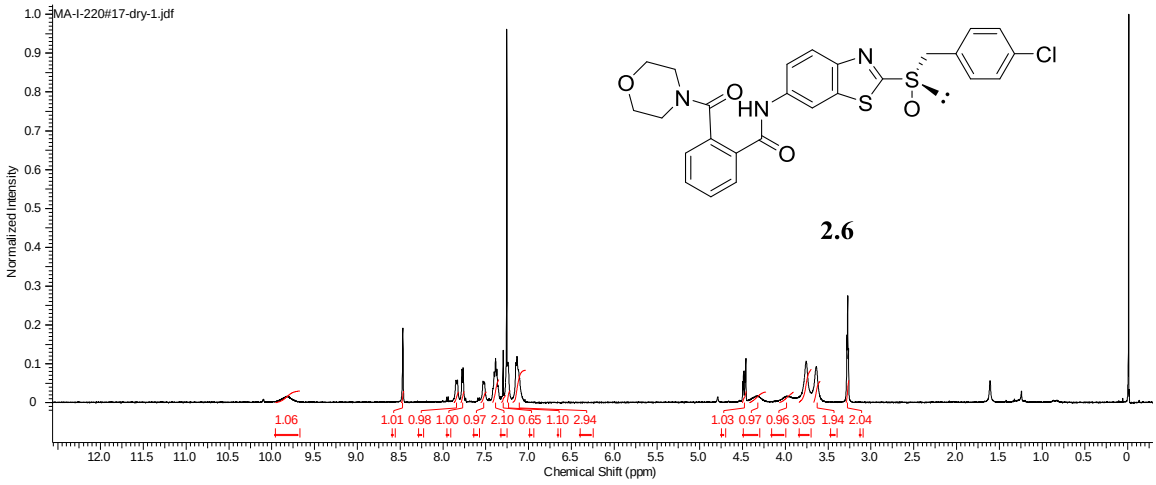

Figure 80. ^{1}H NMR Spectra of Compound **2.6**.

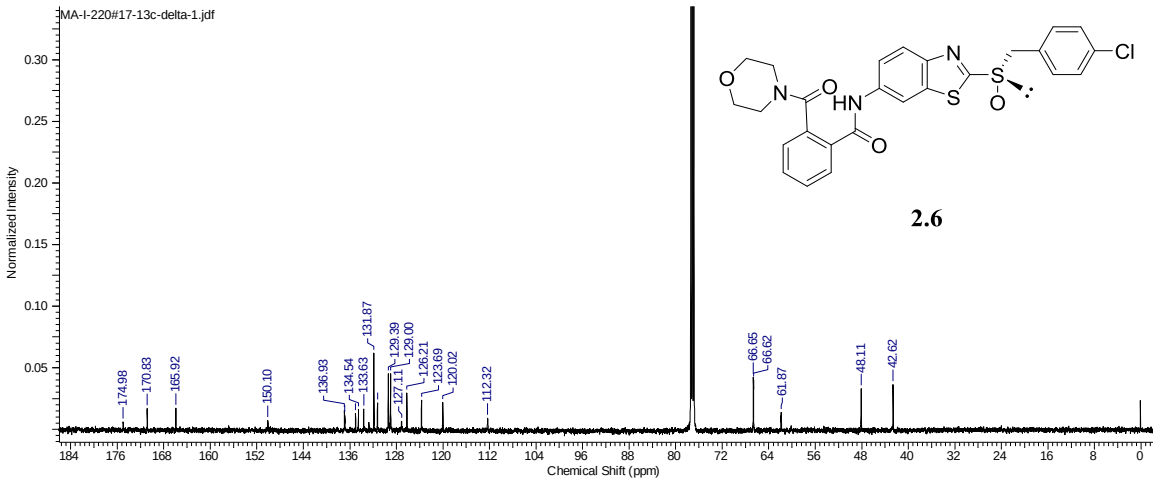

Figure 81. ^{13}C NMR Spectra of Compound **2.6**.

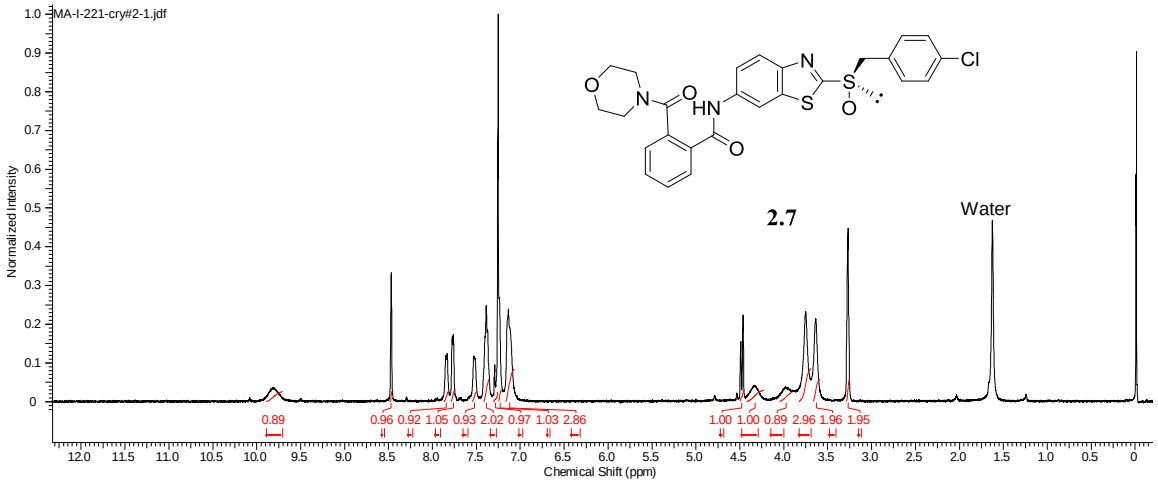

Figure 82. ^{1}H NMR Spectra of Compound **2.7**.

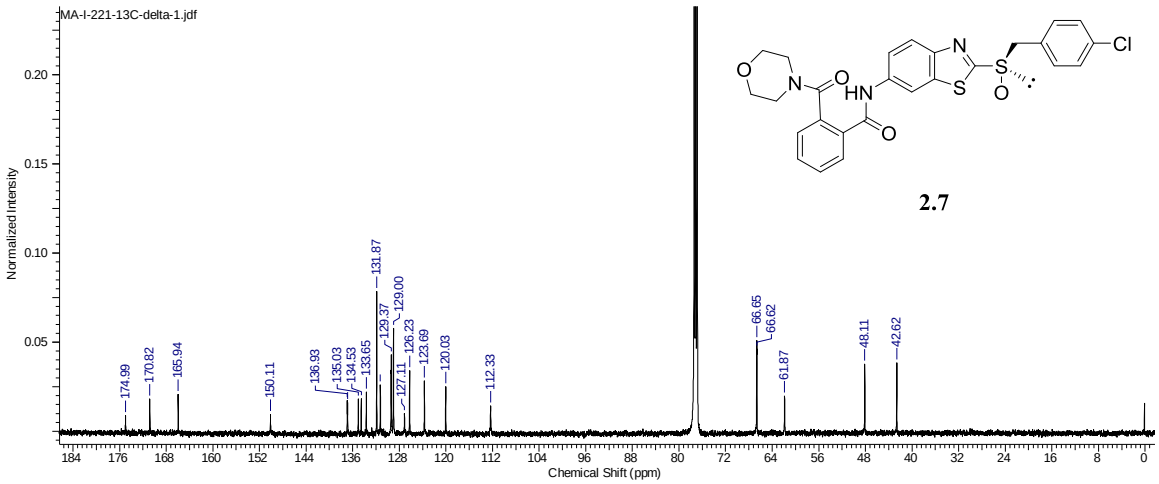

Figure 83. ^{13}C NMR Spectra of Compound **2.7**.

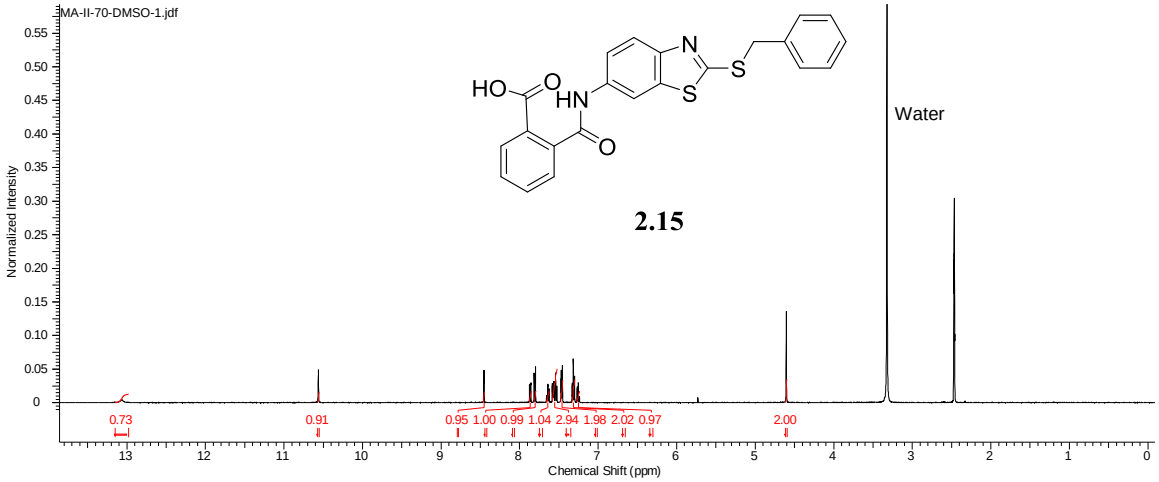

Figure 84. ^{1}H NMR Spectra of Compound **2.15**.

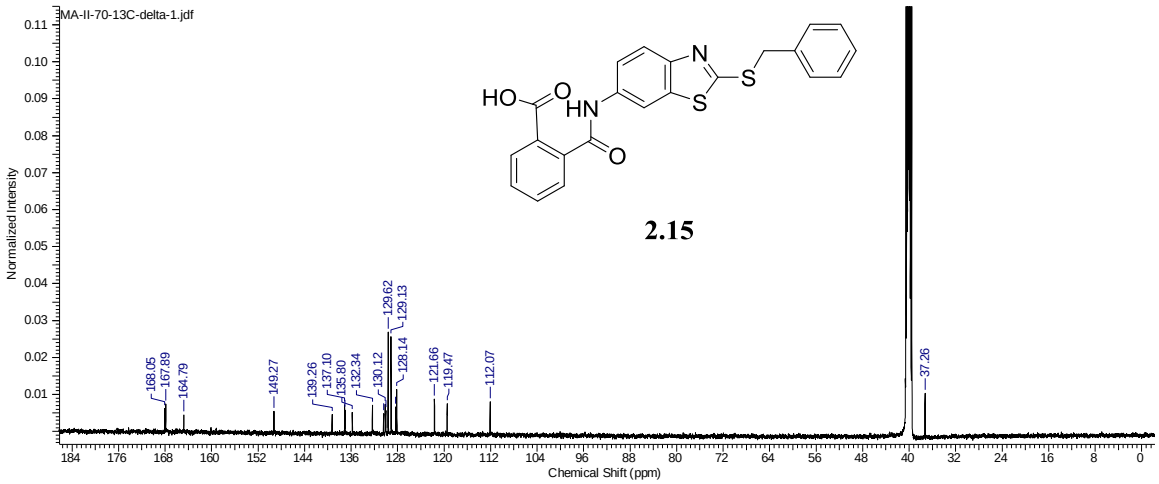

Figure 85. ^{13}C NMR Spectra of Compound **2.15**.

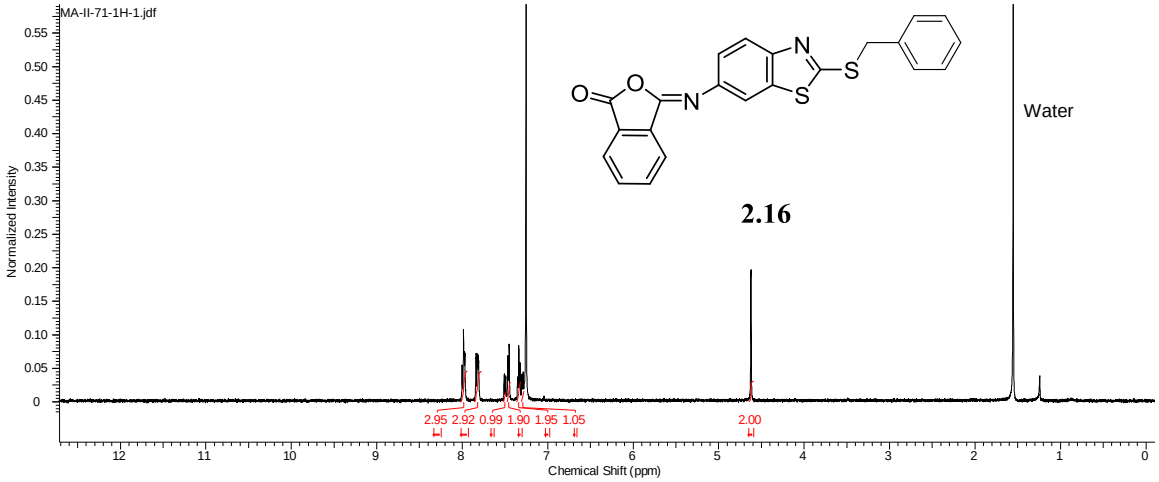

Figure 86. ^{1}H NMR Spectra of Compound **2.16**.

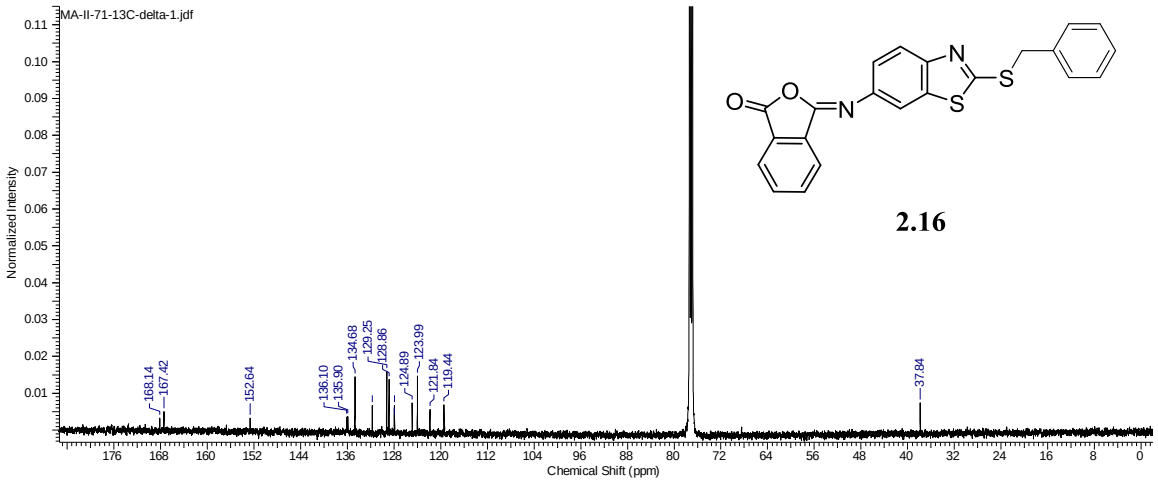

Figure 87. ^{13}C NMR Spectra of Compound **2.16**.

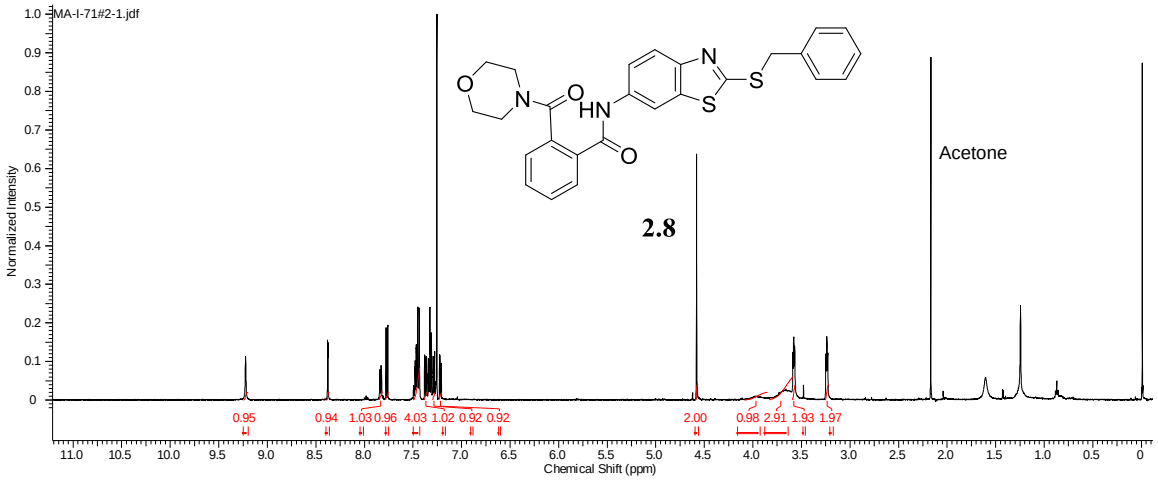

Figure 88. ^{1}H NMR Spectra of Compound **2.8**.

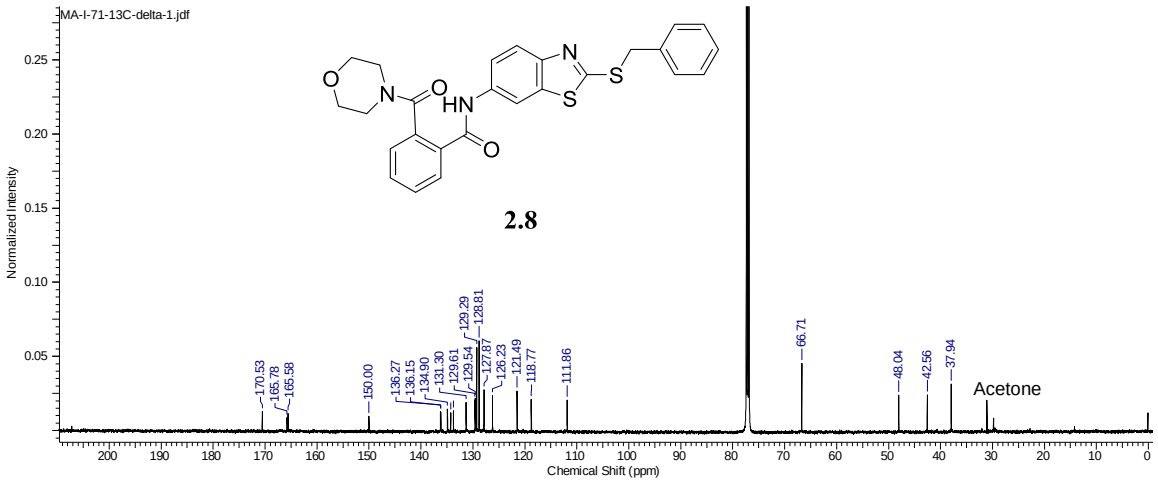

Figure 89. ^{13}C NMR Spectra of Compound **2.8**.

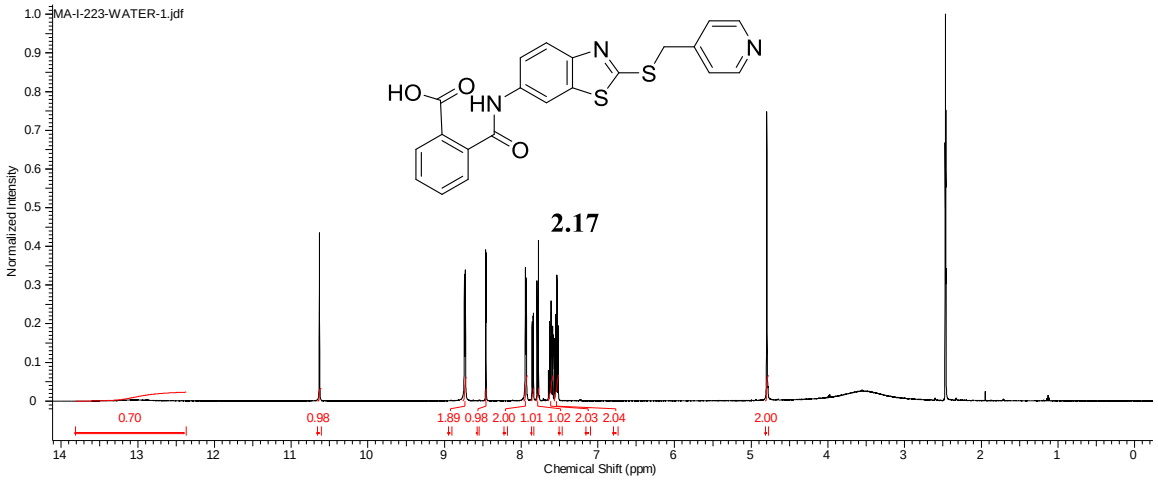

Figure 90. ^{1}H NMR Spectra of Ccompound **2.17**.

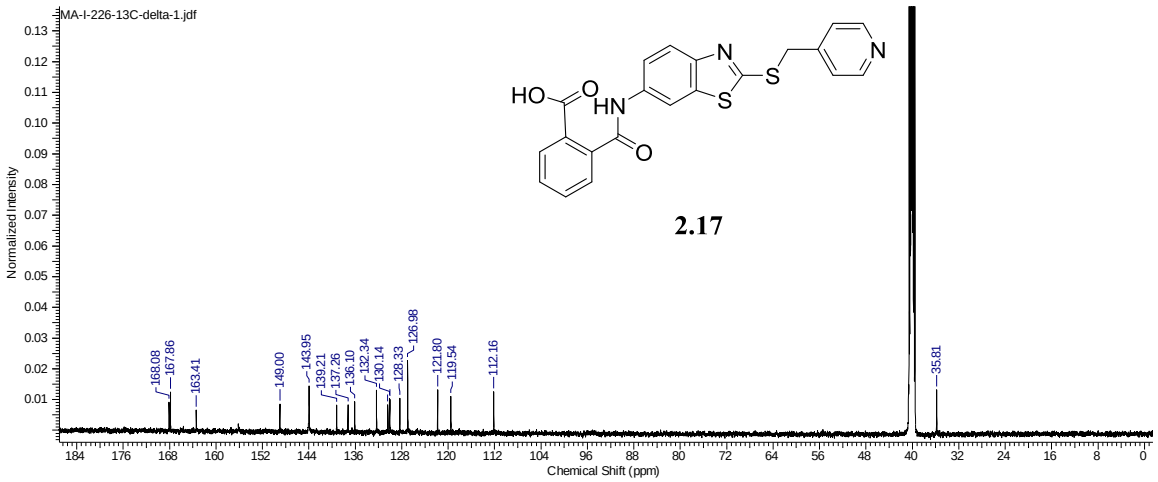

Figure 91. ^{13}C NMR Spectra of Compound **2.17**.

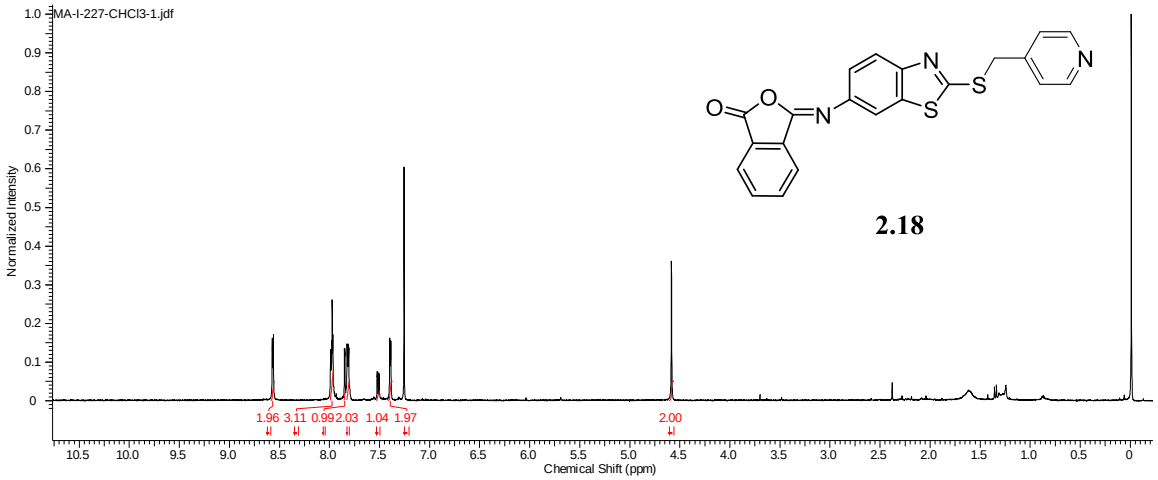

Figure 92. ^{1}H NMR Spectra of Compound **2.18**.

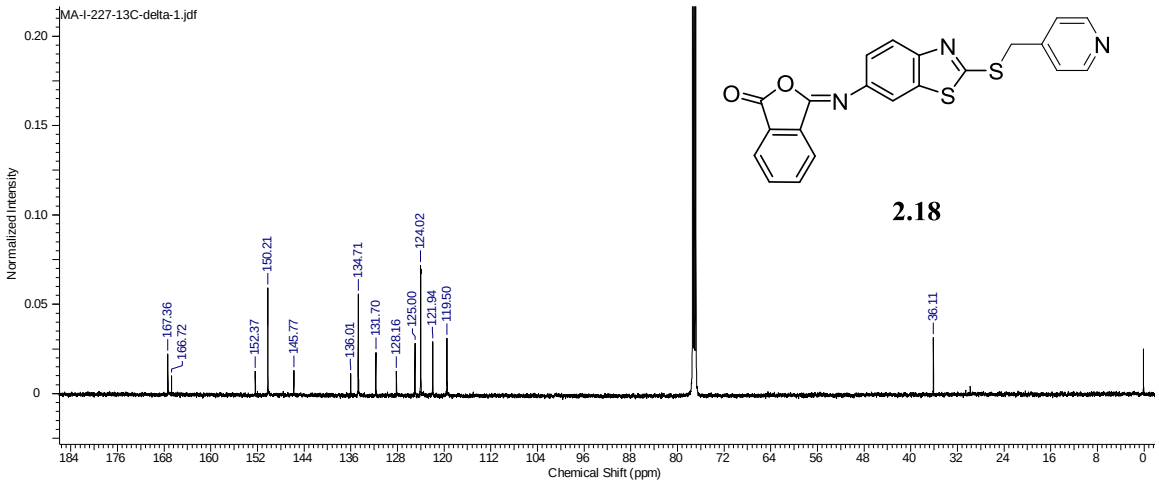

Figure 93. ^{1}H NMR Spectra of Compound **2.18**.

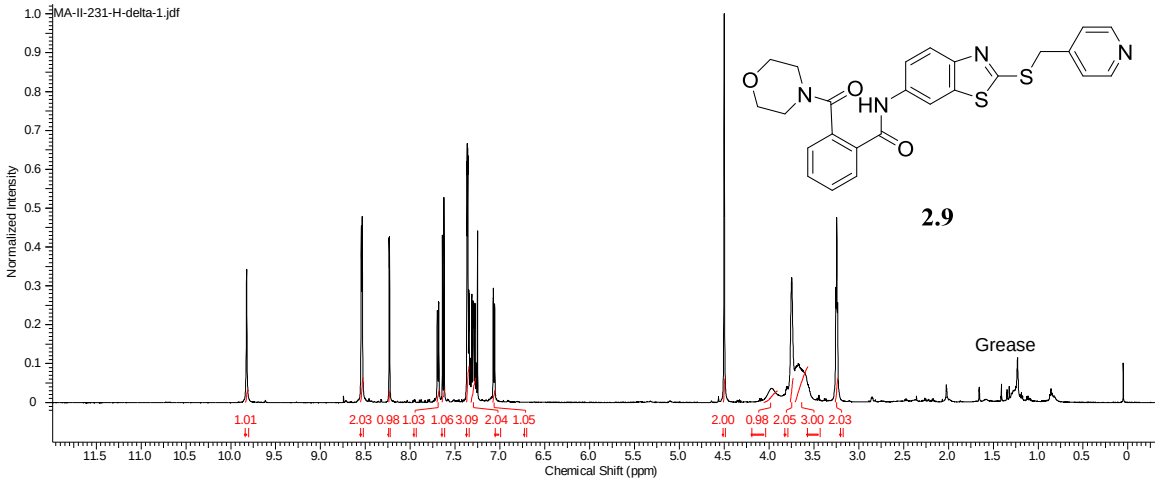

Figure 94. ^{1}H NMR Spectra of Compound **2.9**.

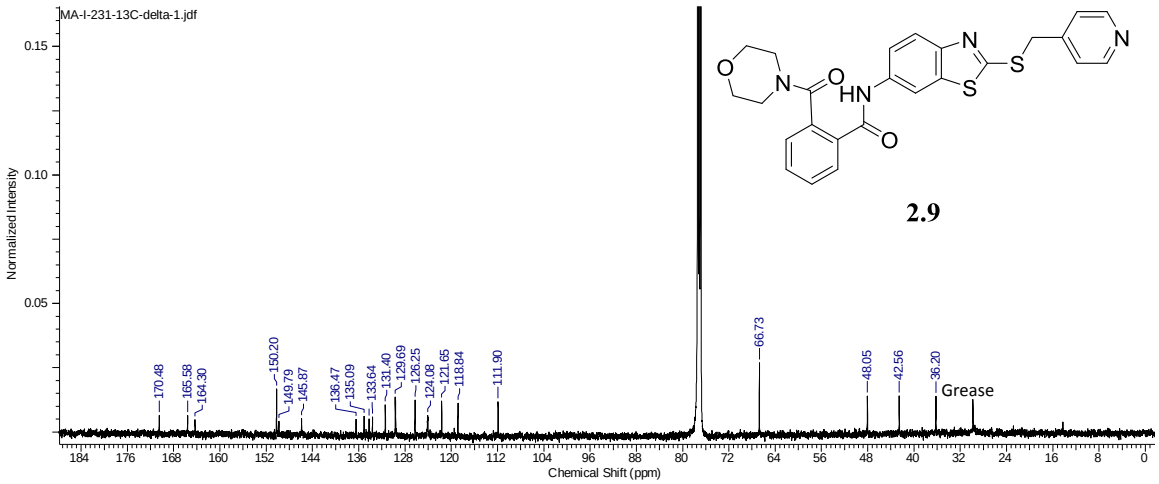

Figure 95. ^{13}C NMR Spectra of Compound **2.9**.

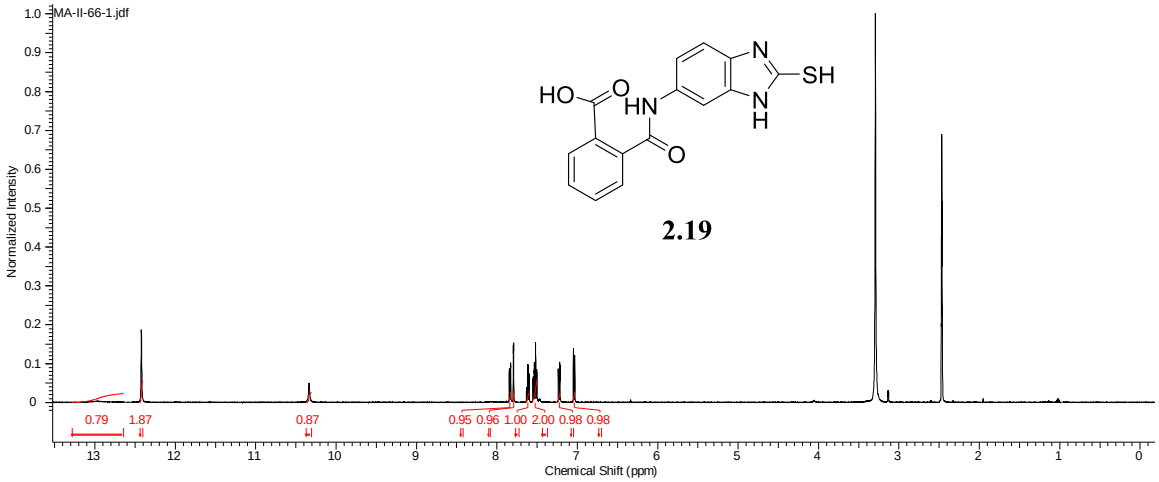

Figure 96. ^{1}H NMR Spectra of Compound **2.19**.

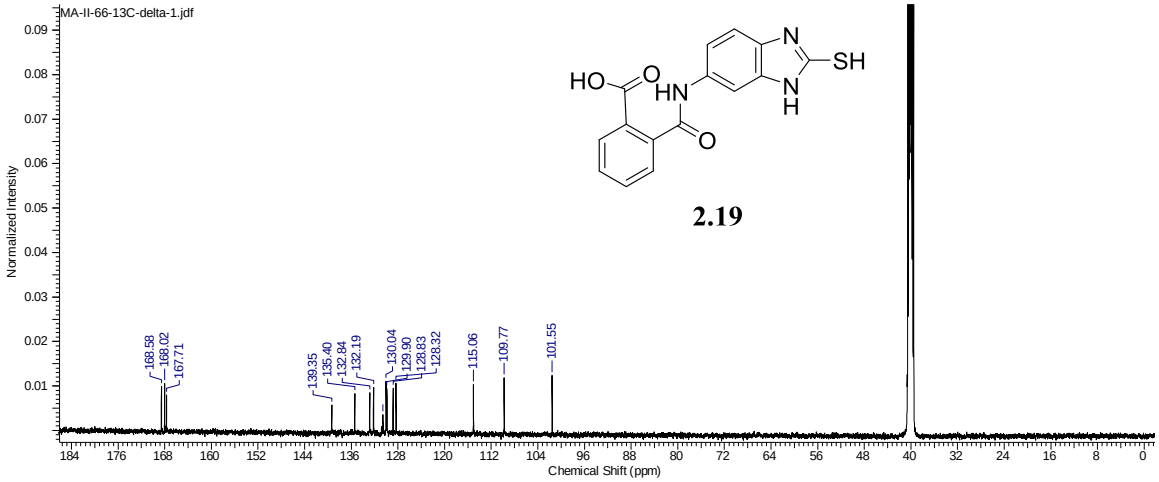

Figure 97. ^{13}C NMR Spectra of Compound **2.19**.

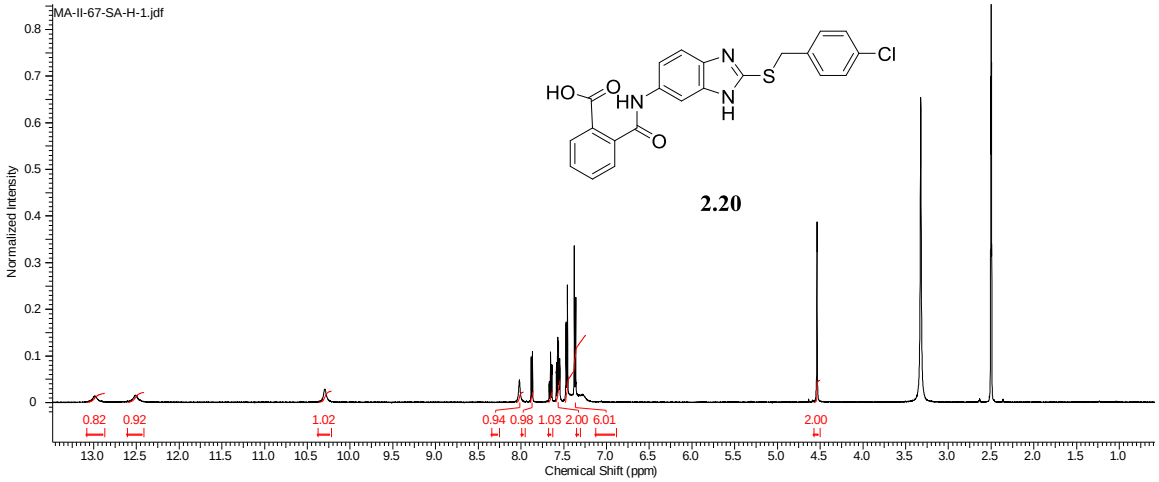

Figure 98. ^{1}H NMR Spectra of Compound **2.20**.

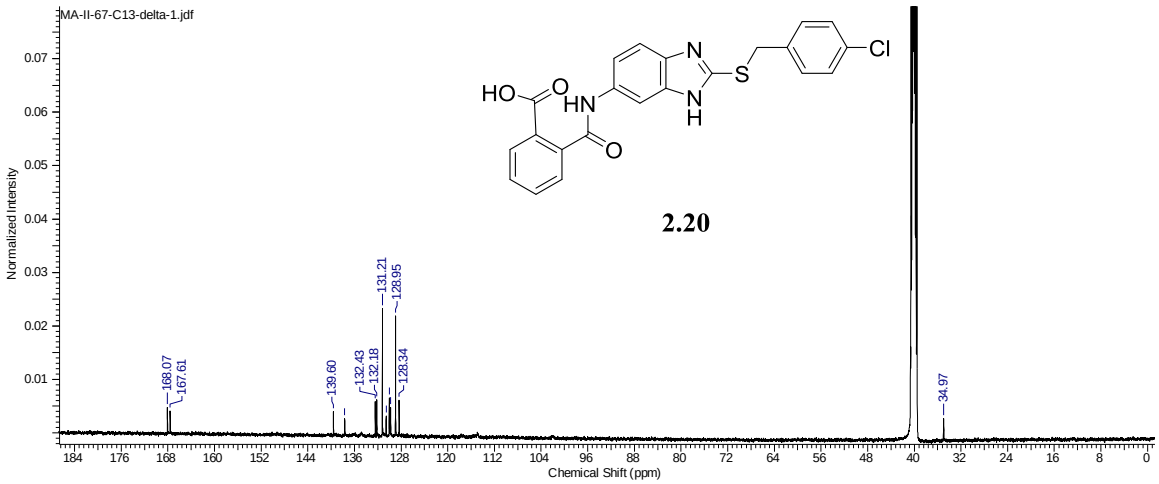

Figure 99. ^{13}C NMR Spectra of Compound **2.20**.

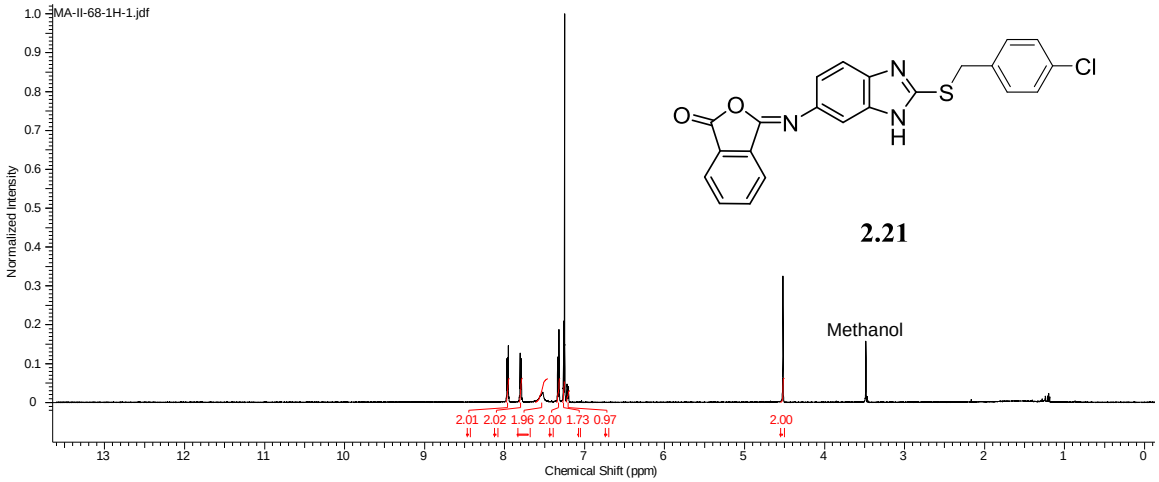

Figure 100. ^{1}H NMR Spectra of Compound **2.21**.

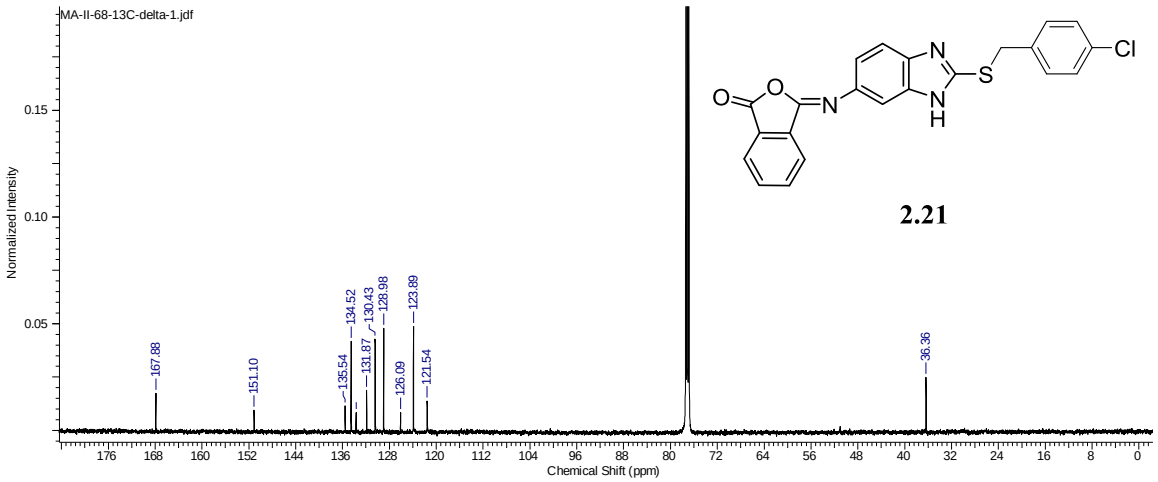

Figure 101. ^{13}C NMR Spectra of Compound **2.21**.

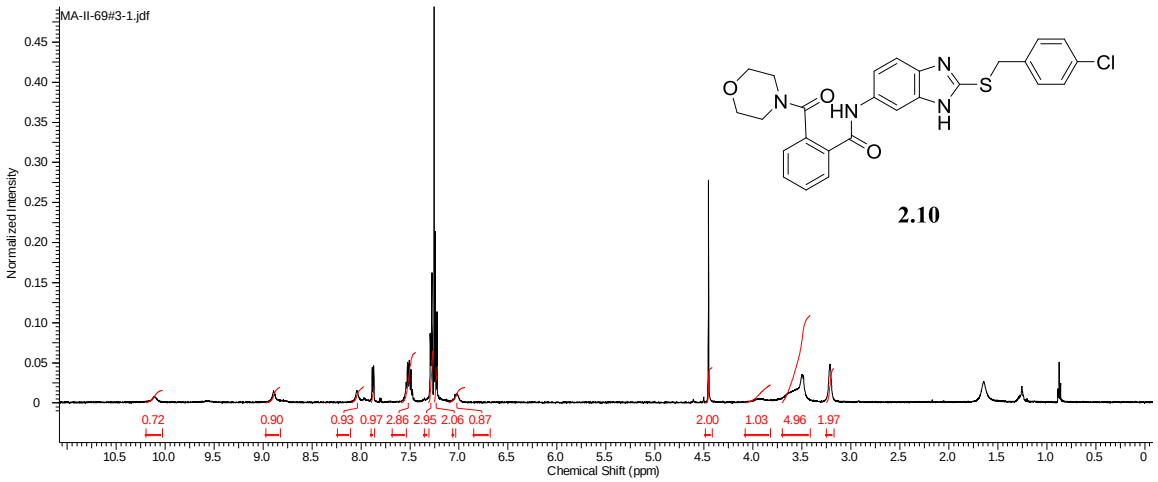

Figure 102. ^{1}H NMR Spectra of Compound **2.10**.

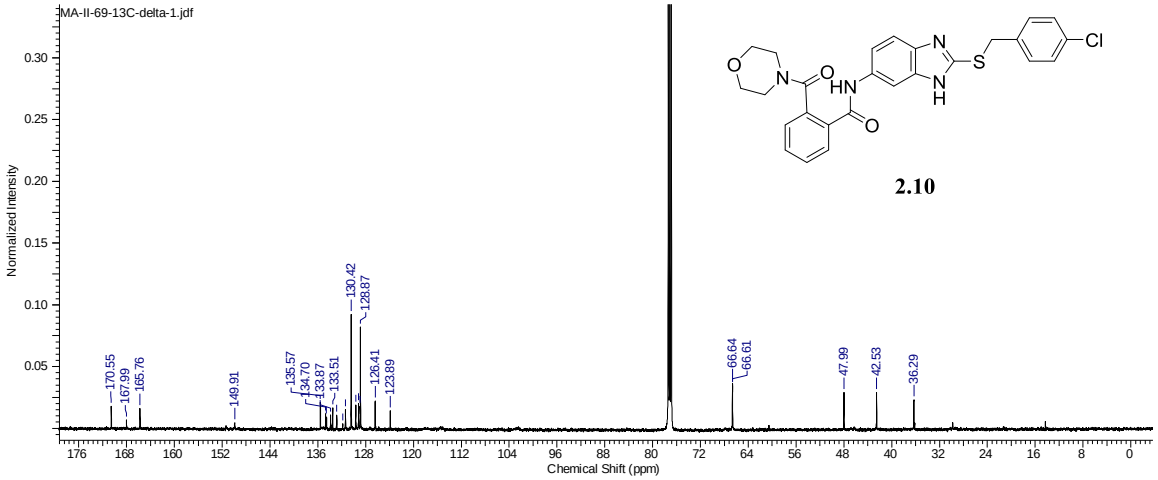

Figure 103. ^{13}C NMR Spectra of Compound **2.10**.

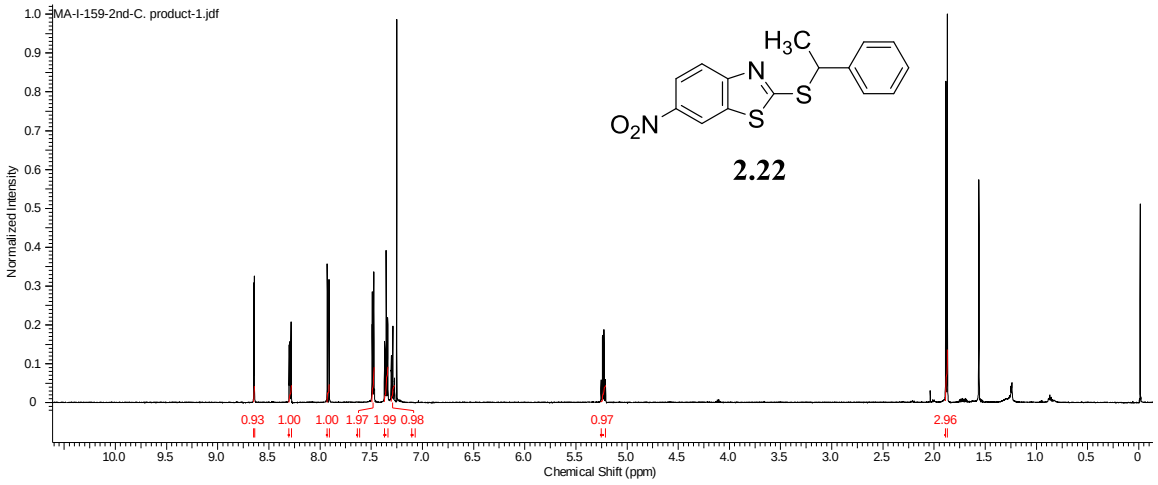

Figure 104. ^{1}H NMR Spectra of Compound **2.22**.

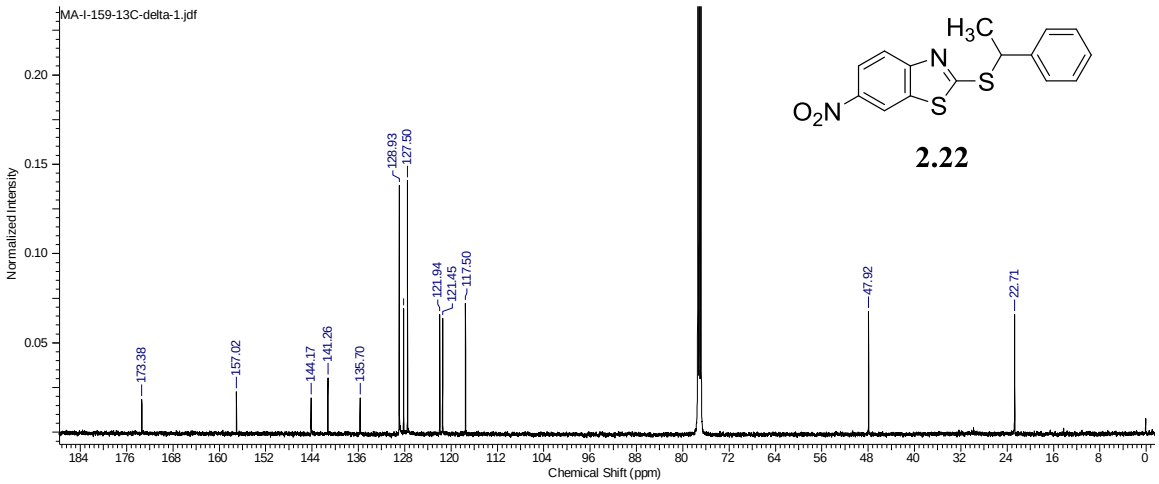

Figure 105. ^{13}C NMR Spectra of Compound **2.22**.

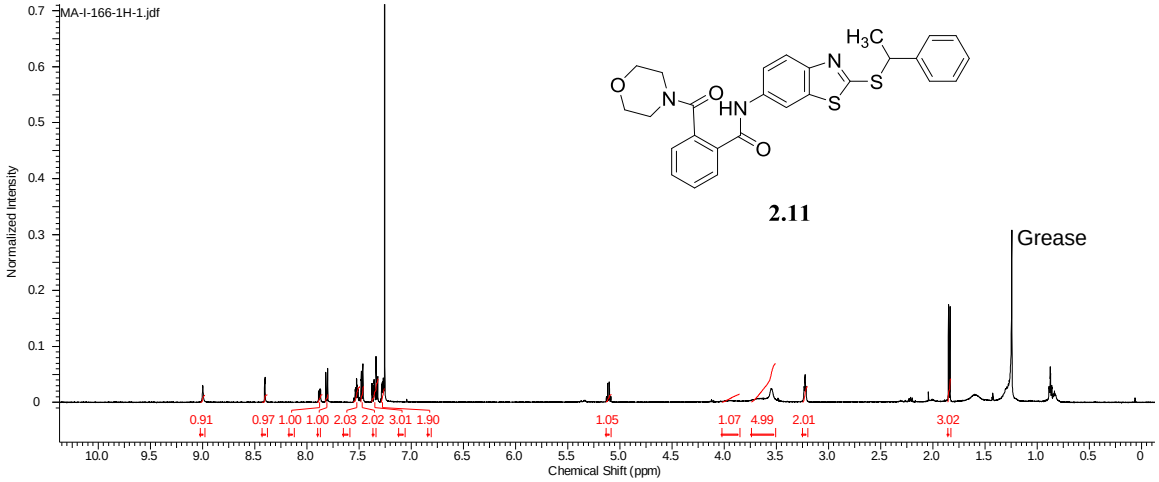

Figure 106. ^{1}H NMR Spectra of Compound **2.11**.

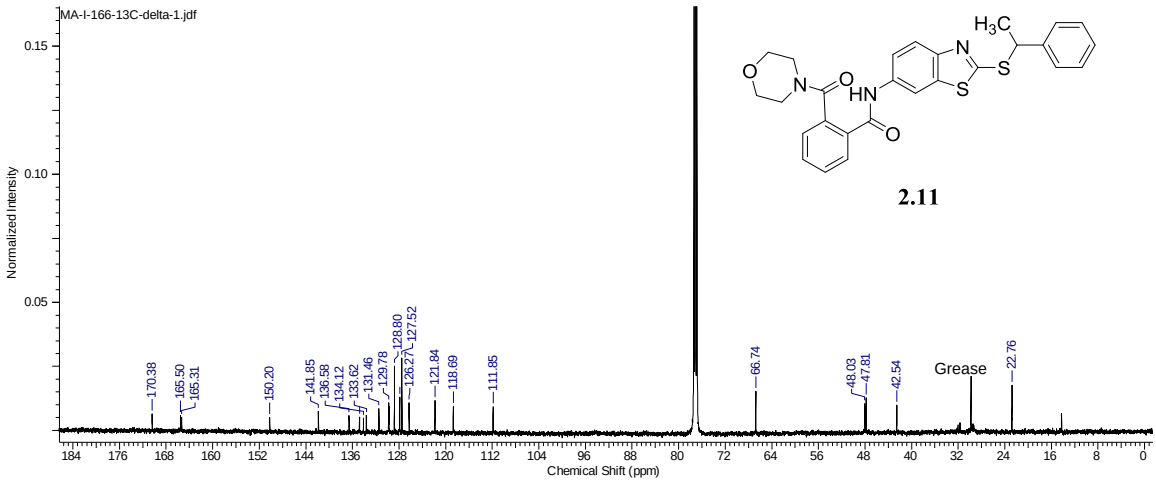

Figure 107. ^{13}C NMR Spectra of Compound **2.11**.

References

[1] O'Dowd, B. F.; Nguyen, T.; Marchese, A.; Cheng, R.; Lynch, K. R.; Heng, H. H.; Kolakowski, L. F. Jr.; George, S. R. Discovery of three novel G-protein-coupled reseptor genes. *Genomics* **1998**, *47*, 310-313.

[2] Wang, J.; Simonavicius, N.; Wu, X.; Swaminath, G.; Reagan, J.; Tian, H.; Ling, L. Kynurenic Acid as a Ligand for Orphan G Protein-coupled Receptor GPR35. *J. Biol. Chem.* **2006**, *281*, 22021-22028.

[3] Horikawa, Y.; Oda, N.; Cox, N. J.; Li, X.; Orho-Melander, M.; Hara, M.; Hinokio, Y.; Lindner, T. H.; Mashima, H.; Schwarz, P. E. H.; Bosque-Plata, L. D.; Horikawa, Y.; Oda, Y.; Yoshiuchi, I.; Colilla, S.; Polonsky, K. S.; Wei, S.; Concannon, P.; Iwasaki, N.; Schulze, J.; Baier, L. J.; Bogardus, C.; Groop, L.; Boerwinkle, E.; Hanis, C. L.; Bell, G. Genetic variation in the gene encoding calpain-10 is associated with type 2 diabetes mellitus, *Nature Genetics*, **2000**, *26*, 163-175.

[4] Ohshiro, H.; Tonai-Kachi, H.; Ichikawa, K. GPR35 is a functional receptor in rat dorsal root ganglion neurons, *Biochem. Biophys. Res. Commun*. **2008**, *365*, 344-348.

[5] Shrimpton, A. E.; Braddock, B. R.; Thomson, L. L.; Stein, C. K. Hoo, J. J. Molecular delineation of deletions on 2q37.3 in three cases with an Albright hereditary osteodystrophy-like phenotype. *Clin. Genet.* **2004**, *66*, 537-544.

[6] Leonard, J. N.; Chu, Z. L.; Unett, D. J.; Gatlin, J. E.; Gaidarov, I.; Qui, J.; Skinner, P. J.; Boatman, P.D. GPR35 and modulators thereof for the treatment of metabolic-related disorders, US 20070077602 A1.

[7] Okumura, S.; Baba, H.; Kumada, T.; Nanmoku, K.; Nakajima, H.; Nakane, Y.; Hioki, K.; Ikenaka, K. Cloning of a G-protein-coupled receptor that shows an activity to transform NIH3T3 cells and is expressed in gastric cancer cells. *Cancer Sci*. **2004**, *95*, 131-135.

[8] Kotsikorou, E.; Madrigal, K. E.; Hurst, D. P.; Sharir, H.; Lynch, D. L.; Heynen-Genel, S.; Milan, L. B.; Chung, T. D. Y.; Seltzman, H. H.; Bai, Y.; Caron, M. G.; Barak, L.; Abood, M. E.; Reggio, P. H. Identification of the GPR55 Agonist Binding Site Using a Novel Set of High Potency GPR55 Selective Ligands. *Biochemistry* **2011**, 50, 5633–5647.

[9] Zhao, P.; Lane, T. R.; Gao, H. G.; Hurst, D. P.; Kotsikorou, E.; Le, L.; Brailoiu, E.; Reggio, P. H.; Abood, M. E.; Crucial positively charged residues for ligand activation of the GPR35 receptor, *J Bio. Chem.*, **2014**, 6, 3625-38.

[10] Zhao, P.; Sharir, H.; Kapur, A.; Cowan, A.; Geller, E. B.; Adler, M. W.; Seltzman, H. H.; Reggio, P. H.; Heynen-Genel, S.; Sauer, M.; Chung, T. D.; Bai, Y.; Chen, W.; Caron, M. G.; Barak, L. S.; Abood, M. E. Targeting of the orphan receptor GPR35 by pamoic acid: a potent activator of extracellular signal-regulated kinase and beta-arrestin2 with antinociceptive activity. *Molecular pharmacology* **2010,** *78*, 560-568.

[11] Baell, J. B.; Holloway, G. A. New substructure filters for removal of pan assay interference compounds (PAINS) from screening libraries and for their exclusion in bioassays, *J. Med. Chem.* **2010**, *7*, 2719-2740.

[12] Ballesteros, J. A.; Weinstein, H. Integrated Methods for the Construction of Three Dimensional Models and Computational Probing of Structure Function Relations in G Protein-Coupled Receptors. In *Methods in Neuroscience*, Sealfon, S. C., Ed. Academic Press: San Diego, CA, 1995; Vol. 25, pp 366-428 - Chapter 19.

[13] McAllister, S. D.; Hurst, D. P.; Barnett-Norris, J.; Lynch, D.; Reggio, P. H.; Abood, M. E. Structural mimicry in class A G protein-coupled receptor rotamer toggle switches: the importance of the F3.36(201)/W6.48(357) interaction in cannabinoid CB1 receptor activation. *J Biol Chem* **2004,** *279*, 48024-48037.

[14] Diaz. de Toranzo, E. G.; Brieux, J. A. Syntheses of Unsymmetric *o*-Phthalic Acid Diamides. *J. Med. Chem.*, **1967**, *10*, 982–983.

[15] Mountford, S. J.; Campi, E. M.; Robinson, A. J.; Hearn, M. T. W. Synthesis of *N*-heterocyclic ligands for use in affinity and mixed mode chromatography. *Tetrahedron,* **2011**, *67*, 471-485.

[16] Cotton, H.; Elebring, T.; Larsson, M.; Li, L.; Sörensen, H.; von Unge, S. Asymmetric synthesis of esomeprazole. *Tetrahedron: Asymmetry* **2000,** *11*, 3819-3825.

[17] Nishide, K.; Miyamoto, T.; Kumar, K.; Ohsugi, S.; Node, M. Synthetic equivalents of benzenethiol and benzyl mercaptan having faint smell: odor reducing effect of trialkylsilyl group. *Tetrahedron Lett.* **2002**, *43*, 8569-8573.

CHAPTER III

DESIGN, SYNTHESIS, AND BIOLOGICAL EVALUATION OF PYRAZOLE DERIVATIVES

Introduction

Almost two decades ago GPR35 was discovered and classified as an orphan GPCR receptor. However, the areas of GPR35 research still lack the basic pharmacological tools. These tools necessitate a need to characterize the GPR35 receptor, to define the chemistry and biochemistry of this receptor, to elucidate the mechanism of action of this receptor, and finally to use this information to explicate the therapeutic advantages of this receptor. The key to the pharmacological tool is finding a ligand with high potency and selectivity at GPR35 receptor to serve as a research probe. Also of importance, GPR35 has been described as a novel therapeutic target due to the association of this receptor with the numbers of major diseases and disorders (see Chapter I, Introduction).

In our previous work, benzothiazole **3.20** (Figure 108) was used as a probe for the ligand-based homology model optimization. This work provided precise analysis on the nature of the residue at binding pocket by means of a structure-activity relationship study. The result was used for developing and refining the GPR35 homology model. However, the search for potent and selective ligand with antagonist activity at GPR35 was still our major aim. Thus, in this chapter we report the design, synthesis, and evaluation of a

GPR35 antagonist based on pyrazole **3.19** structure (Figure 109), plus design, synthesis, and antimicrobial evaluation of pyrazole derivatives.

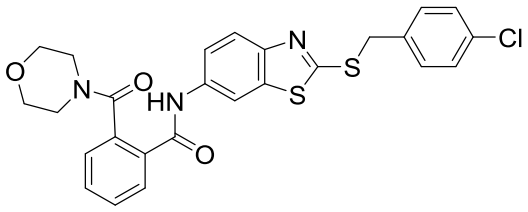

3.20 (CID1231538)
IC_{50} = 0.55 μM

Figure 108. GPR35 Antagonist (CID1231538).

Design of GPR35 Antagonists

Pyrazole **3.19** (Figure 3.2) is the most potent GPR35 antagonist observed to this point. This pyrazole was discovered and identified as the best GPR35 antagonist of ~300,000 compounds assessed in an image-based high-content primary screening performed at the Sanford-Burnham Institute Molecular Libraries Probe Production Center.

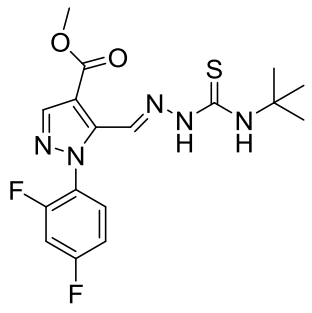

3.19 (CID2745687)
IC_{50} = 160 nM

Figure 109. GPR35 Antagonist (CID2745687).

Pyrazole **3.19** displayed high antagonism activity at GPR35, however this compound has a thiourea hydrazone functionality. Compounds with rhodanine related rings, pyrazolidine rings, activated hydrazones, or compounds with potential Micheal acceptors have been recommended to be excluded from libraries screening results, as described as Pan Assay Interference Compounds (PAINS).[11] These compounds were recommended to be excluded due to the misleading potential through various chemical effects including structure reactivity, chemical instability, chelation, or aggregation. Due to the potential chemical instability or resonance probability of thiourea hydrazone functionality of pyrazole **3.19**, pyrazole **3.19** could adopt a conformational change that could lead to the formation of rhodanine related ring (Figure 110). This pyrazolidine ring could produce chemical reactivity similar to the rhodanine ring. On account of these reasons and concerns, pyrazole **3.19** was selected as a lead for designing new GPR35 antagonist by avoiding thiourea hydrazone functionality.

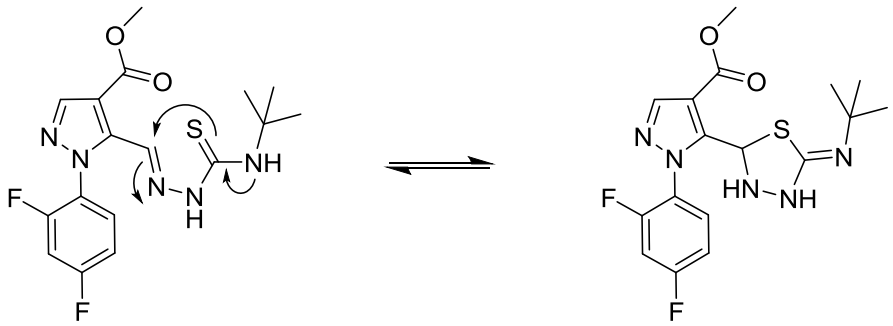

Figure 110. Potential Formation of PAINS Ring.

Pyrazole **3.19** was docked into the GPR35 homology model to predict the conformational interactions with the residues at the binding site. Residues R164 and

Q3.29(93) provides hydrogen bonding with the ester oxygen of pyrazole **3.19** with N-H—O distances of 2.6 Å and 2.8 Å, respectively. Q 3.29(93) also provides hydrogen bonding to the hydrazone hydrogen with O—H-N distance of 2.9 Å. Residue H6.52(234) provides aromatic staking interactions with the difluro aromatic ring (Figure 111).

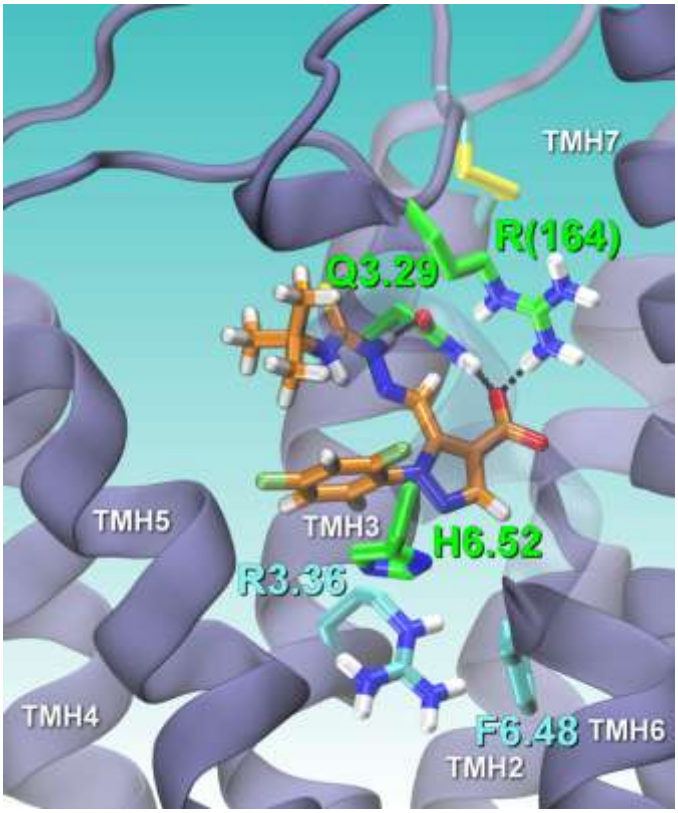

Figure 111. Docking and Key Interactions of Pyrazole **3.19** with GPR35.

Three different scaffolds were designed based on the core structure of pyrazole **3.19** (Figure 111). The scaffolds preserve the aryl pyrazole core while the urea functionality replaces the thiourea. The first scaffold contained alkene function in place of hydrazone. The second scaffold comprised a phenylenediamine ring, whereas the third scaffold comprised triazole ring (Figure 112). The designed analogs were docked into the

GPR35 homology model inactive state (R) to predict the interaction or the lack of interactions with the residues at the binding site. The docking process predicted that the phenylenediamine scaffold possessed preferable interaction with the helices of the GPR35 model (R).

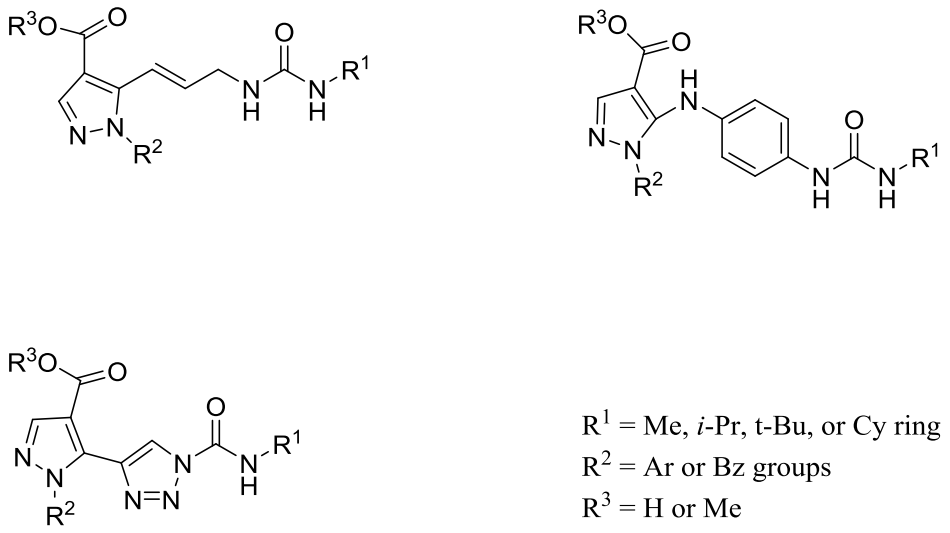

Figure 112. GPR35 Proposed Scaffolds.

Docking of amino pyrazole **3.1** into the homology model of GPR35 (Figure 112) indicated that amino pyrazole **3.1** possessed a handful of favorable interaction with the binding site. Specifically, residue R164 and Q3.29(93) provides hydrogen bonding with carboxylic acid oxygen with N-H—O distances of 2.6 Å and 2.7 Å, respectively. Q 3.29(93) also provides hydrogen bonding to amine hydrogen with O—H-N distance of 3.1Å. Residue R(167) and R4.60(151) provide hydrogen bonding with the urea oxygen with N-H—O distances of 3.0 Å and 2.8 Å, respectively. Residue H6.52 (234) provides aromatic stacking interactions with difluoro aromatic ring (Figure 113).

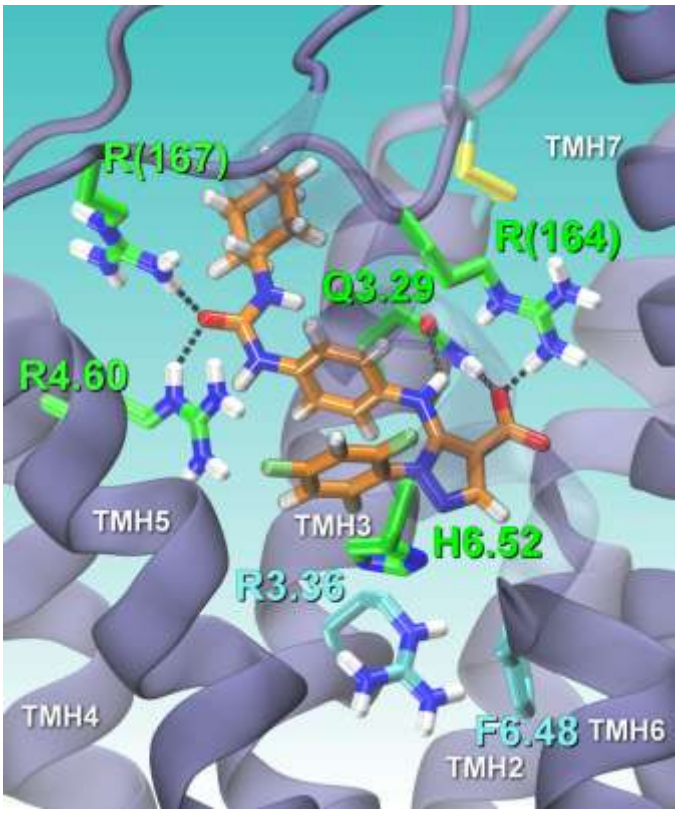

Figure 113. Docking and Key Interactions between Pyrazole **3.1** and GPR35.

Analogs **3.20**-**3.31** were proposed based on the docking of amino pyrazole **3.1** into the GPR35 homology model (Figure 114). Synthesis and biological evaluation of these analogs aimed to reach a potent GPR35 antagonist via structure-activity relationship studies. This was achieved by varying the urea substituent (analogs **3.20**-**3.26**), replacing carboxylic acid with a primary amide (analog **3.27**), functionalizing the phenylenediamine ring (analog **3.28**), replacing pyrazole with pyrrole ring (analog **3.29**), removing the amino pyrazole function (analog **3.30**), and finally addition of methylene between the pyrazole and the attached aryl group (analog **3.31**).

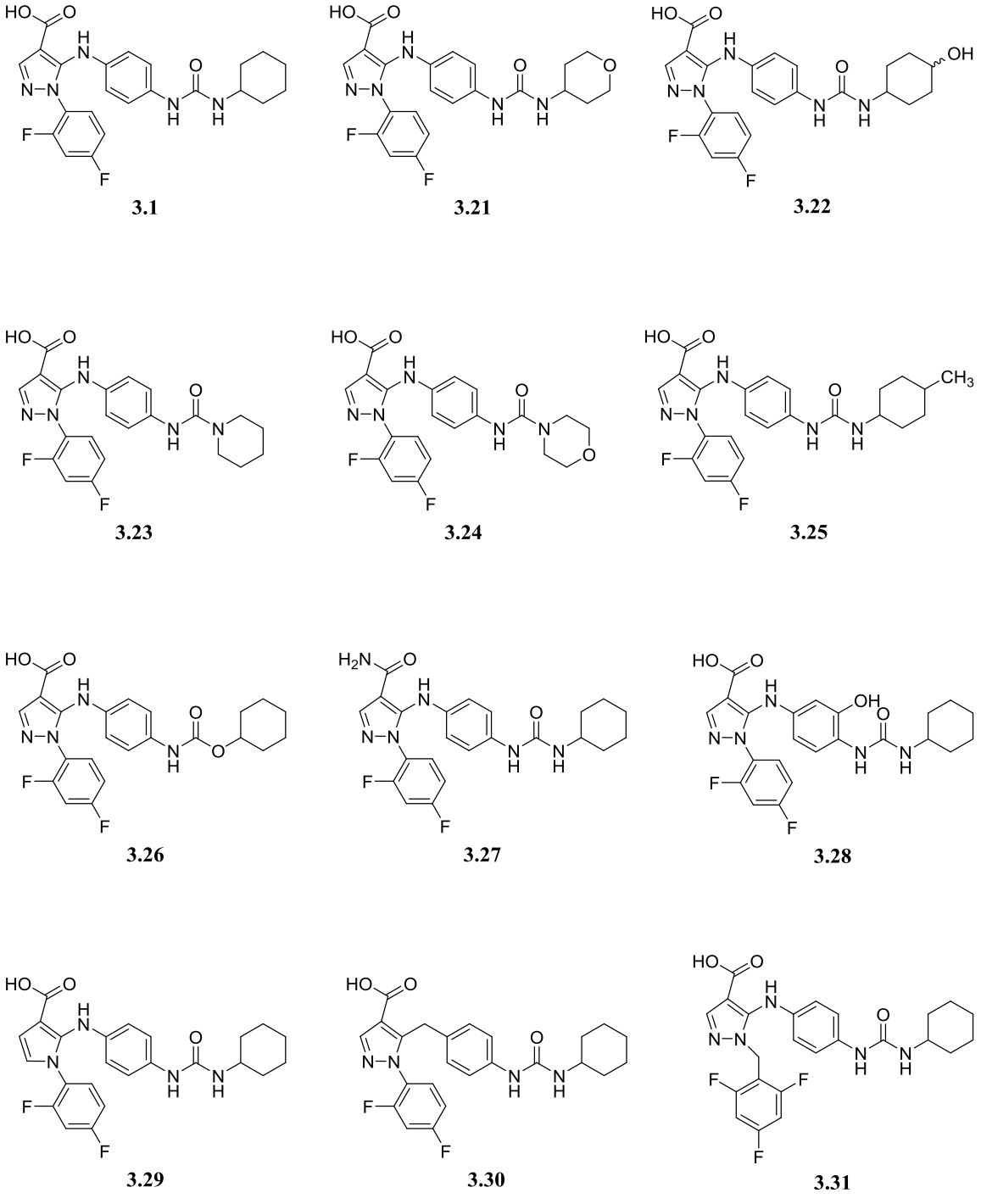

Figure 114. GPR35 Antagonist Analogs.

Synthesis of Pyrazole Analogs

The proposed synthetic route was initiated by examining amino pyrazole **3.1** to test the synthetic route and to optimize experimental conditions. Scheme 3.1 exemplified the reterosynthetic analysis to synthesize amino pyrazole **3.1**. Buchwald-Hartwig cross coupling reaction was proposed as main step in this route. Amino pyrazole **3.1** will be achieved by deesterification of amino pyrazole **3.32** which will be prepared through Buchwald-Hartwig coupling of pyrazole **3.33** and urea **3.4**. The Buchwald-Hartwig substrate **3.33** would be prepared from the reaction of pyrazole **3.3** with triflic achydride under basic condition. Urea **3.4** could be prepared through corbonylation of 1,4 phenylendiamine and cyclohexylamine using triphosgene (Figure 115).

The synthetic route initiated with the formation of dimethyl ethoxymethylenemalonate **3.15** through a condensation of triethyl ortho formate and dimethyl malonate catalyzied by zinc chloride.[7] Addition of **3.15** to a refluxing solution of phenylhydrazine **3.16** in water produced pyrazole **3.3** in good yield. Treatment of **3.3** with triflic anhydride and triethylamine produced triflate **3.33** in 96% yields (Figure 116).

With triflate **3.33** in hand, the Buchwald-Hartwig reaction was first examined using urea **3.4**, However, no reaction was taking place and recovery of starting materials was observed by the NMR. Many different Buchwald-Hartwig reactions using different substrates, ligands, bases, and solvents, resulted in recovery of starting materials or formation of unknown products (Figure 117). In addition to Buchwald-Hartwig coupling, Ullmann-type coupling was also attempted using several substrates. However, all these attempted found to be unsuccessful (Figure 117).

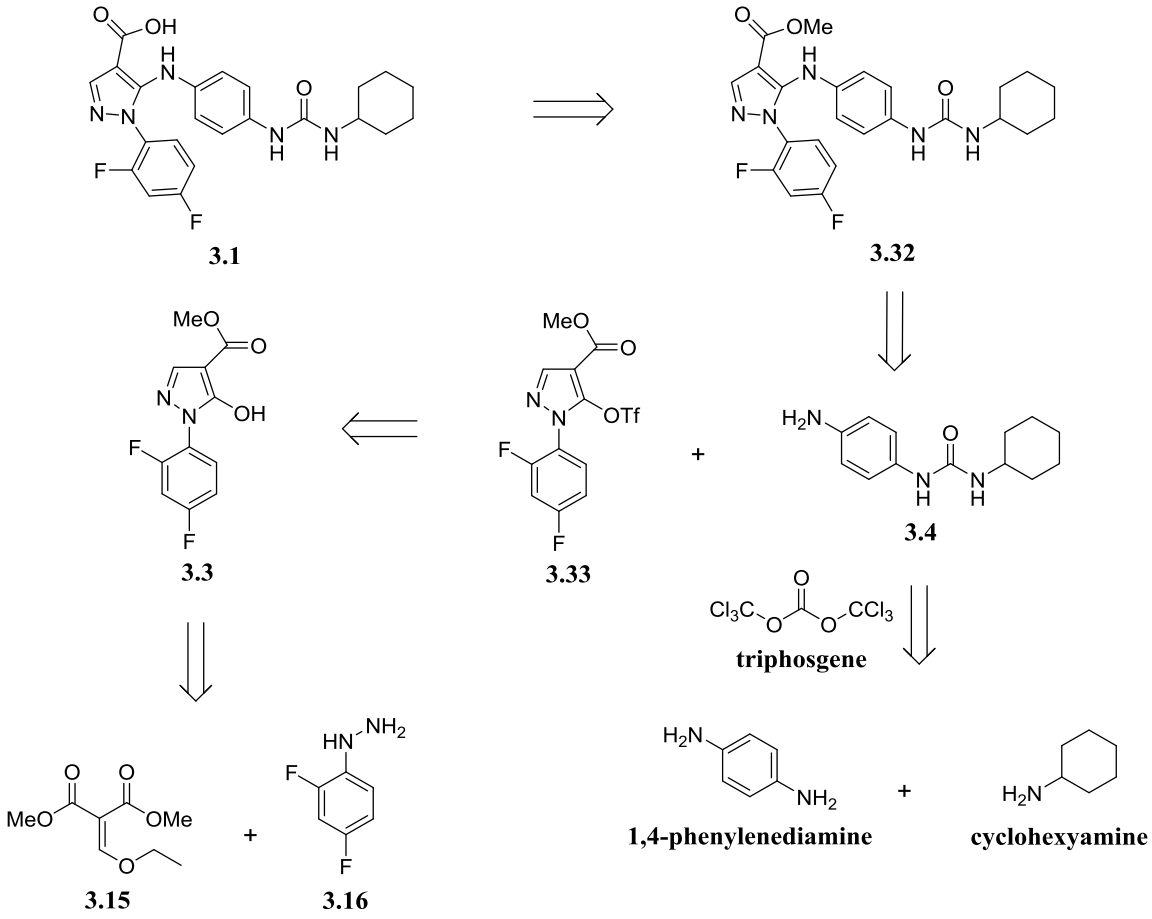

Figure 115. Reterosynthetic Analysis of Amino Pyrazole **3.1**.

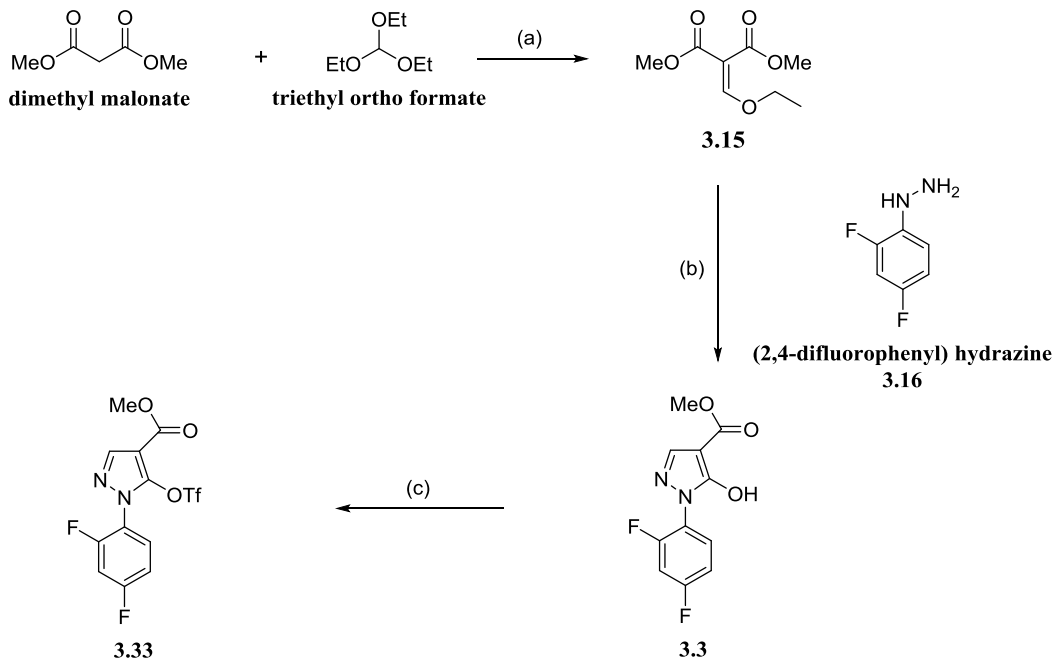

Figure 116. Synthesis of Buchwald-Hartwig Substrate **3.33**. Reagents and conditions: (a) Ac_2O, $ZnCl_2$ 100°C-150°C, 17 hr, 82% (b) **3.16**, K_2CO_3, H_2O, 120°C, 17 hr, 70% (c) Tf_2O, TEA, DCM, 30 °C, 3 hr, 96%.

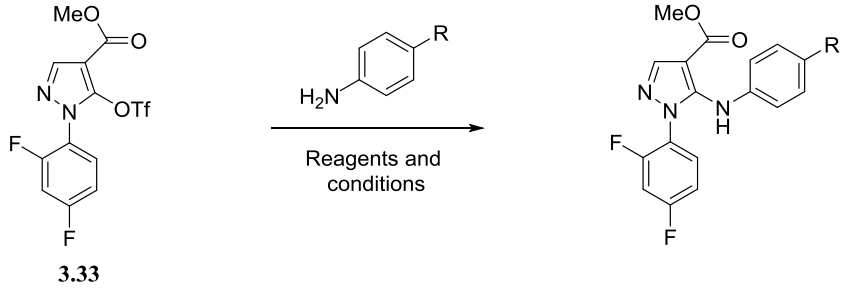

Figure 117. Coupling Reaction Experiments. Reagents and conditions: 1. R = $NHCOC_6H_{11}$, Cs_2CO_3, Xantphos, $Pd(OAc)_2$, THF, 100 °C; 2. R = NO_2, Cs_2CO_3, Xantphos, $Pd(OAc)_2$, toulene, 115 °C; 3. R = NO_2, Cs_2CO_3, Xantphos, $Pd(OAc)_2$, 1,4 dioxane, 115 °C; 4. R = $NHCOC_6H_{11}$, TEA, PPh_3, $Pd(OAc)_2$, DMF, 100 °C; 5. R = H, Cs_2CO_3, Xantphos, $Pd(OAc)_2$, THF, 100 °C; 6. R = H, Cs_2CO_3, PPh_3, $Pd(OAc)_2$, DMF, 65 °C; 7. R = NH_2, TEA, $Pd(PPh_3)_2Cl_2$, CuI, DMF, 100 °C; 8. R = NH_2, Cu, K_2CO_3, H_2O, 100 °C; 9. R = H, Cu, K_2CO_3, H_2O, 100 °C; 10. R = NH_2, Cu, K_2CO_3, DMF, 80 °C; 11. R = NO_2, Cu, K_2CO_3, DMF, 80 °C; 12. R = H, Cu, K_2CO_3, DMF, 80 °C; 13. R = $NHCOC_6H_{11}$, Cu, Cu_2O, K_2CO_3, n-butanol, 130 °C; 14. R = NH_2, BuLi, THF, 0 °C - 25 °C; 15. R = NO_2, NaH, DMF, 70 °C; 16. R = NH_2, THF, 25 °C; 17. R = NH_2, NaH, THF, 25 °C; 18. R = NH_2, HCl (conc.), EtOH, 25 °C; 19. R = H, NaH, THF, 25 °C.

Due to the ineffectiveness of Buchwald-Hartwig coupling reactions and Ullmann-type reactions, nucleophilic attack of the nitrogen of the amine function was suggested to attach the nitrogen at position 3 of the pyrazole ring. Scheme 3.3 showed many experiments under different conditions including aniline, 4-nitroaniline, or phenylenediamine, nevertheless, none of these attempted were successful in achieving the desired product. Surprisingly, the products of some of these reactions were found to be sulfonamides as confirmed by mass spectroscopy and NMR (Figure 3.8).

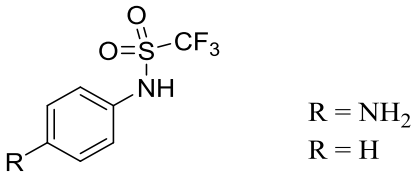

Figure 118. Formation of Sulfonamide.

Due to the unexpected formation of the sulfonamides, replacement of the hydroxyl group of pyrazole **3.3** with chlorine instead of triflate was suggested as a solution. Reaction of pyrazole **3.3** with phosphorous oxychloride ($POCl_3$), thionyl chloride ($SOCl_2$), or aluminum chloride ($AlCl_3$) were found to be ineffectual. Many reactions were also attempted, including Finkelstein conditions, which resulted in recovery of starting materials (Figure 119).

Although multiple trails to replace the hydroxyl group of pyrazole **3.3** with chlorine failed, the desired product was synthesized using 2 equivalents of phosphorous oxychoride and pyridine. A sealed reaction of pyrazole **3.3**, phosphorous oxychloride and pyridine under 200 °C produced carboxylic acid pyrazole **3.17** instead of the methyl ester

(Figure 120). The formation of carboxylic acid believed to be resulted from replacement of methyl ester by nucleophilic chloride followed by hydrolysis of the acyl chloride during workup to form the carboxylic acid.

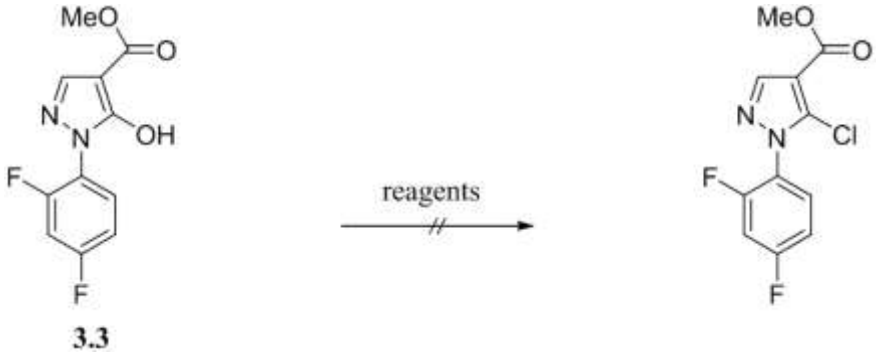

Figure 119. Replacement of Hydroxyl Group with Chlorine. Reagents: 1. $POCl_3$; 2. $POCl_3$, CH_3CN; 3. $AlCl_3$, CH_3CN; 4. $AlCl_3$, 1,4 dioxane; 5. $SOCl_2$; 6. $SOCl_2$, DMF; 7. KCl, acetone; 8. PPh_3, Cl_3CCN, toluene.

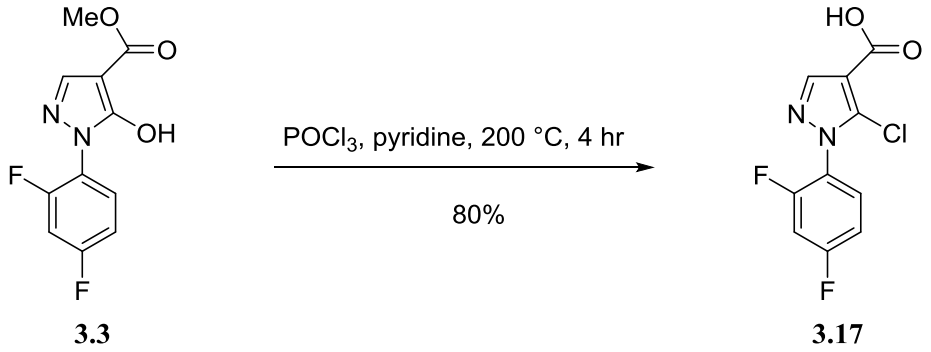

Figure 120. Synthesis of Pyrazole **3.17**.

In order to prepare the first analog to test the validity of initial hypothesis, the urea **3.4** prepared using commercially available cyclohexyl isocyanate and 1,4 phenylenediamine. Coupling of pyrazole **3.17** and urea **3.4** produced analog **3.1** in 82% (Figure 121).

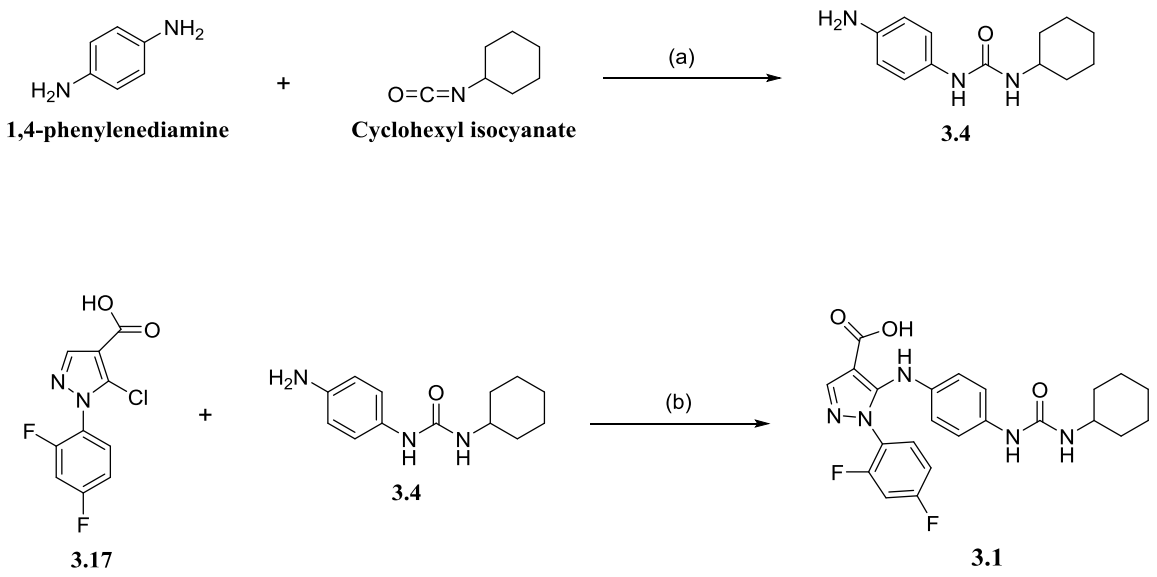

Figure 121. Synthesis of Pyrazole **3.1**. Reagents and conditions: (a) benzene, 27°C, 17 hr, 93% (b) TEA, THF, 27 °C , 17 hr, 82%.

The activity of analog **3.1** as an antagonist at GPR35 was examined using β-arrestin-2-recruitment assay performed at Dr. Abood's lab. This assay revealed that compound **3.1** is completely inactive as a GPR35 antagonist. According to this finding, esterification of pyrazole **3.1** was suggested to mimic the function of the parent. Pyrazole **3.1** was subjected to numbers of experimental condition to convert the acid to methyl ester; however the conversion was ineffective (Figure 122).

Compound **3.2** was proposed as alternative solution to the failed esterification of pyrazole **3.1** for a number of reasons. Compound **3.2** provided protection of the carboxylic acid in the form of an amide instead of unfeasible ester. Compound **3.2** could be synthesize easily by the reaction of urea **3.4** with pyrazole **3.18**, which was accessed from reaction of pyrazole **3.3** with phosphorous oxychloride (Figure 123).

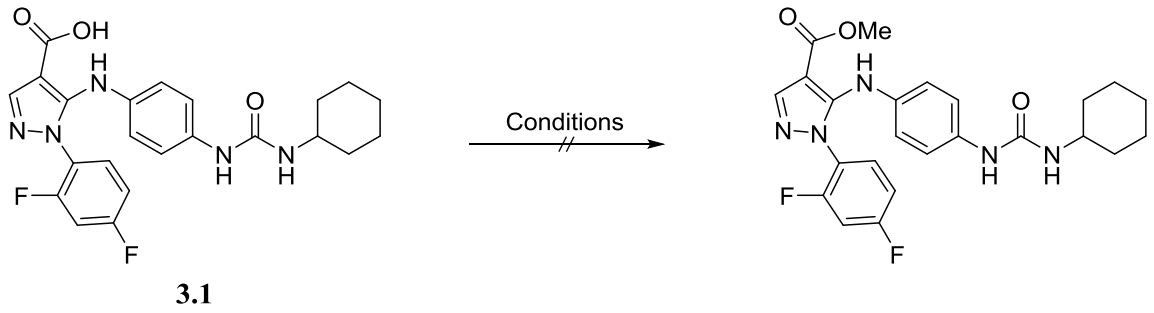

3.1

Figure 122. Esterification of Pyrazole **3.1**. Conditions: 1. $(CH_3)_3SiCHN_2$, dry MeOH; 2. $(CH_3)_3SiCHN_2$, DMF, dry MeOH; 3. MeOH, H_2SO_4; 4. MeOH, DCC, DMAP; 5. MeI; 6. (i) $POCl_3$ (ii) MeOH.

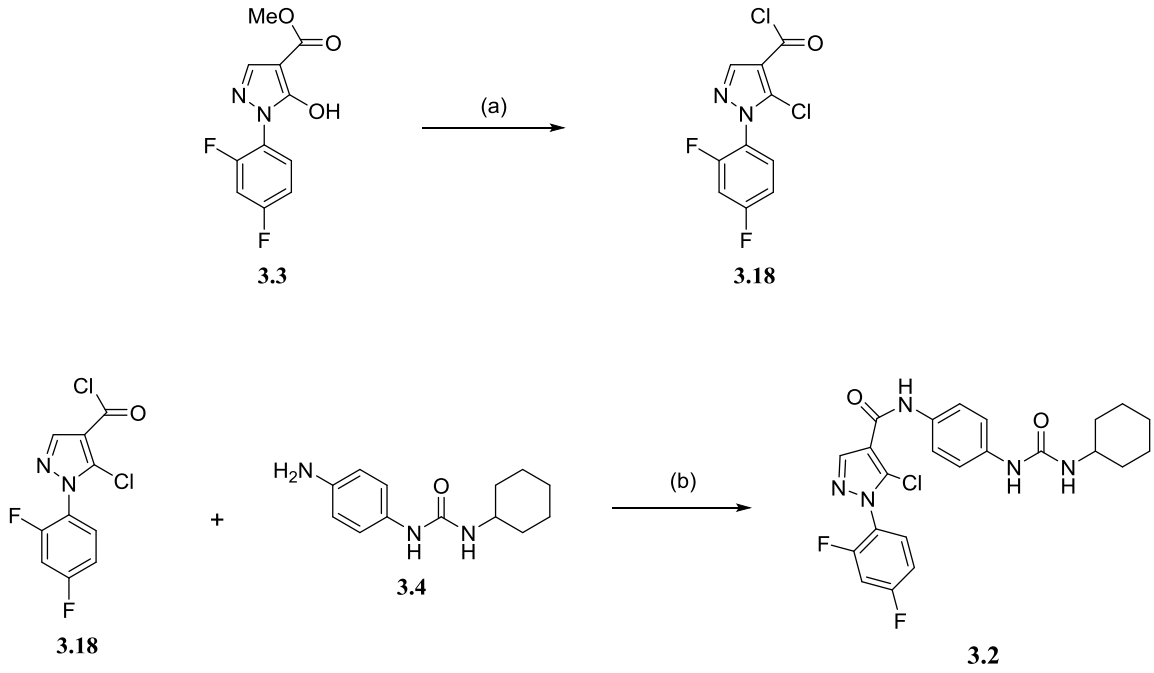

3.3 **3.18** **3.18** **3.4** **3.2**

Figure 123. Synthesis of Pyrazole **3.2**. Reagents and conditions: (a) $POCl_3$, pyridine, 200 °C, 17 hr, 92%; (b) TEA, THF, rt., 30 min, 75%.

Comparable to amino pyrazole **3.1**, pyrazole **3.2** was also inactive as a GPR35 antagonist. This finding supports our initial hypothesis that the thio urea hydrazone is perhaps the cause of the antagonism activity at GPR35 receptor. These results proved that

this scaffold lacks the active feature as GPR35 antagonist. This approach is the basis to discontinue pursing the synthesis of the analogs of this scaffold.

Although these pyrazoles displayed inactive antagonist activity at GPR35 receptor, careful literature screening proved that this family of compound is completely novel. The novelty of these compounds drove our attention to evaluate their biological prosperities. Anti-microbial evaluation of this family of compounds was performed at Dr. Cech lab.

Design, Synthesis, and Anti-microbial Evaluation of 5-substituted 1-Aryl-4-Carboxy Pyrazole Derivatives

Methicillin-resistant Staphylococcus aureus (MRSA) remains a serious threatening health problem due to the emerging resistance to existing anti-microbial drugs. Anti-microbial drug resistance is largely due to the intense use of same family of anti-microbial drugs.[1] The scarcity in anti-microbial drugs and limited scaffold urges the need for new structural lead with potentially unique mode of action and different resistance mechanism.

In recent years, a nitrogen five-membered heterocyclic ring, pyrazole, has gained special consideration as a result of its significant biological properties including anti-cancer,[2] anti-microbial,[3] anti-bacterial, anti-fungal,[4] and anti-inflammatory.[5] Although not many natural pyrazoles are existing, pyrazole ring is ubiquitous in many of synthetic drugs, for instance the anti-inflammatory drugs Celecoxib and Ramifenazone (Figure 124).[6]

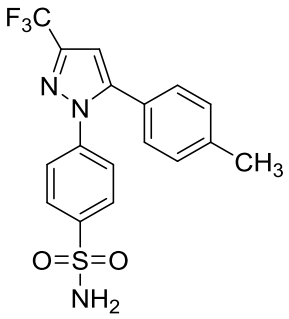

Celecoxib

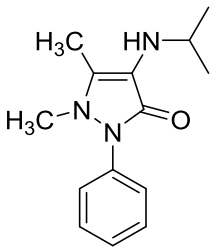

Ramifenazone

Figure 124. Anti-inflammatory Drugs Contain Pyrazole Core.

Motivated by these reasons and continuous resistance of anti-microbial drugs, and with our curiosity to biologically evaluate these structurally novel pyrazoles compounds, we report herein the design, synthesis, and initial structure-activity relationships study of this novel pyrazole derivates as potential anti-microbial agents.

The synthetic route to synthesize compounds **3.1** and **3.2** initiated with the formation of dimethylethoxymethylene malonate **3.15** through a condensation of dimethylmalonate and triethyl ortho formate catalyzied by zinc chloride (Figure 125).[7] Addition of **3.15** to a refluxed solution of 2,4-diflourophenylhydrazine (**3.16)** in water produced pyrazole **3.3** in 70% yield.[8] Treatment of pyrazole **3.3** with phosphorous oxychloride ($POCl_3$) and pyridine produced intermediate **3.17** after basic workup or intermediate **3.18** without the basic workup in 80% and 92% yields respectively. Urea **3.4** was synthesized in 93% yield by the addition of cyclohexylisocyanate to a solution of phenylenediamine in benzene.[9] Nucleaphilic addition of the amine function of urea **3.4** to intermediates **3.17** or **3.18** produced the final analogs **3.1** (82%) and **3.2** (75%) respectively.

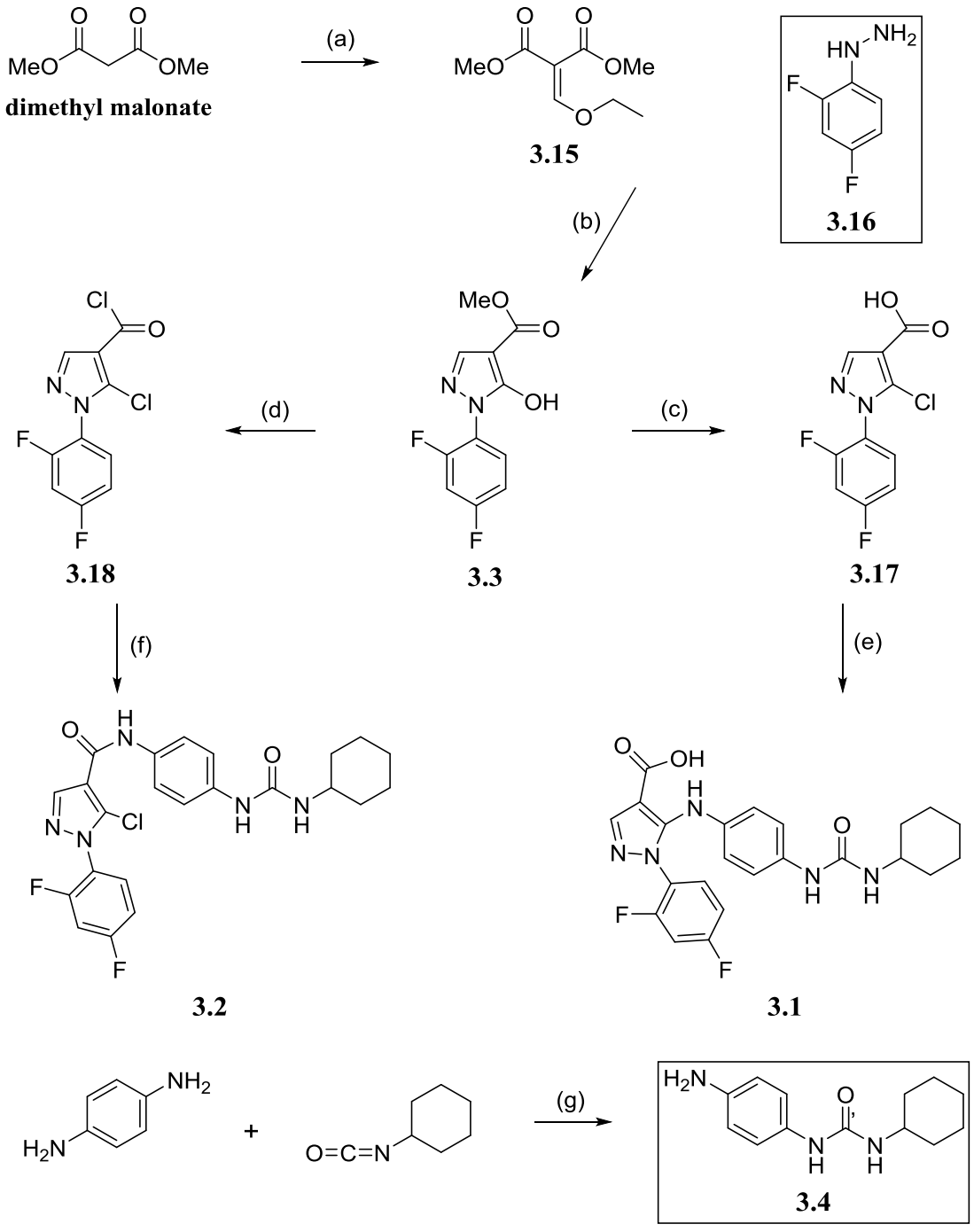

Figure 125. Synthetic Route of Pyrazoles **3.1** and **3.2**. Reagents and conditions: (a) $CH(EtO)_3$, Ac_2O, $ZnCl_2$ 100 °C-150 °C, 17 hr, 82%; (b) **16**, K_2CO_3, H_2O, 120 °C, 17 hr, 70%; (c) $POCl_3$, pyridine, 200 °C, 4 hr, 80%; (d) $POCl_3$, pyridine, 200 °C, 17 hr, 92%; (e) **4**, TEA, THF, 27°C , 17 hr, 82%; (f) **4**, TEA, THF, rt, 30 min, 75%; (g) benzene, 27°C, 17 hr, 93%

Pyrazole **3.5** was synthesized in 78% yield by the addition of ethyl iodide to a solution of pyrazole **3.3** and potassium carbonate in DMF (Scheme 3.10). Addition of intermediate **3.18** to a solution of aniline in THF produced pyrazole **3.6** in 93% yield.

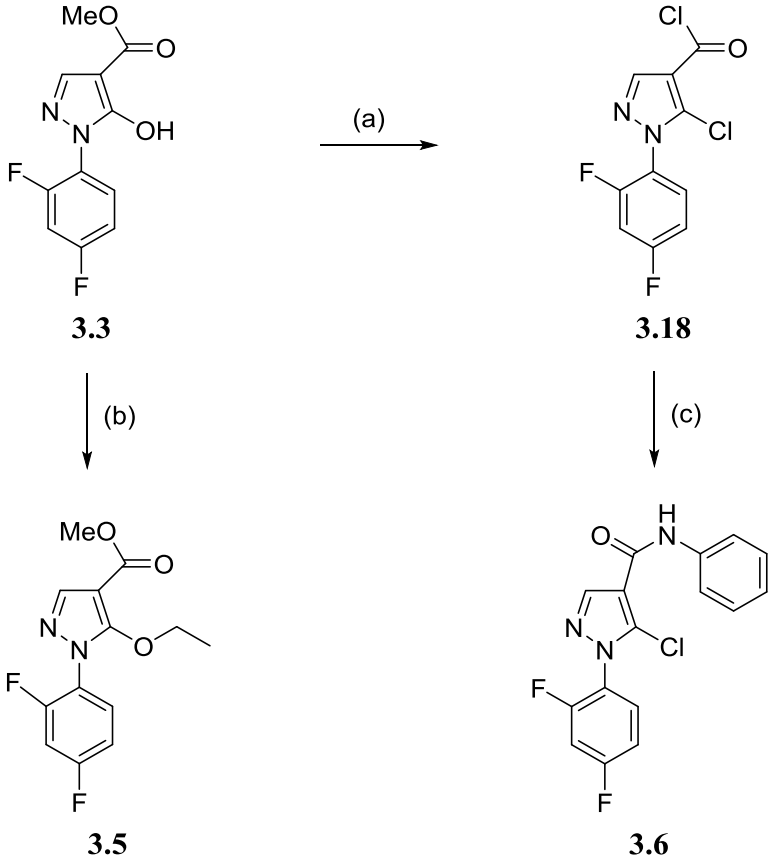

Figure 126. Synthesis of Pyrazoles **3.5** and **3.6**. Reagent and conditions: (a) $POCl_3$, Pyridine, 200 °C, 17 hr, 92%; (b) CH_3CH_2I, K_2CO_3, DMF, 78%; (c) aniline, TEA, THF, rt, 4 hr, 93%.

Synthesized pyrazoles **3.1**-**3.6** were evaluated for their anti-microbial activity using agar diffusion assay. Each compound was suspended in DMSO and diluted with Mueller Hinton broth for a final test concentration of 6 and 10 µM of 2% DMSO solution. Staphylococcus aureus (SA1199) was added at a standardized CFU/mL

concentration and allowed to incubate for 24 hours at 37 °C and turbidity was measured at OD 600 nm. The percent growth inhibition was calculated at the concentrations listed in Table 3.1. The antimicrobial drug, berberine was used as reference drug (or control) to compare the inhibition potency of the synthesized pyrazoles.

The anti-microbial activities of pyrazoles **3.1**-**3.6** directed us to conduct an initial structure-activity relationships study on pyrazole **3.3** (Figure 127). Diversification of the aryl group was done to examine the effect of inductive, electron withdrawing and electron donating groups on the antimicrobial activity of the pyrazole. Aryl amine or ether functionality at position 5 of pyrazole **3.3** created novel structural pyrazoles. Careful literature screening showed that biological evaluation of pyrazole-5-amine derivatives has not been explored. Finally, anti-microbial evaluations of 4-carboxylic acid pyrazoles are yet to be explored.

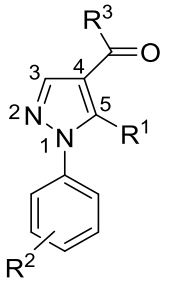

Figure 127. Structure-activity Relationships of Pyrazole Derivatives.

Pyrazole **3.7** and **3.8** were synthesized using a similar method to the synthesis of pyrazole **3.3**.[8] Addition of intermediate **3.15** to a solution of phenylhydrazine or 4-methoxyphenylhydrazine hydrochloride in water produces pyrazoles **3.7** in 81% yield and **3.8** in 95% yield (Scheme 3.11). Pyrazole **3.9** was synthesized in 43% yield by the

addition of intermediate **3.15** to a cold solution of 4-nitrophenylhydrazine hydrochloride and K_2CO_3 in methanol.

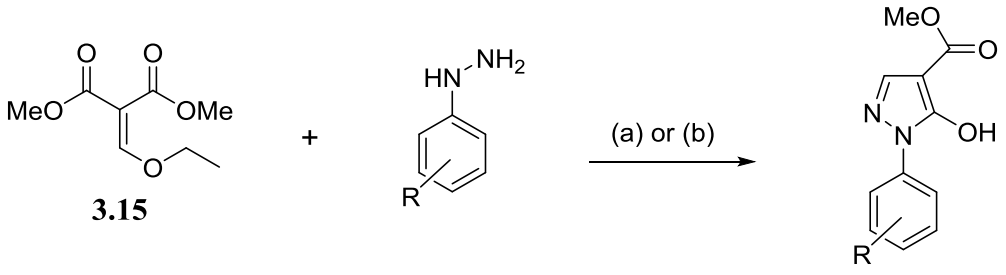

3.7: R = H
3.8: R = *p*-OMe
3.9: R = *p*-NO_2

Figure 128. Diversification of the 1-aryl Pyrazole. (a) K_2CO_3, H_2O, 120°C, 17 hr, **3.7**: 81%, **3.8**: 95% (b) K_2CO_3, EtOH, 0°C to rt, 1 hr, 43%

Replacement of the 2,4-diflourophenyl ring with phenyl or 4-methoxyphenyl groups resulted in significant increase in the anti-microbial activity. Pyrazoles **3.7** and **3.8** exhibited percent inhibition of 62% and 54% at 6 µM respectively (Table 3.1). Our tactic was to examine the effect of substitution of the aryl group of the pyrazole with electron withdrawing and electron donating groups on the anti-microbial activity in order to select the effective pyazole as a lead for compound development. Thus, pyrazole **3.8** was selected for further diversification. Addition of benzyl bromide or 4-chlorobenzyl chloride to a solution of pyrazole **3.8** and K_2CO_3 in DMF at 50 °C produces pyrazole **3.10** (72%) and **3.11** (84%) respectively (Figure 129).

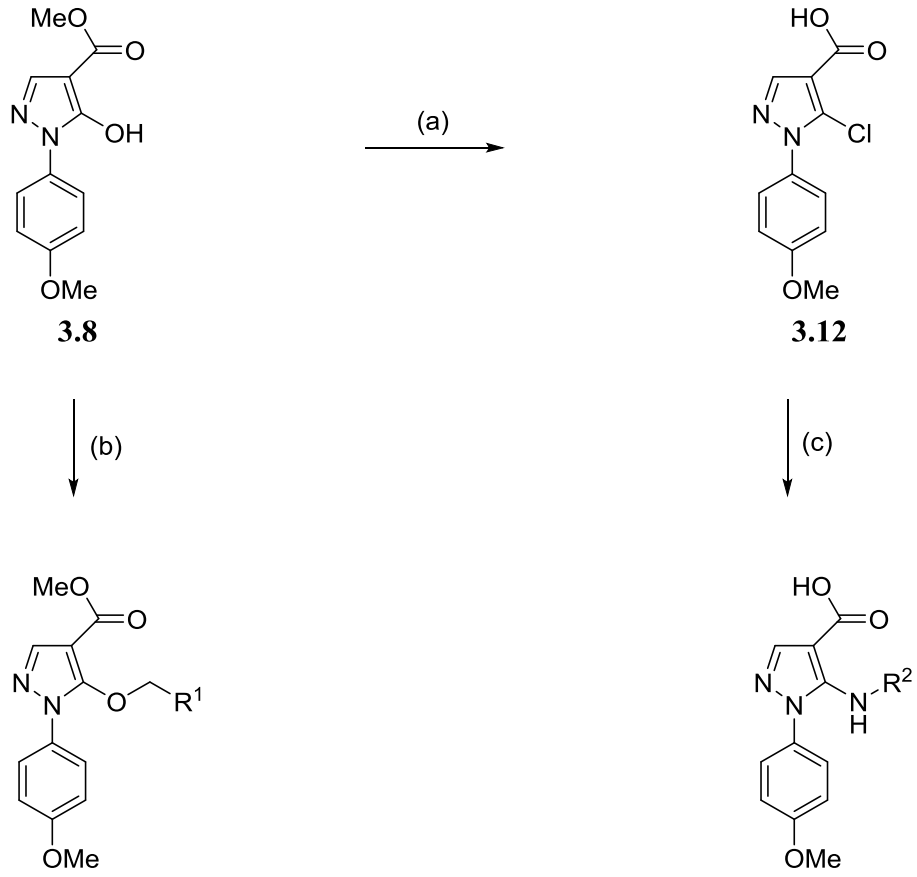

3.10: $R^1 = C_6H_5$
3.11: $R^1 = p\text{-}C_6H_4Cl$
3.13: $R^2 = C_6H_5$
3.14: $R^2 = p\text{-}C_6H_5NH_2$

Figure 129. Synthesis of 5-substituted Pyrazoles. Reagents and conditions: (a) $POCl_3$, pyridine, 200°C, 4 hr, 67% (b) benzyl bromide or 4-chlorobenzyl chloride, K_2CO_3, DMF, 50°C, 17 hr, **3.10**: 72%, **3.11**: 84% (c) aniline or 1,4-phenylenediamine, triethylamine, THF, 27 °C, 17 hr, **3.13**: 67%, **3.14**: 89%.

Treatment of pyrazole **3.8** with $POCl_3$ and pyridine produce pyrazole **3.12** in 67 % yield (Scheme 3.12). Pyrazole **3.12** was used as intermediate in the synthesis of pyrazoles **3.13** and **3.14**. Pyrazoles **3.13** in 67% yield and **3.14** in 89% yield were synthesized by the addition of intermediate **3.12** to a solution of aniline or

phenylenediamine in THF respectively. We also attempted to examine the effect of electron deficient aniline at position 5 on the antimicrobial activity of the pyrazole. However, reaction of **3.12** with nitroaniline proved to be ineffectual.

Results and Discussion

The structure-activity relationships study of the synthesized pyrazoles provides considerable information (Table 7). One of the most important findings is that urea **3.4** is an inactive anti-microbial agent. This finding determined that the moderate potency of compounds **3.1** and **3.2** was due to the pyrazole core. Among the synthesized compounds, pyrazoles **3.3**, **3.5**, **3.7**, **3.8**, and **3.11** exhibited good anti-microbial activities with percentage inhibition of 42%, 47%, 62%, 54% and 48% at 6 μM, respectively. In contrast, pyrazoles **3.6**, **3.13** and **3.14** exhibited poor anti-microbial activity with percentage inhibition of 14%, 18% and 11% at 6 μM, respectively.

Analysis of the anti-microbial activities showed that the aryl group has slight influence on the antimicrobial activity. However, a phenyl group (**3.7**) and an electron donating aryl groups (**3.8**) slightly increase the anti-microbial activity of the pyrazoles. The slight improvement of the anti-microbial activity presumed to be due to increasing electron density on the pyrazole core. With exceptional of pyrazole **3.10**, pyrazoles with an ether function at position 5 of the pyrazole exhibited a significant increase in the anti-microbial activity of pyrazole derivatives (**3.5**, **3.11**). On the contrary, amine function at position 5 decreases the anti-microbial activity drastically (**3.13**, **3.14**). This difference could be electronic in nature or due to the potential protonated state of the amine. Additionally, while an ester substitution at position 4 of the pyrazole appears to be

favorable function, amide substitution at position 4 diminished the anti-microbial activity (**3.6**).

Table 7

Anti-microbial Activity of Pyrazoles **1-14**

Compound ID	Structure	% Inhibition at 6 μM	% Inhibition at 10 μM
3.1	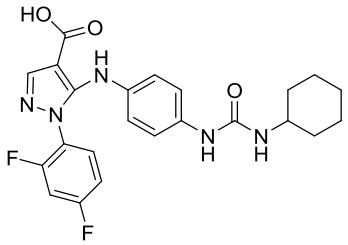	30 ±1	18 ± 16[a]
3.2	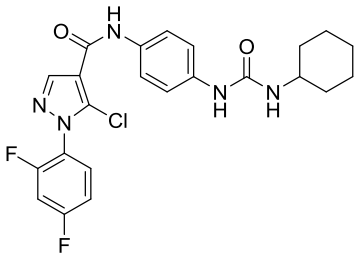	42 ±13	42 ±13
3.3	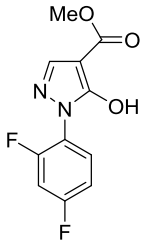	18 ±2	41±12
3.4	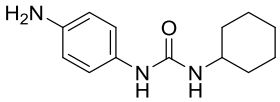	N.I.	N.I.
3.5	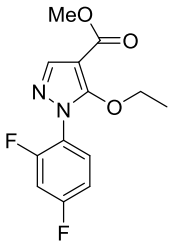	47±9	32±14

Table 7

(Cont.)

Compound ID	Structure	% Inhibition at 6 μM	% Inhibition at 10 μM
3.6	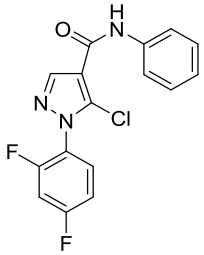	14±1	N.I.
3.7	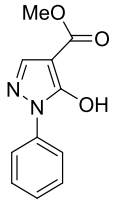	62±3	54±1[a]
3.8	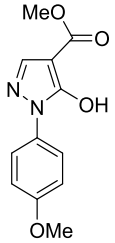	54±1	43±3[a]
3.9	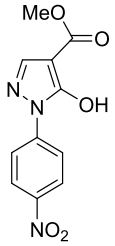	40 ±17	8 ±3[a]
3.10	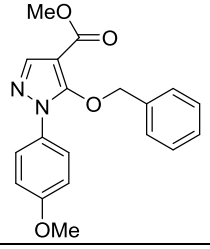	24 ±10	21 ±15[a]

Table 7

(Cont.)

Compound ID	Structure	% Inhibition at 6 μM	% Inhibition at 10 μM
3.11	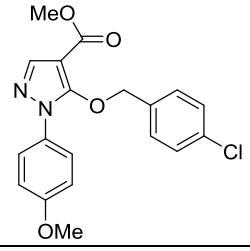	48±9	47±4[a]
3.12	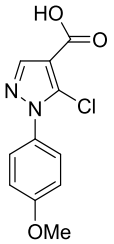	24±1	12±2[a]
3.13	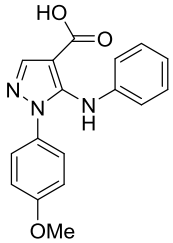	18 ±12	15±12[a]
3.14	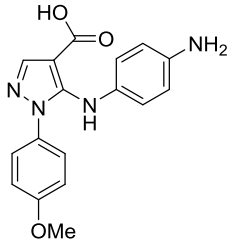	11±8	15±9[a]

[a] compounds tested at 12 μM; N.I. = no inhibition.

The initial structure-activity relationships study for a family of pyrazoles that act as anti-microbial agents proves that an increase electron density on the pyrazole core has a positive influence on the activity. An aryl amine at position 5 should provide greater effect on the pyrazole ring than the ether function. However, pyrazoles with an ether

function at position 5 are significantly active anti-microbial agents than the 5-amino pyrazoles. This perhaps is due to the presence of the carboxylic acid function at position 4 of the pyrazole ring. Deprotonation of the acid and formation of zwitterion ion with the amine function could decrease the solubility of pyrazole **3.13** and **3.14** in the broth. However, protection of the acid in the form of an ester is a requisite to validate this hypothesis. This initial study presents the design and synthesis of a novel scaffold with anti-microbial activity that will serve as a research tools or basis for designing and developing novel anti-microbial drugs.

Experimental Procedures

All anhydrous reactions were performed in oven dried glassware under a nitrogen atmosphere. All commercial reagents and solvents were used without further purification. Chromatographic purification was performed using silica gel (60 Å, 32-63μm). Analytical thin-layer chromatography (TLC) was performed on SiO_2 plates and visualizing by UV irradiation at 254 nm. NMR spectra were recorded in $CDCl_3$, methanol-d_4, acetone-d_6, acetonitrile-d_3 or DMSO-d_6 using JEOL ECA spectrometer (500 MHz for ^{1}H, 125 MHz for ^{13}C). Coupling constants, *J*, are reported in hertz (Hz) and multiplicities are listed as singlet (s), doublet (d), triplet (t), doublet of doublets (dd), triplet of doublets (td), quintet (quint), multiplet (m), etc. High resolution mass spectra were acquired on a Thermo Fisher Scientific LTQ Orbitrap XL MS system using electrospray ionization (ESI).

Following a reported procedure,[7] dimethyl malonate (2.10 mL, 2.42 g, 18.3 mmol) and zinc chloride (0.05 g, 0.37 mmol) were added to stirring solution of triethyl ortho formate (2 mL, 1.78 g, 18.3 mmol) in acetic anhydride (10 mL). The reaction mixture was stirred at 100 °C for 2 hours and then at 150 °C overnight (Figure 130). The reaction mixture was filtered to remove zinc chloride then the solvent was evaporated using rotary evaporator under reduced pressure. The mixture was kept on high vacuum for overnight to produce reddish brown oil (2.80 g, yield 82%) which is used for the next step without further purification. The product matched spectral data from reference 7.[7]

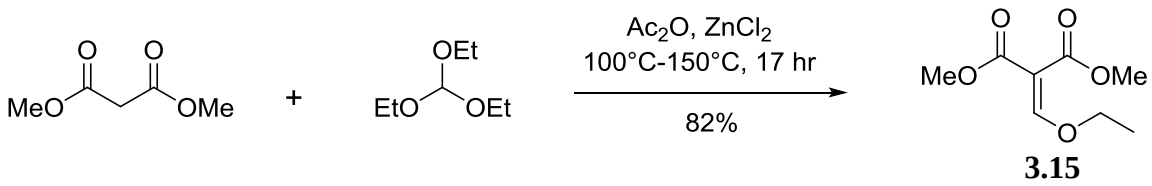

3.15

Figure 130. Synthesis of Dimethyllethoxymethylene Malonate **3.15**.

Following a reported procedure,[8] dimethylethoxymethylene malonate (**3.15**) (0.94 g, 5.0 mmol) was added to a solution of potassium carbonate (0.69 g, 5.0 mmol) and phenyl hydrazine (0.54 g, 5.0 mmol) in water (25 mL) and the reaction mixture was refluxed at 120 °C for overnight (Figure 131). The reaction mixture was then cooled and washed with ethyl acetate (6 X 15 mL). The aqueous layer was then acidified to pH 2 using hydrochloric acid (2 N). The resultant precipitate was collected by vacuum filtration, washed with water and dried under high vacuum. Recrystallization from methanol gives the desired product as pale yellow powder (0.88 g, yield 81%).

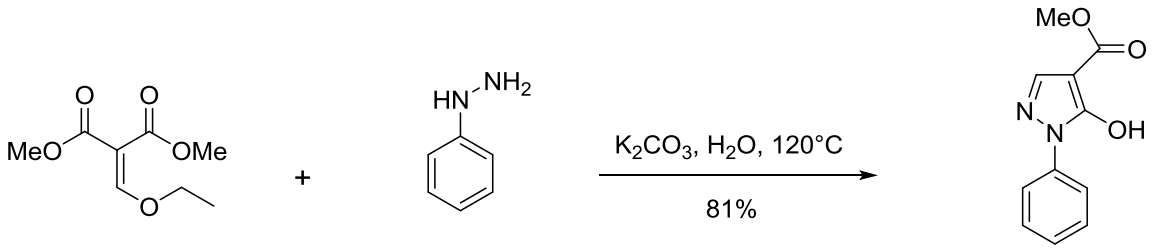

3.15 **3.7**

Figure 131. Synthesis of Analog **3.7**.

^{1}H NMR (500 MHz, $CDCl_3$) δ 9.71 (br. s, 1H), 7.79 (d, *J* = 7.4 Hz, 2H), 7.77 (s, 1H), 7.47 (t, *J* = 8.0 Hz, 2H), 7.33 (t, *J* = 7.4 Hz, 1H), 3.90 (s, 3H).

^{13}C NMR (126 MHz, $CDCl_3$) δ 166.8, 156.7, 138.5, 137.6, 129.3 (2C), 127.3, 121.4 (2C), 95.0, 51.8.

HRMS (ESI): $C_{11}H_{11}N_2O_3[M+H]^+$, Calculated: 219.07697, Found: 219.07575.

Dimethylethoxymethylene malonate (**3.15**) (0.50 g, 2.66 mmol) was added to a solution of potassium carbonate (0.73 g, 5.31 mmol) and 4-methoxyphenylhydrazine hydrochloride (0.46 g, 2.66 mmol) in water (20 mL) and the reaction mixture was refluxed at 120 °C overnight (Figure 132). The reaction mixture was then cooled and washed with ethyl acetate (6 X 10 mL). The aqueous layer was then acidified to pH 2 using hydrochloric acid (2 N). The resultant precipitate was collected by vacuum filtration, washed with water and dried over high vacuum. Recrystallization from methanol gives the desired product as pale yellow powder (0.62 g, yield 95%).

^{1}H NMR (500 MHz, $CDCl_3$) δ 9.59 (br. s, 1H), 7.73 (s, 1H), 7.65 (d, *J* = 9.2 Hz, 2H), 6.97 (d, *J* = 9.2 Hz, 2H), 3.89 (s, 3H), 3.84 (s, 3H).

^{13}C NMR (126 MHz, $CDCl_3$) δ 166.7, 158.7, 156.2, 138.2, 130.7, 123.2 (2C), 114.3 (2C), 94.7, 55.6, 51.7.

HRMS (ESI): $C_{12}H_{13}N_2O_4$ $[M+H]^+$, Calculated: 249.08753, Found: 249.08627.

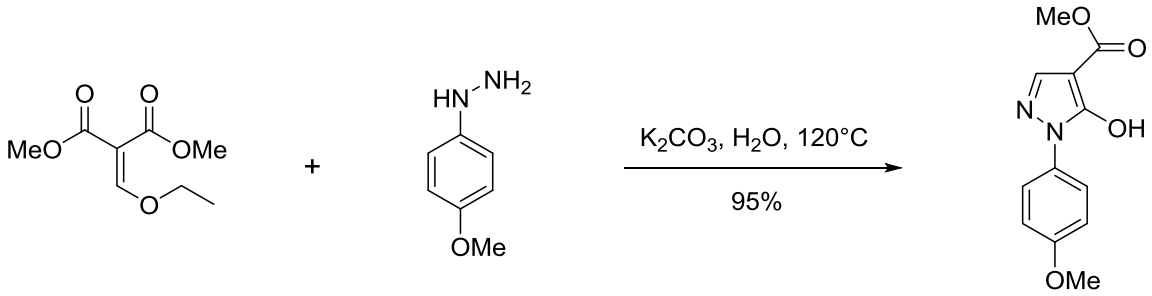

3.15 **3.8**

Figure 132. Synthesis of Analog **3.8**.

To a solution of potassium carbonate (0.30 g, 2.12 mmol) and 4-nitrophenylhydrazine hydrochloride (0.20 g, 1.06 mmol) in methanol (15 mL) at 0 °C, was added dimethyl ethoxy methylene malonate (**3.15**) (0.20 g, 1.06 mmol) and the reaction mixture was stirred at room temperature for 2 hours (Figure 133). Methanol was removed under reduced pressure. Water (20 mL) was then added and the mixture was washed with DCM (4 X 10 mL). The aqueous layer was acidified to pH 2 using hydrochloric acid (2N) and resultant precipitate was collected by vacuum filtration, washed with water and dried under high vacuum. Recrystallization from methanol gives the desired product as dark yellow powder (0.12 g, yield 43%).

^{1}H NMR (500 MHz, $CDCl_3$) δ 10.17 (br. s, 1H), 8.34 (d, *J* = 9.2 Hz, 2H), 8.10 (d, *J* = 9.2 Hz, 2H), 7.81 (s, 1H), 3.93 (s, 3H).

^{13}C NMR (126 MHz, $CDCl_3$) δ 145.7, 142.6, 139.6, 125.6, 125.0 (2C), 120.7 (2C), 118.6, 95.8, 52.1.

HRMS (ESI): $C_{11}H_{10}N_3O_5$ $[M+H]^+$, Calculated: 264.06205, Found: 264.06091.

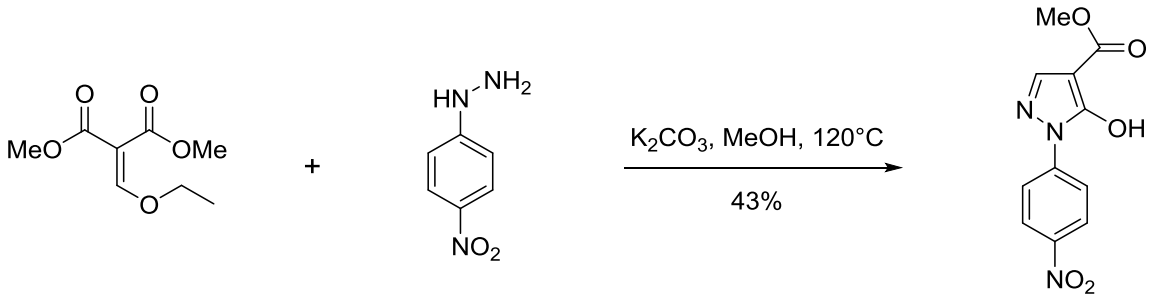

3.15 **3.9**

Figure 133. Synthesis of Analog **3.9**.

To a solution of methyl 5-hydroxy-1-(4-methoxyphenyl)-1H-pyrazole-4-carboxylate (**3.8**) (0.05 g, 0.20 mmol) and potassium carbonate (0.30 g, 0.20 mmol) in DMF at room temperature, was added benzyl bromide (0.03 g, 0.02 mL, 0.20 mmol) and the mixture was stirred at ambient temperature for 17 hours (Figure 134). Water (15 mL) was added and the product was extracted with ethyl acetate (4 X 20 mL). Organic layers were combined, washed with water, dried over anhydrous Na_2SO_4 and evaporated under reduced pressure. The crude oil was purified by short silica fritted column and then cold ether was added to precipitate the product, 0.053 g, 72% yield.

^{1}H NMR (500 MHz, $CDCl_3$) δ 7.91 (s, 1H), 7.36 (d, *J* = 9.2 Hz, 2H), 7.26 - 7.30 (m, 2H), 7.23 - 7.25 (m, 1H), 7.17 - 7.21 (m, 2H), 6.89 (d, *J* = 9.2 Hz, 2H), 5.34 (s, 2H), 3.87 (s, 3H), 3.83 (s, 3H).

^{13}C NMR (126 MHz, $CDCl_3$) δ 163.0, 159.1, 154.1, 141.6, 135.2, 130.8, 128.9 (2C), 128.8, 128.5 (2C), 125.3 (2C), 114.1 (2C), 100.8, 55.6, 51.5 (2C).

HRMS (ESI): $C_{19}H_{19}N_2O_4$ $[M+H]^+$, Calculated: 339.13448, Found: 339.13304.

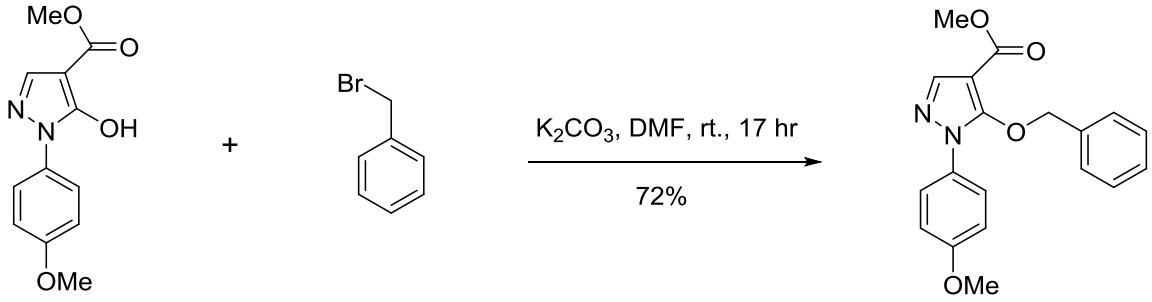

3.8 **3.10**

Figure 134. Synthesis of Analog **3.10**.

To a solution of methyl 5-hydroxy-1-(4-methoxyphenyl)-1H-pyrazole-4-carboxylate (**3.8**) (0.05 g, 0.20 mmol) and potassium carbonate (0.30 g, 0.20 mmol) in DMF, was added 4-chlorobenzyl chloride (0.03 g, 0.20 mmol) and the mixture was stirred at 50 °C for 4 hours (Figure 135). Water (15 mL) was added and the product was extracted with ethyl acetate (4 X 20 mL). Organic layers were combined, washed with water, dried over anhydrous Na_2SO_4 and evaporated under reduced pressure. The product was purified by precipitation out of an ethyl acetate and hexane mixture to obtain 0.064 g, 84% yield.

^{1}H NMR (500 MHz, $CDCl_3$) δ 7.90 (s, 1H), 7.35 (d, *J* = 9.17 Hz, 2H), 7.20 (d, *J* = 8.59 Hz, 2H), 7.10 (d, *J* = 8.59 Hz, 2H), 6.90 (d, *J* = 9.17 Hz, 2H), 5.30 (s, 2H), 3.87 (s, 3H), 3.85 (s, 3H).

^{13}C NMR (126 MHz, $CDCl_3$) δ 163.0, 159.2, 153.9, 141.6, 134.8, 133.7, 130.6, 130.2 (2C), 128.7 (2C), 125.3 (2C), 114.1 (2C), 100.8, 76.5, 55.7, 51.5.

HRMS (ESI): $C_{19}H_{18}ClN_2O_4$ $[M+H]^+$, Calculated: 373.09551, Found: 373.09389.

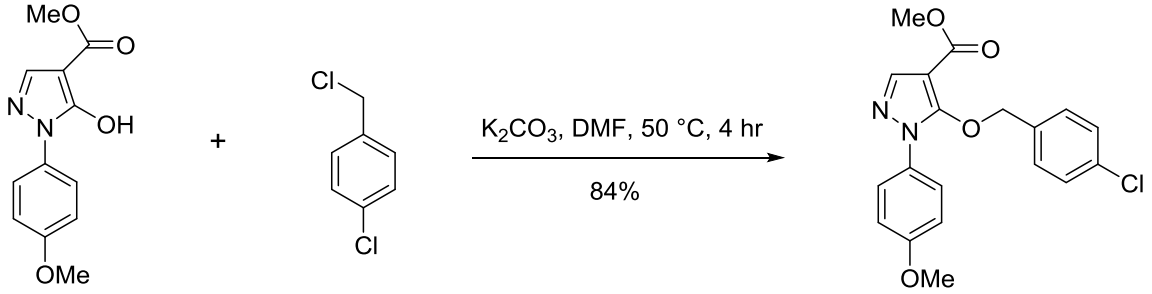

3.8 **3.11**

Figure 135. Synthesis of Analog **3.11**.

In an oven dried tube, phosphorous oxychloride (0.20 mL, 0.33 g, 2.18 mmol) and pyridine (0.18 mL, 0.17 g, 2.18 mmol) were added to methyl 5-hydroxy-1-(4-methoxyphenyl)-1H-pyrazole-4-carboxylate (**3.8**) (0.27 g, 1.09 mmol) at 0 °C and the tube was quickly sealed (Figure 136). The mixture was heated for 200 °C for 4 hours. The tube was opened and submerged in an ice bath. Then aqueous sodium bicarbonate was added carefully to pH 8. The product was extracted by ethyl acetate (3 X 20 mL). The organic layers were combined, washed with aqueous sodium bicarbonate (3 X 10 mL), and dried over anhydrous sodium sulfate. The mixture was concentrated and ether was added to precipitate the product, 0.18 g, 67% yield.

^{1}H NMR (500 MHz, $CDCl_3$) δ 8.21 (s, 1H), 7.45 (d, *J* = 9.2 Hz, 2H), 7.03 (d, *J* = 9.2 Hz, 2H), 3.88 (s, 3H).

^{13}C NMR (126 MHz, $CDCl_3$) δ 160.4, 156.3, 143.0, 133.1, 130.1, 127.0 (2C), 114.5 (2C), 110.8, 55.7.

HRMS (ESI): $C_{11}H_{10}ClN_2O_3$ $[M+H]^+$, Calculated: 253.03799, Found: 253.03685.

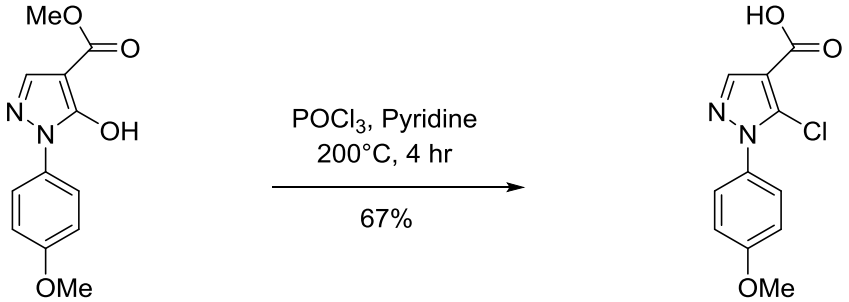

3.8 **3.12**

Figure 136. Synthesis of Analog **3.12**.

To stirred solution of aniline (0.01 mL, 0.01 g, 0.16 mmol) and triethylamine (0.02 mL, 0.01 g, 0.16 mmol) in dry THF was added 5-chloro-1-(4-methoxyphenyl)-1H-pyrazole-4-carboxylic acid (**3.12**) (0.04 g, 0.16 mmol) and the mixture was stirred at 27 °C for overnight (Figure 137). THF was evaporated using rotary evaporator under reduced pressure. The residue was dissolved in water (10 mL) and acidified to pH 2 using hydrochloric acid (2 N). The product was extracted with ethyl acetate (3 X 15 mL). The organic layers were combined, washed with 5% aqueous hydrochloric acid (4 X 10 mL), dried over anhydrous sodium sulfate and evaporated off to dryness using rotary evaporator. The resultant solid was suspended in ether and stirred vigorously for 10 min. The precipitate was collected by vacuum filtration and further dried on high vacuum to obtained 0.03 g, yield 67%.

^{1}H NMR (500 MHz, Acetonitrile-d_3) δ 8.48 (br. s., 1H), 8.13 (s, 1H), 7.66 (d, *J* = 8.6 Hz, 2H), 7.45 (d, *J* = 9.2 Hz, 2H), 7.32 - 7.37 (m, 2H), 7.10 - 7.14 (m, 1H), 7.06 (d, *J* = 9.2 Hz, 2H), 3.84 (s, 3H).

^{13}C NMR (126 MHz, Acetonitrile-d_3) δ 160.3, 159.4, 139.9, 138.6, 130.6, 129.2, 128.9 (2C), 127.3 (2C), 124.2, 120.3 (2C), 115.0, 114.4 (2C), 55.5.

HRMS (ESI): $C_{17}H_{16}N_3O_3$ $[M+H]^+$, Calculated: 310.11917, Found: 310.11870.

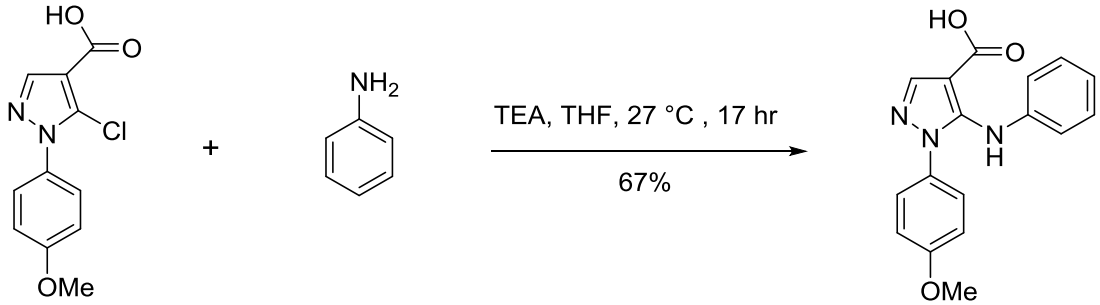

Figure 137. Synthesis of Analog **3.13**.

To stirred solution of phenylenediamine (0.02 g, 0.20 mmol) and triethyl amine (0.03 mL, 0.02 g, 0.20 mmol) in dry THF (6 mL) was added 5-chloro-1-(4-methoxyphenyl)-1H-pyrazole-4-carboxylic acid (**3.12**) (0.05 g, 0.20 mmol) and the mixture was stirred at 27 °C overnight (Figure 138). THF was evaporated using rotary evaporator under reduced pressure. The residue was dissolved in water (10 mL) and acidified to pH 2 using hydrochloric acid (2N). The product was precipitated upon extraction with ethyl acetate. Half of the solvent was evaporated and precipitate was collected by vacuum filtration, washed with water, and dried on high vacuum. 0.06 g was obtained, 89% yield.

^{1}H NMR (500 MHz, Methanol-D_3) δ 8.25 (s, 1H), 7.85 (d, *J* = 8.6 Hz, 2H), 7.45 (d, *J* = 8.6 Hz, 2H), 7.36 (d, *J* = 9.2 Hz, 2H), 7.10 (d, *J* = 9.2 Hz, 2H), 3.87 (s, 3H).

^{13}C NMR (126 MHz, Methanol-D_3) δ 160.65, 160.62, 139.6 (2C), 139.0, 130.2 (2C), 127.1 (2C), 123.0 (2C), 121.7 (2C), 114.6, 114.1 (2C), 54.8.

HRMS (ESI): $C_{17}H_{17}N_4O_3$ $[M+H]^+$, Calculated: 325.13007, Found: 325.12924.

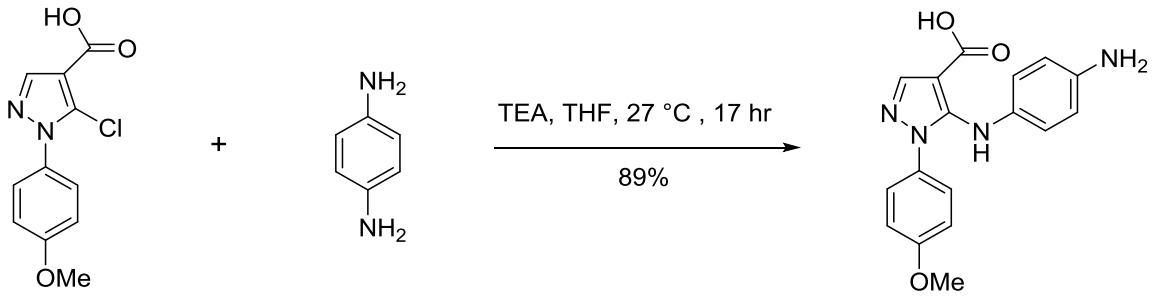

3.12 **3.14**

Figure 138. Synthesis of Analog **3.14**.

Dimethylethoxymethylene malonate (**3.15**) (1.50 g, 7.97 mmol) was added to a solution of potassium carbonate (1.10 g, 7.97 mmol) and 2,4 diflourophenylhydrazine (1.15 g, 7.97 mmol) in water (30 mL) and the reaction mixture was refluxed at 120 °C overnight (Figure 139). The reaction mixture was then cooled and washed with ethyl acetate (6 X 20 mL). The aqueous layer was then acidified to pH 2 using hydrochloric acid (2N). The resultant precipitate was collected by vacuum filtration, washed with water and dried under high vacuum. Recrystallization from aqueous methanol gives the desired product as pale yellow powder (1.41 g, yield 70%).

^{1}H NMR (500 MHz, $CDCl_3$) δ 9.38 (br. s, 1H), 7.80 (s, 1H), 7.43 - 7.52 (m, 1H), 6.97 - 7.03 (m, 2H), 3.89 (s, 3H).

^{13}C NMR (126 MHz, $CDCl_3$) δ 166.3, 162.9 (dd, J = 10.8, 252 Hz), 157.5, 156.6 (dd, J = 13.2, 256.7 Hz), 139.7, 129.1 (d. J = 10.8 Hz), 121.0 (dd, J = 3.6, 12 Hz), 112.1 (dd, J = 3.6, 22.8 Hz), 105.3 (dd, J = 22.8, 26.4 Hz), 94.4.

HRMS (ESI): $C_{11}H_9F_2N_2O_3$ $[M+H]^+$, Calculated: 255.05812, Found: 255.05689.

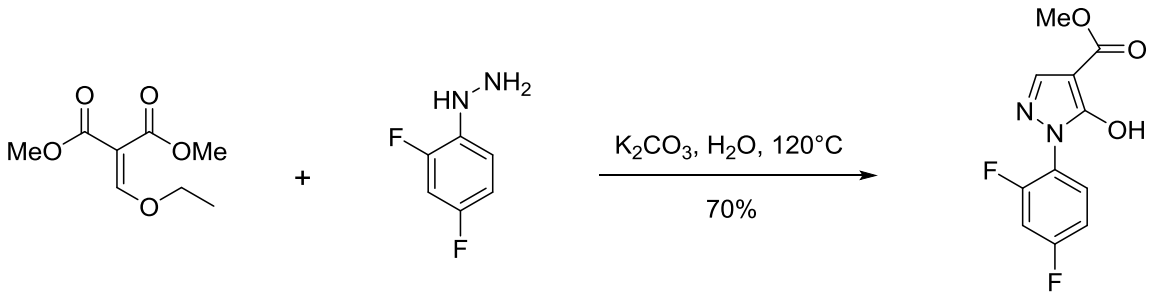

3.15 **3.3**

Figure 139. Synthesis of Analog **3.3**.

To a solution of methyl 1-(2,4-difluorophenyl)-5-hydroxy-1H-pyrazole-4-carboxylate (**3.3**) (0.02 g, 0.08 mmol) and potassium carbonate (0.01 g, 0.08 mmol) in DMF (3 mL) at room temperature, was added iodoethane (0.006 mL, 0.01 g, 0.08 mmol) and the mixture was stirred at ambient temperature for 17 hours (Figure 140). Water (15 mL) was added and the product was extracted with ethyl acetate (4 X 20 mL). The organic layers were combined, washed with water, dried over anhydrous Na_2SO_4 and evaporated under reduced pressure. The crude was purified by column chromatography to obtain 0.02 g of product as white solid (78% yield).

^{1}H NMR (500 MHz, $CDCl_3$) δ 7.95 (s, 1H), 7.39 - 7.46 (m, 1H), 6.96 - 7.03 (m, 2H), 4.52 (q, *J* = 7.3 Hz, 2H), 3.84 (s, 3H), 1.27 (t, *J* = 7.2 Hz, 3H).

^{13}C NMR (126 MHz, $CDCl_3$) δ 162.8 (dd, J = 10.8, 252 Hz), 162.7, 157.1 (dd, J = 13.2, 256.7 Hz), 156.0, 143.1, 129.7 (dd, J = 10.8 Hz), 121.8 (dd, J = 3.6, 12.0 Hz), 112.0 (dd, J = 3.6, 22.8 Hz), 105.1 (dd, J = 22.8, 26.4 Hz), 99.4, 72.2, 51.5, 15.3.

HRMS (ESI): $C_{13}H_{13}F_2N_2O_3$ $[M+H]^+$, Calculated: 283.08942, Found: 283.08818.

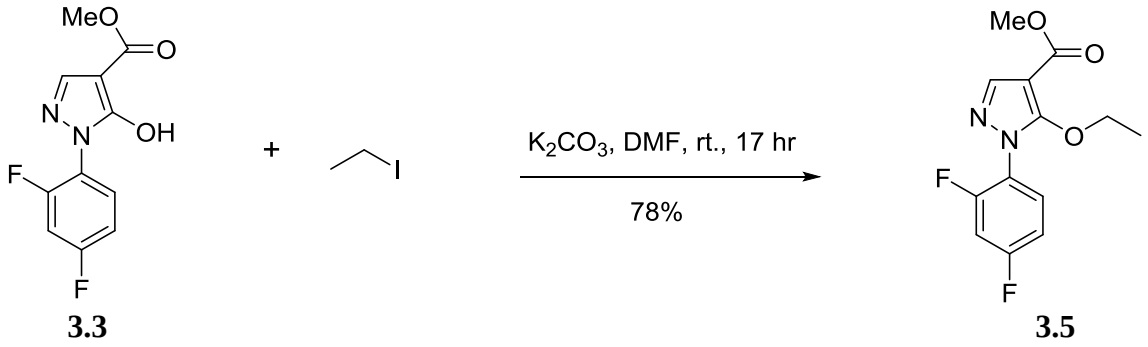

Figure 140. Synthesis of Analog **3.5**.

In an oven dried tube, phosphorous oxychloride (0.15 mL, 0.24 g, 1.57 mmol) and pyridine (0.12 mL, 0.12 g, 1.57 mmol) were added to methyl 1-(2,4-difluorophenyl)-5-hydroxy-1H-pyrazole-4-carboxylate (**3.3**) (0.2 g, 0.79 mmol) at 0°C and the tube was quickly sealed (Figure 141). The mixture was heated for 200 °C for 4 hours. The tube was submerged in an ice bath then aqueous sodium bicarbonate was added carefully to pH 8. The product was extracted by ethyl acetate (3 X 20 mL). The organic layers were combined, washed with aqueous sodium bicarbonate (3 X 10 mL), dried over anhydrous sodium sulfate, and evaporated to dryness using rotary evaporator under reduced pressure. The resultant product was dissolved in diethyl ether (20 mL), stirred for 15 minutes then filtered under vacuum. The ether was evaporated off and the product was dried to produce a beige solid (0.16 g, yield 80%).

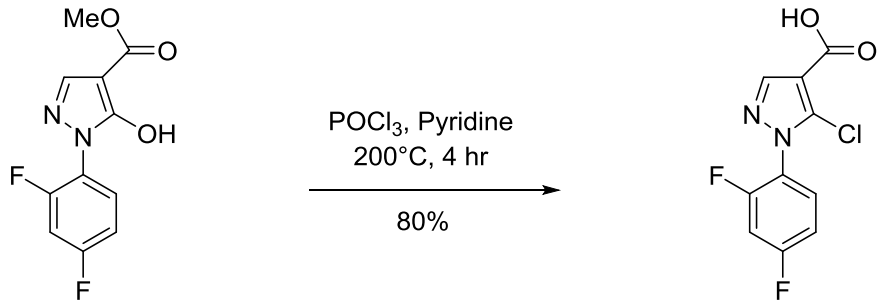

3.3 **3.17**

Figure 141. Synthesis of Compound **3.17**.

^{1}H NMR (500 MHz, Acetone-d_6) δ 8.47 (s, 1H), 7.83 (td, J_d = 5.7, J_t = 8.6 Hz, 1H), 7.44 - 7.50 (m, 1H), 7.32 - 7.38 (m, 1H).

^{13}C NMR (126 MHz, Acetone-d_6) δ 163.9 (dd, *J* = 12, 252 Hz), 157.5 (dd, *J* = 13.2, 254.3 Hz), 155.9, 143.8, 135.1, 131.1 (d, *J* = 10.8 Hz), 121.6 (dd, *J* = 4.8, 13.2 Hz), 112.7 (dd, *J* = 3.6, 22.8 Hz), 110.6, 105.4 (dd, *J* = 24, 27.6 Hz).

HRMS (ESI): $C_{10}H_6ClF_2N_2O_2$ $[M+H]^+$, Calculated: 259.00859, Found: 259.00766.

In an oven dried tube, phosphorous oxychloride (0.22 mL, 0.36 g, 2.36 mmol) and pyridine (0.19 mL, 0.19 g, 2.36 mmol) were added to methyl 1-(2,4-difluorophenyl)-5-hydroxy-1H-pyrazole-4-carboxylate (**3.3**) (0.3 g, 1.18 mmol) at 0 °C and the tube was quickly sealed (Figure 142). The mixture was heated for 200 °C for overnight. The reaction mixture was cooled to room temperature then transferred via syringe to a short silica fritted column and eluted under vacuum with 150 mL of a mixture of ethyl acetate and hexane (2/98). The solvent was evaporated using rotary evaporator under reduced pressure followed by high vacuum drying to produce the intended product, light beige colored (0.3 g, yield 92%).

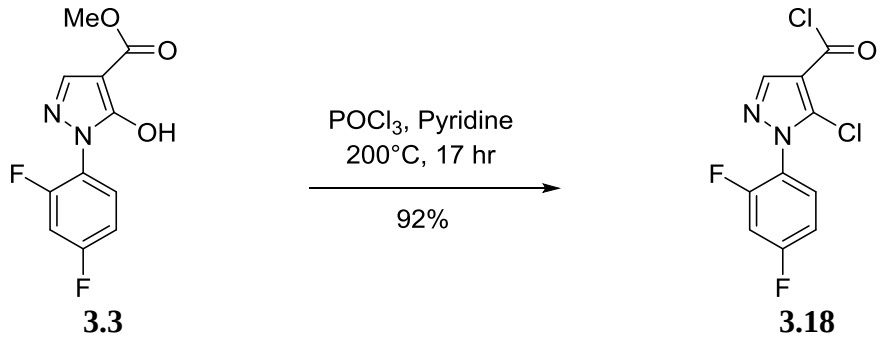

3.3 **3.18**

Figure 142. Synthesis of Compound **3.18**.

^{1}H NMR (500 MHz, Acetone-d_6) δ 8.43 (s, 1H), 7.83 (td, J_d = 5.7, J_t = 8.6 Hz, 1H), 7.44 - 7.50 (m, 1H), 7.33 - 7.38 (m, 1H).

^{13}C NMR (126 MHz, Acetone-d_6) δ 164.9 (dd, *J* = 10.8, 252 Hz), 158.6, 158.2 (dd, *J* = 13.2, 254.3 Hz), 146.2, 135.6, 131.8 (d, *J* = 10.8 Hz), 122.2 (dd, *J* = 3.6, 12 Hz), 116.4, 113.7 (dd, *J* = 3.6, 22.8 Hz), 106.3 (dd, *J* = 22.8, 27.6 Hz).

HRMS (ESI): $C_{10}H_5C_{l2}F_2N_2O$ $[M+H]^+$, Calculated: 276.97470, Found: 276.97362.

To stirred solution of aniline (0.02 mL, 0.02 g, 0.18 mmol) and triethyl amine (0.03 mL, 0.02 g, 0.18 mmol) in THF (8 mL) was added 5-chloro-1-(2,4-difluorophenyl)-1H-pyrazole-4-carbonyl chloride (**3.18**) (0.05 g, 0.18 mmol) and the mixture was stirred at room temperature for 1 hour (Figure 143). THF was evaporated off using rotary evaporator under reduced pressure. The residue was dissolved in ethyl acetate, washed with 5% aqueous HCl (3 X 10 mL), and dried over sodium sulfate. Product was precipitated in the ethyl acetate layer during solvent evaporation under reduced pressure. The crystals were collected by vacuum filtration (0.06 g, 93% yield).

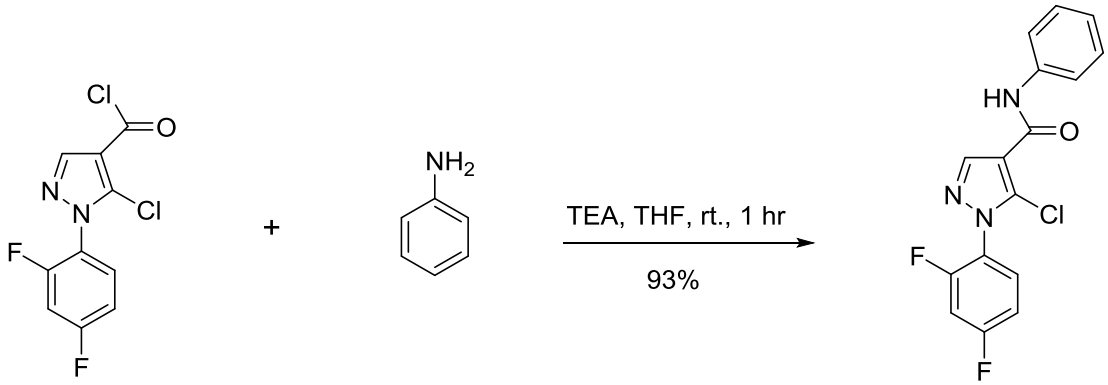

Figure 143. Synthesis of Analog **3.6**.

^{1}H NMR (500 MHz, $CDCl_3$) δ 8.26 (s, 1H), 7.94 (br. s., 1H), 7.61 (d, *J* = 8.02 Hz, 2H), 7.45 - 7.52 (m, 1H), 7.37 (t, *J* = 8.02 Hz, 2H), 7.16 (t, *J* = 7.45 Hz, 1H), 7.02 - 7.10 (m, 2H).

^{13}C NMR (126 MHz, $CDCl_3$) δ 163.7 (dd, J = 10.8, 254.3 Hz), 158.6, 157.5 (dd, J = 12.00, 256.7 Hz), 142.9, 137.4, 130.3 (dd, J = 9.6 Hz), 129.3 (2C), 128.3, 124.9, 121.6 (dd, J = 3.6, 12.0 Hz), 120.4 (2C), 115.7, 112.5 (dd, J = 3.6, 22.8 Hz), 105.5 (dd, J = 22.8, 26.4 Hz).

HRMS (ESI): $C_{16}H_{11}ClF_2N_3O$ $[M+H]^+$, Calculated: 334.05587, Found: 334.05454.

Following a reported procedure,[9] to stirred solution of 1,4-phenylene diamine (0.2 g, 1.85 mmol) in benzene was added cyclohexyl isocyanate (0.24 mL, 0.23 g, 1.85 mmol) and the mixture was stirred at 27 °C under nitrogen atmosphere overnight (Figure 144). The solid formed was collected by filtration, washed with benzene, collected and dried on high vacuum. A white powder product was obtained (0.43 g, yield 93%).

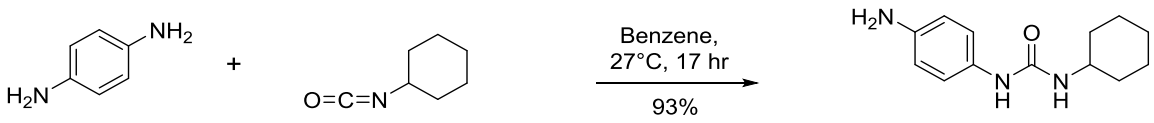

3.4

Figure 144. Synthesis of Urea **3.4**.

^{1}H NMR (500 MHz, DMSO-d_6) δ 7.75 (s, 1H), 6.98 (d, *J* = 8.6 Hz, 2H), 6.45 (d, *J* = 8.6 Hz, 2H), 5.79 (d, *J* = 7.4 Hz, 1H), 4.64 (br. s., 2H), 3.34 - 3.48 (m, 1H), 1.72 - 1.83 (m, 2H), 1.60 - 1.69 (m, 2H), 1.52 (m, 1H), 1.22 - 1.34 (m, 2H), 1.05 - 1.21 (m, 3H).

^{13}C NMR (126 MHz, DMSO-d_6) δ 155.5, 143.7, 130.3, 120.5 (2C), 114.7 (2C), 48.0, 33.7 (2C), 25.8, 24.9 (2C).

HRMS (ESI): $C_{13}H_{20}N_3O$ $[M+H]^+$, Calculated: 234.16064, Found: 234.15929.

To stirred solution of N-(4-aminophenyl)-N-cyclohexyl urea (**3.4**) (0.09 g, 0.39 mmol) and triethyl amine (0.05 mL, 0.04 g, 0.39 mmol) in dry THF (10 mL) was added 5-chloro-1-(2,4-difluorophenyl)-1H-pyrazole-4-carboxylic acid (**3.17**) (0.10 g, 0.39 mmol) and the mixture was stirred at 27 °C for overnight (Figure 145). THF was evaporated using rotary evaporator under reduced pressure. The residue was dissolved in water and acidified to pH 2 using hydrochloric acid (2N). The product was extracted with ethyl acetate (3 X 20 mL). The organic layers were combined, washed with 5% aqueous hydrochloric acid (4 X 15 mL), dried over anhydrous sodium sulfate and solvent was evaporated off to dryness using rotary evaporator. The resultant paige pinkish solid was suspended in ether and stirred vigorously for 10 min. The white precipitate was collected by vacuum filtration and further drying on high vacuum to obtain 0.14 g, yield 82%.

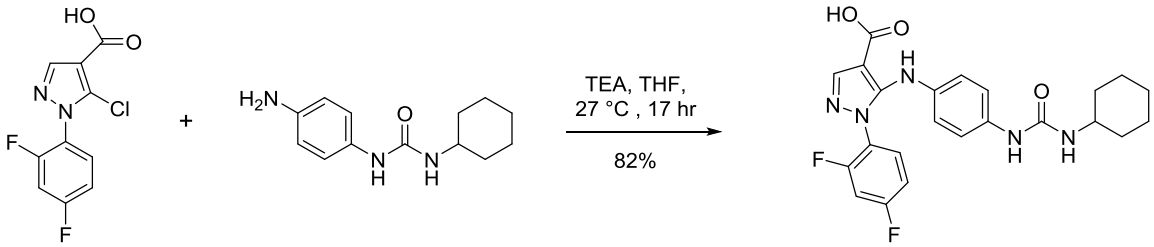

3.17 **3.4** **3.1**

Figure 145. Synthesis of Analog **3.1**.

^{1}H NMR (500 MHz, Acetone-d_6) δ 9.19 (s, 1H), 8.29 (s, 1H), 7.80 (s, 1H), 7.71 (dt, J_d = 5.7, J_t = 8.6 Hz, 1H), 7.59 (d, *J* = 9.2 Hz, 2H), 7.43 (d, *J* = 9.2 Hz, 2H), 7.37 - 7.42 (m, 1H), 7.26 - 7.31 (m, 1H), 5.68 (d, *J* = 8.0 Hz, 1H), 3.53 - 3.61 (m, 1H), 1.84 - 1.92 (m, 2H), 1.67 (td, J_t = 3.8, J_d = 13.6 Hz, 2H), 1.52 - 1.59 (m, 1H), 1.27 - 1.37 (m, 2H), 1.12 - 1.21 (m, 3H).

^{13}C NMR (126 MHz, Acetone-d_6) δ 163.6 (dd, *J* = 10.8, 250.7 Hz) , 158.5, 157.6 (dd, *J* = 13.2, 254.3 Hz), 154.6, 140.8, 137.2, 132.6, 131.1(d, *J* = 10.8 Hz), 130.8, 122.2(dd, *J* = 3.6, 13.2 Hz), 120.7 (2C), 118.1(2C), 115.6, 112.5 (dd, *J* = 3.6, 22.8 Hz), 105.2 (dd, J = 24.0, 27.6 Hz), 48.3, 33.4(2C), 25.6 (2C), 24.8.

HRMS (ESI): $C_{23}H_{24}F_2N_5O_3$ $[M+H]^+$, Calculated: 456.18472, Found: 456.18297.

N-(4-aminophenyl)-N-cyclohexyl urea (**3.4**) (0.04 g, 0.16 mmol) and triethylamine (0.03 mL, 0.02 g, 0.16 mmol) were stirred in THF (6 mL) at room temperature for 15 min before 5-chloro-1-(2,4-difluorophenyl)-1H-pyrazole-4-carbonyl chloride (0.05 g, 0.18 mmol) was added (Figure 146). The consumption of the pyrazole was completed after 0.5 hours (monitored by TLC). THF was evaporated off using rotary evaporator under reduced pressure. The residue was dissolved in ethyl acetate and

washed with 5% aqueous HCl (3 X 10 mL). The product was precipitated in the ethyl acetate layer during the washing process. Half of the solvent was removed and a white crystal product was collected by vacuum filtration (0.06 g, yield 75%).

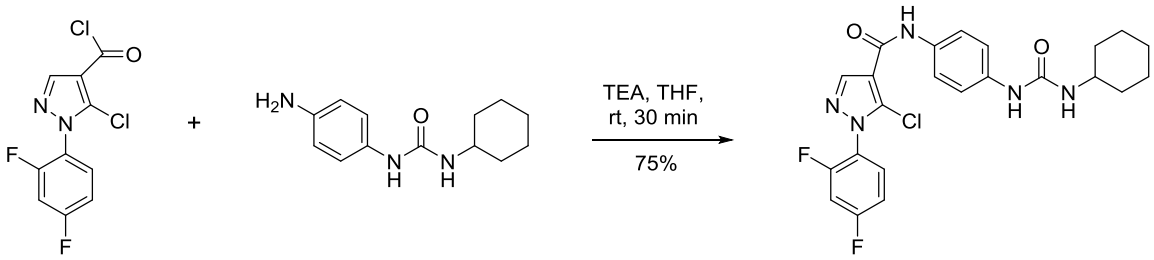

3.18 **3.4** **3.2**

Figure 146. Synthesis of Analog **3.2**.

^{1}H NMR (500 MHz, DMSO-d_6) δ 9.95 (s, 1H), 8.44 (s, 1H), 8.25 (s, 1H), 7.78 (dt, J_d = 5.70, J_t = 8.60 Hz, 1H), 7.65 - 7.71 (m, 1H), 7.53 (d, J = 8.6 Hz, 2H), 7.35 - 7.39 (m, 1H), 7.34 (d, J = 8.6 Hz, 2H), 6.02 (d, J = 8.0 Hz, 1H), 3.41 - 3.50 (m, 1H), 1.76 - 1.84 (m, 2H), 1.62 - 1.69 (m, 2H), 1.49 - 1.58 (m, 1H), 1.25 - 1.36 (m, 2H), 1.10 - 1.24 (m, 3H).

^{13}C NMR (126 MHz, DMSO-d_6) δ 163.2 (dd, J= 10.8, 250.7 Hz) , 158.7, 157.2 (dd, J = 13.2, 254.3 Hz), 154.7, 141.3, 137.0, 132.3, 131.5 (d, J = 10.8 Hz), 131.1, 121.8 (dd, J = 3.6, 12.0 Hz), 121.3 (2C), 118.0 (2C), 115.3, 113.1 (dd, J = 3.6, 22.8 Hz), 105.9 (dd, J = 24, 27.6 Hz), 47.9, 33.3 (2C), 25.6, 24.7(2C).

HRMS (ESI): $C_{23}H_{23}ClF_2N_5O_2$ $[M+H]^+$, Calculated: 474.15083, Found: 474.14879.

NMR Spectra

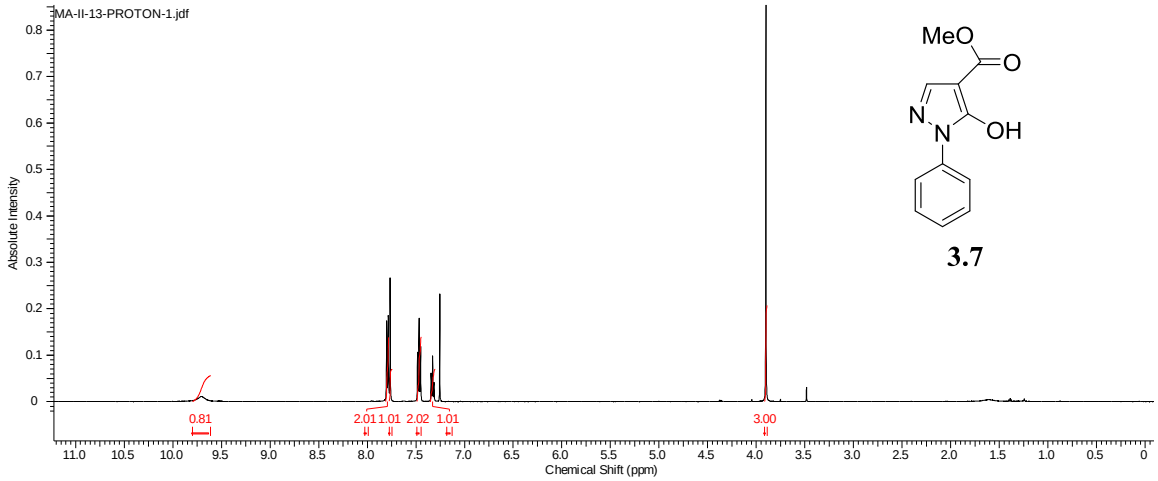

Figure 147. ^{1}H NMR Spectra of Compound **3.7**.

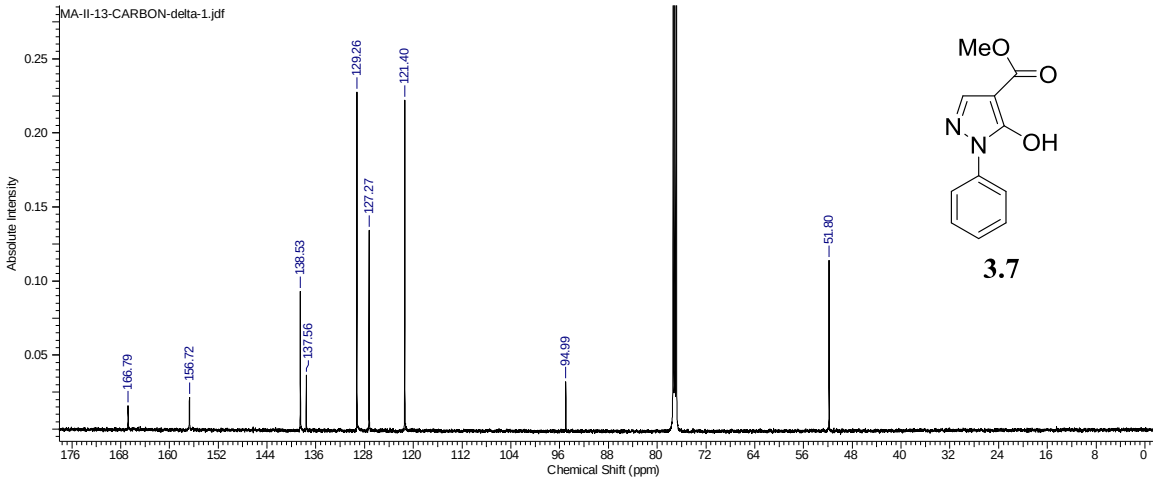

Figure 148. ^{13}C NMR Spectra of Compound **3.7**.

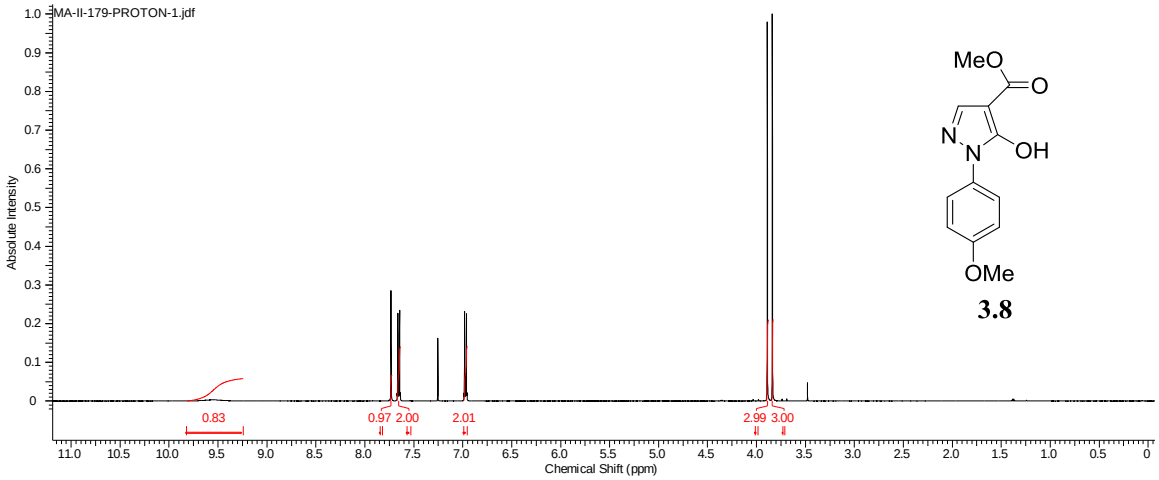

Figure 149. ^{1}H NMR Spectra of Compound **3.8**.

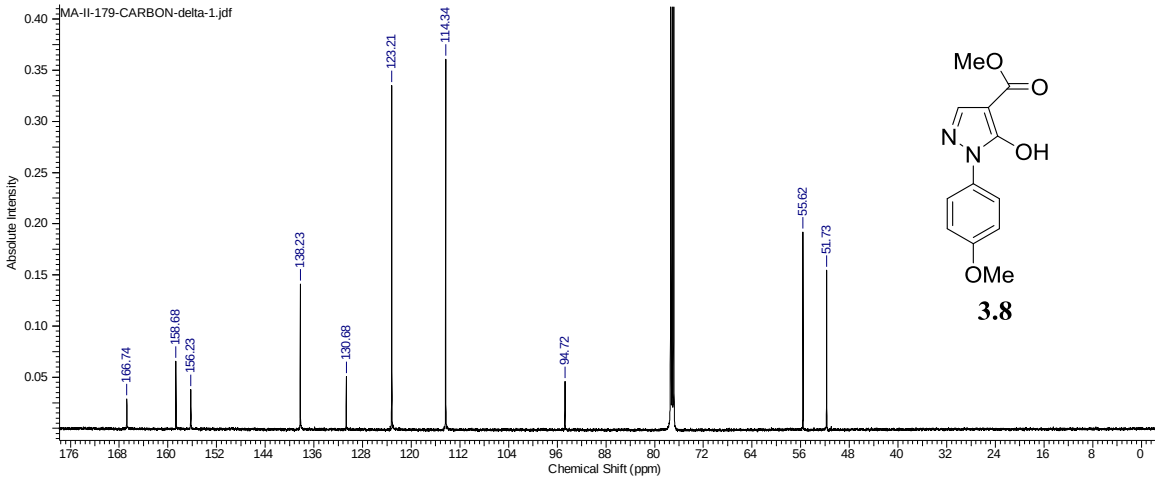

Figure 150. ^{13}C NMR Spectra of Compound **3.8**.

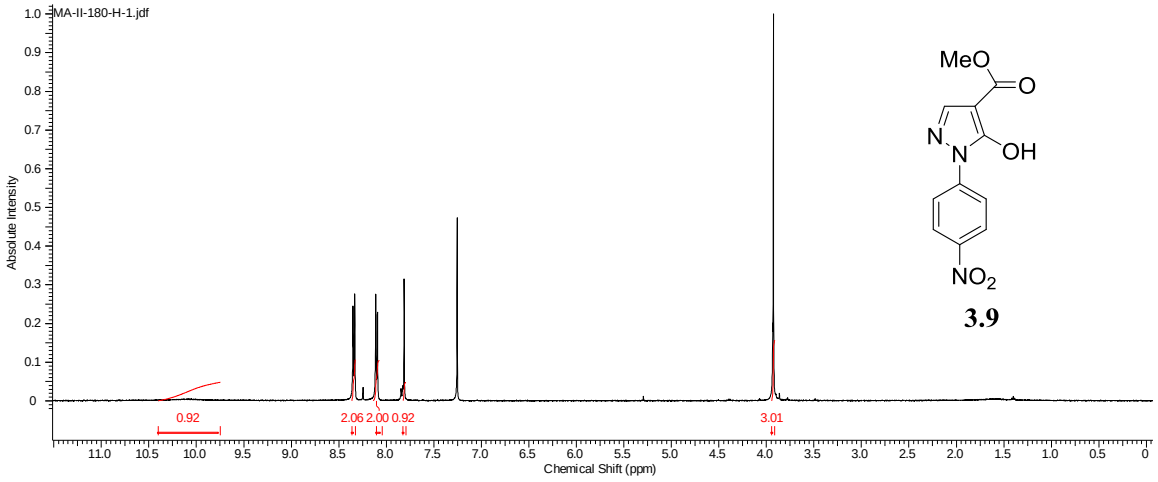

Figure 151. ^{1}H NMR Spectra of Compound **3.9**.

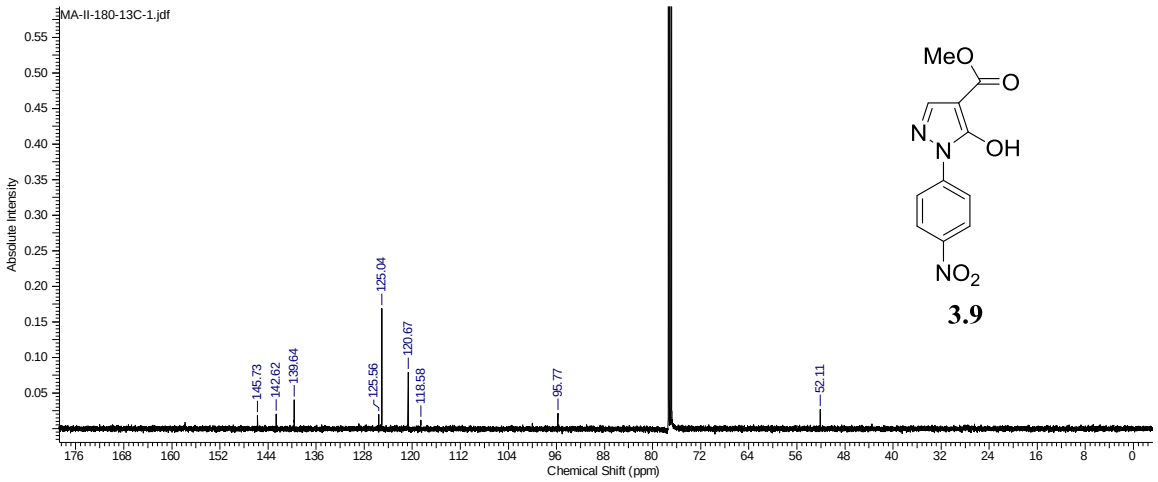

Figure 152. ^{13}C NMR Spectra of Compound **3.9**.

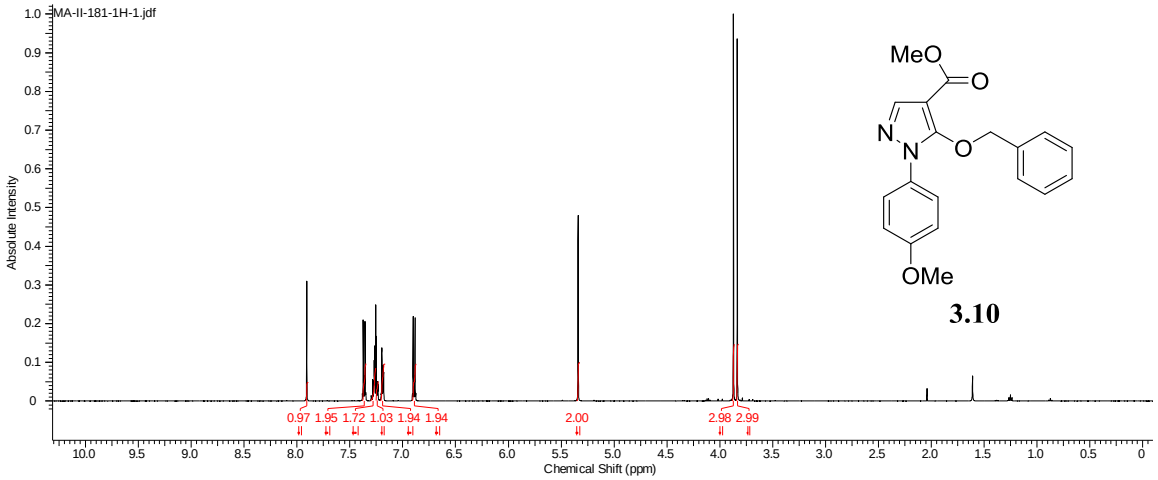

Figure 153. ^{1}H NMR Spectra of Compound **3.10**.

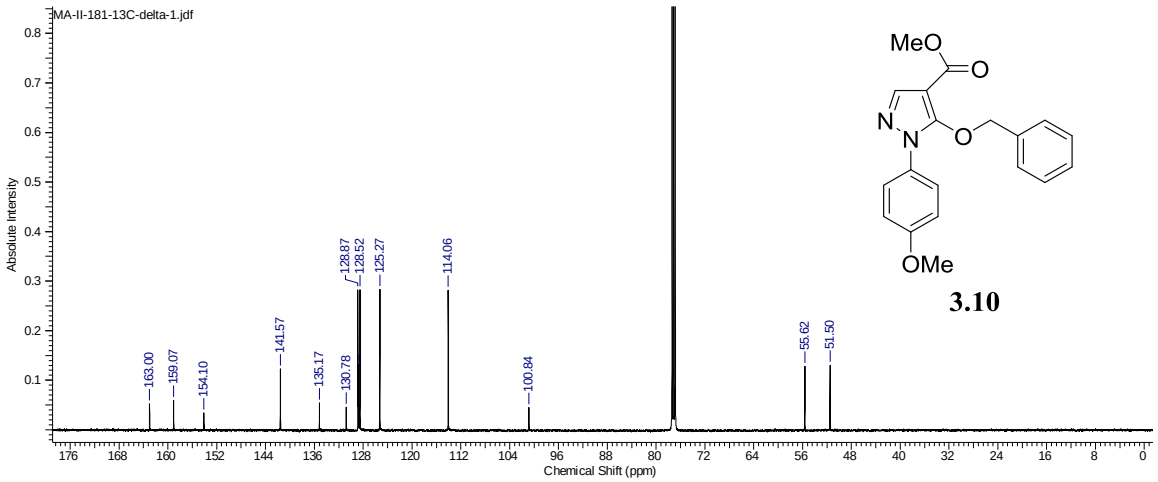

Figure 154. ^{13}C NMR Spectra of Compound **3.10**.

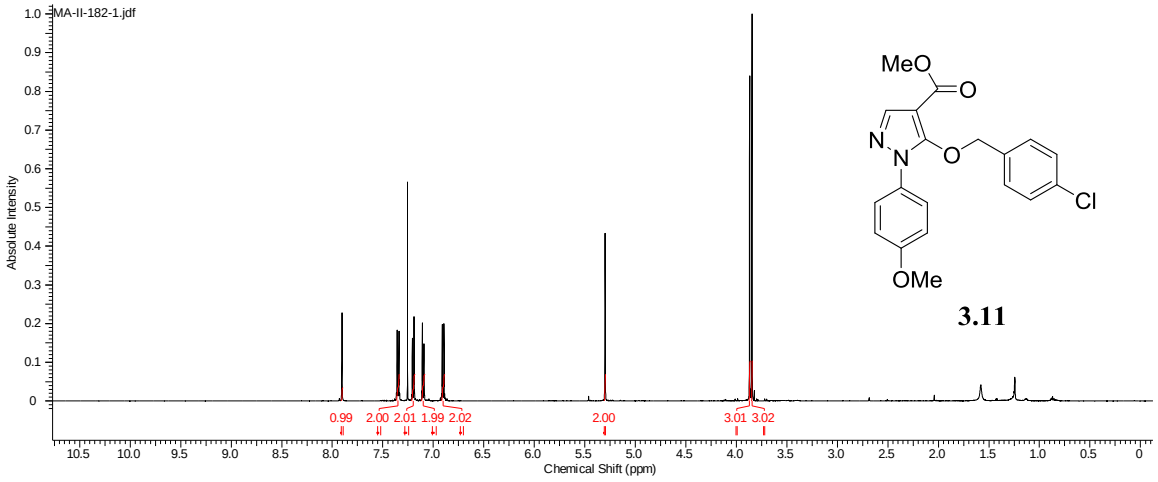

Figure 155. ^{1}H NMR Spectra of Compound **3.11**.

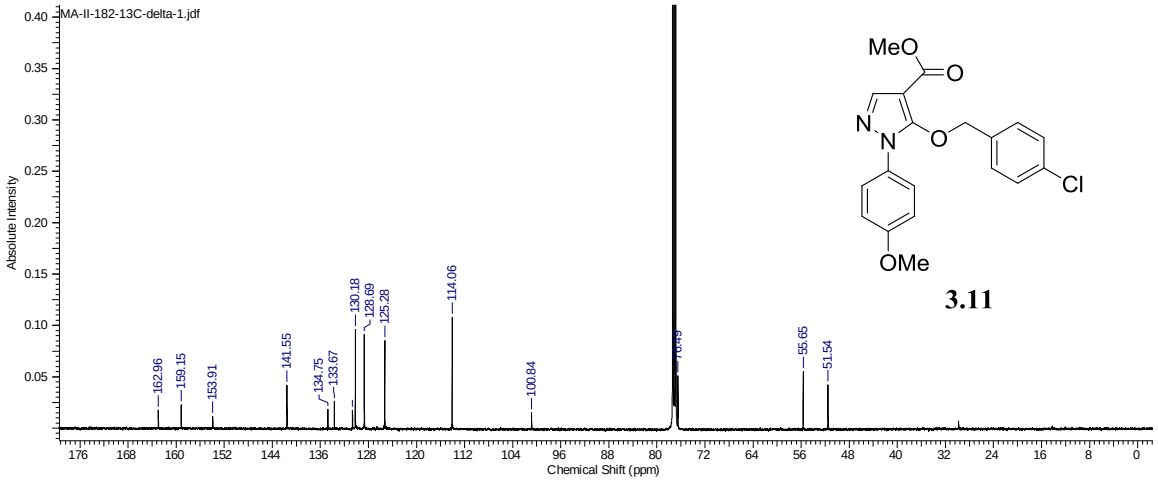

Figure 156. ^{13}C NMR Spectra of Compound **3.11**.

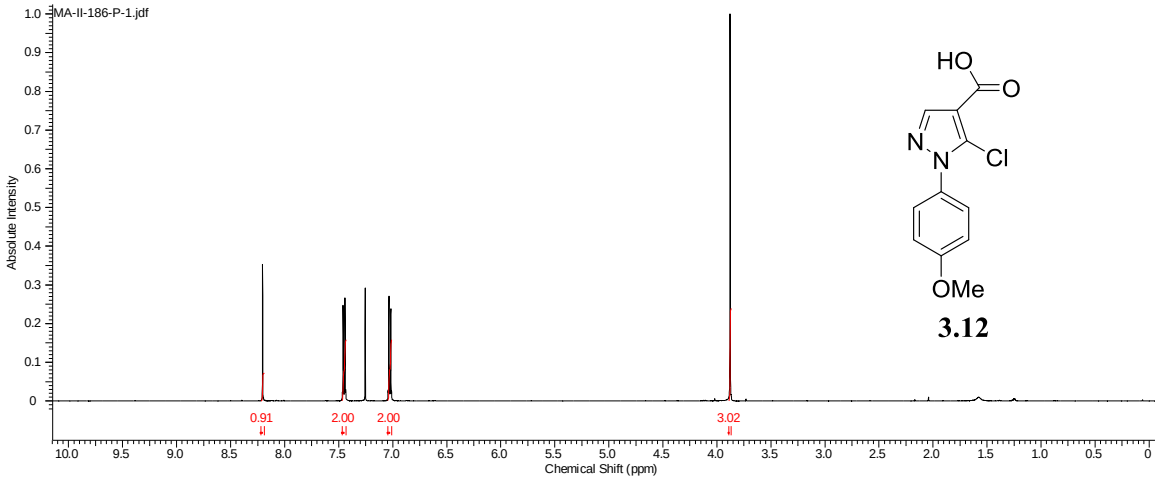

Figure 157. ^{1}H NMR Spectra of Compound **3.12**.

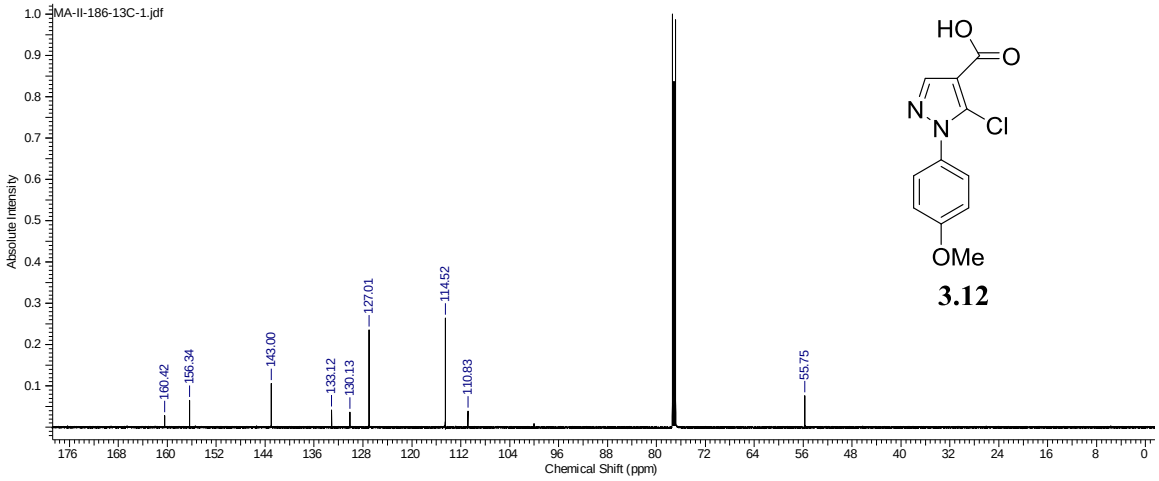

Figure 158. ^{13}H NMR Spectra of Compound **3.12**.

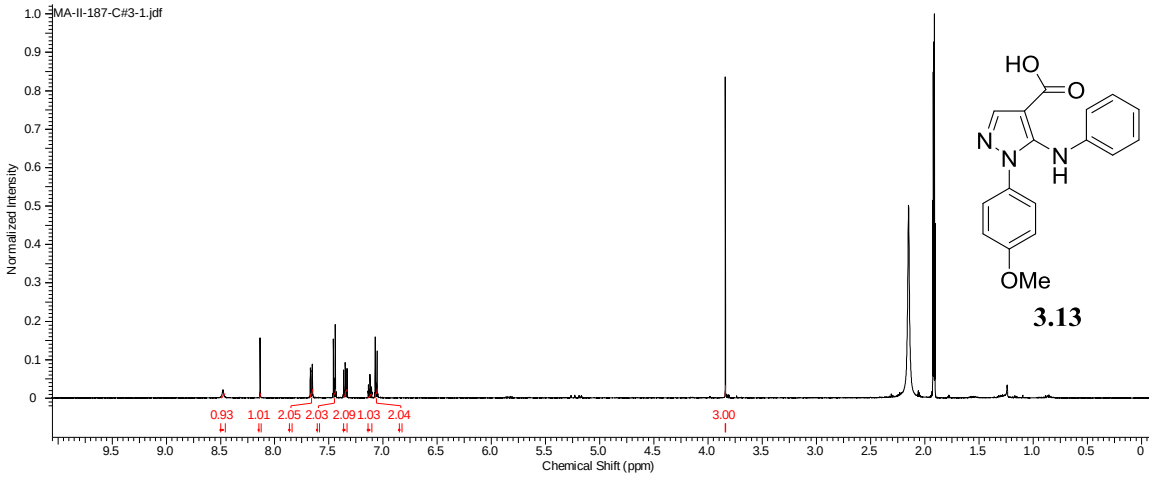

Figure 159. ^{1}H NMR Spectra of Compound **3.13**.

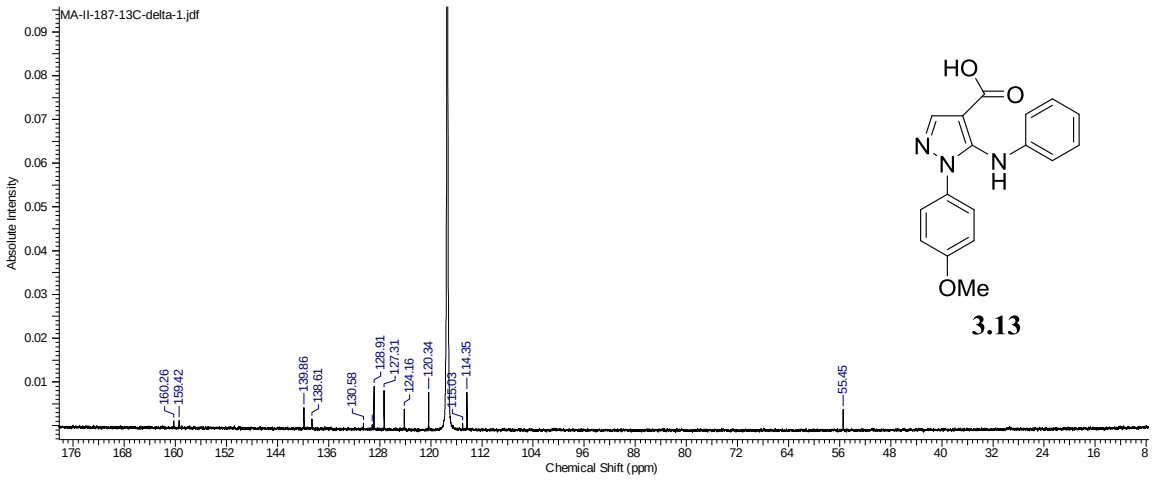

Figure 160. ^{13}C NMR Spectra of Compound **3.13**.

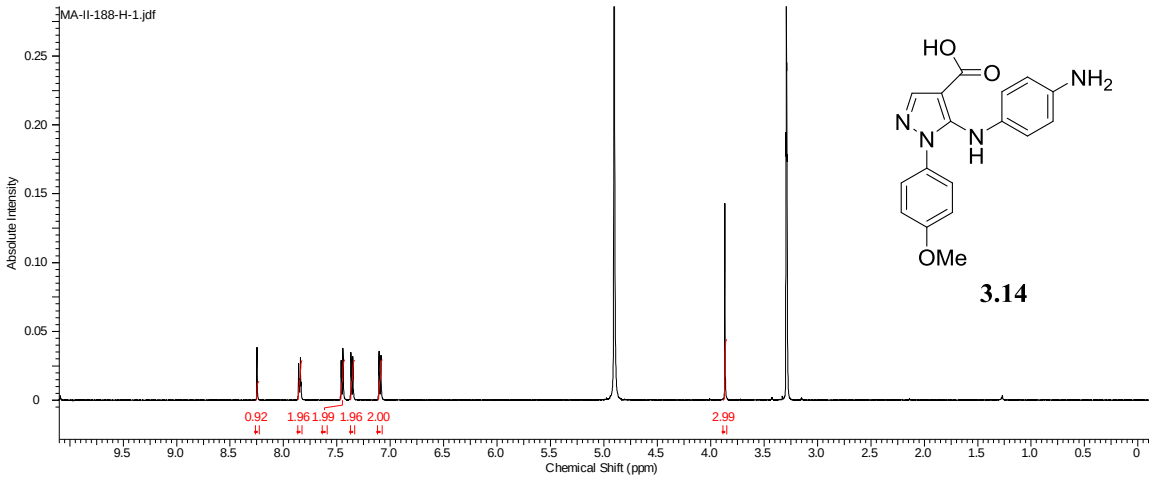

Figure 161. ^{1}H NMR Spectra of Compound **3.14**.

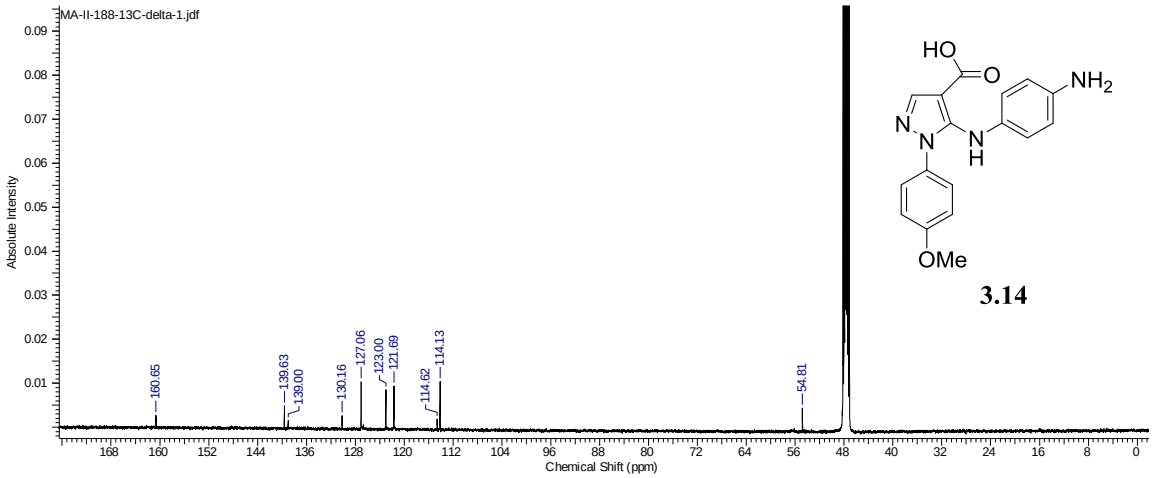

Figure 162. ^{13}C NMR Spectra of Compound **3.14**.

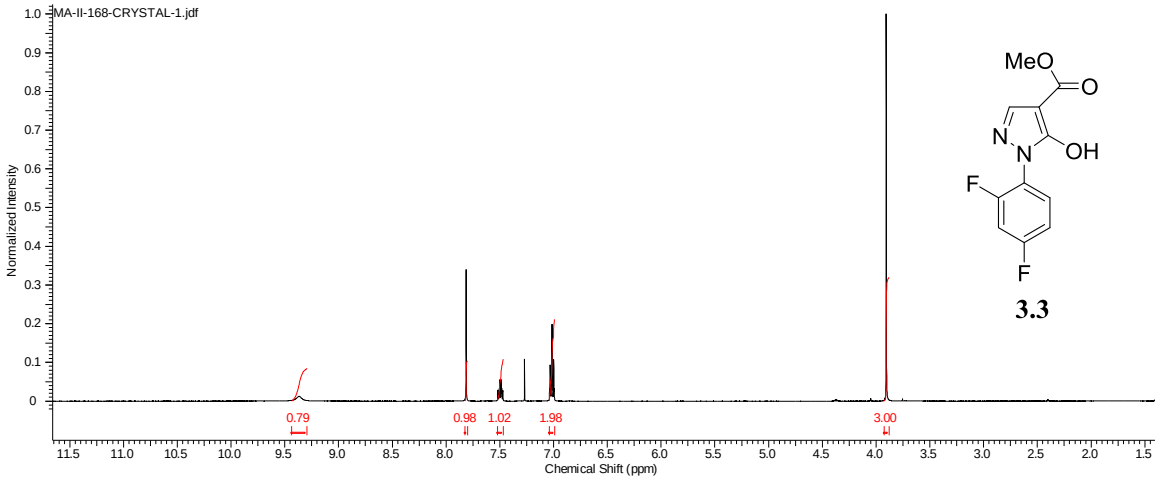

Figure 163. ^{1}H NMR Spectra of Compound **3.3**.

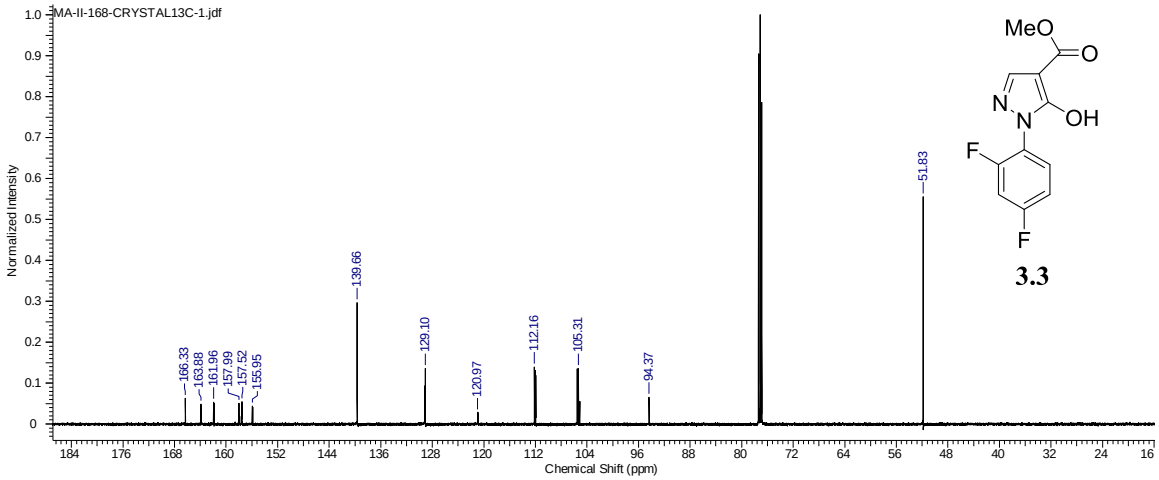

Figure 164. ^{13}C NMR Spectra of Compound **3.3**.

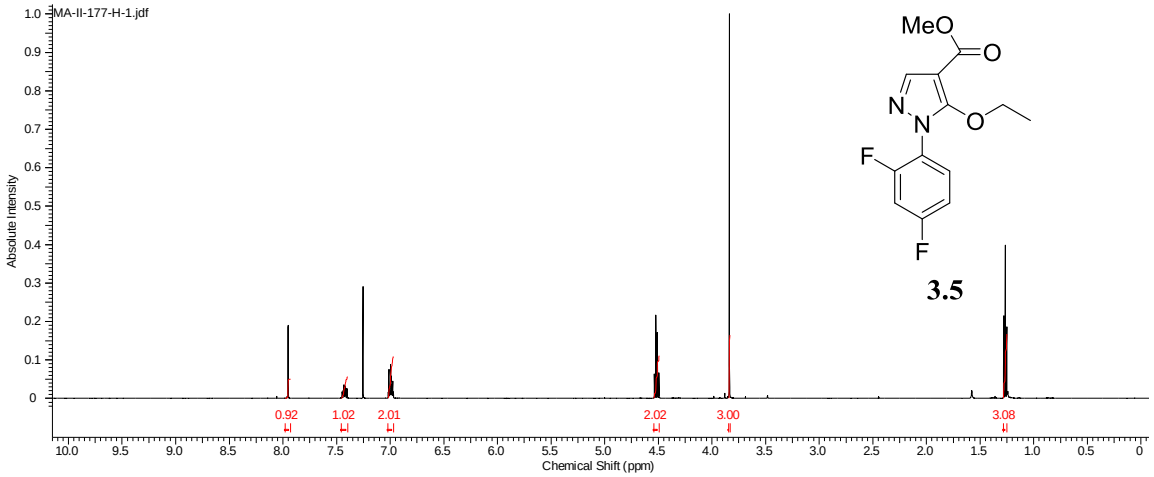

Figure 165. ^{1}H NMR Spectra of Compound **3.5**.

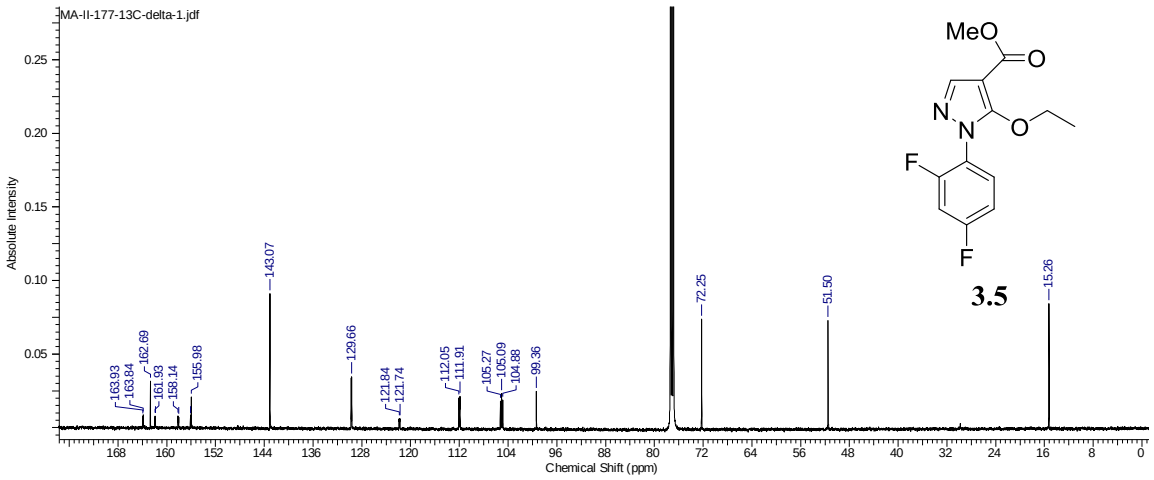

Figure 166. ^{13}C NMR Spectra of Compound **3.5**.

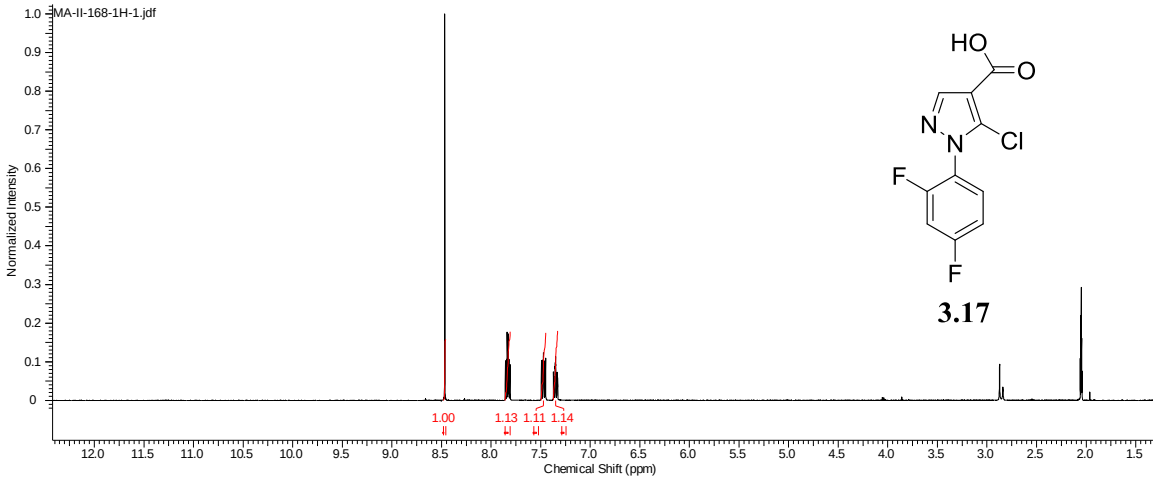

Figure 167. ^{1}H NMR Spectra of Compound **3.17**.

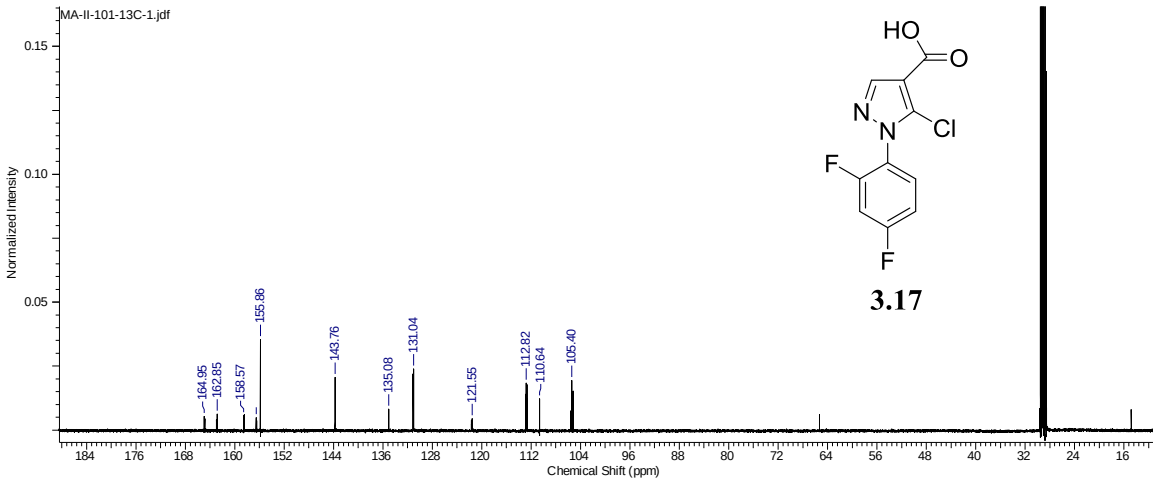

Figure 168. ^{13}C NMR Spectra of Compound **3.17**.

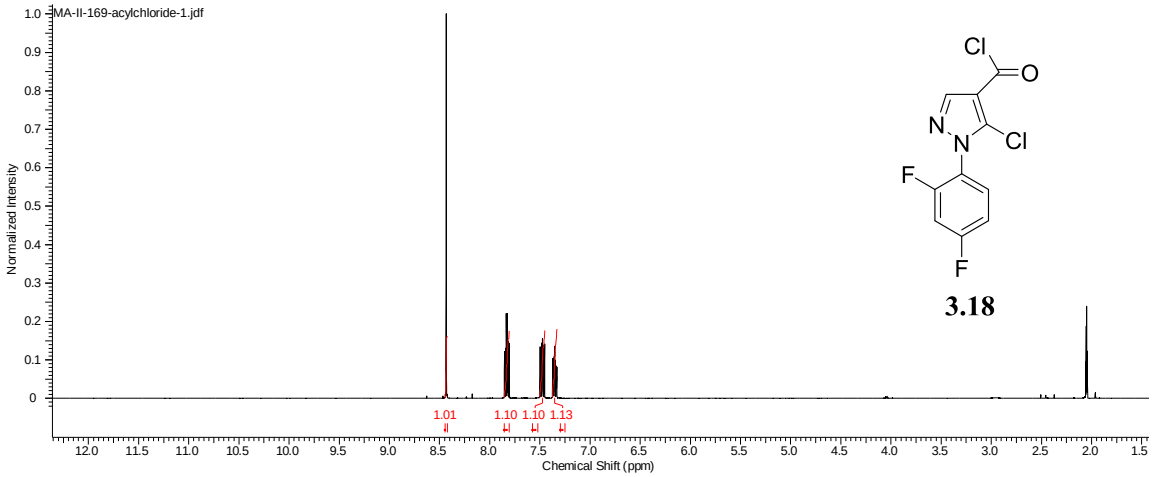

Figure 169. ^{1}H NMR Spectra of Compound **3.18**.

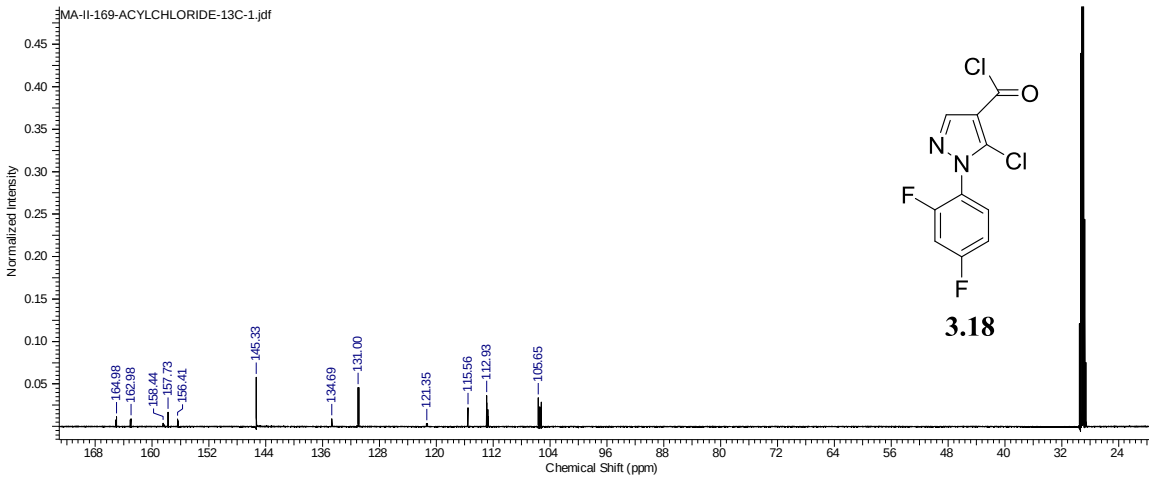

Figure 170. ^{13}C NMR Spectra of Compound **3.18**.

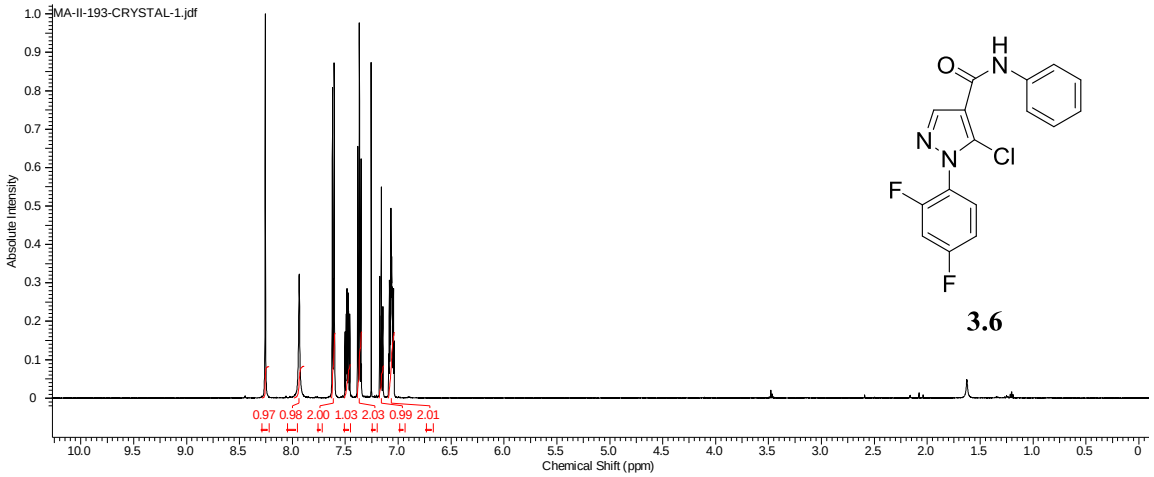

Figure 171. ^{1}H NMR Spectra of Compound **3.6**.

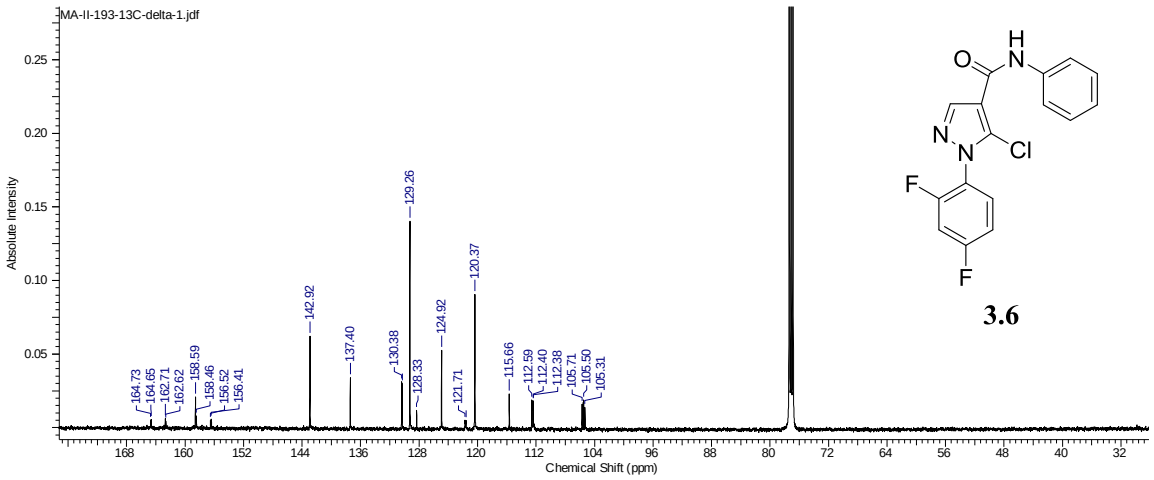

Figure 172. ^{13}C NMR Spectra of Compound **3.6**.

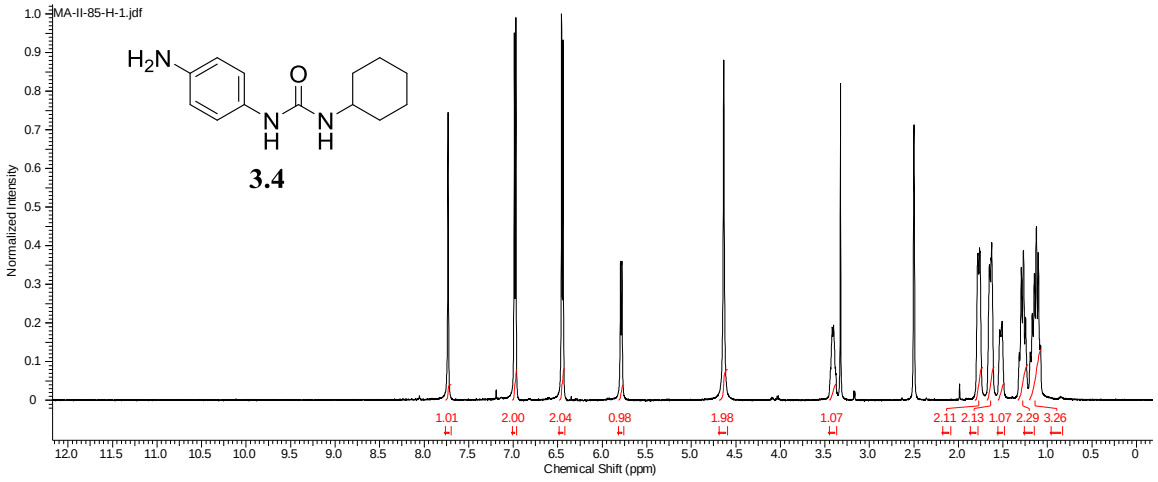

Figure 173. ^{1}H NMR Spectra of Compound **3.4**.

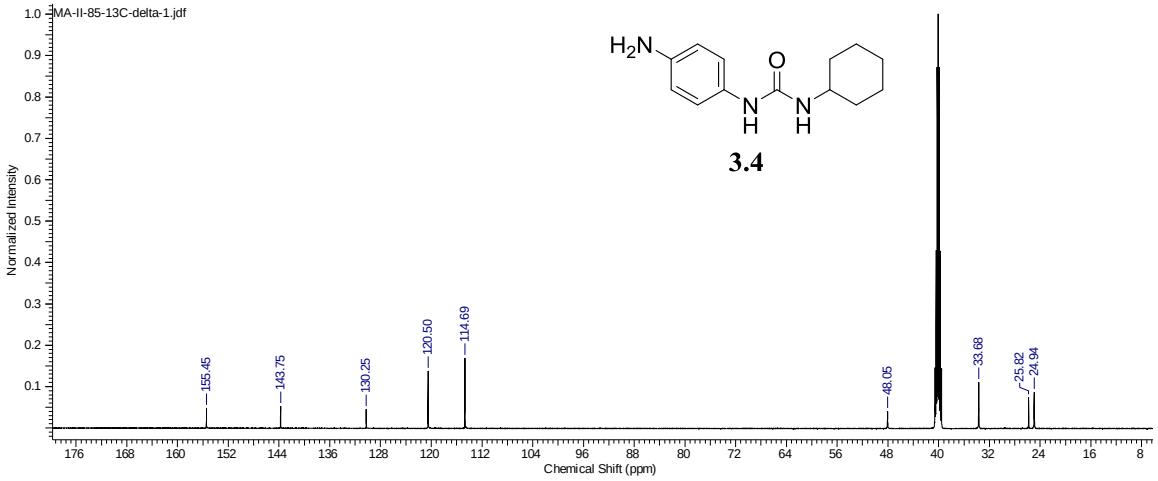

Figure 174. ^{13}C NMR Spectra of Compound **3.4**.

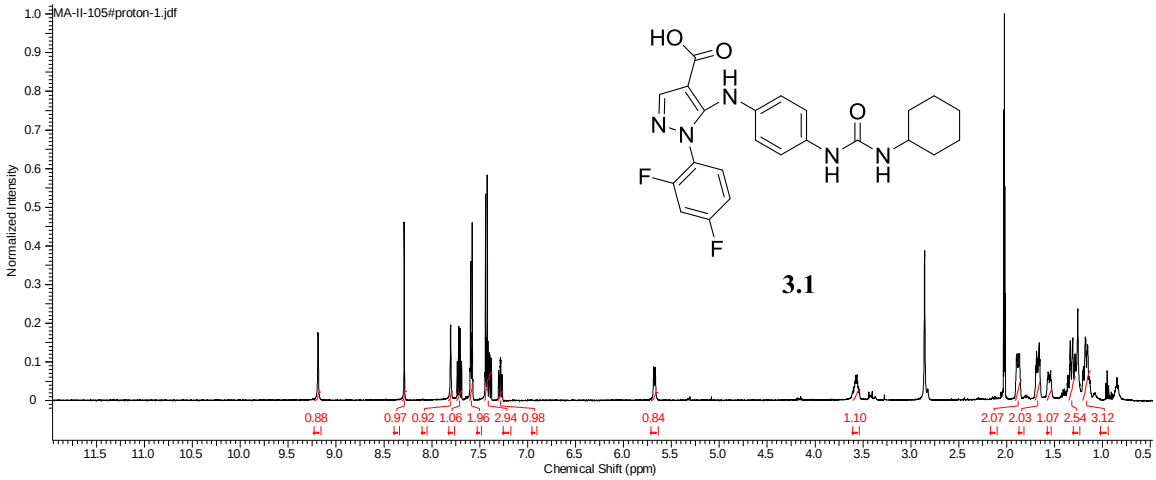

Figure 175. ^{1}H NMR Spectra of Compound **3.1**.

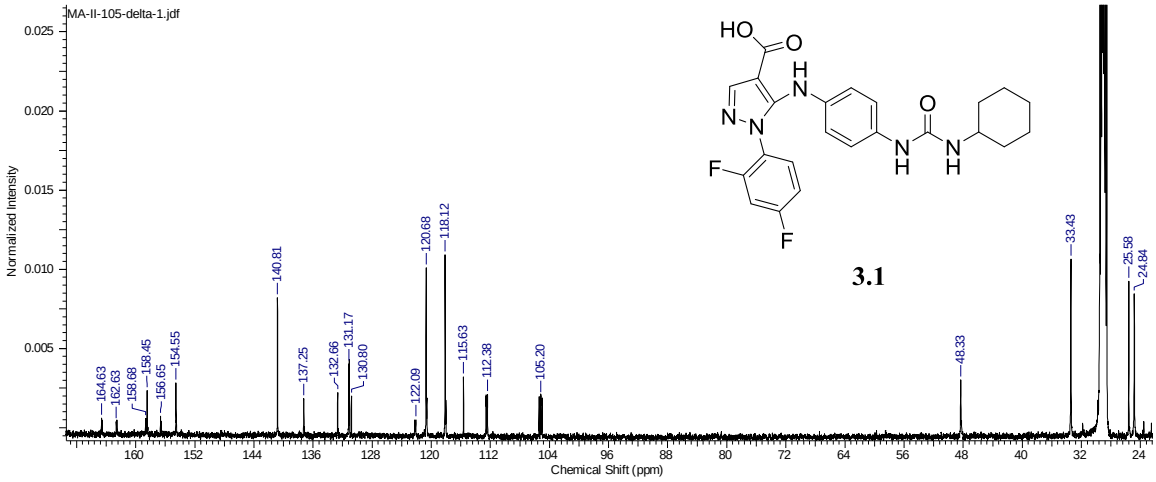

Figure 176. ^{13}C NMR Spectra of Compound **3.1**.

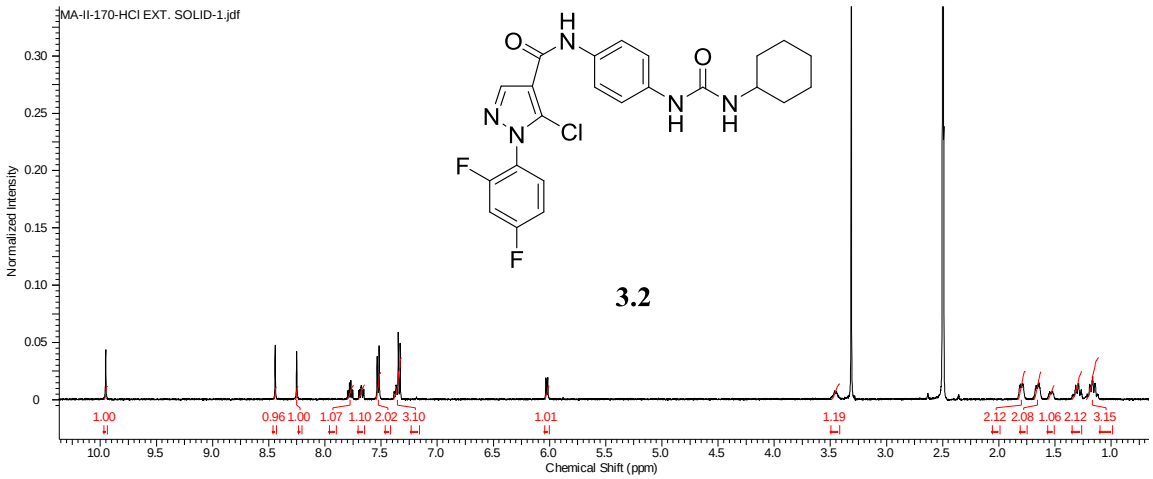

Figure 177. ^{1}H NMR Spectra of Compound **3.2**.

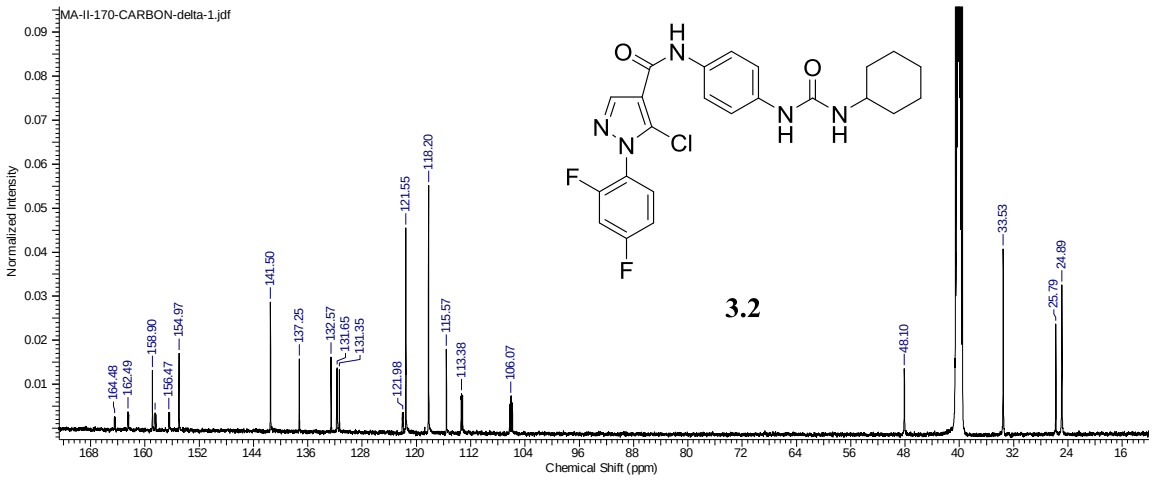

Figure 178. ^{13}C NMR Spectra of Compound **3.2**.

References

[1] O'Daniel, P. I.; Peng, Z.; Pi, H.; Testero, S. A.; Ding, D.; Spink, E.; Leemans, E.; Boudreau, M. A.; Yamaguchi, T.; Schroeder, V. A.; Wolter, W. R.; Llarrull, L. I.; Song, W.; Lastochkin, E.; Kumarasiri, M.; Antunes, N. T.; Espahbodi, M.; Lichtenwalter, K.; Suckow, M. A.; Vakulenko, S.; Mobashery, S.; Chang, M. Discovery of a New Class of Non-β-lactam Inhibitors of Penicillin-Binding Proteins with Gram-Positive Antibacterial Activity, *J. Am. Chem. Soc*. **2014**, *136*, 3664–3672.

[2] Balbi, A.; Anzaldi, M.; Macciò, C.; Aiello, C.; Mazzei, M.; Gangemi, R.; Castagnola, P.; Miele, M.; Rosano, C.; Viale, M. Synthesis and biological evaluation of novel pyrazole derivatives with anticancer activity. *Eur. J. Med. Chem*. **2011**, *46*, 5293–5309.

[3] Ningaiah, S.; Bhadraiah, U. K.; Doddaramappa, S. D.; Keshavamurthy, S.; Javarasetty, C. Noval pyrazole integrated 1,3,4-oxadiazoles: Synthesis, characterization and antimicrobial evaluation. *Bioorg. Med. Chem. Lett.* **2014**, 24, 245-248.

[4] Mert, S.; Kasimogullari, R.; Ica, T.; Colak, F.; Altun, A.; Ok, S. Synthesis, structure-activety relationships, and in vitro antibacrerial and antifungal activity evaluations of noval pyrazole carboxylic and dicarboxylic acid derivatives. *Eur. J. Med. Chem*. **2014**, *78*, 86-96.

[5] Khloya, P.; Kumar, S.; Kaushik, P.; Surain, P.; Kaushik, D.; Sharma, P. Synthesis and biological evaluation of pyrazolylthiazole carboxylic acids as potent anti-inflammatory-antimicrobial agents. *Bioorg. Med. Chem. Lett.* **2015**, 25, 1177–1181.

[6] Tewari, A. K.; Singh, V. P.; Yadav, P.; Gupta, G.; Singh, A.; Goel, R. K.; Shinde, P.; Mohan, C. G. Synthesis, Biological evaluation and molecular study of pyrazole derivatives as selective COX-2 inhibitors and anti-inflammatory agents. *Bioorg. Chem.* **2014**, *56*, 8-15.

[7] Sreenivas, B.; Akhila, M.; Mohammed, B. Synthesis and Biological Evaluation of Pyrimidine Analogs as Potential Antimicrobial Agents. *Int. J. Pharm. Pharm. Sci.*, **2012**, *4*, 306-310.

[8] Taylor, A. W.; Cook, R. T. A direct preparation of 2-aryl-4-ethoxycarbonyl-3-pyrazolin-5-ones from aryl hydrazines. *Tetrahedron*, **1987**, *43*, 607-616.

[9] Henderson, S. A.; Matthews, B. R. Heterocyclic Angiogenesis Inhibitors. U. S. Patent WO 2002030886 A2, April 18, **2002.**